Identification, optimization and characterization of pharmacological tools for the cannabinoid-activated orphan G protein-coupled receptor GPR18 and related receptors

Dissertation

zur

Erlangung des Doktorgrades (Dr. rer. nat.)

der

Mathematisch-Naturwissenschaftlichen Fakultät

der

Rheinischen Friedrich-Wilhelms-Universität Bonn

vorgelegt von

Clara Tabea Schoeder

aus

Bad Oldesloe

Bonn 2017

Angefertigt mit Genehmigung der Mathematisch-Naturwissenschaftlichen Fakultät der Rheinischen Friedrich-Wilhelms-Universität Bonn

Die vorliegende Arbeit wurde in der Zeit von April 2013 bis Juli 2017 am Pharmazeutischen Institut der Rheinischen Friedrich-Wilhelms-Universität Bonn unter der Leitung von Prof. Dr. Christa E. Müller durchgeführt.

Für meine Eltern

Contents

1. INTRODUCTION

1.1. Concepts in Medicinal Chemistry

A major goal in medicinal chemistry is the development of drugs that act in the intended way at a selected target. This process includes the identification and validation of hit and lead structures, their pharmacological and toxicological characterization and the study of their structure-activity relationships to optimize potency and selectivity, as well as physicochemical and pharmacokinetic properties.

Nowadays, there are many ways to identify hit and lead structures for further development. One of the most frequently used techniques, especially in an industrial environment, is high-throughput screening, which means automated testing of large compound libraries in a suitable test system. This procedure has the advantage of being fast and allows the testing of a large number of compounds. However, it also has some draw-backs. It is a very expensive undertaking, which needs an automated test system. Not all pharmacological assays are suitable for automatization, especially when it comes to cell-based assays that involve the exchange of media or filtering and washing steps. Another necessity is a large and diverse compound library. A relatively new method is computer-based virtual screening of huge compound libraries by using structural information of the target from crystal structure analysis or, if not available, from a homology model.

Another possibility to identify new lead structures is by knowledge-based approaches. Already established ligands and information of the endogenous ligand can be used to identify a suitable lead structure. This is also termed "ligand-based approach".

Lead structures not seldom arise from natural products. In plants, bacteria, fungi, algae and animals a broad diversity of chemical structures exist, which can be tested for biological activity, and which have already been optimized by evolution for interacting with proteins.

When identifying an active compound ('hit compound'), it has to be evaluated for its suitability as a lead structure. Some small modifications can be undertaken to optimize the compound's properties, a process, which is called "hit-to-lead" optimization. A good lead structure needs to fulfill some physiochemical requirements: an acceptable molecular weight and logP or logD value, solubility in aqueous solutions, positions on the scaffold that can be chemically modified, and a sufficient stability. It also should not have been reported to be toxic or contain functional groups that are known to have toxic effects. One has to investigate if the compound has been used for other purposes or whether it has already been described as a drug for some other target. Depending on the target of interest, a high degree of selectivity may be a requirement.
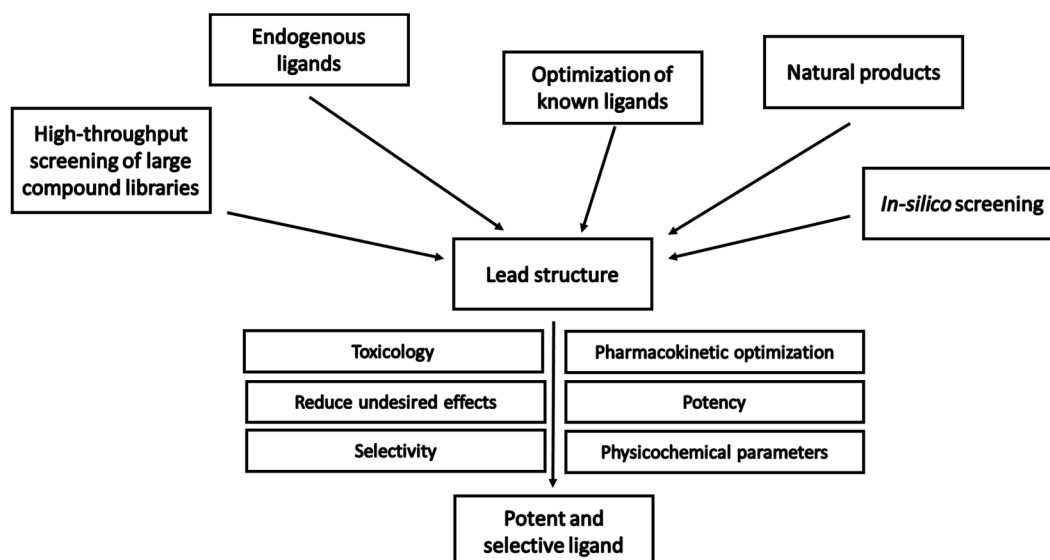
Figure 1: Development of potent and selective ligands in medicinal chemistry

1.2. G protein-coupled receptors

1.2.1. G protein-coupled receptors in medicinal chemistry

The major common function of a G protein-coupled receptor (GPCR) can be described as transmission of an extracellular signal to the intracellular site, where it causes a response in the cell via a G protein and/or β-arrestin. GPCRs respond to a broad diversity of ligands, including peptides, lipids, nucleotides, biogenic amines, hydrogen ions and light. Over 800 GPCRs exist in the human genome.[1] Some of these GPCRs have been targeted by drugs, before the structure and function of the receptor had been known. Many crucial (patho-)physiological events in the body are mediated via GPCRs.

In 2006, the group of Brian Kobilka solved the crystal structure of the first human GPCR. They crystallized the β_2-adrenergic receptor, a major drug target, and described its function on a molecular basis.[2] This insight into their molecular structure fueled research on GPCRs. Brian Kobilka was awarded the Nobel Prize in 2012 together with Robert Lefkowitz, who discovered β-arrestin signaling of GPCRs.

All GPCRs can be subdivided according to their phylogenetic relationship. The largest group consists of the so-called class A rhodopsin-like receptors. This family can be subdivided based on their phylogenetic relationships into four subfamilies (α-δ). The α-subfamily contains many well-known drug targets such as the adenosine, the serotonin, the cannabinoid, the melanocortin receptors and the opsins. The γ-subfamily comprises many peptide receptors, such as the opioid and chemokine receptors. The δ-branch receptors are the most diverse class, and include the P2Y receptors and the PAR receptors, but also contains many uncharacterized receptors with unknown function.[1]
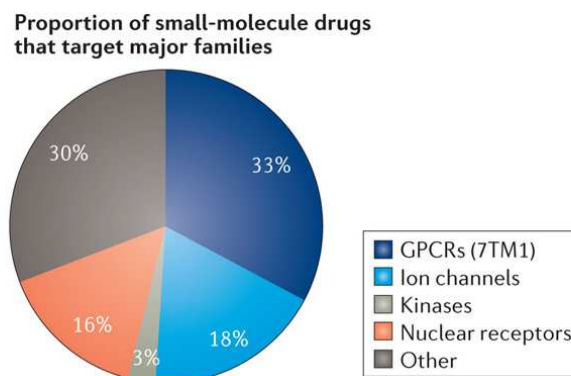
Figure 2: Approved small molecule drugs by targets. Picture was taken from Santos *et al.*[3]

GPCRs have been proven to be very druggable targets in the past and over 30% of all marked drugs target GPCRs (Figure 2).[3] Through the human genome project, it became clear that there are many more receptors than had not been known before. The function of some of them has not yet been described, nor their role in (patho)physiological conditions. To target these yet poorly characterized receptors may provide many drugs for diseases that today can only insufficiently be treated.

1.2.2. Structure and function of GPCRs

The major common feature of GPCRs are the seven transmembrane spanning domains. The N-terminus of the protein can be found extracellularly, the C-terminus intracellularly. GPCRs can be activated by a multitude of ligands including peptides, lipids, nucleotides, biogenic amines, protons and even light. The binding of an agonist results in a conformational change that leads to the activation of so-called G proteins. G proteins consist of three subunits (α,β,γ) and bind guanosine diphosphate (GDP) in their inactivate state. Upon activation by the GPCR, GDP is exchanged for guanosine triphosphate (GTP) and the α-subunit dissociates from the G protein complex. Depending on the type of G_α subunit different effects in the cell are mediated. A $G_{\alpha s}$ protein stimulates adenylate cyclase resulting in the formation of cyclic adenosine monophosphate (cAMP). The cAMP-dependent protein kinase A can then mediate further effects in the cell. A $G_{\alpha i}$ subunit inhibits adenylate cyclase and therefore inhibits the formation of cAMP. $G_{q/11}$ activates phospholipase C that forms inositol trisphosphate (IP_3) and diacylglycerol (DAG) from phosphatidylinositol-4,5-bisphosphate (PIP_2). IP_3 triggers the release of calcium ions (Ca^{2+}) in the cell. There are also further G proteins, as for example $G_{12/13}$, which activates small GTPases like RhoA leading to the recruitment of transcription factors such as nuclear factor of activated T-cells (NFAT), nuclear factor 'kappa-light-chain-enhancer' of activated B-cells (NFκB) or serum-response element (SRE). The $G_{\beta\gamma}$ subunit is able to induce a K^+ ion influx into the cell by activating the so-called G protein-coupled inwardly-rectifying potassium channels (GIRKs) causing hyperpolarization. The G protein signal is abrogated by the G_α subunit-inherent GTPase activity. Thus, GTP is cleaved to GDP and the G protein returns into its inactive state.

The activated GPCR is phosphorylated to stop the activation signal. Phosphorylation triggers the recruitment of β-arrestin, a structural protein that mediates the internalization of the GPCR through clathrin-coated pits. Furthermore, β-arrestin can address signaling pathways on its own, as for example the mitogen-activated protein kinase (MAPkinase) pathway, which induces the phosphorylation of extracellular-signal regulated kinase (ERK).

In Figure 3, the main structural features of a GPCR are depicted, exemplarily for the cannabinoid receptor 1 (CB_1).
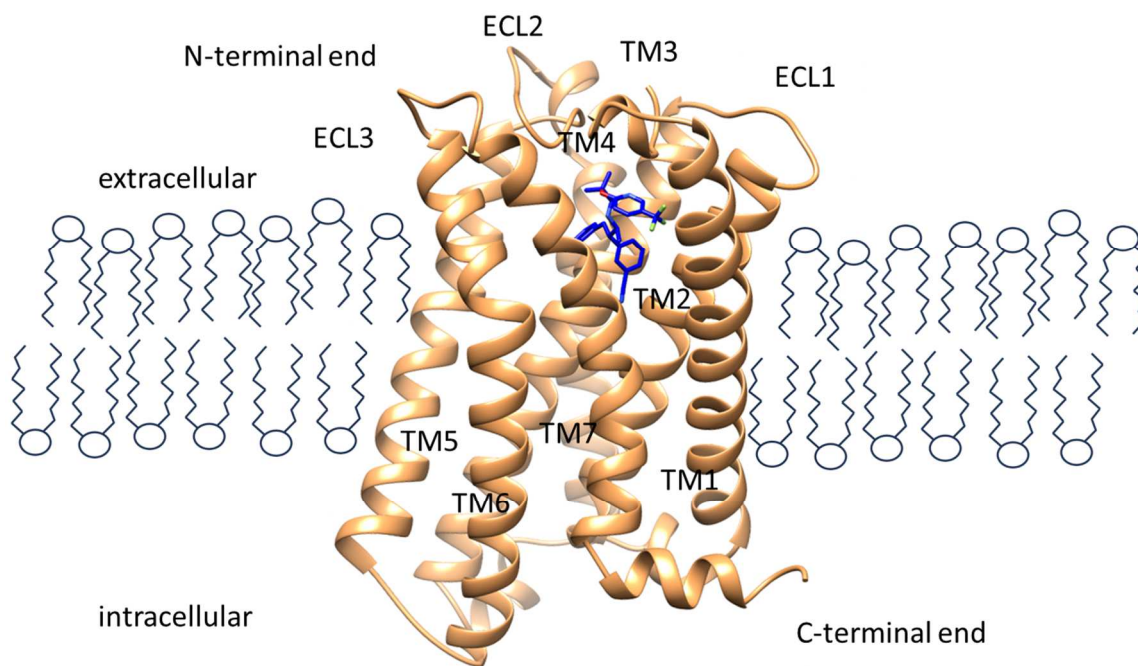
Figure 3: The cannabinoid receptor 1 (5U09), TM = transmembrane domain, ECL = extracellular loops

1.2.3. Measurement of GPCR activation

In medicinal chemistry, the interactions of compounds with their targets are studied and the compounds are optimized to obtain the desired action at the target of interest. To study compound target interaction quantifiable assays are needed. As described above, GPCR activation induces different effects in the cell. Some of them can be quantified to study compound receptor interaction.

Some types of read-out depend on the G_α subunit, to which the receptor is coupled, to analyze the change in the levels of a product of GPCR activation. Other read-outs are independent of the type of G protein involved.
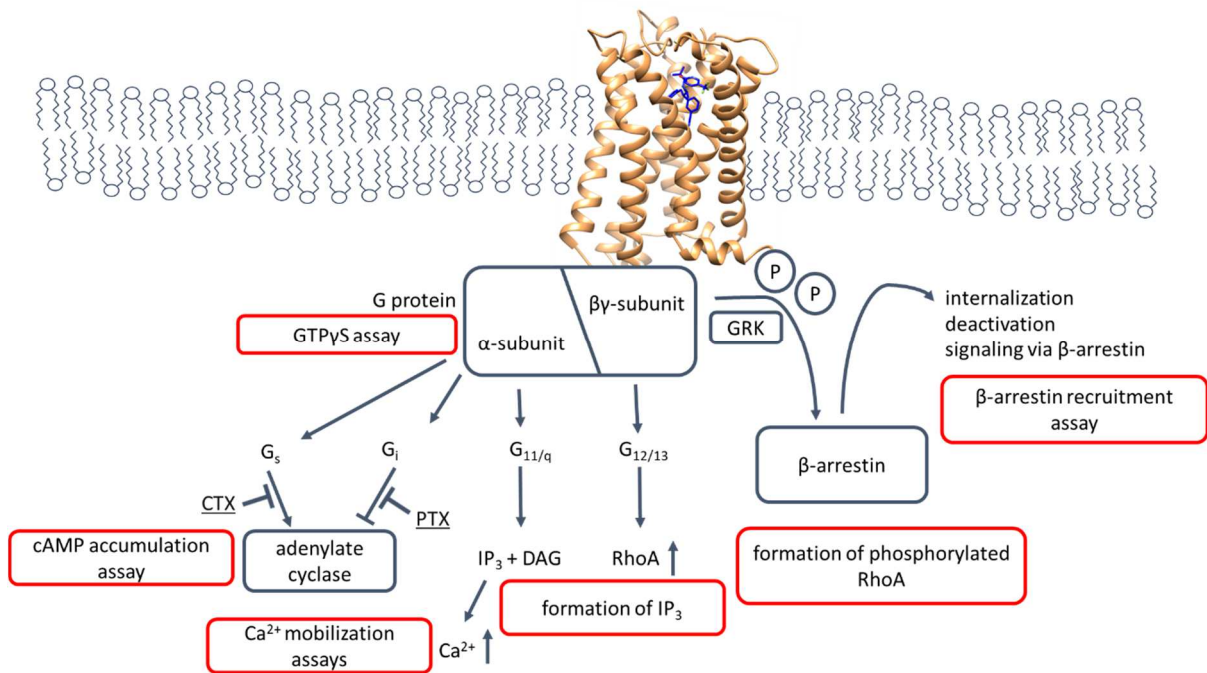
Figure 4: Possibilities to measure GPCR activation, (CTX = cholera toxin; PTX = pertussis toxin; GRK = G protein-coupled receptor kinase)

A rather universal read-out for the activation of a G protein is the [^{35}S]GTPγS assay, for which a hydrolytically stable radioactively labeled GTP analog is applied. When the GPCR is activated, the G protein exchanges GDP for GTP, but it is not able to cleave the applied [^{35}S]GTPγS, which can be quantified via liquid scintillation counting after separating bound from free radioligand, e.g. filtration.

For measuring the activation of G_s- and G_i-coupled receptors the accumulation of cAMP can be quantified. Cells usually have relatively low amounts of cAMP, therefore, the inhibition of cAMP formation by G_i proteins can in most cases only be assessed in the presence of the direct adenylate cyclase activator forskolin. The G_i response can be blocked by "uncoupling" receptor and G protein with PTX (pertussis toxin), while the G_s response can be blocked with CTX (cholera toxin).[4]

The $G_{q/11}$ or G_q response results in an increase in intracellular calcium ions. This can be measured in the presence of Ca^{2+}-sensitive fluorophors. The formation of IP$_3$ can be measured with an enzyme-linked immunosorbent assay (ELISA). The same is true for the activation of RhoA.

The G protein response in the cell is also influenced by the amount of the G protein of interest. If the G protein of interest is only available in low amounts the signal will be small or not quantifiable. Moreover, GPCRs can be promiscuous signaling through different G proteins. Another aspect when choosing an assay system are the costs. Antibodies, for example, are mostly very expensive and require many working steps, for example, washing steps. Therefore, they are mostly unsuitable for high-throughput screening approaches.

β-arrestin recruitment can be measured as a read-out for GPCR activation. It is a G protein-independent way to observe receptor activation. One possibility is the labeling of β-arrestin with a fluorescent marker and the visual observation of the recruitment process. When the receptor is also labeled with a fluorescent dye, the activation can be measured when the proteins come in close proximity by FRET (Förster Resonance Energy Transfer). Another possibility is the enzyme complementation assay. In this assay an enzyme that produces a readable output (for example, cleaves a substrate that leads to a chemoluminescence signal) is bound to β-arrestin, only lacking a small but essential part which is fused to the GPCR. When the receptor is activated and β-arrestin is recruited, the enzyme is complemented and ready to cleave its substrate. The advantage is the very specific read-out for only one receptor with a high amplification rate of the signal. Draw-backs are the possibility of interaction of test compounds with the enzyme.[5] β-Arrestin assays have been proven very valuable tools especially when investigating poorly characterized receptors.

Independently from the measurable cellular response, the binding affinity of a radiolabeled ligand can be determined. Here, a highly potent ligand is necessary, which binds to the receptor. When radioactively labeled, the amount of bound ligand can be quantified. The independence from downstream signaling is one of the major advantages of the binding approach. Furthermore, the tissue distribution of a GPCR can be investigated by labeling it with a high affinity radioligand. However, the binding study itself gives no information on the functionality of the receptor. Especially, when it comes to poorly characterized receptors, this technique cannot always be used, due to the lack of highly potent compounds.[6]

1.2.4. New trends in GPCR drug discovery

For a long time, a ternary complex of ligand-GPCR-G-protein interaction has been used to describe GPCR-ligand interactions: $L + R + G \rightarrow LR + G \rightarrow LRG$.

However, an activated GPCR can have different effects, depending on the ligand and the corresponding conformational state. For example, it can be able to address different downstream effects. Some GPCRs are able to signal through different G proteins (either depending on the ligand or the availability of the G protein in the cell). Another effect is the signaling through either β-arrestin or a G protein pathway. This phenomenon is known as biased signaling. Compounds that induce a conformation of the receptor that only leads to the activation or inhibition of a certain signaling pathway are called "biased" ligands.[7] This concept can be of advantage when one signal pathway leads to undesired side effects while the other one generates the intended effect.

Compounds inducing a partial activation or inhibition are so-called partial agonists or antagonists. They can be of interest when a full activation or inhibition causes side effects.

For many GPCRs a constitutive activity has been reported, which means a constant activation without the presence of an agonist. Inverse agonists are antagonists that are able to reduce the constant activity. Constitutive activity of GPCRs has been discussed to be a target of interest especially in cancer.[8]

Another concept of great interest is the development of allosteric ligands. The binding site of the endogenous ligand defines the orthosteric binding site, whereas allosteric interactions occur in a different binding site. An allosteric ligand changes the conformation of a receptor protein in such a way that the affinity and/or efficacy of the endogenous ligand is altered. This can result in desirable therapeutic effects.[9]

GPCRs have been reported to form homodimers and heterodimers. The special interaction of certain receptors and their mutual interaction may provide new targets for drug discovery. GPCR homodimer and heterodimer pharmacology needs to be further investigated to generate reliable concepts for medicinal chemistry.[9]

For every therapeutic option, a certain kind of ligand may be desired that has advantages over another one.

1.3. Cannabinoid receptors

The cannabinoid receptors (CB receptors) are named after the most famous compound group that interact with them. The effects and structures of cannabinoids have been known long before it became clear on which targets they act. The psychoactive effects of Δ^9-tetrahydrocannabinol (Δ^9-THC) derived from the plant *Cannabis sativa* has been described as a major psychoactive constituent in the late 1950s. Although a specific site of action for this compound and its derivatives had been postulated and characterized by radioligand binding,[10] the cannabinoid receptor 1 (CB_1) was not identified before 1990, when it was cloned for the first time.[11]

The endogenous ligand of the CB_1 receptor was identified in the early 1990s, shortly after the identification of the CB receptors. Anandamide (arachidonoylethanolamide, AEA) was extracted from porcine brain tissue and later on characterized in various test systems to evoke the same pharmacological responses as previously known CB receptor agonists.[1214; 13,13] It was therefore postulated to be the endogenous ligand of the CB receptor. In 1993, another CB receptor was discovered which was differently expressed, predominantly in the immune system.[15] Later on, a second endogenous fatty acid derivative was reported as an endogenous agonist for both cannabinoid receptors, 2-arachidonoyl-*sn*-glyercerol (2-AG).[16]

Anandamide is primarily produced from *N*-acylphosphatidylethanolamide (NAPE) in the membrane by the enzyme *N*-acyl phosphatidylethanolamide phospholipase D (NAPE-PLD), whereas 2-AG can be formed by the cleavage of diacylglycerols by diacylglycerollipase (DAGL). Anandamide is degraded by fatty acid amide hydrolase (FAAH) to arachidonic acid and ethanolamine, whereas 2-AG is cleaved by monoacylglycerol lipases (MAGL) to arachidonic acid and glycerol. These enzymes control the formation and degradation of the endocannabinoids and represent possible targets in medicinal chemistry.

In 2016, the crystal structure of the CB_1 receptor was solved independently by two groups. The structures contain the antagonists taranabant and AM6538, respectively. Information from these structural insights will help to guide future ligand development for CB receptors.[17,18]
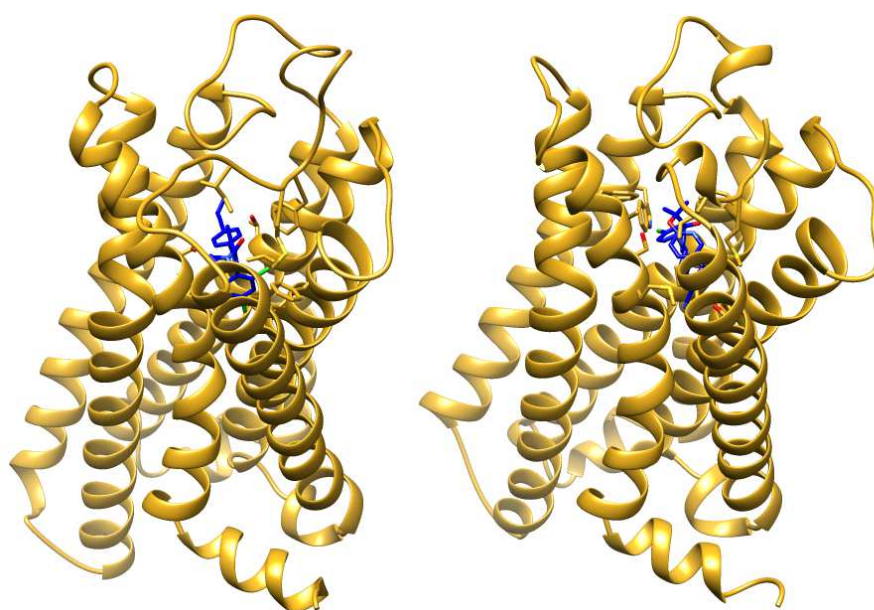
Figure 5: Crystal structures of CB_1; on the left side PSB:5UO9, on the right side PSB: 5TGZ

1.3.1. Physiological role of the cannabinoid receptors

The CB_1 receptor was postulated to be the most highly expressed GPCR in the brain. Its expression was reported in hippocampus, cortex, basal ganglia and cerebellum, where the receptor can primarily be found presynaptically on both, excitatory glutamatergic and inhibitory GABAergic neurons.[19] Activated GABA-ergic neurons produce endocannabinoids at the postsynaptic end and activate the presynaptically distributed CB receptors. Upon activation, they suppress the neurotransmitter release and thus the postsynaptic neuron cannot fire action potentials as frequently as before. This retrograde modulation of transmission is called depolarization-induced suppression of inhibition and is one of the key features of cannabinoid functionality in the brain.[20,21,22] However, postsynaptic expression of CB receptor has also been reported.[19]

The CB$_1$ receptor displays in pleiotropic effects. It modulates the formation of anorexigenic leptin and orexigenic ghrelin in the brain, both major factors to control appetite and food intake.[23] Additionally, the CB$_1$ receptor is involved in peripheral energy homeostasis by increasing the biosynthesis of fatty acids and triglycerides and by decreasing lipolysis.[23] CB$_1$ activation further leads to prolonged hypotension and bradycardia. For the CB$_2$ receptor a protective role for the ischemic heart has been described. [24,25]

The CB$_2$ receptor is mainly expressed in the immune system. It was found in almost all immune cells and seems to be involved in the migration of immune cells in maturation and. It promotes chemotaxis and chemokine formation. The immunosuppression by CB$_2$ activation is a new possibility to target inflammatory diseases and pain. Especially, as the CB$_2$ receptor was also found in microglia in the brain, the activation of CB$_2$ receptors mediates immunosuppressive effects in neuroinflammation. [26,27]

The cannabinoid receptor 2 plays a key role in the formation of bones, where it can be found both in osteoclasts and osteoblasts. In CB$_2^{-/-}$ knock out mice the bone mass is significantly reduced. Therefore, the activation by CB$_2$ receptor agonists could serve as a future treatment for osteoporosis.[28,29]

1.3.2. Medicinal chemistry of cannabinoid receptor ligands

Compounds displaying affinity for CB receptors can be divided into four structurally different compound classes: the endogenous ligands for the two CB receptors, anandamide and 2-AG; Δ^9-THC related phenolic compounds; *N*-alkyl-indoles originally designed by Huffman *et al*. and pyrazoles, as for example the CB$_1$ receptor antagonist rimonabant, as well as other compounds, which do not belong to any of these groups.
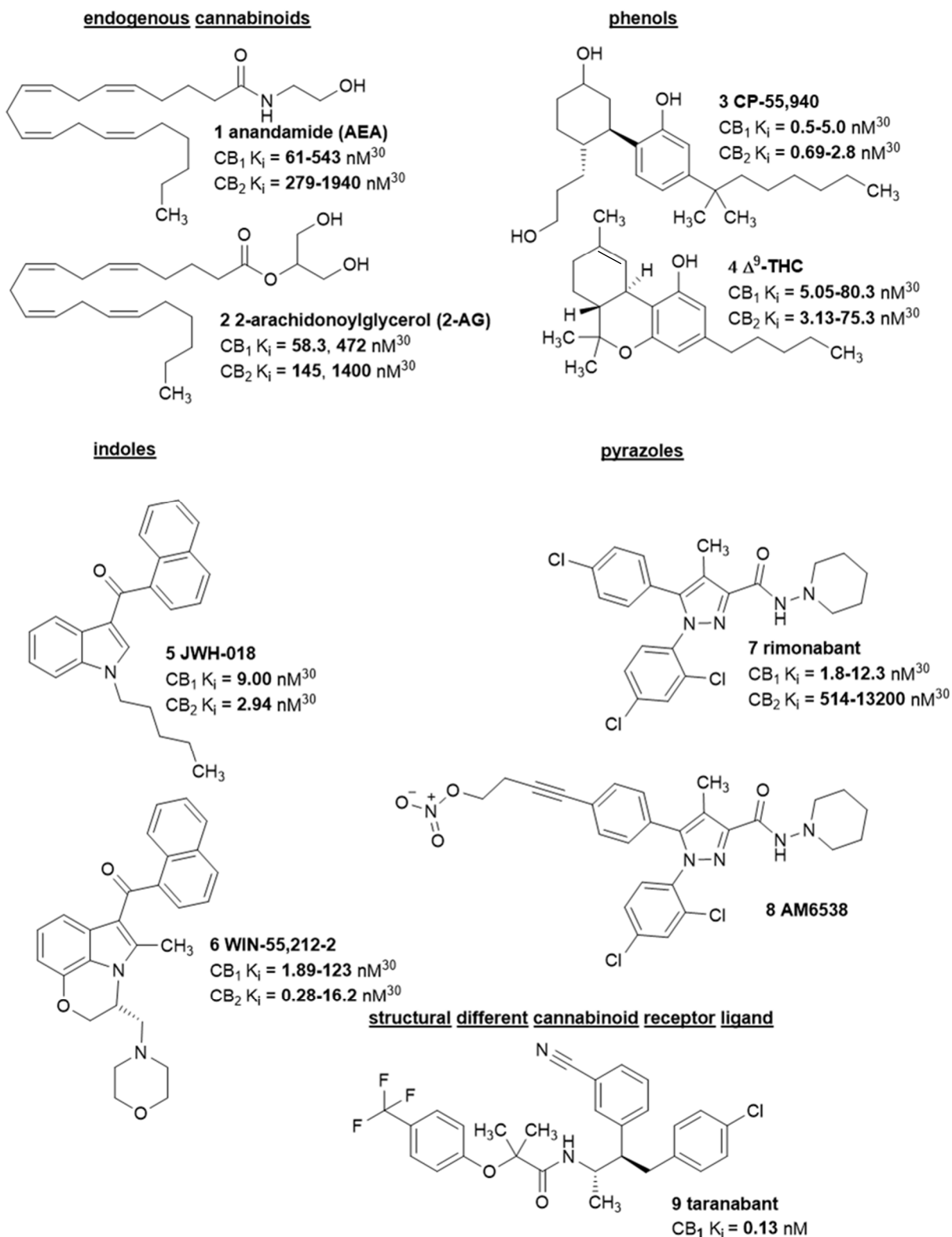
Figure 6: CB receptor ligands

The cannabinoid receptors both have been of great interest with regard to drug development. CB_1 agonists and their effects have been known for a long time. They are also the first group of CB receptor ligands that have been approved for medicinal use.

In Germany, the partial-synthetic dronabinol can be prescribed for the treatment of cancer- or AIDS-derived anorexia, kachexia and nausea. Nevertheless, it has to be prescribed and is treated as a controlled substance with all the accompanying formalities. It can be manufactured in the pharmacy shop from the crude drug, since no industrial product is distributed in Germany, but in the US it is sold under the tradename Marinol® as capsules. Repeatedly, Δ^9-THC has been in discussion to be used for the treatment of multiple sclerosis, Morbus Crohn, Colitis ulcerosa and glaucoma. As a combination therapy together with cannabidiol (CBD), it was approved as a buccal spray (Sativex®) in several European countries. The fixed combination of Δ^9-THC and CBD and can be prescribed as an add-on therapy for multiple sclerosis patients, who did not benefit from other therapies.[31] It was further discussed to be beneficial in the treatment of chronic neuropathic pain.[32] A synthetic derivative of Δ^9-THC, nabilone, was developed by Eli Lilly and launched as a treatment against emesis and as a tranquilizer in the 1980s.[33]

The draw-back of CB_1 receptor agonists has always been their psychoactive side-effects, which makes them controlled drugs in most Western countries. To circumvent this problem some therapeutic options have been discussed. Local administration or development of peripherally acting cannabinoid receptor agonists could prevent the central side effects. Further, the anandamide-metabolizing enzymes fatty acid amide hydrolase could serve as a target, but unfortunately severe side-effect have been reported in phase I studies.[34,35]

CB_1 receptor antagonists have been developed for obesity.[36] With rimonabant (Acomplia®, SR141716A) a drug was already marketed for this indication in Europe. The beneficial potential, especially when discussed in the context of the reported side-effects, led the FDA to refuse the approval of rimonabant. The reported side-effects, especially depression and suicidal behavior, led to the withdrawal of rimonabant.[37] This experience emphasizes the complexity of the cannabinoids' actions in the brain. Although several other CB_1 receptor antagonists had been advanced, none of them entered into clinical development. New therapeutic options in the field of CB_1 antagonists are allosteric modulators of CB_1 receptors or peripherally acting CB_1 antagonists.[38]

As the potential of CB_1 receptor antagonists will always be limited by undesirable central side-effects, the interest in CB_2 receptor ligands is emerging. The main distribution of CB_2 in the immune system has made it an interesting target for neuropathic pain, immunologic diseases, cancer and osteoporosis.[39] It is nowadays well accepted that CB_2 is also expressed in the brain, especially in microglia, which is involved in inflammatory processes in the brain. The activation of CB_2 has an immunosuppressive and anti-inflammatory effect. Especially, as there is no evidence of psychoactive side-effects, CB_2 agonists are of great interest. Therefore, selective CB_2 agonists are proposed as future drugs for diseases such as multiple sclerosis and Huntington's disease.[40] Furthermore, central CB_2

agonists offer a possible treatment for neuroinflammatory diseases, as for example Alzheimer's disease.[41,42]

CB$_2$ antagonists have not been of interest for drug discovery so far, but might become interesting in the context of immuno-oncology.

Table 1: Possible application of ligands for CB receptors

	(Possible) indication	Drugs
CB$_1$ agonists	Kachexia, nausea and emesis, multiple sclerosis, neuropathic pain	Dronabinol (Marinol®), Sativex® (Δ^9-THC, CBD), Nabilone
CB$_1$ antagonists	Obesity, adipositas	Rimonabant (Acomplia®) withdrawn because of side effects
CB$_2$ agonists	Inflammation, neuroinflammatory diseases, e.g. multiple sclerosis, Huntington's disease etc. osteoporosis	-

New CB receptor ligands may open up new therapeutic indications in the furture.

1.3.3. Off-target effects of cannabinoid receptor ligands

Cannabinoids can also act at other targets. For example, they influence the transient receptor potential cation vanilloid (TRPV) channels. These are thermosensitive cation channels involved in pain formation, which respond to the activation by lipid-like compounds, for example *N*-acyldopamine and similar lipids including anandamide. [43,44]

Lake *et al*. investigated the characteristic effect of direct cannabinoid-induced vasodilatation and observed that the anandamide-induced vasodilatory effects can neither be blocked with the CB$_1$ antagonist/inverse agonist rimonabant, nor mimicked by the CB$_1$ receptor agonist Δ^9-THC. The authors concluded that anandamide acts at an additional site and hypothesized that an endothelial anandamide receptor exist which is different from CB$_1$ and CB$_2$.[45] Anandamide-induced vasorelaxtion of rat mesenteric arteries persists also in CB$_1^{-/-}$-CB$_2^{-/-}$ double knock-out mice. They further showed that abnormal-cannabidiol (abn-CBD), a regioisomer of CBD, both of which are inactive at the CB receptors, can also induce this effects. The mesenteric vasodilation is endothelium-dependent and can be blocked by CBD. They concluded from their experiments that an additional site of action for vasodilation exists in the endothelium for anadamide, and proposed a putative 'abn-CBD-receptor'.[46] This putative 'abn-CBD' receptor has been further investigated, especially in rat mesenteric arteries. O-1918, an inactive cannabinoid-like compound, was shown to inhibit the vasodilatory signal and also to inhibit abn-CBD-

induced phosphorylation of p42/44 MAP kinases and B/Akt kinases in HUVEC cells, an endothelial cell line, in a $G_{i/o}$-dependent manner.[47]

1.4. Orphan G protein-coupled receptors

Orphan GPCRs are GPCRs with yet unidentified endogenous ligands. Through the human genome project many more GPCRs were discovered than the known receptors. Over 800 GPCRs can be found in the human genome, about 400 when excluding the olfactory GPCRs. From them, still over 100 remain orphan receptors.[48]

In reverse pharmacology approaches screening for endogenous ligands is conducted, but the success rate of deorphanization has been decreasing.[49,50] Different methods have been used to map known transmitters to newly identified receptors, first of all by reports of interactions and tissue distribution. Later on, orphan receptors were screened for new ligands, however with mixed success.

Nevertheless, the (patho)physiological role of an orphan receptor can be investigated with surrogate ligands instead. Potent and selective ligands for orphan receptors can help to understand their role and validate them as targets for further therapeutic use.
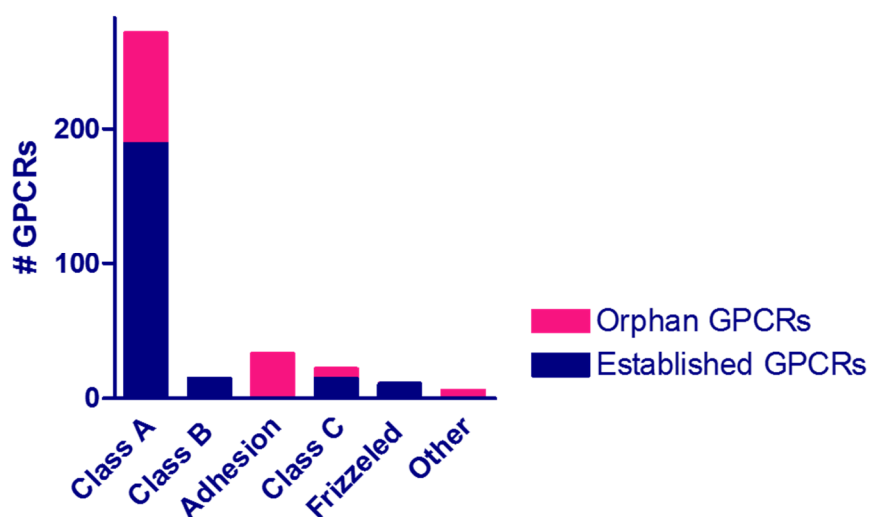
Figure 7: All non-sensory GPCRs, according to NC-IUPHAR classification (Source: http://www.guidetopharmacology.org/)

In the class A rhodopsin-like GPCR subfamily almost one hundred orphan GPCRs can be found. Many of them belong to the δ-branch. Among others, two orphan GPCRs (GPR18 and GPR55) are located in this group of receptors, to which also the purinergic P2Y but also peptide-activated and lipid-activated receptors belong. These two orphan receptors have been reported to interact with cannabinoids.

1.4.1. GPR18

GPR18 has been firstly described by Gantz *et al.* in 1997. They detected a so far unknown GPCR in canine parietal cells and a human colorectal adenocarcinoma cell line (Colo 320DM) by using relaxed low-stringency PCR, when they were trying to clone a possible bombesin receptor. Furthermore, they investigated expression levels of this new receptor and found GPR18 highly expressed in spleen and testis, and also in thymus, peripheral leukocytes and small intestine.[51] Therefore, they proposed its involvement in immunological processes.

Phylogenetically, GPR18 belongs to the δ-branch class A rhodopsin-like GPCRs.[1] Many orphan receptors can be found in this branch. Interestingly, the CB receptors belong to the α-branch of class A GPCRs and are therefore genetically unrelated to the two orphan GPCRs. For GPR18, it is remarkable that there is no very closely related receptor. GPR34 can be considered as closest relative, and GPR183 (EBI2) shares the highest sequence identity. Both of them are also orphan GPCRs, for GPR34 lyso-phosphatidylserine,[52] and for GPR183 oxysterols have been proposed as an endogenous ligand.[53]
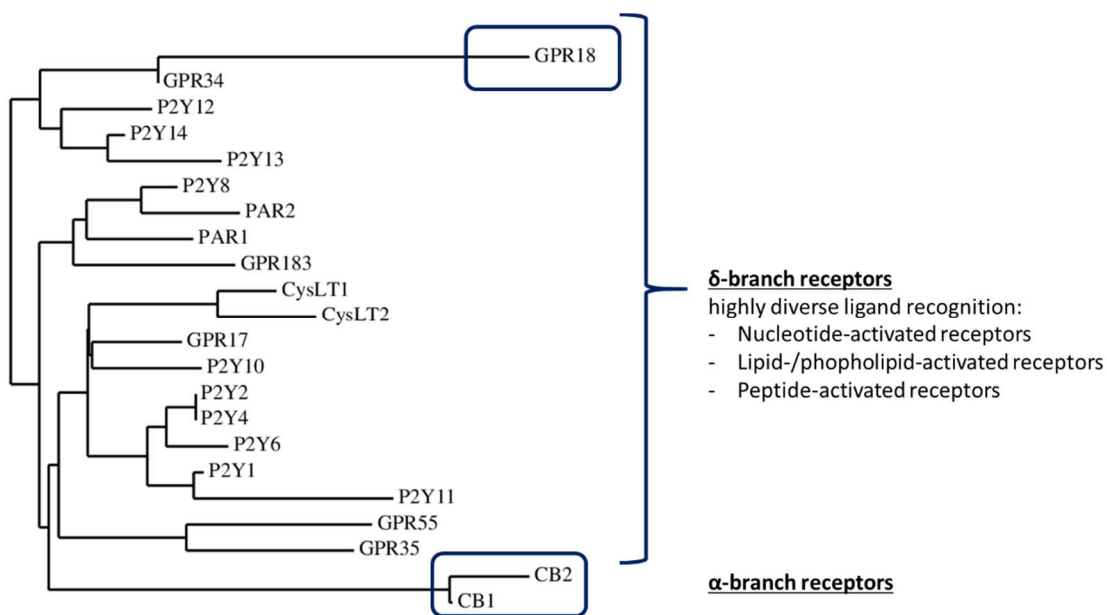
Figure 8: Phylogenetic relationship of GPR18 and GPR55 (phylogenetic tree designed with phylogeny.fr [55-57])

In chapter 1.3.3, we showed that a putative 'abn-CBD receptor' has been proposed that induces vasodilatation in the endothelium. The endothelial expression of GPR18 has been investigated in another study, which focused on the role of endogenous cannabinoids in epithelial cells. GPR18 and CB$_1$ receptors were expressed along with TRPV1 channel, and these are involved in the regulation of inflammatory responses of the vascular bed.[58] Endothelial cells also build the surface of the blood brain barrier, where GPR18 like CB$_1$ and CB$_2$ receptors were reported to be expressed. CB$_2$ activation reduced the migration by tumor cells, but the role of GPR18 in this respect has not been clearly characterized by now.[59]

Endogenous ligands have been proposed for GPR18. In 2006, Kohno *et al*. introduced *N*-arachidonoylglycine (NAGly) as GPR18 agonist. Kohno *et al.* were investigating chemokine receptor 4 (CXCR4)-like GPCRs in lymphoid cell lines and found GPR18 to be highly expressed, especially in HUT102 cells, a T-cell lymphoma cell line. To identify an endogenous ligand for GPR18, they screened a lipid library in Ca^{2+}-mobilization assays on GPR18-transfected cells, and detected a signal induced by NAGly. They confirmed their finding by cAMP accumulation assays in CHO cells stably expressing the receptor and reported an IC_{50} value of 20 ± 8 nM. Their signal was abolished upon pretreatment with PTX, a G_i protein-decoupling agent.[60]

NAGly (Figure 9) has been known before. It was found to be a substrate for FAAH,[61] and suppressed pain in a formalin-induced tonic pain test.[61] Although, it is structurally related to anandamide, the endogenous ligand of the cannabinoid receptors, it does not interact with them.[62] However, it has been reported to inhibit the glycine transporter 2a (GIYT2a)[63] and to increase calcium ion signals in primary β-cells.[64] It was also proposed as an endogenous mediator with anti-inflammatory potential.[65]

10 *N*-Arachidonoylglycine (NAGly)
CB_1: K_i = >10 μM[66,62]
CB_2: K_i = >10[66]
GIYT2a: IC_{50} = 5.1 μM[63]
FAAH: IC_{50} = 7.0-4.1 μM[61]
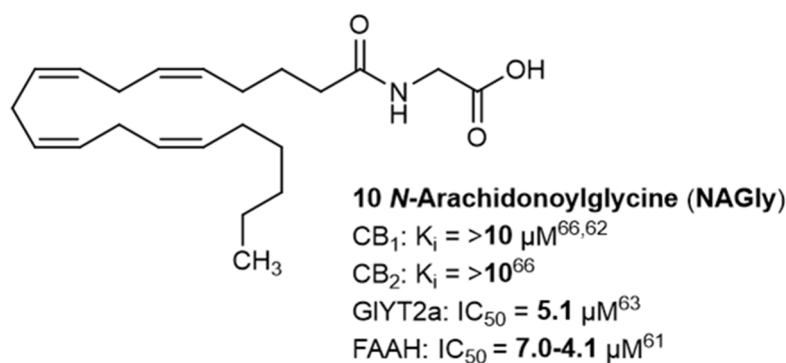
Figure 9: Chemical structure of *N*-arachidonoylglycine

Conjugates of other fatty acids with the amino acid glycine are also possible. For the condensation product of palmitoic acid and glycine calcium influx in adult dorsal root ganglia was reported, and its involvement in anti-inflammatory and nociceptive processes was also suggested.[67]

While characterizing a distinct site of action for endogenous cannabinoids in microglia McHugh *et al*.[68] investigated also a possible involvement of the putative abn-CBD receptor. They found microglial migration strongly increased by NAGly and by abn-CBD in BV-2 cells, a mouse immortalized microglial cell line. p44/42 MAP kinase phosphorylation was enhanced, not only in BV-2 cells but also in HEK293 cells overexpressing GPR18. The authors demonstrated the antagonism of the already mentioned O-1918 and *N*-arachidonoylserine. They concluded from their experiments that GPR18 and the abnormal-cannabinoid receptor are the same and NAGly is the endogenous agonist.[69] With an siRNA knock-down experiment, they further supported their hypothesis that GPR18 mediates NAGly-induced migration in BV-2 cell lines.[70] The microglial expression of GPR18 could also been observed by Malek *et al*. who found mRNA levels in primary rat microglia elevated after LPS treatment.[71]

McHugh *et al*. continued with research on the endometrial cell line HEC-1B, an epithelial uterus adenocarcinoma, which also showed increased migration in the presence of NAGly, but even more pronounced in the presence of AEA. They unsuccessfully tried to block the response with a selective CB$_1$ antagonist (SR141716A). However, it was sensitive to SR144528, a selective CB$_2$ antagonist. They demonstrated that AEA can be transformed into NAGly in HEC 1B, as already shown by Bradshaw *et al*. They concluded that NAGly-induced migration in this endometrial cell line is mediated by GPR18. Therefore, GPR18 has been proposed as target for endometriosis, a severe female disease of the uterus.[72]

GPR18 was also discovered to be involved in the regulation of intraocular pressure. By being expressed in ciliary and corneal epithelium and also trabecular meshwork, it was proposed to play a role in the regulation of the intraocular pressure mediated by NAGly, which can be found in the tissue in amounts of 0.268 pmol/l. Along GPR18, they also showed cannabinoid receptor CB$_1$ to be expressed and involved.[73] In the studies of McIntyre *et al*. GPR18 has been found in the epithelial retinal microvasculature. NAGly and abn-CBD abolished endothelin-induced vasoconstriction.[74]

The involvement of NAGly in inflammatory processes has been investigated by Burstein *et al*. Inflammation becomes chronic when the natural resolution factors fail to stop the inflammatory process. Burstein *et al*. observed that NAGly enhances resolution factors (PGJ and LXA$_4$) in different myeloid and lymphoid cell lines (compare Table 2). They proposed a GPR18 mediated pathway due to a partial blocking of the resolution response by GPR18 antibodies.[75]

In macrophages, Takenouchi *et al*. described GPR18 to be mainly expressed in the so-called M1 macrophages, a classical proinflammatory stage. They investigated the cell viability in the presence of different concentrations of NAGly. When 30 μM NAGly was supplied, the cell viability was significantly reduced. By blocking specific pathways in the cells known to mediate cell death, they identified p38 MAP kinases and MEK involved in the process. GPR18 therefore might be involved in NAGly-induced apoptosis signals in macrophages.[76] The expression of GPR18 in the M1 macrophages was also reported by Jablonski *et al*. GPR18 and CD38, an ectonucleotidase, together with the formyl peptide 2 receptor were proposed as M1 stage markers, because of their exclusive expression in this cell type.[77] The M1 stage of macrophages is known to be induced by bacterial infections. The resolution of the M1 stage abrogates the inflammatory process. When the M1 stage is not resolved proinflammatory stages can occur resulting in chronic inflammation. The M1 stage has been linked to inflammatory diseases as arteriosclerosis and also multiple sclerosis.[78]

Abn-CBD-stimulated responses, which might be mediated by GPR18, have also been reported in the rostral ventrolateral medulla, resulting in a lowered blood pressure. GPR18 was shown together with CB$_1$ expression. In these specialized neurons, adiponectin and NO were enhanced as reactive

oxygen species were reduced.[79] The authors concluded on a $G_{i/o}$ protein-mediated effect via the PI3K/Akt pathway, which finally leads to an enhanced level of adiponectin and nNOS.[80]

GPR18 has been detected to be highly expressed in metastatic melanoma by Qin *et al*. Melanoma is one of the most aggressive skin cancers for which not many therapeutics are available. Therefore, GPR18 could be a possible target for melanoma treatment.[81]

In contrast to the previous studies, Yin *et al*. did not monitor any activation of GPR18 by NAGly when they were screening a lipid library in the PathHunter™ test system by DiscoveRx[82], an enzyme complementation assay for β-arrestin recruitment. Furthermore, Lu *et al*. were also not able to report NAGly-induced GPR18 activation, although they investigated a range of possible cellular responses. In their experiments measuring Ca^{2+} currents, which can be mediated by $G_{i/o}$ proteins, they observed no GPR18-mediated response, but NAGly was able to increase the Ca^{2+} currents independent of GPR18. The same was true for potassium channels. They were further not able to show any production or decrease of cAMP levels in GPR18-transfected cells. From their experiments they concluded GPR18-independent pathways to be responsible for NAGly-related observations.[83]

Finley *et al*. also investigated the response of cells to NAGly and could not observe any GPR18-mediated signal, neither on calcium mobilization nor on changes in the cAMP level. However, GPR18 showed a high degree of trafficking. In comparison to the cannabinoid receptor 1, it shows lower cell surface expression. When trying to find a suitable endogenous cell line to further test GPR18 activation, they investigated its expression in the already reported BV-2 and HEC-1a and HEC-1b cell lines but could not detect it.

In another study on small intestininal CD8αα-positive T cells, NAGly did not show any migratory effect on GPR18-expressing cells. However, GPR18 was found to be important for the appropriate maturation and movement of intraepithelial lymphocytes.[84] CB_2 receptor-independent migration of primary murine macrophages has also been found to be mediated by GPR18 or GPR55, but both receptors do not response to the CB_2 agonists applied (JWH-133 and HU-308). The response could be abolished by pretreatment with PTX.[85] The authors concluded that there is an additional site of action for the mentioned CB_2 agonists which is neither GPR18 nor GPR55.[85] Becker *et al*. further investigated the function of GPR18 in intraepithelial lymphocytes both in wildtype mice and in GPR18-deficient mice. The number of the intraepithelial lymphocytes did not change between the knock-out and the wildtype mice, but when a bone marrow transplantation was carried out the wildtype mice reconstituted the intraepithelial lymphocyte function better than the knock-out mice.[86]

In an attempt to explain discrepancies between reported results, Console-Bram *et al*. investigated both cannabinoid ligands (Δ^9-THC, abn-CBD, O-1918 and O-1602) and NAGly in MAPK signaling, Ca^{2+} mobilization and β-arrestin signaling. They found both cannabinoid compounds and NAGly to stimulate

Ca^{2+} increase in the cell. This signal was sensitive not only to PTX but also to a G_q inhibitor. However, only Δ^9-THC and partly also CBD, produced a signal in a β-arrestin assays. The authors concluded that biased signaling of the compounds towards β-arrestin or G_q or G_i took place.[87]

Table 2: Reported expression levels of GPR18

Reported expression of GPR18	Source
Testis, Spleen, thymus, peripheral leukocytes, small intestine	Gantz et al. 1997[51]
Lymphoid cell lines (HUT102, MOLT-4, MT-2, MT-4, Jurkat, HUT78)	Kohno et al. 2006[60]
Peripheral lymphocytes: $CD4^+$, $CD4^+CD45RA^+$, $CD4^+CD45RO^+$, $CD8^+$ and $CD19^+$-positive; but not in non-lymphoid cell lines	
BV-2 cells (mouse), primary microglia	McHugh et al. 2010[69]
Metastatic melanoma, primary melanoma cells	Qin et al. 2010[81]
HEC-1B, endothelial adenocarcinoma of the uterus	McHugh et al. 2012[72]
U937, HL60, MOLT4, RAJI	Burstein et al. 2011[75]
RAW264.7 (a macrophage cell line)	Takenouchi et al. 2012[76]
Ciliary and corneal epithelium, trabecular meshwork	Cardwell et al. 2013[73]
Neurons of the rostral ventrolateral medulla (RVLM) in the brainstem (together with CB_1)	Penumati et al. 2014[79]
Endothelial cell lines (HUVEC, HCAEC, brain, liver, and lung derived endothelial cell lines), peripheral blood mononuclear cell (PBMC)	Wilhelmsen et al. 2014[58]
Retinal cells	McIntyre et al. 2014[74]
Brain endothelial cells	Hasko et al. 2014[59]
CD8αα-intraepithelial lymphocytes	Wang et al. 2014[84]
Primary murine macrophages	Taylor et al. 2015[85]
Rat primary microglial cultures	Malek et al. 2015[71]
Peripheral blood polymorph nuclear neutrophils, monocytes and macrophages, intraepithelial lymphocytes	Chiang et al. 2015[88]
Intraepithelial lymphocytes	Becker et al. 2015[86]
M1 stage macrophages	Jablonski et al. 2016[77]
Glioblastoma cell lines	Finlay et al. 2016[89]
Sperm	Flegel et al. 2016[90]
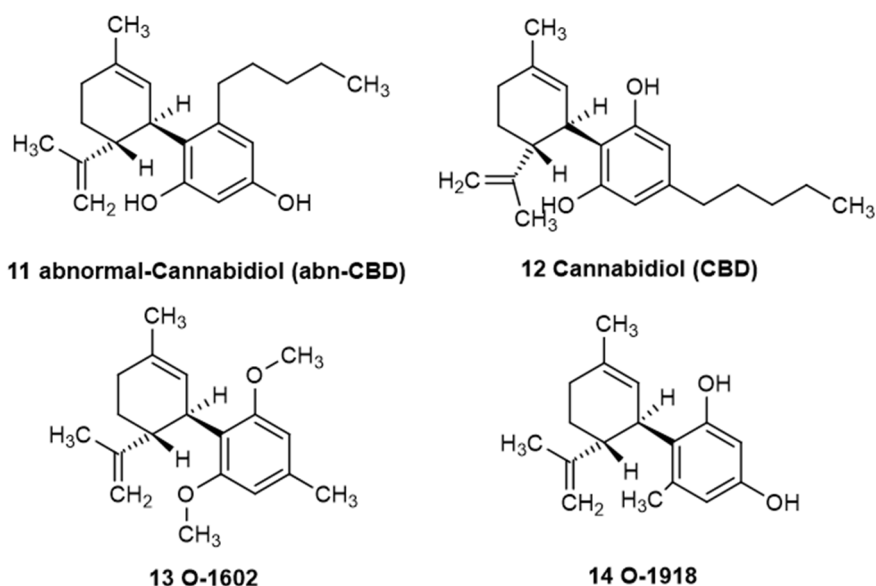
Figure 10: Chemical structure of cannabinoids proposed to act on GPR18

The fatty acid derivative resolvin D2 was reported to solve inflammatory processes. Chiang *et al*. investigated the action of resolvin D2 on macrophages, where it stimulated the formation of cAMP. The effect was attenuated in GPR18-deficient mice. GPR18 deficient mice did not show any apparent pathological phenotype. In cells overexpressing GPR18 tritium-labeled resolvin D2 methyl ester showed a K_D value of 9.6 nM in a radioligand binding assay and was displaced by resolvin D2. The authors proposed resolvin D2 as the endogenous ligand of GPR18. Furthermore, they investigated the effects of NAGly, which displaced the radiolabeled resolvin D2-methyl ester.[88] It also reduced the bacterial titer of *Staphylococcus aureus* after infection significantly, which took not place in GPR18 deficient mice.

However, resolvin D2 (see Figure 11) is a chemical entity with poor stability. This has to be taken into account when working with this compound.[91]

Resolvin D2 was known before to be a lipid mediator produced by leukocytes to abolish inflammatory processes.[92] An involvement in wound healing, prevention of thrombosis, prevention of neuroinflammation e.g. Parkinson's disease[93] and revasculization processes after ischemic events were also proposed for the lipid.[94] It showed inhibition of TRPV1 and TRPA1 channels (IC_{50} = 0.1 nM and 2 nM, respectively), which could be blocked by PTX pretreatment. The authors therefore concluded the involvement of a GPCR.[95]
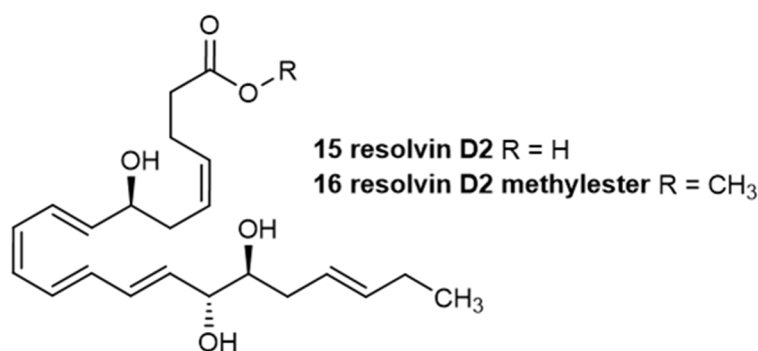
Figure 11: Chemical structure of resolvin D2

Two antagonists for GPR18 have been described so far. One of them was identified in extracts of a marine sponge. The diketopipierazine amauromine is not only a potent CB_1 receptor antagonist (with a K_i value of 0.178 µM), but also a GPR18 antagonist with potency in the low micromolar range.[96]

Another antagonist, **PSB-CB-5** (**17**), was obtained by optimization of a hit compound that was identified in a small screening campaign. Rempel *et al.* had screened compounds in β-arrestin assays (DiscoveRx) against 10 µM $Δ^9$-THC. They investigated preliminary structure-activity relationships of this compound class and described **PSB-CB-5** (**17)** as the first potent and select antagonist of GPR18. They also investigated the selectivity of the compound, which was found to be not active at the related GPR55. It showed no affinity to the CB_1, but a weak affinity to CB_2 with a K_i value of 4.03 µM, resulting a 14-fold selectivity for GPR18 versus CB_2.[66]

17 PSB-CB-5
GPR18 IC_{50} = **0.279** µM[66]
GPR55 IC_{50} = >10 µM[66]
hCB_1 K_i = >10 µM[66]
hCB_2 K_I = **4.03** µM[66]

18 Amauromine
GPR18 IC_{50} = **3.74** µM[96]
GPR55 IC_{50} = >10 µM[96]
hCB_1 K_i = **0.178** µM[96]
hCB_2 K_I = >10 µM[96]
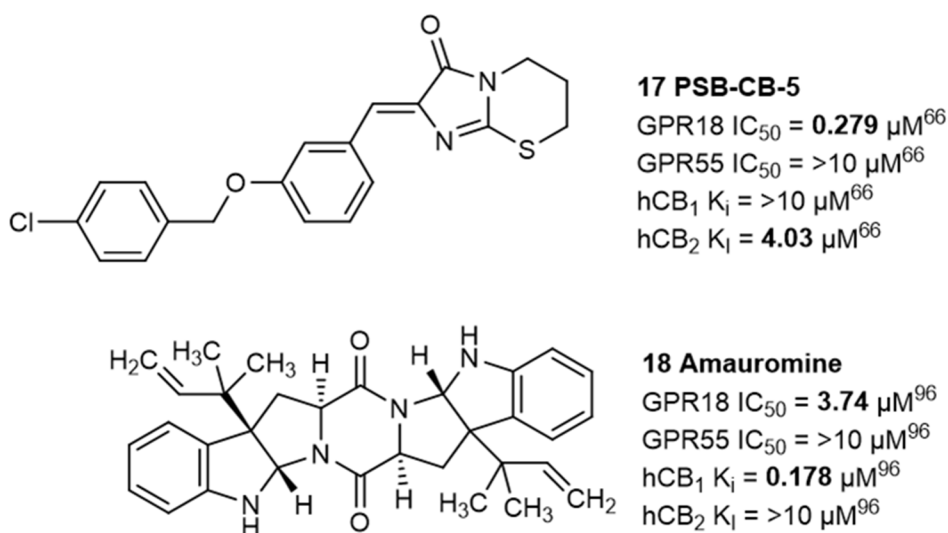
Figure 12: Chemical structures of GPR18 antagonists **PSB-CB-5** and amauromine

Possible therapeutic options of GPR18 have yet to be confirmed. But, as has been discussed above, its predominant involvement in inflammatory processes suggests a role in resolution of inflammation. Thus, by activating GPR18 in the case of an inflammatory disease, the progression of the process might be attenuated. Several groups have reported a GPR18 expression in M1 macrophages, which is linked

to inflammatory diseases, including neuroinflammatory diseases. However, the involvement of GPR18 in neuroinflammation and a possible advantage of GPR18 activation needs further confirmation.
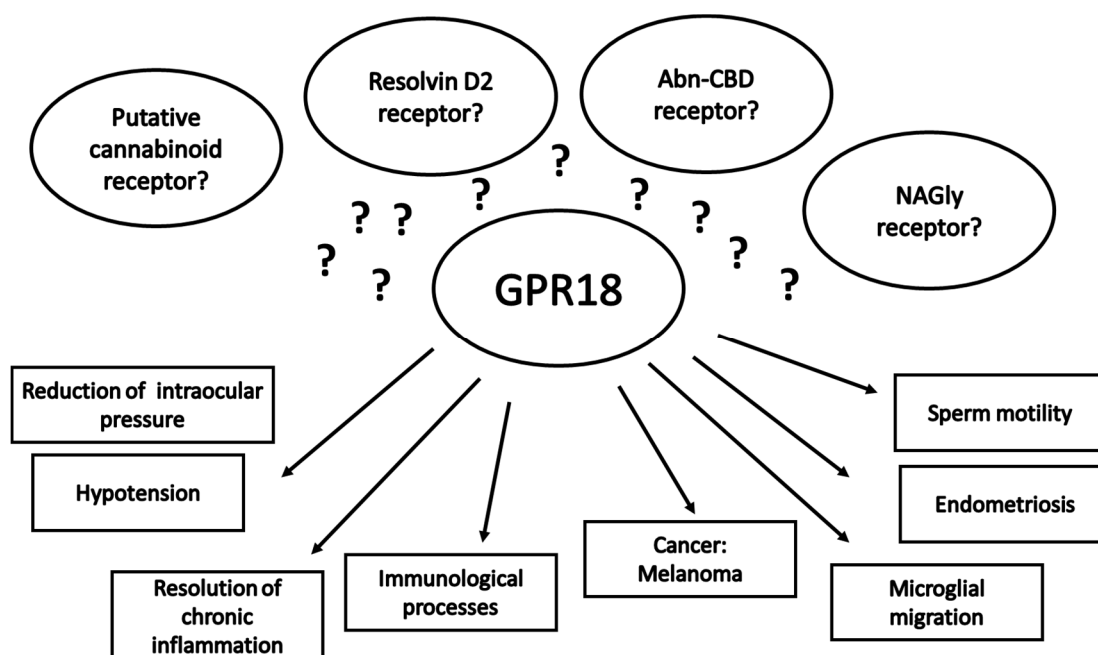
Figure 13: Possible physiological roles of GPR18

GPR18 has also been discussed in relation to cancer and migratory processes. Here, antagonizing the GPR18 activity would lead to the desired therapeutic effects.

Unfortunately, the uncertain situation on GPR18 agonists makes it very hard to rely on published results. Unselective compounds reduce the significance of a study. The inconsistent studies on the activation of GPR18 by NAGly complicate the evaluation of GPR18 effects. Whenever GPR18 pharmacology is studied the effects of the applied agonists or antagonists have to be characterized in detail. Therefore, selective and potent compounds, both agonists and antagonists are required to fully understand the role of GPR18 in physiology and disease.

1.4.2. GPR55

GPR55 was firstly identified in 1999 along with another orphan GPCR, GPR52. It was found to be highly expressed in the putamen and in the caudate nucleus.[98] From early on, it was suggested that GPR55 might be a receptor involved in the off-target effects of cannabinoids and discussed contradictorily.[99,100] Phylogenetically, it is closely related to the orphan GPCR GPR35, a receptor that has been proposed to interact with kynurenic acid and lysophosphatidic acid.[101]

In 2007, Oka *et al.* proposed an endogenous ligand for GPR55 distinct from the endogenous cannabinoids, also a fatty acid derivative.[102] The so-called lysophosphatidylinositol (LPI) consists of a

fatty acid that is linked to glycerol, which is esterified with a phosphate group. To the phosphate group inositol is bound The chemical description "lyso" means that one of the glycerol hydroxyl groups is unsubstituted, not esterified with a fatty acid. In nature, many different fatty acids can be bound to glycerol, and the type of fatty acid can determine the bioactivity. In a study by Oka *et al.*, LPI from soybeans was used and proved to elevate calcium transients in GPR55 transfected HEK cells but not in mock-transfected cells. Further, ERK phosphorylation was enhanced. Therefore, the authors concluded that LPI is a new ligand for GPR55.[102] Furthermore, they studied the exact species of LPI, since LPI can be regarded as a molecular mixture because of the different fatty acids potentially present. For example, soybean LPI mostly contains palmitoic acid (2-lyso-LPI). Oka *et al.* found in total 37.5 nmol/g LPI in rat brain tissue mostly stearic acid derivatives (2-lyso-LPI, 50.5 %) and furthermore arachidonic acid derivatives (1-lyso-LPI, 22.1%). The latter was found to be the most potent species to activate GPR55, namely 2-arachionoyl-glycero-phosphatidyl-inositol (2-AG-PI) with EC_{50} value of 30 nM in calcium mobilization assays. Therefore, they concluded that this might be the true endogenous ligand.[103,104]

However, also other endogenous substrates have been discussed to be the endogenous ligands for GPR55. Guy *et al.* reported lyso-phosphatidyl-β-D-glucoside to be released from glial cells to target GPR55, thereby directing the growth of nociceptive axons. This was found to be abolished in GPR55 knock-out mice.[105]
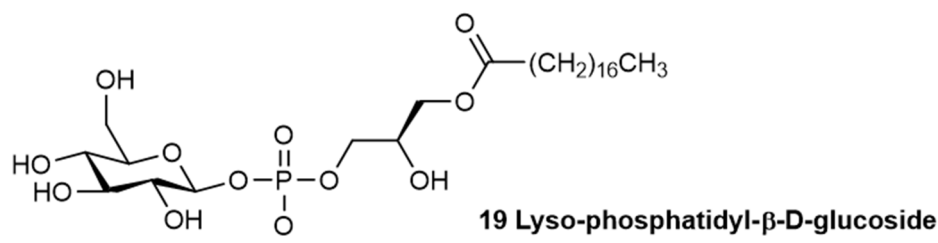
Figure 14: Chemical structure of lyso-phosphatidyl-β-D-glucoside

GPR55 was reported to signal via the $G_{\alpha 13}$ pathway by different independent groups.[106,107,108] The $G_{\alpha 13}$ pathway leads to oscillatory calcium transients and the activation of NFAT via RhoA (a small GTPase).[107]

20 2-AGPI

21 LPI
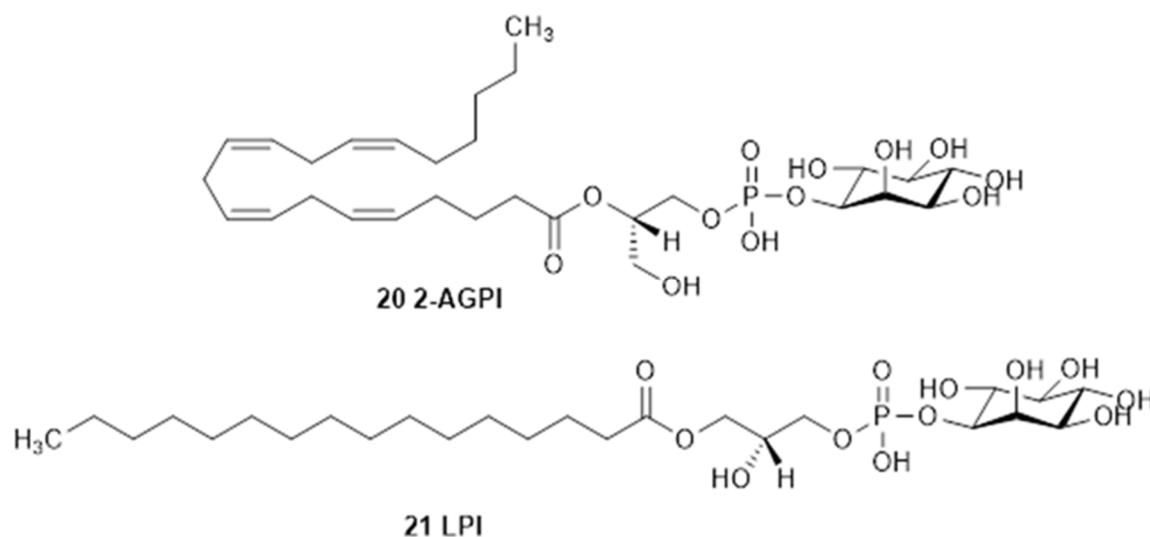
Figure 15: Chemical structures of 2-arachidonoyl-lysophosphatidyl-inositol (2-AGPI) and 1-Stearyl-2-lysophosphatidylinositol (LPI)

GPR55 was shown to be sensitive to abn-CBD, but reports on the potency differ largely.[109] Moreover, effects of abn-CBD still persisted in GPR55$^{-/}$ knock-out mice.[110]

GPR55 and the CB$_1$ have been reported to be co-expressed in some tissues. Kargl *et al*. investigated the possibility of the mutual effect of the receptors in HEK cells and found CB$_1$ co-expression to inhibit GPR55-induced activation of transcription factors such as NFκB and SRE. CB$_1$-induced effects were increased.[111] Similarly, CB$_1$ and GPR55 were shown to interact in the striatum, especially with regard to NFAT activation.[112] CB$_2$ receptors and GPR55 were also reported to form functional heteromers in cancer cells, for example, in a brain glioblastoma cell line. It was proposed that GPR55 activation silences CB$_2$ activation.[113] Functional cross-talk was also investigated in cells overexpressing both receptors, where GPR55 MAPK signaling was enhanced, and NFAT, NF-κB and cAMP response element activation was reduced in the presence of CB$_2$ receptors.[114]

Ryberg *et al*. reported very potent interactions of cannabinoids with GPR55 determined in [^{35}S]GTPγS assays.[106] However, many groups could not confirm similar potencies in their assay systems. In Table 3, some reported activities are shown exemplarily to demonstrate the diverse and controversial results of cannabinoid ligands at GPR55. Some groups tried to evaluate cannabinoid ligands in a special assay system to clarify the role of cannabinoids at GPR55. Anavi-Goffer *et al*. investigated cannabinoids in ERK-phosphorylation assays and postulated an allosteric mode of action for AM-251 and Δ^9-THC.[115] All groups observe an activation of GPR55 by LPI independent from the applied test system. However, the EC$_{50}$ values vary between the different test systems and research groups. Henstridge *et al*. investigated the activation of GPR55 by LPI in various test system, e.g. reporter-gene assays, phosphorylation of kinases and the label-free dynamic mass redistribution, and reported EC$_{50}$ values from about 10 nM to 1 μM.[116] Nevertheless, an activation of GPR55 by LPI was

always observable. Cannabinoids have also been investigated by other research groups. However, the results on the cannabinoids are very diverse and contradictory, ranging between nanomolar potencies and inactivity. Therefore, the effect of cannabinoids on GPR55 should always be studied, before applying them to pharmacological purposes, as they are no reliable tools. Different small molecule agonist and antagonist have been developed which are selective against the CB receptors. They will be introduced in the following.

Table 3: Reported effects of cannabinoids at GPR55

		EC_{50} or IC_{50}
1	AEA	**0.0183 µM** (agonist, GTPγS-assay[a])[106] **>30 µM** (no response, β-arrestin assay[b])[118], antagonist at 10 µM (β-arrestin assay[c])[119]
2	2-AG	**0.003 µM** (agonist, GTPγS-assay[a])[106] inactive at 5 µM (Ca^2 increase[d])[117] **>30 µM** (no response, β-arrestin assay[b])[118]
3	CP55,940	**0.005 µM** (agonist, GTPγS-assay[a])[106] inactive at 5 µM (Ca^2 increase[d])[117]; no response (ERK-phosphorylation[e])[115] **>30 µM** (no response, β-arrestin assay[b])[118],
4	Δ[9]-THC	**0.008 µM** (agonist, GTPγS-assay[a])[106] **>30 µM** (no response, β-arrestin assay[b])[118]
6	WIN55212,2	**>30 µM** (no response, GTPγS-assay[a])[106] inactive at 5 µM (Ca^2 increase[d])[117] **>30 µM** (no response, β-arrestin assay[b])[118]
7	Rimonabant	**3.9** µM (agonist, β-arrestin assay[b])[118], no response (ERK-phosphorylation[e])[115]
12	CBD	**0.445 µM** (antagonist, GTPγS-assay[a])[106] inactive at 3 µM (Ca^2 increase[d])[117] **>30 µM** (no response, β-arrestin assay[b])[118]
21	LPI	**1.2** µM (agonist, β-arrestin assay[b])[118] **0.045 µM** (agonist, Ca^{2+} oscillation[f])[107]; **1.10** µM (NFAT activation[g]), **0.074** µM (ERK-phosphorylation[g]), **0.093** µM CREB-phosphorylation[g]), **1.9** µM (NFκB activation[g]), **0.009** µM (dynamic mass redistribution[g])[116]

[a]membrane preparations of HEK cells, stably transfected with human GPR55
[b]U2OS cells, stably transfected with GPR55 and β-arrestin-2-GFP, redistribution of β-arrestin-2-GFP monitored imaged using a fluorescence microscope
[c]U2OS cells, stably transfected with GPR55 and β-arrestin-2-GFP, redistribution of β-arrestin-2-GFP monitored imaged using a fluorescence microscope
[d]CHO and HEK293 cells, stably transfected with GPR55
[e]HEK293 cells, stably expressing 3xHA-GPR55 were used
[f]HEK293 cells, stably expressing 3xHA-GPR55 were used
[g]HEK293 cells, stably transfected with 3xHA-GPR55 were used

The NIH Molecular Libraries Program initiated a screening campaign to identify small molecule ligands for GPR55. Agonists of three different scaffolds were found and investigated to study structure-activity relationships and selectivity (compound **22-24**, see Figure 16). They shared some features as the central amide bond.[120,121] LPI and these agonists were further docked into a homology model of

GPR55 to predict possible binding modes and involved amino acids. The authors proposed an inverted L-or T-shape of the agonists binding to the receptor with their long lipophilic residue pointing deep into the binding pocket, interacting phenylalanine residues providing a hydrophobic environment. The polar head group can be found close to the extracellular loops, filling the upper top of the binding pocket and interacting with K2.60, a lysine that forms ionic interaction with the phosphate group of LPI. The agonists (compound **22-24**) identified in the screening campaign mostly mimics this orientation.[122] Binding of compound **24** was investigated in mutagenesis studies and crucial residues were identified which interact both with LPI and also with compound **24** (chemical structure in Figure 16).[123] Another homology modeling approach came to the same observation regarding the residue K2.60.[124]

Partial agonists were described by Morales *et al*., who used a cell impedance assay to investigate a group of chromenopyrazoles (compound 26, Figure 16). They identified ligands with high potency, but moderate efficacy. The most potent ligand showed an EC_{50} value of 0.0004 µM and an efficacy of 51%. The selectivity profile was also investigated and the CB_2 receptor showed some affinity to the ligands.[125]

A screening approach of GlaxoSmithKline (GSK) identified compound **25** as agonist at GPR55 with an EC_{50} value of 0.631 µM. However, the compound was more potent at the glycine transporter 1 (GlyT1).[120] Yrjölä *et al.* developed biphenylic suolfonamides (compound **27** and **28**), which showed a very high potency. Their physicochemical properties however were not favorable.[126]

Although some agonists have been described for GPR55, no radioligand was developed until now. Some of the agonists were not potent enough and others were not selective. Further compound optimization is needed to obtain compounds with a high potency and suitable physicochemical properties.

22 ML-185 (CID 1374043)
GPR55: EC_{50}= **0.658** µM (β-arrestin, FRET)[119]
GPR35: EC_{50} > 32 µM (β-arrestin, FRET)[119]
CB_1 IC_{50} > 32 µM (β-arrestin, FRET)[119]
CB_2 IC_{50} > 32 µM (β-arrestin, FRET)[119]

23 ML-186 (CID 15945391)
GPR55: EC_{50}= **0.305** µM (β-arrestin, FRET)[119]
GPR35: EC_{50} > 32 µM (β-arrestin, FRET)[119]
CB_1 IC_{50} > 32 µM (β-arrestin, FRET)[119]
CB_2 IC_{50} > 32 µM (β-arrestin, FRET)[119]

24 ML-184 (CID 2440433)
GPR55: EC_{50}= **0.263** µM (β-arrestin, FRET)[119]
GPR35: EC_{50} > 32 µM (β-arrestin, FRET)[119]
CB_1 IC_{50} = **21.75** µM (β-arrestin, FRET)[119]
CB_2 IC_{50} = **15.1** µM (β-arrestin, FRET)[119]

25 GSK522373A
GPR55 EC_{50} = **0.631** µM (Yeast Exoglucanase assay)[126]
GlyT1 IC_{50} = **0.0794** µM (Scintillation proximity assay)[126]
CB1 EC_{50} = **>30** µM (Yeast Exoglucanase assay)[126]

26
GPR55 EC_{50} = **0.0004** µM (51% activation; HEK293[124]
cell impedance measurement, xCellLigaence)[124]
hCB_1 K_i > 40 µM (radioligand binding)[124]
hCB_2 K_i = **1.073** µM (radioligand binding)[124]

R =

27
GPR55 EC_{50} = **0.002** µM (HEK293, calcium mobilization
assays)[128]

R =

28
GPR55 EC_{50} = **0.002** µM (HEK293, calcium mobilization
assays)[128]

Figure 16: Chemical structures of synthetic GPR55 agonists

The NIH Molecular Libraries Program further identified and studied a group of antagonists (compound **29-31**, Figure 17). They share some structural properties with the agonists described above especially in shape. The highest potency displayed compound **29** (ML-193) with an IC_{50} value of 0.221

26

µM. The other antagonist were less potent.[127] Compound **30** was modified to study structure-activity relationships (Meza-Avina *et al.*) They tried different substitutions at the phenylcyclopropyl residue und observed slightly increased inhibitory activity when compared to the original *para*-methyl substitutions with *para*-chloro residues, up to an IC_{50} value of 0.64 µM (in β-arrestin assays). A pyridine ring instead of the phenyl ring at the oxadiazole core was also beneficial.[128]

Rempel *et al.* identified and optimized coumarine-derived compounds as GPR55 antagonist. The most potent antagonist was **PSB-SB-489** (**32**) with an IC_{50} of 0.113 µM, however, this compound was unselective against the CB receptors. The most selective antagonist of this series **PSB-SB-487** (**33**) showed an IC_{50} value of 1.77 µM.[129] GSK also identified an antagonist, which was investigated by Kargl *et al.* in various test system, where it showed potencies from 0.48 – 1.99 µM.[130]

Comparably to the agonists, a possible binding pose of GPR55 antagonists was investigated by Kotsikorou *et al.* They proposed antagonists to bind closer to the surface of the receptor than the typical L-shaped agonists, where they possibly stabilize the M3.36-F6.48 ionic lock with aromatic or heteroaryl residues.[131]

GPR55 antagonists described so far are not potent enough to be further developed as radioligand. Therefore, further compound optimization is needed to enhance potency and also optimize the physicochemical properties.

29 ML-193 (CID1261822)
GPR55 IC$_{50}$ = **0.221** µM (β-arrestin, FRET)[132]
CB$_1$ IC$_{50}$ = **24.6** µM (β-arrestin, FRET)[132]
CB$_2$ IC$_{50}$ > 32 µM (β-arrestin, FRET)[132]
GPR35 IC$_{50}$ > 32 µM (β-arrestin, FRET)[132]

30 ML-192 (CID1434953)
GPR55 IC$_{50}$ = **0.702** µM (β-arrestin, FRET)[132]
CB$_1$ IC$_{50}$ > 32 µM (β-arrestin, FRET)[132]
CB$_2$ IC$_{50}$ > 32 µM (β-arrestin, FRET)[132]
GPR35 IC$_{50}$ > 32 µM (β-arrestin, FRET)[132]

31 ML-191 (CID 23612552)
GPR55 IC$_{50}$ = **1.076** µM (β-arrestin, FRET)[132]
CB$_1$ IC$_{50}$ > **17.1** µM (β-arrestin, FRET)[132]
CB$_2$ IC$_{50}$ > 32 µM (β-arrestin, FRET)[132]
GPR35 IC$_{50}$ > 32 µM (β-arrestin, FRET)[132]

32 PSB-SB-489
GPR55 IC$_{50}$ = **0.113** µM (β-arrestin assay, CHO cells)[125]
GPR18 IC$_{50}$ = **12.5** µM (β-arrestin assay, CHO cells)[125]
hCB$_1$ K$_i$ = **1.17** µM (radioligand bindind)[125]
hCB$_2$ K$_i$ = **0.292** µM (radioligand bindind)[125]

33 PSB-SB-487
GPR55 IC$_{50}$ = **1.77** µM (β-arrestin assay, CHO cells)[125]
GPR18 IC$_{50}$ = **>10** µM (β-arrestin assay, CHO cells)[125]
hCB$_1$ K$_i$ = **>10** µM (radioligand binding)[125]
hCB$_2$ K$_i$ = **>10** µM (radioligand binding)[125]

34 AF060
GPR55 IC$_{50}$ = **3.25** µM (β-arrestin assay, CHO cells)[131]
CB$_1$ K$_i$ = **0.313** µM (radioligand binding)[131]
CB$_2$ K$_i$ = **0.281** µM (radioligand binding)[131]

35 CID16020046
GPR55 IC$_{50}$ = **0.48 - 1.99** µM
(Calcium mobilization, NFAT, SRE, NFκB activation)[147]

Figure 17: Chemical structures of synthetic GPR55 antagonists

1.4.2.1.   Therapeutic potential of GPR55

GPR55 mRNA levels were reported in small intestine, spleen, testis, thymus, brain and colon by Oka et al.[108] Broad expression of GPR55 in the brain has been reported. When investigating GPR55$^{-/-}$ knock-out mice for CNS performance, Wu et al. did not detect any prominent difference compared to wildtype littermates. When knock-out mice were challenged with complex motor coordinative tasks they performed worse, indicating a role of GPR55 in motor control.[134] As already mentioned above, GPR55 was also found to be involved in the axon growth of nociceptive neurons. The receptor was further described to be involved in the axon growth of retinal ganglionic cells guiding the growth of

axons. When blocked growth was attenuated, and could be rescued with LPI. Knockout mice were found to have smaller growth cones of the axons than wildtype mice.[135] Obara *et al.* found GPR55 but not CB receptors to be expressed in the PC-12 cell line, a model cell line for brain diseases. LPI induced retraction of neurites, but cannabinoids did not. GPR55-independent mechanisms of pain reduction have also been investigated and the direct activation of calcium^{2+}-channels was proposed.[136,137] In microglial cells the expression of GPR55 has been reported, where LPI treatment in the presence of interferon-γ induced ERK-phosphorylation.[138] LPI further showed neuroprotective effects by inducing microglial migration.[139]

These reports indicate a possible role of GPR55 in axon growth and sensation, especially in pain mediating neurons. GPR55 might therefore be an interesting target for neuropathic pain.[140,141] Its possible role in microglial cells, which control inflammatory processes in the brain, indicate GPR55 to be a possible target for neuroinflammation.

Andradas *et al.* found GPR55 expressed in several cancer cell lines, including breast cancer, pancreatic cancer, skin cancer and glioblastoma. The expression was correlated to cancer types with bad prognosis, late stage, and highly proliferative behavior mediated via ERK signaling.[142] It was also reported in ovarian and prostate cancer cells, where it also promoted proliferation. The authors proposed an autocrine stimulation of GPR55 by released LPI.[143] In glioblastoma, the high expression levels correlated well with bad prognosis.[144] This was also found for triple negative breast cancer cells, which showed more tendency to metastasis when associated with high GPR55 expression.[145] GPR55 was also detected in MDA-MB-231 breast cancer cell line, and evoked LPI-induced migration.[146] Kargl *et al.* investigated the inactivation of GPR55 by GPCR associated sorting protein 1 (GASP-1), which induces the internalization of GPR55 after prolonged agonist stimulation and could therefore be a target of interest for highly active GPR55.[147] They further found GPR55 involved in the migration of colon carcinoma cells and their ability to attach to endothelial cells. By blocking GPR55 with the antagonist **35**, the metastatic process could be attenuated.[148] The antagonism of GPR55 was therefore proposed for antitumor therapy.

GPR55 and the CB$_2$ receptor have been reported to be co-expressed in neutrophils. The receptors pathways interference lead to a GPR55 modulated CB2 response in the migration behavior of neutrophils.[149] Furthermore, GPR55 and CB$_1$ are also co-expressed in the rat brain.[112] This cross-talk might be used to circumvent CB receptor side-effects. We discussed above that new strategies are needed to address the CB receptors in therapy. GPR55 might be such a therapeutic options, when it fine-tunes CB receptor signaling, it might prevent undesired side-effects. However, the effects of GPR55 and CB$_1$ or CB$_2$ co-expression have to be described more in detail and the action of GPR55 agonists and antagonists with its effects on CB$_1$ and CB$_2$ signaling has further to be investigated.

By blocking GPR55 with the antagonist **35** in mice, inflammatory responses in colitis could be reduced. Especially, the recruitment of macrophages and lymphocytes was attenuated and led to reduced levels of inflammation markers. The authors proposed GPR55 to play a role in chronic bowel diseases.[150] This was corroborated by a study comparing different GPR55 expression levels in inflammatory bowel disease.[151]

GPR55 has been found to be augmented in obese and type 2 diabetic compared to non-obese subjects.[152] GPR55 agonists triggered insulin secretion.[153] The influence of GPR55 on calcium levels was investigated in myocytes, where it fine-tunes calcium response depending on the receptor localization.[154] In GPR55$^{-/}$ knock-out mice compared to wildtype mice, an age-related effect of GPR55 absence resulted in ventricular dysfunction.[155] GPR55$^{-/-}$ knock-out mice were further reported to show increased fat and insulin resistance, mainly accompanied with reduced physical activity, but not with an altered feeding behavior.[156] Another report of GPR55$^{-/-}$ knock-out mice showed an altered activity behavior during the night with an overall lower energy expenditure but no distinguishable other differences to wildtype mice.[157]

The CB$_2$ has already been mentioned in the context of osteoporosis. GPR55 was also found to be expressed in osteoclasts, a cell type that derives from macrophages. The proposed endogenous ligand LPI caused an inhibition of osteoclast formation, which did not occur in knock-out mice. Interestingly, the bone mass of male GPR55$^{-/-}$ mice was increased, whereas no difference could be observed in female knock-out mice.[158] GPR55-mediated effects should be further investigated to elucidate its role in bone homeostasis.

Since GPR55 triggers endothelial proliferation via *N*-arachidonoylserine, it was linked to wound healing.[159] The antagonist **35** was reported to inhibit LPI-induced endothelial wound healing.[130]

GPR55 has also been discussed as a candidate target to treat cannabinoid compound addiction.[160]

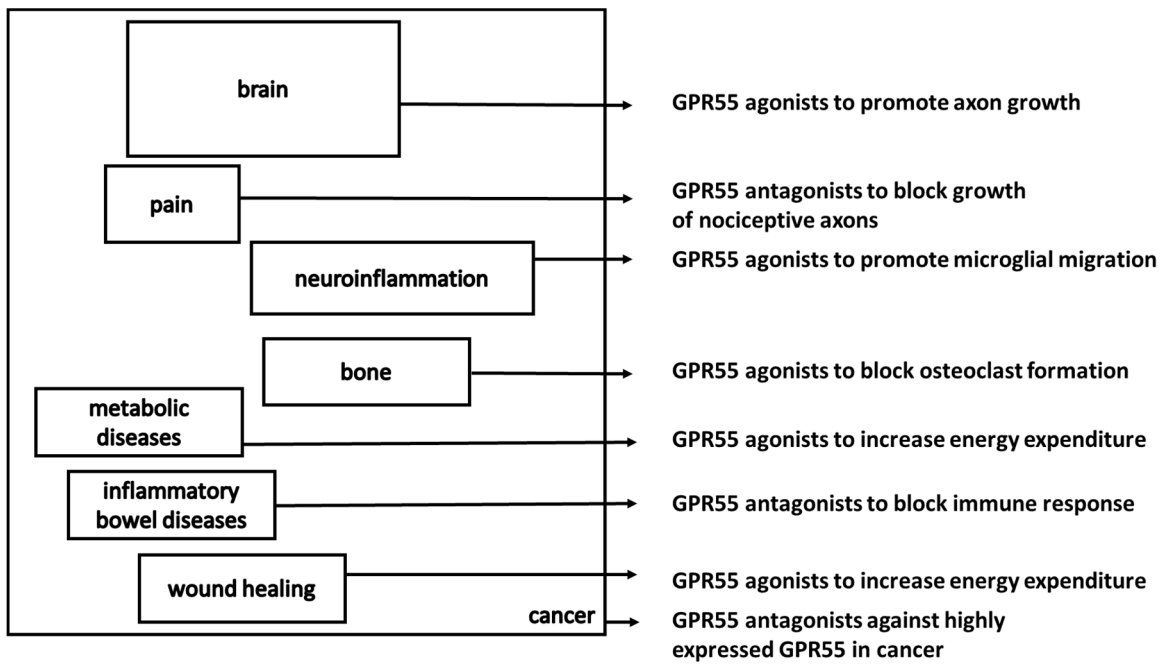Figure 18: Proposed effects of GPR55 agonists and antagonists

Altogether, GPR55 could be a target especially for cancer, where antagonists would be desirable. The reported effects of GPR55 in the central nervous system are of very great interest. However, the role of GPR55 in the brain needs further to be investigated, both the physiological as the immunological role. The results on bowel inflammation are very promising.

2. AIM OF THE STUDY

The involvement of a specific receptor in a disease can be investigated by its activation and inhibition and observing the resulting effects. To this end, potent and selective agonists and antagonists with suitable physicochemical properties are required as pharmacological tools.

GPCRs are the largest group of membrane proteins that represent important drug targets. However, there are still around 100 so-called orphan receptors for which the endogenous ligand is not known. The (patho)physiological characterization of these receptors and their validation as drug targets requires well-characterized tool compounds.

The aim of this study has been the development of tool compounds for the orphan GPCRs GPR18 and GPR55. In case of GPR18, the proposed endogenous agonist, *N*-arachidonoylgylcine (NAGly) has been controversially discussed and is questionable. Poorly characterized compounds limit the reliability of experiments. Therefore, we want to develop potent and selective tool compounds. Rempel *et al*. were already successful in developing the first potent and selective antagonist for GPR18, namely PSB-CB-5, an imidazothiazinone derivative. This compound class will be further studied and the structure-activity relationships will be extended. We further want to develop GPR18 agonists with suitable physicochemical properties. To achieve this, the compound library of the Pharma-Zentrum Bonn will be screened in β-arrestin recruitment assays. This compound library consists of different sublibraries, based on structural properties. This ensures a high hit rate upon screening a small number of appropriate compounds. The identification of hit compounds will be followed by a broad characterization. This includes determination of the dose-dependency of the observed effect, investigation of the compound's selectivity and specificity of the observed effect.

A further goal was to develop suitable GPR55 ligands. Therefore, we screened different libraries of the Pharma-Zentrum Bonn. The class of chromen-4-ones has already been described by our group as rather weak GPR55 antagonist. We now wanted to explore the structure-activity relationships of this compound class.

Fuchs *et al*. described biphenylic magnolol derivatives as potent CB receptor ligands. They also investigated them at orphan GPR55 and GPR18. Here, we wanted to expand the structure-activity relationships of this compound class.

In collaboration with the Institute of Forensic Medicine, we wanted to determine the CB receptor affinities of compounds described to be abused in incenses called 'Spice'. We further want to investigate these compounds as possible ligands of GPR18 and GPR55.

3. MEDICINAL CHEMISTRY OF GPR18 AGONISTS AND ANTAGONISTS

3.1. Cannabinoids and cannabinoid-like compounds

3.1.1. Introduction

Cannabinoid and cannabinoid-like compounds have been reported to interact with GPR18 and GPR55, although their effects have been controversially discussed (chapter 1.4.1 and 1.4.2). Here, we wanted to investigate the effects of selected cannabinoids in our established assay system.

Dr. Viktor Rempel established the β-arrestin recruitment system PathHunter™ from DiscoverX, Fremont, CA, USA, in our laboratory for GPR18 and GPR55. This test system is based on a fusion-protein technology, where the receptor of interest is fused to a small sequence of amino acids, which is part of the enzyme β-galactosidase. The major part of β-galactosidase is fused to β-arrestin 2, the most important internalization mediator for many GPCRs. The measurement of β-arrestin recruitment has the advantage of being G protein-independent, which is in this case favorable, as we do not know the explicit G protein through which GPR18 is signalling. G_i protein recruitment has been reported in the literature, but needs to be confirmed. For GPR55, the signaling through $G_{12/13}$ has been reported, which leads to activation of small GTPases as RhoA. This signal tranduction pathway can be measured by Western Blots or ELISA - methods that are not suitable to screen high numbers of compounds. Therefore, we will also use the β-arrestin technology, where we observed a stable response with an EC_{50} value of 1 μM for the reported endogenous agonist LPI.
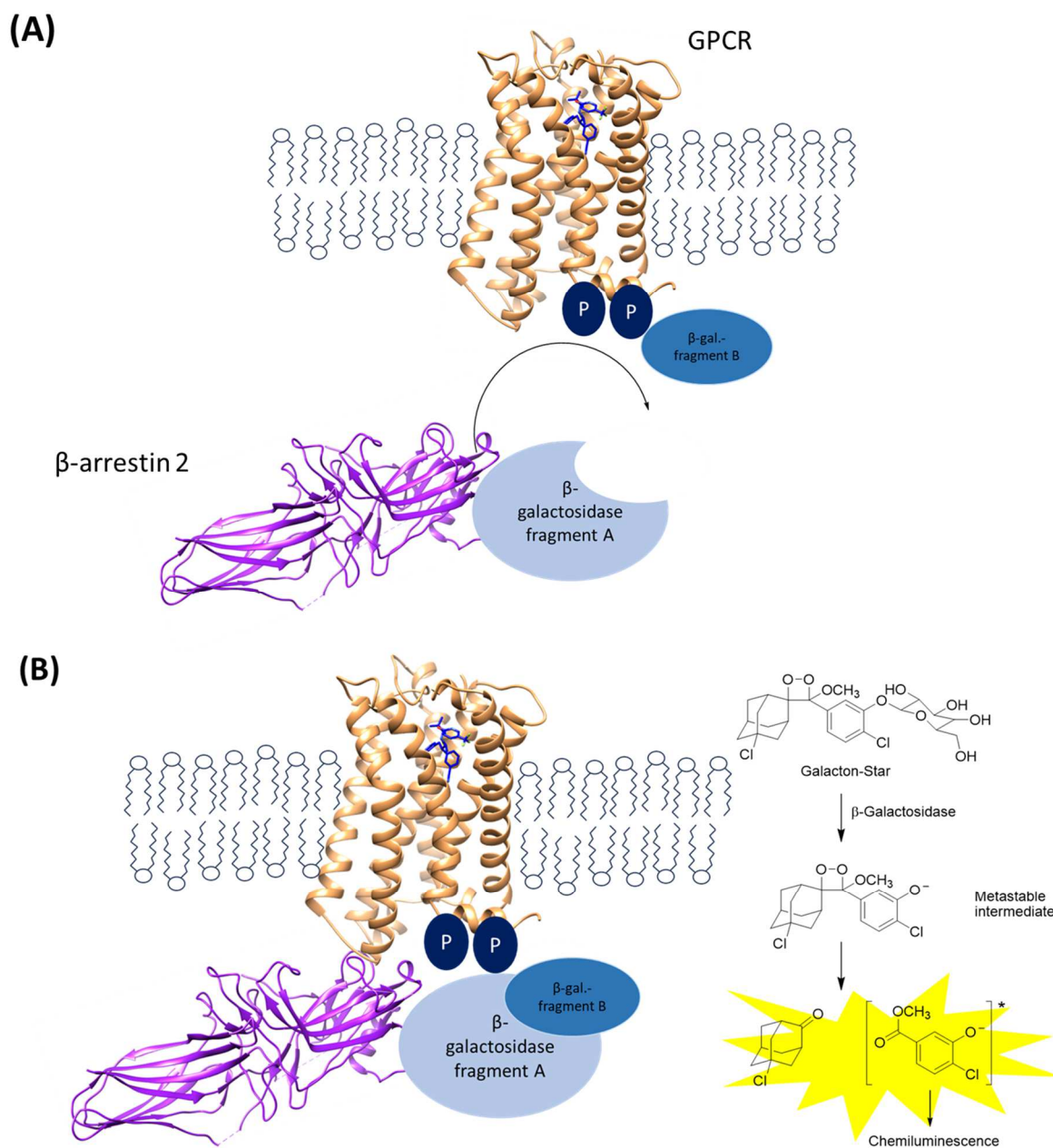
Figure 19: Schematic description of the PathHunter™ β-arrestin recruitment assay (DiscoverX, Fremont, CA, USA

Dr. Viktor Rempel investigated reported ligands for GPR18 and GPR55 in the β-arrestin test system and found NAGly to be inactive. However, he measured a signal for Δ[9]-THC, which was used as a standard agonist in this test system from then on. The activation of GPR18 by Δ[9]-THC can be seen in Figure 20, and could also be confirmed by Console-Bram *et al.*[87]
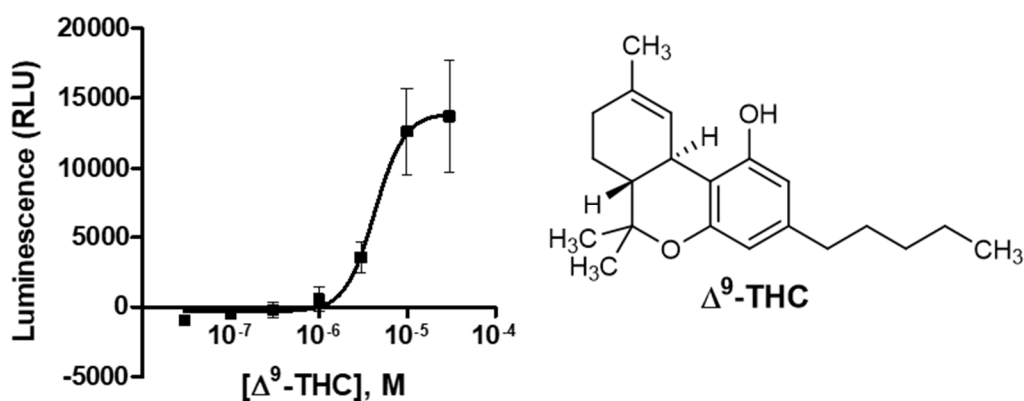
Figure 20: Activation of the human GPR18 in a β-arrestin recruitment assay by Δ^9-THC. Luminescence signal in relative luminescence units (RLU), results by Dr. Viktor Rempel[66]

Table 4: Potencies of Δ^9-THC and NAGly in β-arrestin recruitment assay, results by Dr. Viktor Rempel

		Human GPR18	Human GPR55
	Compound[a]	Agonistic activity	Antagonistic actvity
		$EC_{50} \pm$ SEM (µM)	$IC_{50} \pm$ SEM (µM)
4	Δ^9-THC	4.61 ± 0.50[66]	14.2 ± 5.2[66]
10	NAGly	>10 (15%)[66]	>10 (6%)[66]

[a] chemical structures in chapter 1.3.2 and 1.4.1

Here, additional cannabinoids that regularly have been reported in the context of either GPR18 or GPR55 will be investigated in β-arrestin recruitment assays, namely abn-CBD, CBD, O-1602 and O-1918. In addition, cAMP assays will be performed.

3.1.2. Results for atypical cannabinoids

The results for the atypical cannabinoids CBD, abn-CBD, O-1918 and O-1602 are shown in Table 5.

Table 5: Potencies of atypical cannabinoids in β-arrestin recruitment assays for GPR18 and GPR55

		Human GPR18		Human GPR55	
	Compd.[a]	Antagonistic activity	Agonistic actvity	Antagonistic activity	Agonistic actvity
		$IC_{50} \pm$ SEM (µM)	EC_{50} (µM)	$IC_{50} \pm$ SEM (µM)	EC_{50} (µM)
11	Abnormal cannabidiol (abn-CBD)	>10 (42 ± 7%)	> 10 (-50 ± 11%)	>10 (33 ± 8%)	>10 (-7%)
12	Cannabidiol (CBD)	> 10 (-41 ± 12%)	1.38 ± 0.20	10.7 ± 2.5	>10 (-4%)
13	O-1602	>10 (29 ± 3%)	>10 (7 ± 4%)	>10 (24%)	>10 (1%)
14	O-1918	>10 (16 ± 6%)	> 10 (12 ± 8%)	6.79 ± 0.98	>10 (-8%)

[a] chemical structure in Figure 10

CBD, which is structurally very similar to Δ^9-THC, activated GPR18 with a comparable EC_{50} value of **1.38** µM. The concentration-dependent activation is shown in Figure 21. It should be noted, that the last value of the curve was already lower than the previous value. This effect might be due to low solubility of this very lipophilic compound. Abn-CBD, which also had been reported to target GPR18, did not show any agonistic effect. The two atypical cannabinoids O-1918 and O-1602 were both inactive as agonists and as antagonists.
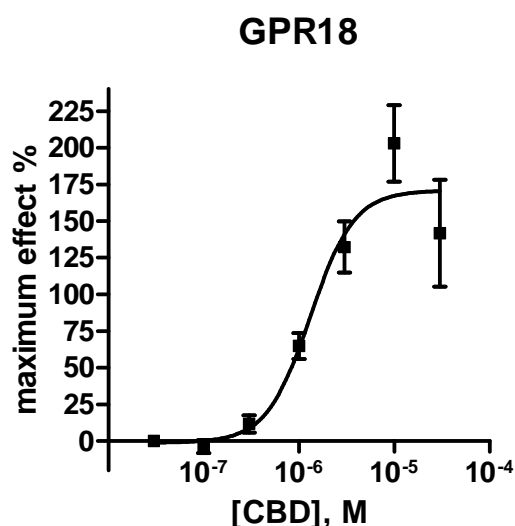

Figure 21: Activation of GPR18 by CBD; maximum effect corresponds to 10 µM Δ^9-THC = 100%

At GPR55 no agonistic activity could be observed for any of the compounds. However, two of them showed antagonistic activity. O-1918 displayed an IC_{50} value of **6.79** µM and CBD of **10.7** µM (see Figure 22).
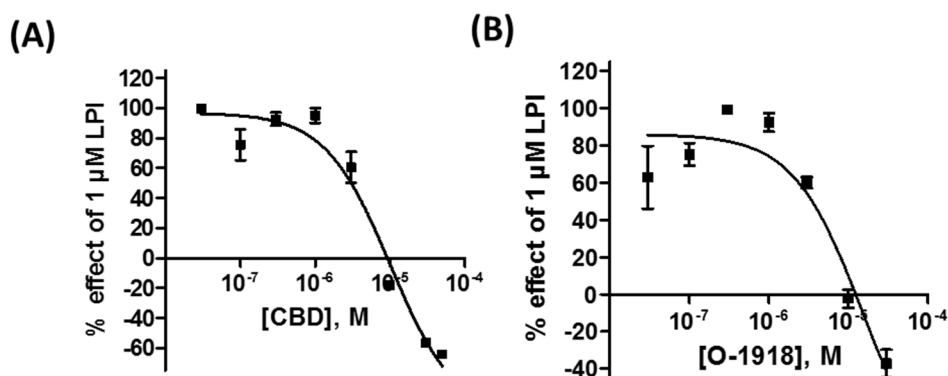

Figure 22: Inhibition of LPI 1 µM-induced β-arrestin signaling by CBD and O-1918

CBD has been proposed for the treatment of psychological disorders such as schizophrenia,[161] anxiety[162] and hypoxic-ischemic encephalopathy.[163] However, the site of action could not be identified. CBD has been reported to interact with a multitude of targets, as equilibrative nucleoside transporter

(ENT), GPR55, 5-HT$_{1a}$ receptor, α_3 and α_1 glycine receptor and TRPA1. In higher concentrations, it also should interact with PPAR-γ, TRPV1 and TRPV2 and inhibit FAAH. Further, it has been reported to act as an antioxidant.

O-1602 has been described as an agonist for GPR55. Peripherally applied to rats it reduced mechanically evoked pain stimuli. Furthermore, O-1602 and CBD were used to target GPR55 in rat intestine, where they reduced LPS-induced effects.[164] However, it was also reported that O-1602 displays anti-inflammatory effects independent of GPR55 and the cannabinoid receptors in colitis in mice.[165] It was further described to increase glucose tolerance via GPR55 in mice.[166] O-1602 also triggers feeding behavior and increased food intake but independent of GPR55.[167]

Here, we could show that the effects reported for the treatment with abn-CBD and O-1602 do not arise from GPR55-mediated β-arrestin signaling. We also did not observe a β-attestin-dependent effect of abn-CBD at GPR18, which was proposed to be the abnormal-cannabinol receptor. However, β-arrestin signaling is not the only signaling pathway that GPCRs address. An effect of one of these compounds could also be mediated via a β-arrestin-independent signaling pathway.

For O-1918 and CBD, we observed a weak inhibition of GPR55. However, these compounds have been reported to interact with many different targets. Although, they interact with LPI-induced β-arrestin signaling, they are no selective tools for GPR55 blockade.

CBD behaved as an agonist at GPR18. This is an interesting finding, as CBD has been reported as a weak/partial agonist at GPR18 before.[168] Its structural similarity to Δ^9-THC is high, therefore it might be assumed that these two compounds interact with the receptor in the same way. In the following experiments Δ^9-THC was used as a standard agonist for GPR18.

3.1.3. Results in cAMP accumulation assays for lipid cannabinoids and NAGly

We followed up on the results by Dr. Viktor Rempel, who studied NAGly and Δ^9-THC in β-arrestin recruitment at GPR18.[66] He did not observe any activating effect of NAGly on GPR18. He prepared a GPR18 expressing Chinese hamster ovary (CHO) cell line (CHO flip-in) and selected two clones. Here, we investigated the effect of NAGly or Δ^9-THC at 10 µM in cAMP accumulation assays. The results can be found in Figure 23. As a control, we also treated CHO K1 cells (lacking GPR18), and the previously used β-arrestin cell line.
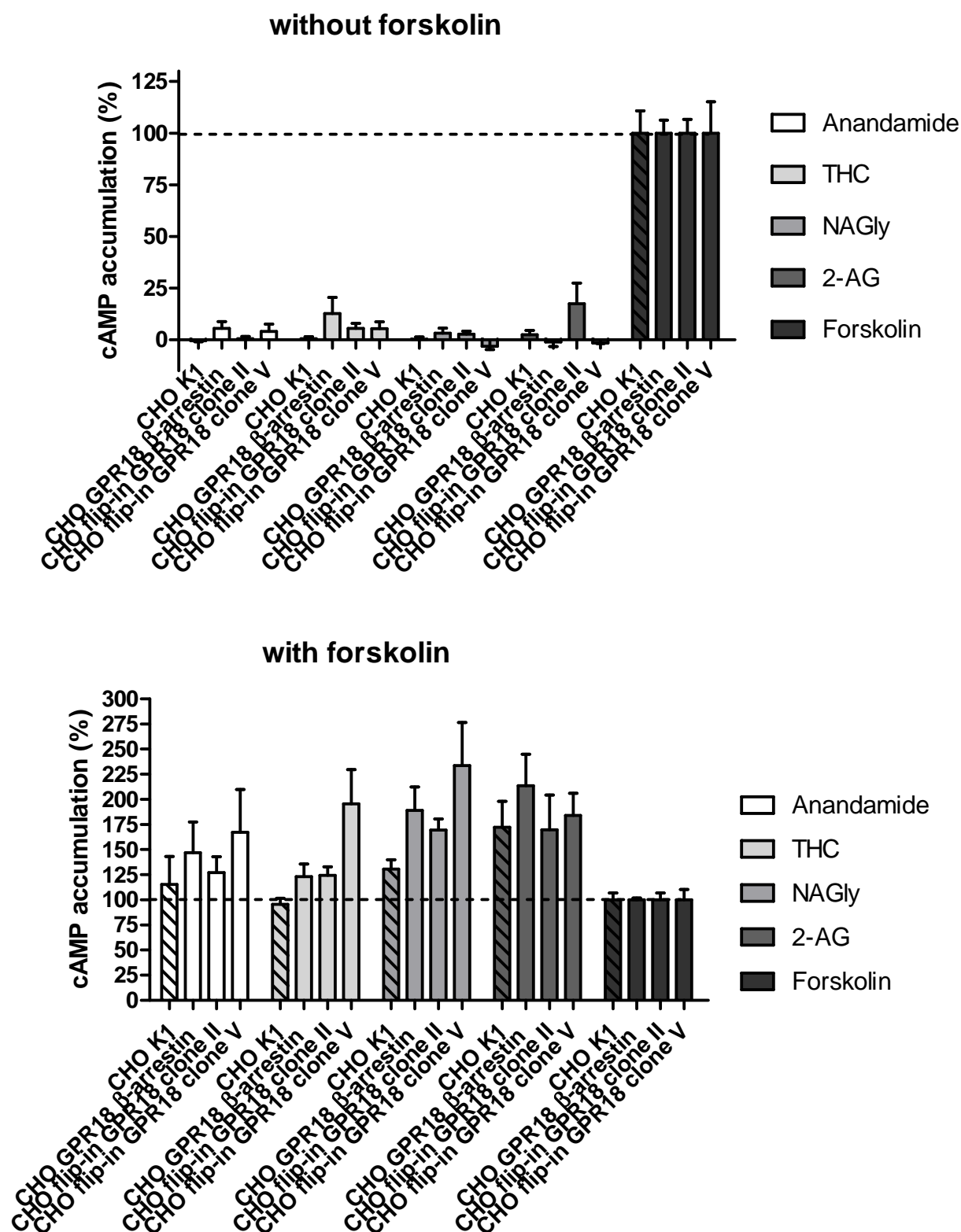
Figure 23: Results of cAMP accumulation assays in presence or absence of 10 µM forskolin, normalized to the forskolin response; compounds were applied in concentration of 10 µM

GPR18 has been reported to be G_i protein-coupled.[60] This means, an activation of GPR18 would result in the inhibition of adenylate cyclase and in a decrease in cAMP levels in the cell. The basal level

of cAMP in the cell is rather low, so it cannot always be measured with high confident. Therefore, the activation of G_i proteins is investigated in the presence of 10 µM forskolin, a compound that activates adenylate cyclase directly.

In Figure 23, the effect of the possible GPR18 ligands NAGly and Δ^9-THC and additionally that of anandamide and 2-AG are depicted. In the upper panal, no forskolin was applied. All compounds were unable to elevate cAMP levels in the cells. The effects have been compared to the activation by 10 µM forskolin which was set at 100%. In the lower panel, the effect of the applied compounds was measured in the presence of 10 µM forskolin. First of all it can be noted that no compound was able to result in a cAMP decrease, meaning that none of the compounds acted in a G_i dependent manner. Anandamide was not able to produce an effect in any of the cell lines. The same was true for 2-AG. Here, the effect in the untransfected CHO-K1 cells was similar as in the transfected cells. This led us conclude that whatever causes the increase in cAMP in the cells is GPR18 independent. Δ^9-THC caused an increase in cAMP predominantly in the CHO flip-in cells (clone V). Also, NAGly caused an increase in cAMP in both flip-in clones.

From these results, it can be concluded that the investigated compounds, especially NAGly and Δ^9-THC, do not cause a G_i protein dependent decrease in cAMP levels.

Whether the increase of cAMP is due to GPR18 further needs to be investigated.

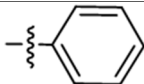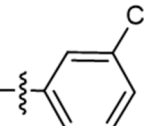## 3.2. Imidazothiazinones as GPR18 antagonists
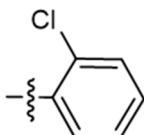
3.2.1. Introduction
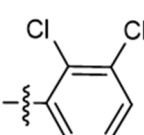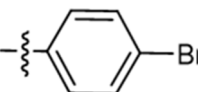
Rempel *et al.* discovered imidazothiazinones as antagonists of the orphan GPR18 by screening a compound library for antagonistic activity versus Δ^9-THC in a β-arrestin recruitment assay. They investigated the structure-activity relationships of this compound class and were able to identify some basic features required for GPR18 inhibition. Subsequently, they developed **PSB-CB-5** (**17**), the first potent and selective GPR18 antagonist, which was further characterized in this thesis.[66] The results presented in this chapter complete previous studies of this first class of GPR18 antagonists.

All investigated compounds were synthesized by the group of Professor Katarzyna Kiéc-Kononowicz in Cracow, Poland, and are part of the compound library of the PharmaZentrum Bonn (PZB).

Previous results for this compound class, which are necessary to understand the structure-activity relationships are as follows: The compounds can roughly be divided into two groups: (i) d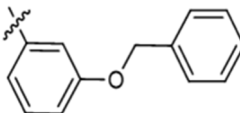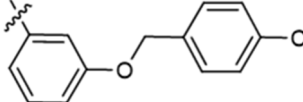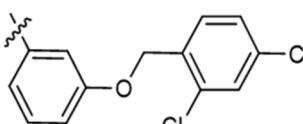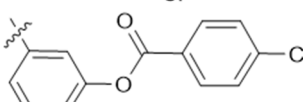erivatives with small substituents at the benzylidene residue and (ii) compounds with larger residues in *meta*-position. As can be seen in Table 6, **PSB-CB-5** (**17**) is the most potent GPR18 antagonist in this series with an IC_{50} value of **0.279** μM. It is a *para*-chlorobenzoyloxy-substituted derivative, one of the largest compounds in this set. The *o,p*-chloro-substituted compound **43** displayed a ten-fold weaker inhibition with an IC_{50} value of **2.55** μM. None of the compounds with smaller residues was able to inhibit GPR18 activation. To test selectivity using the same β-arrestin test system at a related receptor, potency at the orphan GPCR GPR55 was always determined in parallel. Interestingly, some rather small substituents such as chlorine at the benzylidene residue resulted in compounds that were able to inhibit GPR55 activation. However, only the *o*-chloro and the *o,m*-di-chloro benzylidene derivatives were antagonists, but not the *p*-chlorobenzylidene-substituted one. For compounds with larger substituents, e.g. the *p*-chlorobenzoyloxy derivatives of **PSB-CB-5** (**17**), no inhibition could be observed at GPR55. For some of the compounds, thiazepine analogues were obtained, the *p*-chlorobenzyloxy-substituted derivative **45** completely failed to inhibit GPR18 activation, showing that the size was crucial at least in this case. However, compound **43** and **48**, the latter being a thiazepine, showed almost no difference in potency. Interestingly, compound **45** turned out to be a GPR55 agonist of moderate potency with an EC_{50} value of **10.7** μM.[66]

As can be concluded, the structure-activity relationships for this compound class is still incomplete and more modifications are needed to further explore the interaction of imidazothiazinones both with GPR18 and GPR55. The antagonist **PSB-CB-5** (**17**) will be investigated to gain more insight in the functional profile of this compound.

Table 6: Potencies of chosen imidazothiazinones in β-arrestin assays for GPR18 and GPR55, data by Dr. Viktor Rempel[66]

			Human GPR18		Human GPR55	
No	Compd.	Chemical structure	Antagonistic activity IC$_{50}$ ± SEM (µM)	Agonistic actvity EC$_{50}$ (µM)	Antagonistic activity IC$_{50}$ ± SEM (µM)	Agonist activity EC$_{50}$ (µM)
Imidazo[2,1-*b*][1,3]thiazin-3-ones (A)						
36	ChM-13		>10 (5%)	>10 (7%)	>10 (25%)	>10 (32%)
37	B-54		>10 (18%)	>10 (13%)	>10 (35%)	>10 (-33%)
38	ChM-6		>10 (14%)	>10 (-2%)	>10 (42%)	>10 (9%)
39	ChM-1		>10 (6%)	>10 (20%)	**5.09** ± 0.35	>10 (27%)
40	ChM-40		>10 (0%)	>10 (17%)	**6.91** ± 1.04	>10 (3%)
41	ChM-3		>10 (13%)	>10 (-20%)	>10 (16%)	>10 (26%)
42	CB-3		**7.22** ± 3.42	>10 (-4%)	>10 (0%)	>10 (37%)
17	**CB-5** (PSB-CB-5)		**0.279** ± 0.111	>10 (-27%)	>10 (0%)	>10 (21%)
43	CB-4		**2.55** ± 0.71	>10 (-23%)	>10 (0%)	>10 (12%)
44	CB-1		>10 (14%)	>10 (0%)	>10 (16%)	>10 (31%)

Imidazo[2,1-*b*][1,3]thiazepin-3-ones (B)						
45	ChM-72		>10 (32%)	>10 (-3%)	-	**10.7** ± 0.3
46	CB-8		>10 (15%)	>10 (-6%)	>10 (27%)	~10 (52%)
47	CB-9		**6.48** ± 1.20	>10 (-19%)	>10 (43%)	>10 (7%)
48	ChM-73		**4.61** ± 2.36	>10 (-32%)	>10 (33%)	>10 (16%)
Imidazo[2,1-*b*][1,3]thiazin-2-ones (D)						
49	ChM-44		>10 (2%)	>10 (9%)	>10 (0%)	~10 (59%)

3.2.2. Pharmacological evaluation of PSB-CB-5

The concentration-dependent inhibition of GPR18 by **PSB-CB-5** (**17**) determined in a β-arrestin assay is shown in Figure 24. The inhibition of the Δ^9-THC-induced signal reached only up to 60%. Therefore, **PSB-CB-5** (**17**) can be regarded as a partial antagonist versus Δ^9-THC. **PSB-CB-5** (**17**) was also administered in a fixed concentration of 3 µM to different concentrations of Δ^9-THC, showing a rightward shift of the activation curve (experiments by Viktor Rempel).[66] This may indicate a competitive mechanism of inhibition at the binding site.
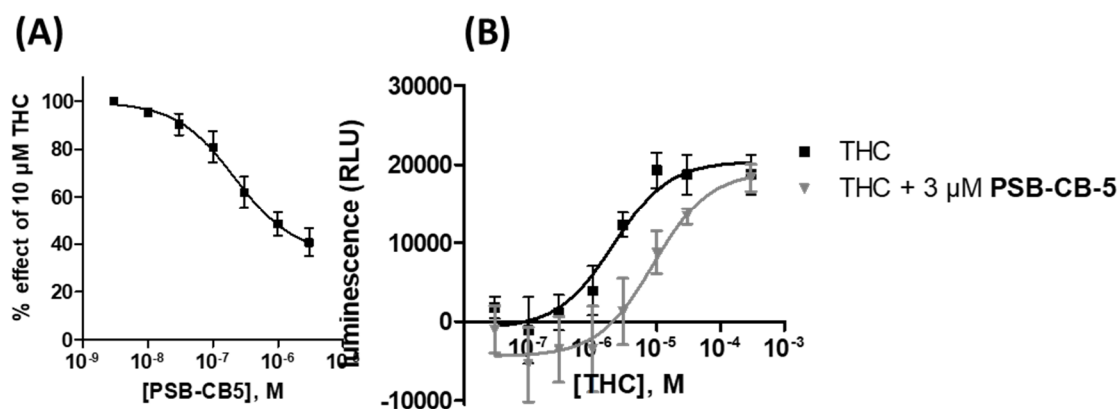

Figure 24: Inhibition of β-arrestin recruitment of human GPR18 by **PSB-CB-5** (**17**) (n = 3)

From the results in 3.1.2, we know that Δ^9-THC does not generate the expected signal in cAMP assays in our test system. To get an idea if or how **PSB-CB-5** (**17**) acts in cAMP assays it was administered with or without 10 µM of forskolin. The results are shown in Figure 25.
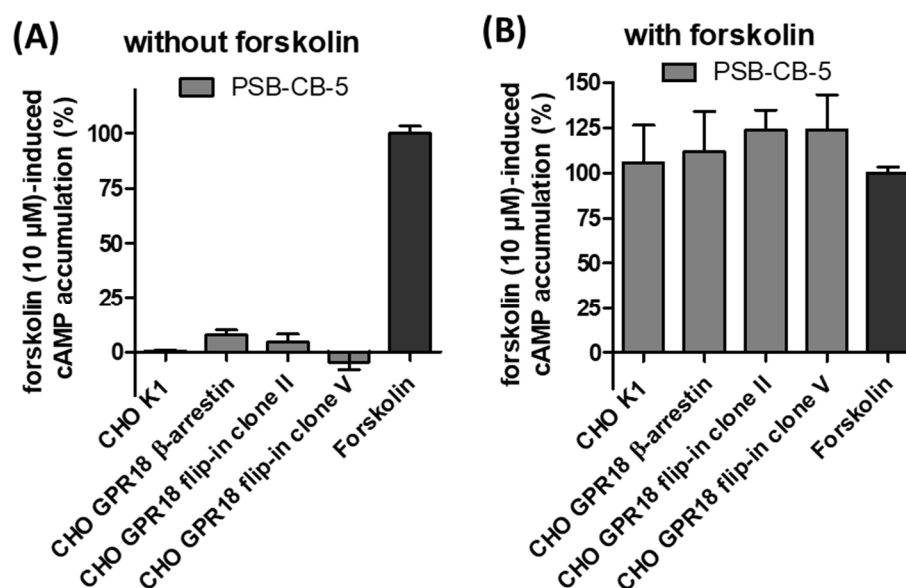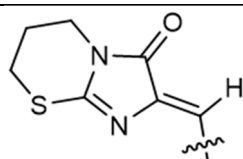

Figure 25: Effects of **PSB-CB-5** (**17**) on cAMP accumulation, in the presence or absence of forskolin in different cell lines stably expressing GPR18

In the absence of forskolin, no cAMP was produced by 10 µM **PSB-CB-5** (**17**). In the presence of forskolin, the cAMP level stayed the same compared to a forskolin control. Therefore, it can be concluded that as expected **PSB-CB-5** (**17**) does not act as an agonist in a G_s or G_i protein-dependent manner at GPR18.

So far, no GPR18 agonist has been identified that activates G_i or G_s. Therefore, **PSB-CB-5** (**17**) cannot be evaluated as an antagonist in cAMP assays.
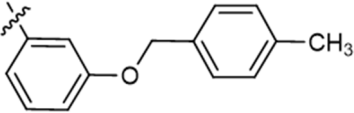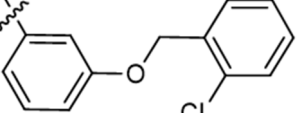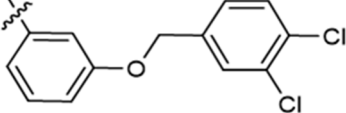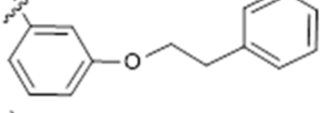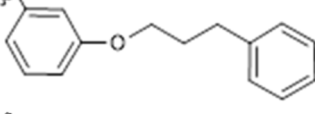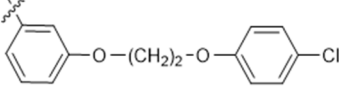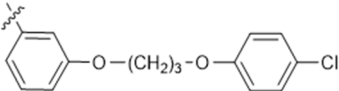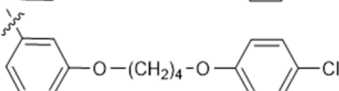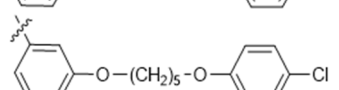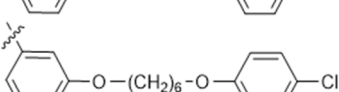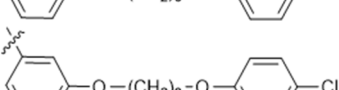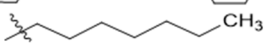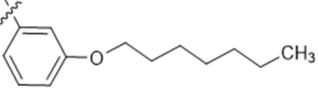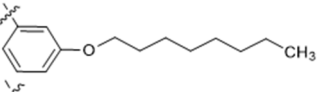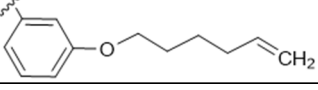
3.2.3. Results for imidazothiazinones in β-arrestin assays

Further compounds of this series were investigated in β-arrestin assays to establish comprehensive structure-activity relationships. All compounds were synthesized by the group of Prof. Kiéc-Kononowicz. Both, the smaller ligands for GPR55 and the larger GPR18 ligands were further modified to systematically analyze the structure-activity relationships. In Table 7, Table 8 and Table 9, the potencies of these compounds are collected. Compounds in Table 7 belong to the class of imidazothiazin-3-ones (group A), which had been proven to be active (see 3.2.1).

Table 7: Potencies of imidazothiazinones at human GPR18 and GPR55 in β-arrestin assays

A

No.	Compd.	Chemical structure					Human GPR18		Human GPR55	
							Antagonistic activity $IC_{50} \pm$ SEM (μM)	Agonistic actvity EC_{50} (μM)	Antagonistic activity $IC_{50} \pm$ SEM (μM)	Agonist activity EC_{50} (μM)

Imidazo[2,1-*b*][1,3]thiazin-3-ones (group A)

No.	Compd.	R^1	R^2	R^3	R^4	R^5	Antagonistic activity $IC_{50} \pm$ SEM (μM)	Agonistic actvity EC_{50} (μM)	Antagonistic activity $IC_{50} \pm$ SEM (μM)	Agonist activity EC_{50} (μM)
50	CB-11	F	H	H	H	H	>10 (17%)	>10 (6%)	**5.56** ± 1.10	>10 (0%)
51	CB-37	Br	H	H	H	H	>10 (12%)	>10 (-2%)	**17.7** ± 6.1	>10 (-6%)
52	CB-41	OH	H	H	H	H	>10 (33%)	>10 (-17%)	>10 (30%)	>10 (-24%)
53	CB-36	CH₃	H	H	H	H	>10 (8%)	>10 (0%)	>10 (39%)	>10 (-5%)
54	CB-39	H	H	F	H	H	>10 (12%)	>10 (12%)	>10 (9%)	>10 (-5%)
55	CB-38	H	H	CH₃	H	H	>10 (15%)	>10 (13%)	>10 (29%)	>10 (-1%)
56	CB-13	F	F	H	H	H	>10 (3%)	>10 (4%)	**3.15** ± 0.20	>10 (0%)
57	CB-46	CH₃	CH₃	H	H	H	>10 (16%)	>10 (-1%)	**20.6** ± 5.8	>10 (-20%)
58	CB-17	OCH₃	OCH₃	H	H	H	>10 (10%)	>10 (10%)	**16.4** ± 5.8	>10 (0%)
59	CB-14	F	H	F	H	H	>10 (6%)	>10 (11%)	**3.46** ± 1.34	>10 (0%)
60	CB-16	Cl	H	Cl	H	H	>10 (14%)	>10 (0%)	**6.76** ± 1.37	>10 (0%)
61	CB-42	Br	H	Br	H	H	>10 (26%)	>10 (16%)	>10 (24%)	>10 (-11%)
62	CB-44	OH	H	OH	H	H	>10 (2%)	>10 (30%)	**11.8** ± 1.8	>10 (-33%)
63	CB-45	CH₃	H	CH₃	H	H	>10 (15%)	>10 (7%)	**2.93** ± 0.30	>10 (-14%)
64	CB-18	Cl	H	H	H	Cl	>10 (0%)	>10 (12%)	>10 (0%)	>10 (15%)
65	CB-43	H	Br	Br	H	H	>10 (17%)	>10 (22%)	>10 (4%)	>10 (-15%)
66	CB-34B	H	OH	OH	H	H	>10 (39%)	>10 (-4%)	**11.0** ± 0.5	>10 (-44%)
67	CB-34A						>10 (21%)	>10 (3%)	>10 (19%)	>10 (-3%)
68	CB-21						>10 (3%)	>10 (6%)	**4.22** ± 1.66	>10 (-30%)
69	CB-20						**1.73** ± 0.371	>10 -9%)	**45.8** ± 21.0	>10 (-19%)

#	Code	Structure				
70	CB-22	(3-position ether, CH₃-substituted benzyl)	**3.59** ± 2.25	>10 (2%)	**9.45** ± 3.71	>10 (-31%)
71	CB-15	(benzyl ether, Cl ortho)	**1.65** ± 0.45	>10 (8%)	>10 (4%)	>10 (10%)
72	CB-19	(benzyl ether, 2× Cl)	**6.16** ± 2.86	>10 (0%)	**11.8** ± 2.1	>10 (4%)
73	CB-23	(phenethyl ether)	>10 (16%)	>10 (8%)	**29.3** ± 13.9	>10 (-42%)
74	CB-24	(phenylpropyl ether)	**1.49** ± 0.387	>10 (-30%)	**6.04** ± 1.62	>10 (-49%)
75	CB-30	O–(CH₂)₂–O–C₆H₄–Cl	**5.00** ± 0.392	>10 (-10%)	**10.1** ± 2.4	>10 (-20%)
76	CB-25	O–(CH₂)₃–O–C₆H₄–Cl	**3.25** ± 1.22	>10 (-16%)	>10 (38%)	>10 (-36%)
77	CB-28	O–(CH₂)₄–O–C₆H₄–Cl	**2.38** ± 1.15	>10 (-16%)	>10 (26%)	>10 (11%)
78	CB-26	O–(CH₂)₅–O–C₆H₄–Cl	**1.14** ± 0.44	>10 (-38%)	**3.77** ± 0.23	>10 (-21%)
79	CB-27	O–(CH₂)₆–O–C₆H₄–Cl	**0.650** ± 0.134	>10 (-37%)	>10 (37%)	>10 (-15%)
80	CB-29	O–(CH₂)₈–O–C₆H₄–Cl	**1.15** ± 0.17	>10 (-25%)	>10 (43%)	>10 (-18%)
81	CB-47A	(alkyl chain, CH₃)	>10 (8%)	>10 (4%)	>10 (44%)	>10 (-14%)
82	CB-48	(O-alkyl chain, CH₃)	>10 (42%)	>10 (21%)	**10.4** ± 2.4	>10 (-8%)
83	CB-55	(O-alkyl chain, CH₃)	**8.63** ± 3.03	>10 (-27%)	**3.70** ± 1.02	>10 (7%)
84	CB-56	(O-alkenyl chain, CH₂)	>10 (33%)	>10 (-9%)	**12.8** ± 3.5	>10 (9%)

[a] Percent inhibition of agonist-induced luminescence signal (GPR18: 10 µM THC; GPR55: 1 µM LPI)
[b] Percent activation compared to agonist-induced luminescence signal (GPR18: 10 µM THC; GPR55: 1 µM LPI)

The GPR55 inhibitors **39** (IC$_{50}$ = **5.09** µM) and **40** (IC$_{50}$ = **6.91** µM) were both chloro-substituted compounds, the first one in the *ortho*-position the latter one in the *ortho-* and *meta*-position of the benzylidene residue. This type of compound was further investigated. The corresponding *ortho-fluoro*-substituted compound **50** showed a quite similar potency as compound **39** with an IC$_{50}$ value of **5.56** µM.

When this substituent was changed to bromo, the potency decreased ((compound **51**: IC_{50} value of **17.7** µM). The *ortho-*,*meta*-difluoro derivative **56** showed a slightly increased potency in comparison to the *ortho-*,*meta*-dichloro-analogue **40** with an IC_{50} value of **3.15** µM. When substituting with di-methyl or di-methoxy residues, the potency decreased. Additionally, the *ortho-*,*para*-difluoro compound **59** showed an IC_{50} value of **3.46** µM, which was in the same range as that of the *ortho-*,*meta*-di-substituted compound **29**. This can also be observed for the corresponding di-chloro-derivatives (compare compound **40** and **60**). The *ortho-*,*para*-dibromo-substituted compound **61** was inactive **61**, as also the hydroxyl-substituted derivative **62**. Interestingly, the *ortho-*,*para*-dimethyl derivative **63** was slightly more active with an IC_{50} value of **2.93** µM. This compound was the most potent compound at GPR55 of the whole series. None of the compounds showed any inhibitory or activating properties at GPR18 up to a concentration of 10 µM. It appears that GPR55 requires compounds with an *ortho*-substitution with a small lipophilic residue as such fluorine or chlorine. Compounds that are only substituted in the *meta-* or *para*-position were not inhibiting GPR55 (e.g. compound **38**, **37** and **54**). None of the compounds showed any activation of GPR55.

Based on the structural properties of the potent and selective GPR18 antagonist **PSB-CB-5** (**17**), further derivatives were synthesized and investigated. **PSB-CB-5** (**17**) itself has a *para*-chlorobenzyloxy residue in the *meta*-position of the benzylidene residue. The corresponding fluorinated compound **68** showed no inhibitory potency at GPR18, but the brominated compound **69** displayed an IC_{50} value of **1.73** µM. The inhibition of Δ^9-THC-induced β-arrestin recruitment by **PSB-CB-5** (**17**) was incomplete and reached only 60% (compare Figure 24 (A)). It can therefore be regarded as a partial antagonist versus Δ^9-THC. However, compound **69** showed a complete inhibition of the signal and acted as a full antagonist. A comparable inhibitory potency was shown by compound **71**, which has a chlorine atom in the *ortho*-position of the benzyloxy residue. The di-chlorinated compound **72** (in the *para-* and *meta*-position) and the methylated compound **70** both showed lower potency, with IC_{50} values of **6.16** µM and **3.59** µM, respectively. The phenylpropyloxy residue of compound **74** led to an IC_{50} value of **1.49** µM. However, the phenylethyloxy derivative **46** was without any activity up to a concentration of 10 µM. A series of phenyloxyalkyloxy-substituted compounds was investigated. The length of the alkyl linker was varied from ethyl to hexyl and octyl. The results for these series of compounds are displayed in Figure 26.
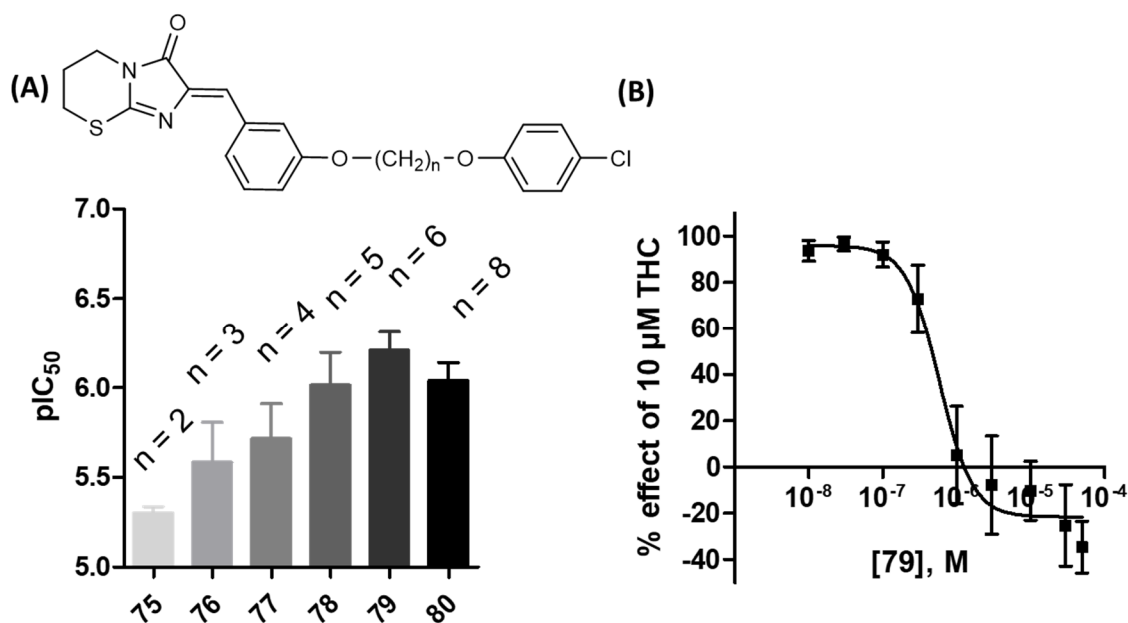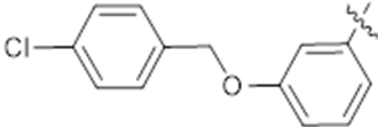
Figure 26: Influence of the methylene chain length of the phenyloxyalkyloxy derivatives on GPR18 inhibitory potency
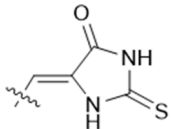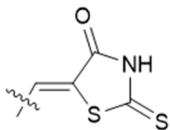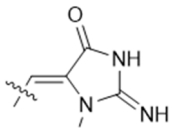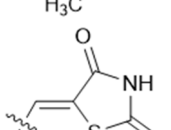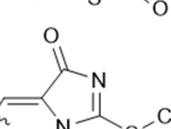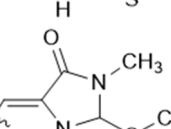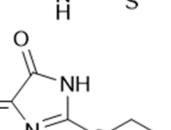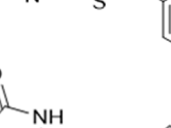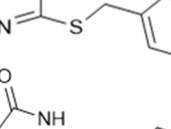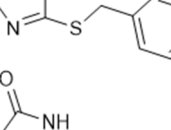
With six methylene groups in the phenyloxyalkyloxy residue and an IC_{50} value of **0.650** µM, compound **79** was the most potent antagonist of this small series of compounds. It is not as potent as the already described compound **PSB-CB-5** (**17**), but as can be seen in Figure 26 (B) the compound showed full inhibition of the Δ^9-THC-induced effect and can be regarded as full antagonist at GPR18, while **PSB-CB-5** (**17**) displayed a maximal effect of only 60%. The compounds with eight or five methylene groups were slightly less potent with potencies of around 1 µM. When the alkyl chain length decreased also the activity decreased. Compound **75** (n = 2) showed weak inhibitory potency at GPR55 with an IC_{50} value of **10.1** µM. Compound **78** (n = 5), which was relatively potent at GPR18 (IC_{50} value of **1.14** µM) showed also moderate inhibitory potency at GPR55 (IC_{50} value of **3.77** µM). There appears to be no clear structural dependency for a compound's activity at GPR55, yet.

Some compounds with alkyl residues instead of the aromatic residue have been investigated. Only the octyloxy derivative **83** led to potency at GPR18 with an IC_{50} value of **8.63** µM. All other aliphatic substitutions were unbeneficial for GPR18 affinity. In contrast, most of them showed at least moderate potency at GPR55.

Instead of varying the benzylidene residue, the imidazothiazinone can be exchanged for different heterocycles, thereby expanding or contradicting the sulfur-containing ring. Furthermore, the importance of the thiazine residue was to be monitored by deleting and exchanging it. The results of these modifications are shown in Table 8.

Table 8: Potencies for oxosulfanylimidazoles as GPR18 and GPR55 antagonists

No.	Compd.	Chemical structure	Human GPR18		Human GPR55	
			Antagonistic activity	Agonistic actvity	Antagonistic activity	Agonist activity
			IC$_{50}$ ± SEM (µM)[a]	EC$_{50}$ (µM)[b]	IC$_{50}$ ± SEM (µM)[a]	EC$_{50}$ (µM)[b]
Imidazo[2,1-*b*][1,3]thiazin-3-ones (A)						
85	CB-59		**33.0** ± 7.8	>10 (-14%)	**32.4** ± 15.2	>10 (5%)
86	CB-61		>10 (22%)	>10 (-38%)	>10 (-18%)	>10 (29%)
87	CB-62		>10 (4%)	>10 (6%)	>10 (-5%)	>10 (22%)
88	CB-63		>10 (-10%)	>10 (-1%)	>10 (-1%)	>10 (22%)
89	CB-60		**13.8** ± 5.4	>10 (31%)	>10 (47%)	>10 (18%)
90	CB-66		>10 (23%)	>10 (-2%)	>10 (35%)	>10 (-2%)
91	CB-70		>10 (3%)	>10 (-17%)	>10 (17%)	>10 (21%)
92	CB-74		>10 (27%)	>10 (23%)	>10 (44%)	>10 (-21%)
93	CB-76		>10 (35%)	>10 (5%)	>10 (41%)	>10 (-10%)
94	CB-71		**2.29** ± 0.72 (max. inhibition: **44**%)	>10 (-11%)	>10 (36%)	>10 (13%)

95	CB-75		>10 (0%)	>10 (4%)	>10 (48%)	>10 (-12%)
96	CB-77		>10 (17%)	>10 (7%)	>10 (33%)	>10 (20%)
97	CB-78		**4.78 ± 1.82**	>10 (2%)	>10 (27%)	>10 (21%)
98	CB-72-1,2		>10 (25%)	>10 (13%)	>10 (19%)	>10 (2%)
99	CB-72-2,3		>10 (40%)	>10 (1%)	>10 (42%)	>10 (-3%)

[a] % inhibition of standard agonist-induced luminescence signal (GPR18: 10 µM Δ^9-THC; GPR55: 1 µM LPI)
[b] % activation compared to standard agonist-induced luminescence signal (GPR18: 10 µM Δ^9-THC; GPR55: 1 µM LPI)

Only two compounds of this set showed an IC_{50} value below 10 µM. These two compounds were **97** (with an IC_{50} value of **4.78** µM and **94** (with an IC_{50} value of **2.29** µM, maximum inhibition: 44%). Both compounds shared a structural feature: an imidazole ring, substituted with a *para*-bromo-benzylthioether (**94**) or a phenylpropylthioether (**97**). There were some compounds, which were also substituted with a benzylthioether, but they were not active at all (for example, compound **92**, **95**, **93**). Compound **94** with its *para*-bromo-benzyl residue had one of the largest lipophilic residue and the lipophilic residue of compound **97** was even larger. It appears to be that the lipophilic bulky residue is necessary for GPR18 inhibition.

The contraction of the heterocyclic system was not successful; none of the compounds with an imidazole was active. The only active compounds **94** and **97** have large lipophilic residues. None of the compounds showed activity at GPR55.

PSB-CB-5 (**17**) contains a *meta*-benzyloxy-residue. A small set of *para*-substituted compounds were synthesized and evaluated, as can be seen in Table 9.

Table 9: Potencies of imidazothiazinones with *para*-orientated benzylidene-residue, results for GPR18 and GPR55

No.	Compd.	Chemical structure	human GPR18		human GPR55	
			antagonistic activity	agonistic actvity	antagonistic activity	agonist activity
			$IC_{50} \pm SEM$ (μM)	EC_{50} (μM)	$IC_{50} \pm SEM$ (μM)	EC_{50} (μM)
Imidazo[2,1-*b*][1,3]thiazin-3-ones (A)						
100	CB-10		**22.2 ± 8.6**	>10 (-12%)	**2.23 ± 0.30**	>10 (-12%)
101	CB-57		>10 (17%)	>10 (18%)	**27.4 ± 11.0**[a]	>10 (11%)
102	CB-12		>10 (48%)	>10 (-5%)	>10 (28%)	>10 (-11%)
103	CB-58		>10 (6%)	>10 (-3%)	>10 (12%)	>10 (8%)
104	CB-84		>10 (34%)	>10 (8%)	>10 (39%)	>10 (-12%)
105	CB-83		>10 (29%)	>10 (18%)	**12.2 ± 4.2**	>10 (-40%)
106	CB-64		>10 (17%)	>10 (-5%)	>10 (25%)	>10 (9%)
107	CB-33		>10 (-5%)	>10 (15%)	>10 (-3%)	>10 (13%)
108	CB-31		>10 (17%)	>10 (10%)	>10 (-25%)	>10 (9%)

109	CB-32		>10 (7%)	>10 (15%)	>10 (-5%)	>10 (12%)
110	CB-65		>10 (16%)	>10 (31%)	>10 (33%)	>10 (-11%)
111	CB-73		>10 (31%)	>10 (2%)	>10 (49%)	>10 (-12%)
112	CB-69		>10 (12%)	>10 (16%)	>10 (13%)	>10 (-1%)
113	CB-35		>10 (13%)	>10 (3%)	>10 (18%)	>10 (-3%)
114	CB-68		>10 (38%)	>10 (22%)	>10 (26%)	>10 (2%)
115	CB-40		>10 (27%)	>10 (9%)	>10 (30%)	>10 (-10%)
Imidazo[2,1-*b*][1,3]thiazepin-3-ones (B)						
116	CB-67		>10 (-14%)	>10 (2%)	>10 (-23%)	>10 (30%)
Imidazo[2,1-*b*][1,3]oxazin-3-ones (C)						
117	CB-80		>10 (8%)	>10 (2%)	**9.09 ± 3.40**[c]	>10 (-10%)
118	CB-86		>10 (-10%)	>10 (11%)	>10 (38%)	>10 (13%)
Imidazo[2,1-*b*][1,3]thiazin-2-ones (D)						
119	CB-47B		>10 (4%)	>10 (6%)	>10 (46%)	>10 (-7%)

[a] % inhibition of standard agonist-induced luminescence signal (GPR18: 10 µM Δ^9-THC; GPR55: 1 µM LPI)

[b] % activation compared to standard agonist-induced luminescence signal (GPR18: 10 µM Δ^9-THC; GPR55: 1 µM LPI)

[c] extrapolated value

The *para*-substituted analogue of **PSB-CB-5** (**17**), compound **100**, was the only compound of this series that showed inhibitory potency for the human GPR18, but with an IC$_{50}$ value of **22.2** µM it is 80-fold weaker as compred to **PSB-CB-5** (**17**). Interestingly, it displayed a higher inhibition for GPR55, which is typically not inhibited by these larger residues. With an IC$_{50}$ value of **2.23** µM, it was ten-fold more active at the human GPR55 than at GPR18. Further compounds of this group were tested and some also showed weak inhibitory potency for GPR55, but compound (**100**) was by far the most potent compound. None of the compounds were active at GPR18.

Altogether, three very different substitution patterns have been evaluated at GPR18 and GPR55. The first hits were further investigated by introducing different substituents in different positions at

the benzylidene residue, and also by replacing the imidazothiazinones by different heterocycles. The results of this study are summarized in Figure 27.
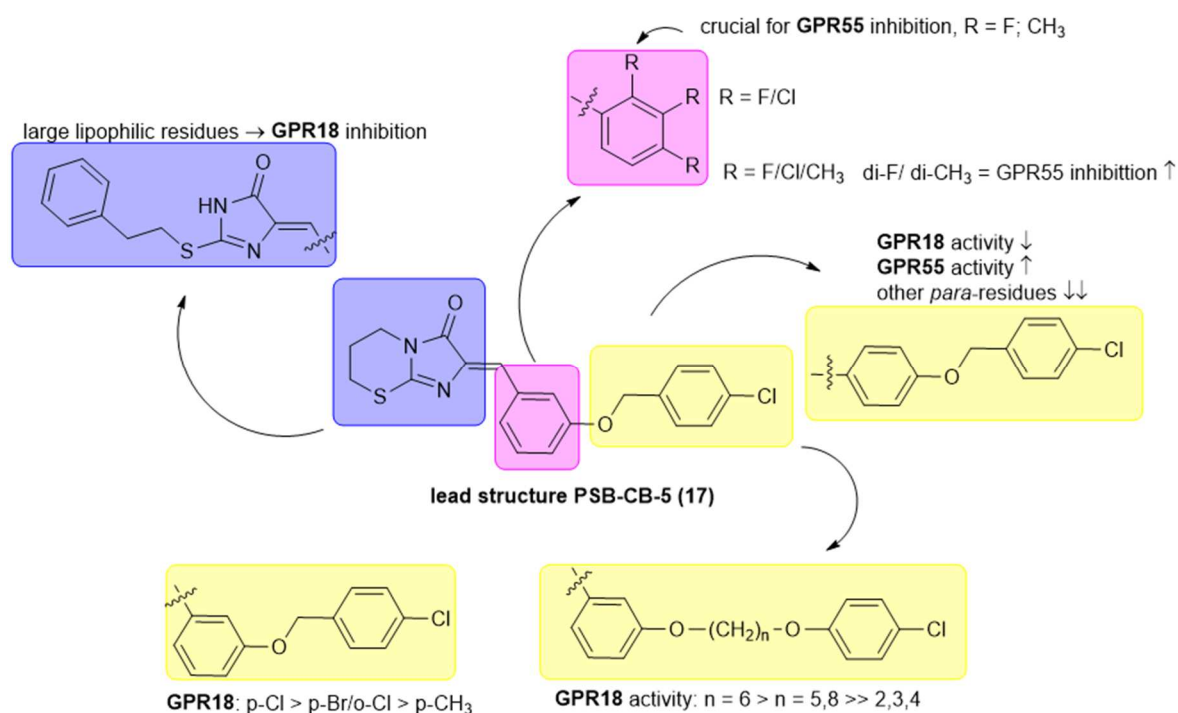
Figure 27: Structure-activity relationships of imidazothiazinones as GPR18 and GPR55 antagonists

PSB-CB-5 (**17**) was the most potent compound of this series with an IC_{50} value of **0.279** μM, but it showed only a partial inhibition of the Δ^9-THC-induced signal. Compound **79** was shown to inhibit the Δ^9-THC-induced signal completely, but displayed a higher IC_{50} value of **0.650** μM. For GPR55 inhibtion, very small residues at the benzylidene residue were crucial, especially, an *ortho*-halogen or *ortho*-methyl residue, which can be combined with a *para*-halogen or a methyl group. The most potent GPR55 antagonist so far was compound **63** with an IC_{50} value of **2.93** μM, but did not show any inhibition of GPR18 up to 10 μM.

The structure-activity relationships of this compound class have been studied extensively at GPR18 and GPR55. 68 new compounds have been investigated and described in this study. **PSB-CB-5** (**17**) is still the most potent GPR18 antagonist.

3.2.4. Selectivity of imidazothiazinones versus cannabinoid receptors

The selectivity of GPR18 and GPR55 antagonists versus both cannabinoid receptors is of major importance. Cannabinoid receptors and orphan GPR18 share the ability to interact with similar ligands. For this study, a binding assay employing the tritiated radioligand CP55,940 was used. CP55,940 is an

agonist ligand of high affinity for both cannabinoid receptors, and therefore a suitable tool to test binding affinity for comparison.

Table 10: Affinities of imidazothiazinones for CB_1 and CB_2 cannabinoid receptor determined in radioligand binding assays versus [^{3}H]CP55,940 (for chemical structures view Table 7, Table 8, and Table 9)

		Radioligandbinding	
No.	Compd.[b]	Human CB$_1$ K_i (µM) vs. [^{3}H]CP55,940 (% inhibition of specific binding)	Human CB$_2$ K_i (µM) vs. [^{3}H]CP55,940 (% inhibition of specific binding)
36	ChM-13[a]	>10 (40%)	>10 (18%)
37	B-54[a]	>10 (25%)	>10 (23%)
38	ChM-6[a]	>10 (30%)	>10 (2%)
39	ChM-1[a]	>10 (0%)	>10 (21%)
40	ChM-40[a]	>10 (12%)	>10 (40%)
41	ChM-3[a]	>10 (29%)	>10 (8%)
42	CB-3[a]	>10 (25%)	**1.11 ± 0.01**
17	**PSB-CB-5**[a]	>10 (0%)	**4.03 ± 0.51**
43	CB-4[a]	**2.09 ± 0.08**	**0.950 ± 0.269**
44	CB-1[a]	>10 (12%)	>10 (0%)
45	ChM-72[a]	**0.251 ± 0.064**	**4.15 ± 0.39**
46	CB-8[a]	**2.16 ± 0.07**	>10 (37%)
47	CB-9[a]	**2.29 ± 0.46**	**0.98 ± 0.23**
48	ChM-73[a]	**3.18 ± 0.49**	**1.65 ± 0.71**
49	ChM-44[a]	>10 (26%)	>10 (19%)
50	CB-11	>10 (13%)	>10 (0%)
51	CB-37	>10 (-16%)	>10 (10%)
52	CB-41	>10 (2%)	> 10 (17%)
53	CB-36	>10 (2%)	>10 (11%)
54	CB-39	>10 (-25%)	>10 (10%)
55	CB-38	>10 (-6%)	>10 (32%)
56	CB-13	>10 (13%)	>10 (0%)
57	CB-46	>10 (-13%)	>10 (25%)
58	CB-17	>10 (18%)	>10 (15%)
59	CB-14	>10 (13%)	>10 (0%)
60	CB-16	>10 (8%)	>10 (24%)
61	CB-42	>10 (7%)	>10 (18%)
62	CB-44	>10 (5%)	>10 (12%)
63	CB-45	>10 (7%)	>10 (-6%)
64	CB-18	>10 (14%)	>10 (4%)
65	CB-43	>10 (35%)	>10 (22%)
66	CB-34B	>10 (13%)	>10 (20%)
67	CB-34A	>10 (11%)	>10 (38%)
68	CB-21	>10 (35%)	>10 (46%)
69	CB-20	>10 (4%)	>10 (4%)
70	CB-22	>10 (22%)	>10 (25%)
71	CB-15	>10 (0%)	>10 (9%)
72	CB-19	>10 (15%)	>10 (0%)
73	CB-23	>10 (24%)	>10 (19%)
74	CB-24	>10 (11%)	>10 (23%)
75	CB-30	>10 (21%)	>10 (-9%)

76	CB-25	>10 (18%)	>10 (-2%)
77	CB-28	>10 (-19%)	>10 (3%)
78	CB-26	>10 (8%)	>10 (-11%)
79	CB-27	>10 (-14%)	>10 (12%)
80	CB-29	>10 (-9%)	>10 (-3%)
81	CB-47A	>10 (32%)	>10 (34%)
82	CB-48	>10 (33%)	>10 (34%)
83	CB-55	>10 (8%)	>10 (19%)
84	CB-56	**2.48** ± 0.27 max. inhibition of radioligand-binding: **75%**	**1.91** ±0.55 max. inhibition of radioligand-binding: **69%**
85	CB-59	>10 (30%)	>10 (19%)
86	CB-61	>10 (47%)	>10 (26%)
87	CB-62	>10 (43%)	**22.8** ± 4.0
88	CB-63	**5.04** ± 1.09 max. inhibition of radioligand-binding: **67%**	>10 (41%)
89	CB-60	**2.21** ± 0.57	**0.591** ±0.031 max. inhibition of radioligand-binding: **73%**
90	CB-66	>10 (19%)	>10 (24%)
91	CB-70	>10 (11%)	>10 (46%)
92	CB-74	>10 (42%)	>10 (19%)
93	CB-76	>10 (36%)	>10 (30%)
94	CB-71	>10 (31%)	>10 (36%)
95	CB-75	>10 (38%)	>10 (22%)
96	CB-77	>10 (15%)	>10 (25%)
97	CB-78	>10 (18%)	>10 (33%)
98	CB-72-1,2	**1.67** ± 0.84 max. inhibition of radioligand-binding: **60%**	>10 (41%)
99	CB-72-2,3	>10 (18%)	>10 (28%)
100	CB-10	>10 (40%)	>10 (12%)
101	CB-57	>10 (21%)	>10 (-11%)
102	CB-12	>10 (-4%)	>10 (-17%)
103	CB-58	>10 (19%)	>10 (20%)
104	CB-84	>10 (33%)	>10 (45%)
105	CB-83	>10 (33%)	**0.668** ± 0.253 max. inhibition of radioligand-binding: (63%)
106	CB-64	>10 (44%)	**0.202** ± 0.086 max. inhibition of radioligand-binding: **69%**
107	CB-33	>10 (35%)	>10 (40%)
108	CB-31	>10 (36%)	> 10 (30%)
109	CB-32	>10 (37%)	> 10 (30%)
110	CB-65	>10 (31%)	**0.853** ± 0.358 max. inhibition of radioligand-binding: (76%)
111	CB-73	>10 (38%)	>10 (46%)
112	CB-69	>10 (49%)	**0.942** ± 0.628
113	CB-35	>10 (36%)	>10 (18%)
114	CB-68	>10 (23%)	>10 (34%)

115	CB-40	>10 (3%)	>10 (22%)
116	CB-67	**2.55 ± 0.22** max. inhibition of radioligand-binding: **62%**	>10 (46%)
117	CB-80	**1.54 ± 0.51** max. inhibition of radioligand-binding: **75%**	>10 (47%)
118	CB-86	>10 (36%)	>10 (45%)
119	CB-47B	>10 (34%)	>10 (44%)

[a] data determined by Dr. Viktor Rempel[66]

[b] for chemical structures see Table 6, Table 7, Table 8 and Table 9

PSB-CB-5 (**17**), the hit compound for GPR18 inhibition, showed a K_i value of **4.03** µM for the CB_2 receptor. This correlates to a 14-fold selectivity for GPR18 over CB_2. Compound **43**, which is also a quite potent GPR18 antagonist, showed a K_i value of **2.09** µM for CB_1 and a K_i value of **0.95** µM for CB_2. These two examples indicate that the selectivity of this compound class needs to be optimized.

To understand the binding behavior of this class of compound completely, all compounds have been evaluated. Compound **106** showed the highest affinity for CB_2 with a K_i value of **0.202** µM but only a partial inhibition of radioligand binding (69%). It is one of the compounds, which have a *para*-substituted benzylidene residue, and were therefore not active at GPR18. Compound **45** showed the highest affinity for CB_1 with a K_i value of **0.251** µM. It is the only GPR55 agonistic compound of this series with an EC_{50} value of **10.2** µM. Four other *para*-substituted compounds (**110**, **112**, **116** and **117**) showed K_i values in the low micromolar or submicromalor range for the CB_2 receptor and two further at the CB_1 receptor. In the group of compounds with different heterocycles linked to the benzylidene residue only compounds **89** and **88** showed some affinity to the CB receptors. They were not active at GPR18 or GPR55. The phenyloxyalkyloxy compound group that was discussed above does not show any affinity to one of the receptors.

In summary, it can be concluded that most of the compounds are selective versus both CB receptors. Only very few compounds show an affinity to one or both CB receptors. The most potent GPR18 antagonist **PSB-CB-5** (**17**) shows a 14-fold selectivity versus CB_2 and no affinity up to concentrations of 10 µM for the CB_1 receptor. Nevertheless, the selectivity should be optimized. Structural features, which led to for CB receptor binding, were especially the thiazepine ring together with the *meta-* or *para-* substituted benzylidene ring. Here bulky, lipophilic residues were preferred, as the *p*-chlorobenzyloxy substituent of compound **45** and **PSB-CB-5** (**17**). However, the *p*-bromobenzyloxy residue was not active. The structure-activity relationships were summarized in Figure 28.

thiazepin: CB_1, CB_2 ↑
thiazin: CB_2
oxysulfanylimidazol: CB_1, CB_2 ↑
imidazothiazol: CB_1

meta

similar affinities

para

R^1, R^2 = H, chloro: CB_2 ↑
R^1, R^2 = Br, F: CB_2 ↓

phenylpropoxy: CB_2 ↑
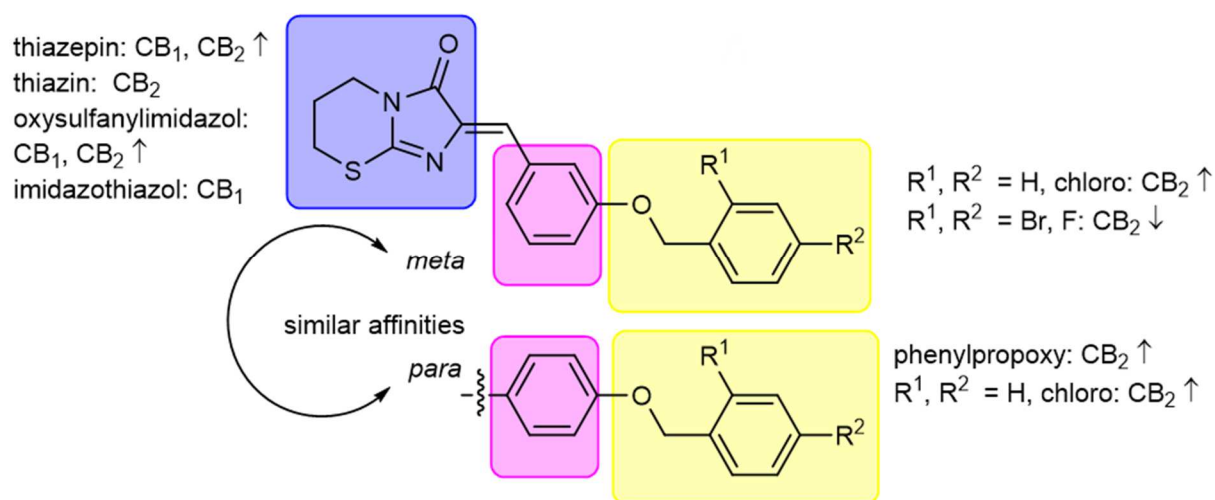R^1, R^2 = H, chloro: CB_2 ↑

Figure 28: Structure-activity relationships for imidazothiazinones at the CB receptors

3.2.5. Selectivity versus GABA$_A$ receptors

Some of the compounds, which were originally included in the screen, had been developed as GABA$_A$ receptor ligands, but had only shown low or moderate binding to the benzodiazepine binding site of the GABA$_A$-receptor.[169] To exclude the possibility that the newly developed GPR18 antagonists also interact with this target the lead compounds were evaluated for their ability to replace radiolabeled diazepame from its binding site at rat brain membrane preparations. For comparison, some of the previously developed compounds were also investiagted together with the most potent GPR18 antagonists (as can be seen in Figure 29).
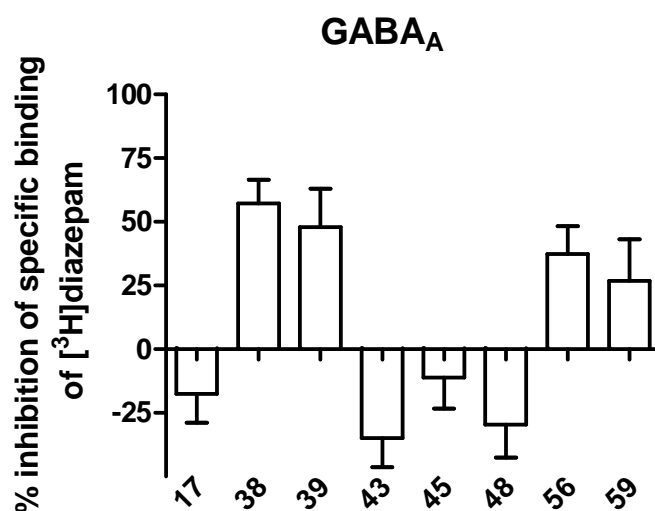
Figure 29: Inhibition of specific binding of [³H]diazepam to rat brain membrane preparations by selected compounds

The two compounds **48** and **38** showed an inhibitory potential – which was expected based on the results reported by Kiéc-Kononowicz *et al.* (2004).[169] For compound **48** the K_i value was determined and found to be slightly higher as the literature value (K_i = **2.2** µM)[169], namely **18.9** µM in our current experiment. Heterologous competition was also performed with unlabeled diazepam to control whether the literature K_D value (4 nM) can be used for further calculation. Diazepam showed a K_i value of **9.72** nM in the heterologous binding experiment, which was in the same range.
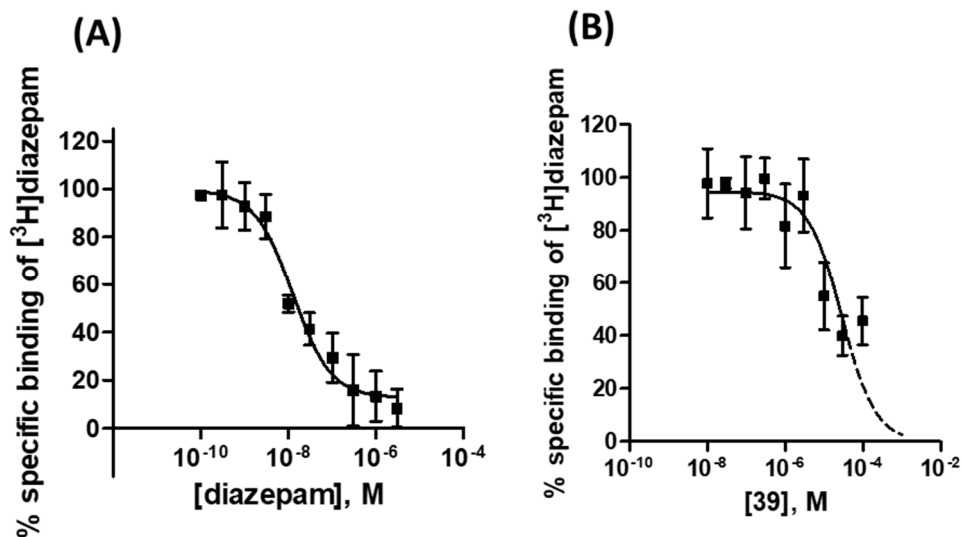

Figure 30: Heterologous competition binding of diazepam (left side) and compound **48** (right side). Compound **48** showed a K_i value of **18.9** ± 5.4 after extrapolation

Most importantly, **PSB-CB-5** (**17**), our optimized GPR18 antagonist, does not show any affinity to the diazepam binding site of $GABA_A$ receptors up to concentrations of 10 µM. This was also true for structurally related compounds such as **43**, **102** and **56**. The optimized structures were no $GABA_A$ receptor ligand and it appears that by optimizing the compounds for GPR18 the $GABA_A$ affinity was lost.

3.2.6. Summary: imidazothiazinones as GPR18 antagonists

In this study, a series of 79 compounds was investigated for their ability to act as antagonists at GPR18 and GPR55. The most potent compound was **PSB-CB-5** (**17**), which was first described by Viktor Rempel, with an IC_{50} value of **0.279** µM, but only partial inhibition of Δ^9-THC-induced β-arrestin recruitment (60%). Three different types of substitutents were evaluated as shown in Figure 31. The results were used to analyze structure-activity relationships for this compound class.
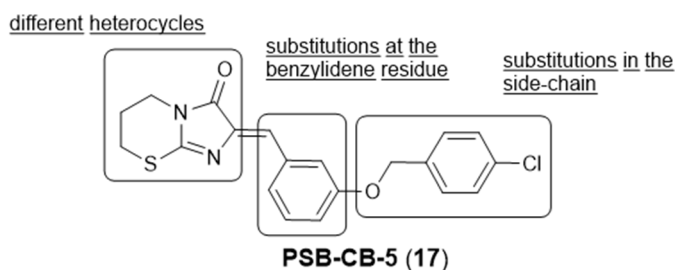
Figure 31: Investigated structural variations of the hit compound **PSB-CB-5** (**17**)

Different heterocycles showed no improvement in potency at GPR18. The thiazepine ring of compound **45** led to a weak GPR55 activation (EC_{50} value of **10.1** μM), but to a loss in GPR18 potency. The substitution pattern of the benzylidene residue was of major importance to distinguish between GPR55 and GPR18 inhibition. Small lipophilic substitutions, such as *o,p*-difluoro and *o,p*- dimethyl led to an improved GPR55 inhibition without affecting GPR18 activation. o*rtho*-Substitution was necessary to achieve GPR55 inhibition. For GPR18, long lipophilic residues in the *meta*-position were crucial for inhibitory potency. **PSB-CB-5** (**17**), the *para*-chlorobenzyloxy compound, showed an IC_{50} value of **0.279** μM with an efficacy of 60% against Δ^9-THC induced β-arrestin recruitment. The *para*-position of the benzyloxy residue needed to be substituted with a lipophilic residue of a certain size; the corresponding bromo-derivative was moderately active, the *para*-fluoro derivative was not active at all. Long lipophilic residues such as a *para*-substituted phenyloxyalkyloxy residues showed also potencies in the submicromolar range. Compound **79** with a hexyl chain was the most potent derivative with an IC_{50} value of **0.650** μM and a maximal inhibition of 100%. This group of compounds showed potency, but their physicochemical properties are not favorable. The imdiazothiazinones are already very lipophilic compounds. By extending the lipophilic residues water-solubility and polarity are decreasing. Therefore, every further optimization should focus on decreasing the size and the lipophilicity of the compounds.
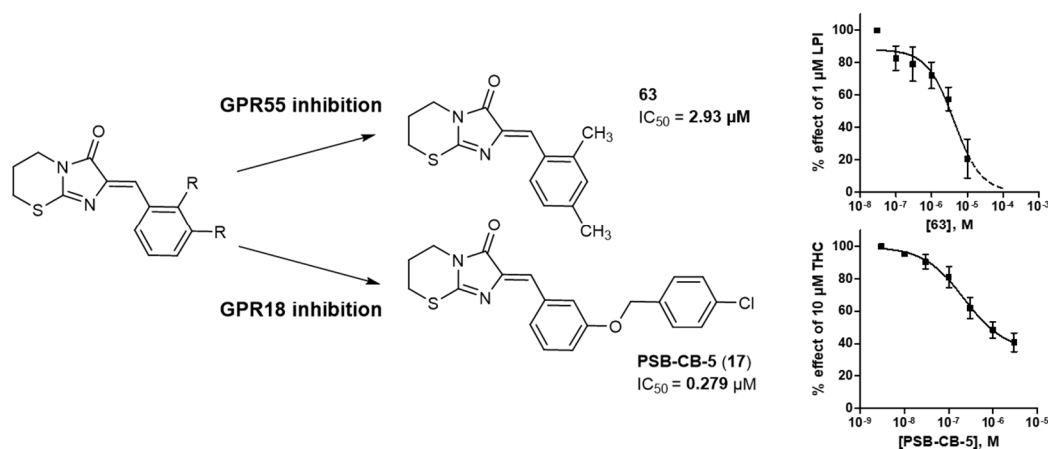

Figure 32: Summary of the results of imidazothiazinones at GPR18 and GPR55

The selectivity of the compounds was also investigated not only against GPR55, but also against the cannabinoid receptors CB_1 and CB_2 and for few compounds also at the benzodiazepine binding site of $GABA_A$ receptors. Compounds with *meta*-substituted benzylidene residues were not active at GPR55, only compounds with small lipophilic residues especially in the *ortho*-position were GPR55 antagonists. A few compounds showed a moderate affinity to CB_1 and CB_2 receptors in radioligand binding assays. Some of the GPR18 antagonists bound weakly to CB_2, as also the most potent compound **PSB-CB-5** (**17**). However, most of the compounds that bind to the CB receptors are not active at the orphan receptors. For selected compounds, $GABA_A$ receptor binding was investigated versus [^{3}H]diezepam. The optimized GPR18 antagonists do not displace [^{3}H]diazepam binding to rat brain cortex. In the future, the selectivity of the compounds against the CB receptors should be further enhanced.

The antagonists for GPR18 were designed to act against the Δ^9-THC-induced β-arrestin signal. As long as no endogenous ligand for GPR18 can be confirmed, it remains unclear whether these antagonists will inhibit the signal of an endogenous ligand. This information would be important to if the antagonists are to be used in native tissues or in animals.

Nevertheless, the here investigated compound class can serve as useful tools to study GPR18 pharmacology and (patho-)physiology.

3.3. GPR18 agonists

3.3.1. Introduction

As has been depicted in chapter 3.1, there is a growing number of compounds discussed to either activate or inhibit GPR18. Unfortunately, very controversial data exist in the literature for these compounds, which make it very difficult to rely on the effects of a compound in a biological system. Especially, as no clear confirmation for an endogenous ligand has been provided, the comparison of results from different test systems remains challenging. There is an urgent need to develop reliable tool compounds, both antagonists and agonists. Here, we want to show the results of an approach to study a new compound class of GPR18 agonists. These agonists are small molecules that do neither have a cannabinoid-like nor a lipid-like structure. For the first time, such synthetic small molecule agonists for the orphan GPR18 will be described.

The here studied compound class was discovered through the screening of a sublibrary of the Pharma-Zentrum Bonn (https://www.pharma.uni-bonn.de/www/pharmchem1/ak-mueller/biblio-thek). An initial hit from this screen was further investigated and could be confirmed. Subsequently, the structure-activity relationships of this compound class were established in cooperation with the group of Prof. Dr. Katarzyna Kiéc-Kononowicz from the Jagiellonian University of Cracow, who supplied the compounds. Selectivity versus cannabinoid receptors and also versus GPR55 was extensively studied. The pharmacological behavior against established antagonists was also studied and led to the assumption that GPR18 probably has more than one binding site. To further elucidate this, a modeling approach was conducted in collaboration with Jens Meiler from the Vanderbilt University including a research stay to learn the method and collect the data. The results of these studies will be presented in the following sub-chapters.

3.3.2. Screening of Pharma-Zentrum Bonn libraries

The Pharma-Zentrum Bonn maintains a professionally managed proprietary compound library. To also enable smaller screening campaigns with up to several hundred compounds, this compound library is subdivided into focused sublibraries. One of these sublibraries was used to screen for agonists and antagonists at the orphan GPR18 against 10 µM Δ^9-THC as an agonist. Compounds were tested at a one-point screen in a concentration of 10 µM. Whenever compounds activated or inhibited GPR18 by more than 50%, they were retested to confirm the result.

One of the screened sublibraries, the xanthine library, consisted of 264 compounds. In the initial agonist screen, one prominent hit could be observed (see Figure 33, marked with an arrow). All

compounds were additionally tested for their potential antagonistic activity. The agonist hit could be confirmed.
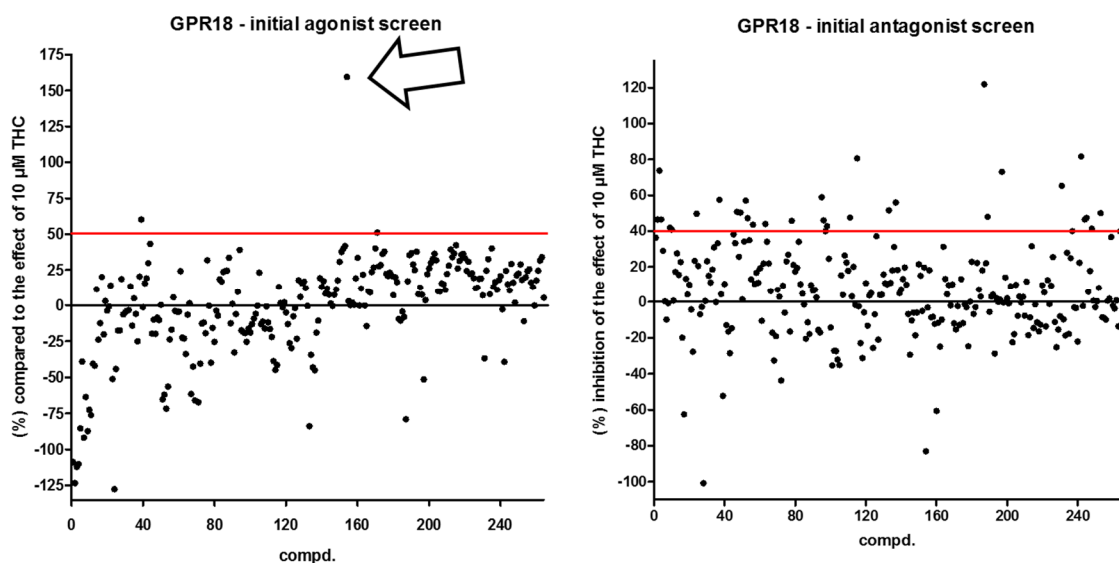

Figure 33: Initial screen of the xanthine sublibrary of the Pharma-Zentrum Bonn at the human GPR18

For the hit compound **182**, the concentration-dependent activation of GPR18 was further tested. As can be seen in Figure 34, the compound acted as full agonist in β-arrestin assays in comparison to the maximal effect of the agonist Δ^9-THC with an EC_{50} value of **0.556** µM. The new agonist was a pyrimido-purindione derivative with an indolylethyl substitution. The indolylethyl-residue is a structural element that can be found quite often in natural products, - it is a component of tryptophan, one of the essential amino acids. Overall, it can be concluded that this compound does not display lipid-like structural properties. It rather displays a peptide-like structure. Further, it is a small molecule agonist with many positions that can further be investigated.
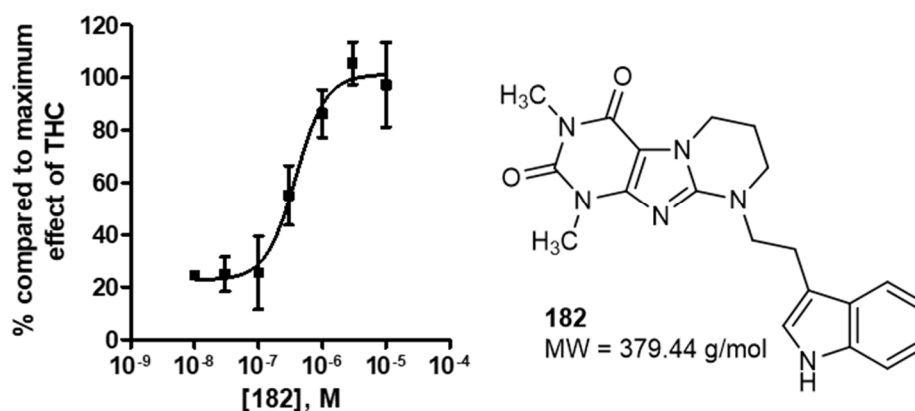

Figure 34: Concentration dependent activation of human GPR18 in β-arrestin assays by compound **182** and chemical structure of compound **182**.

3.3.3. Structure-activity relationship of indolylylethylaminoxanthines
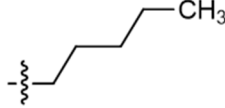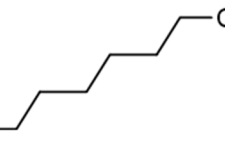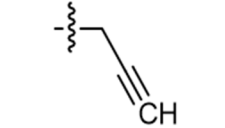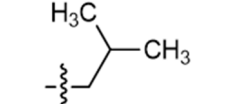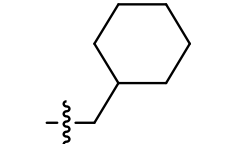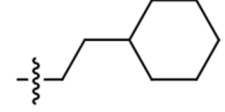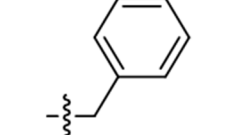
The newly identified compound class has been characterized by exploring the structure-activity relationships. The lead compound **182** consists of a xanthine moiety annelated with a tetrahydropyrimidine and an indolylethyl residue. There were several positions that were investigated for structure-activity relationships. As can be seen in Table 11, the tricyclic compound core has not been maintained in most compounds since it was discovered not to be required. A xanthine core was sufficient, where the N1- and the N7- positions were substituted with lipophilic residues of different sizes.
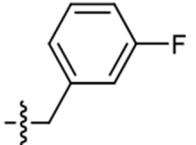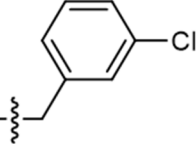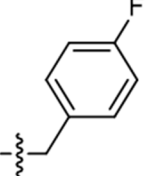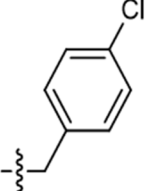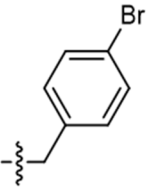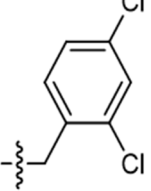
Table 11: Potencies of the indolylethylaminoxanthines at human GPR18 and human GPR55.
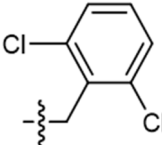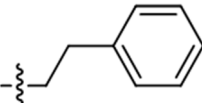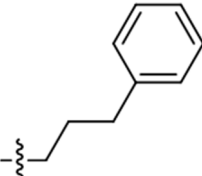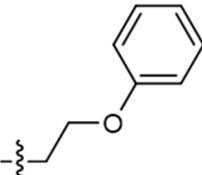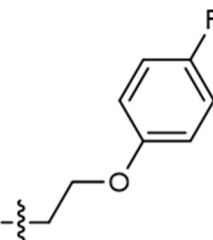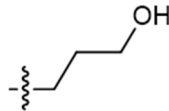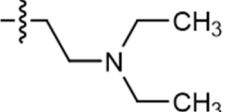
No.	Compd.	Chemical structure		human GPR18		human GPR55	
				Antagonistic activity	Agonistic actvity	Antagonistic activity	Agonistic activity
				$IC_{50} \pm SEM\ (\mu M)^a$	$EC_{50}\ (\mu M)^b$ % efficacy[c]	$IC_{50} \pm SEM\ (\mu M)^a$	$EC_{50}\ (\mu M)^b$
		R^1	R^2				
120	MZ1458	H	H	>10 (-30%)	>10 (33%)	>10 (27%)	>10 (8%)
121	KM-15-1	H	CH_3	>10 (2%)	>10 (14%)	>10 (3%)	>10 (8%)
122	MZ1459	H	(4-chlorobenzyl)	-	**0.329** ± 0.064 (104%)	>10 (32%)	>10 (2%)
123	MZ1416	CH_3	CH_3	-	**0.902** ± 0.148 (132%)	>10 (36%)	>10 (-1%)
124	KM-15-3	(ethyl)	CH_3	>10 (-28%)	>10 (30%)	>10 (11%)	>10 (3%)
125	KM-15-4	(propyl)	CH_3	>10 (-7%)	>10 (15%)	>10 (22%)	>10 (-11%)
126	KM-15-5	(butyl)	CH_3	>10 (-11%)	>10 (11%)	>10 (-27%)	>10 (25%)
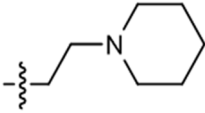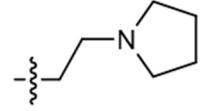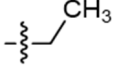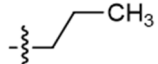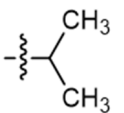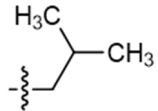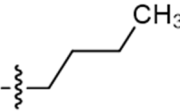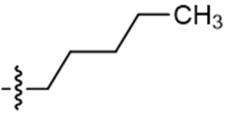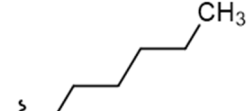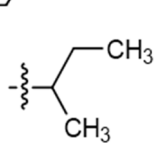
127	KM-15-6	—CH₃	CH₃	>10 (10%)	>10 (25%)	>10 (-21%)	>10 (22%)
128	KM-15-7	CH₃	CH₃	>10 (11%)	>10 (22%)	>10 (-23%)	>10 (10%)
129	KM-15-8	—CH₃	CH₃	>10 (-5%)	>10 (11%)	>10 (-22%)	>10 (14%)
130	KM-15-9	CH	CH₃	>10 (-5%)	>10 (18%)	>10 (-20%)	>10 (-2%)
131	KM-15-10	H₃C CH₃	CH₃	>10 (-25%)	>10 (5%)	>10 (35%)	>10 (3%)
132	KM-15-11	(cyclohexylmethyl)	CH₃	>10 (3%)	>10 (13%)	>10 (9%)	>10 (10%)
133	KM-15-12	(cyclohexylethyl)	CH₃	>10 (-6%)	>10 (3%)	>10 (3%)	>10 (-3%)
134	KM-15-13	(benzyl)	CH₃	>10 (-45%)	>10 (37%)	>10 (-55%)	>10 (14%)
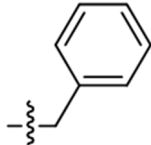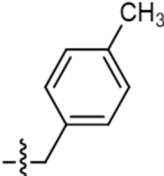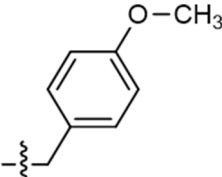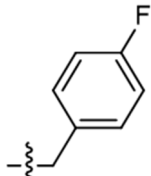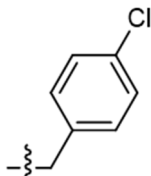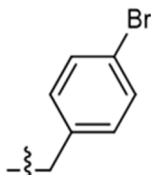
135	KM-15-17		CH_3	>10 (7%)	>10 (26%)	>10 (0%)	>10 (10%)
136	KM-15-14		CH_3	>10 (7%)	>10 (27%)	>10 (-29%)	>10 (29%)
137	KM-15-18		CH_3	>10 (15%)	>10 (28%)	>10 (-20%)	>10 (9%)
138	KM-15-15		CH_3	>10 (28%)	>10 (14%)	>10 (-19%)	>10 (15%)
139	KM-15-16		CH_3	>10 (-27%)	>10 (15%)	>10 (16%)	>10 (17%)
140	KM-15-19		CH_3	>10 (0%)	>10 (30%)	>10 (14%)	>10 (5%)
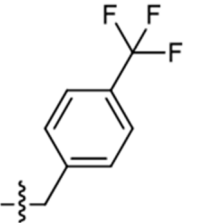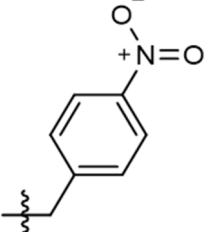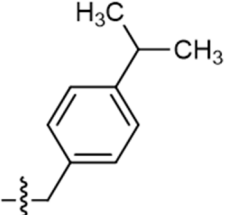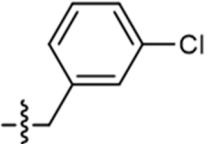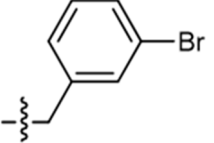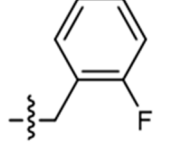
141	KM-15-20		CH_3	>10 (13%)	>10 (18%)	>10 (1%)	>10 (29%)
142	KM-15-21		CH_3	>10 (-4%)	>10 (23%)	>10 (-13%)	>10 (30%)
143	KM-15-22		CH_3	>10 (-11%)	**2.96** ± 0.97 (47%)	>10 (22%)	>10 (16%)
144	KM-15-23		CH_3	>10 (-27%)	**1.67** ± 0.75 (75%)	>10 (13%)	>10 (15%)
145	KM-15-24		CH_3	>10 (-12%)	**1.58** ± 0.55 (70%)	>10 (-6%)	>10 (30%)
146	KM-15-26		CH_3	>10 (-32%)	>10 (28%)	>10 (31%)	>10 (-7%)
147	KM-15-28		CH_3	>10 (-13%)	>10 (44%)	>10 (26%)	>10 (-3%)
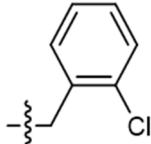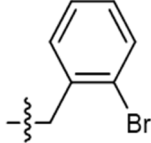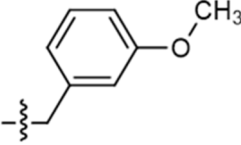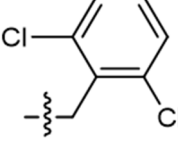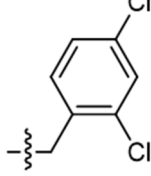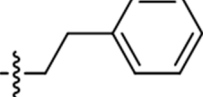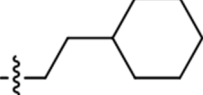
148	KM-15-29		CH_3	>10 (-28%)	>10 (19%)	>10 (14%)	>10 (-15%)
149	KM-15-30		CH_3	>10 (-25%)	>10 (17%)	>10 (7%)	>10 (-13%)
150	MZ1412	CH_3		-	**0.190** ± 0.043 (113%)	>10 (-11%)	>10 (21%)
151	MZ1411	CH_3		-	**0.196** ± 0.059 (127%)	>10 (-9%)	>10 (48%)
152	MZ1439	CH_3		-	**0.0614** ± 0.0136 (69%)	>10 (3%)	>10 (10%)
153	MZ1441	CH_3		-	**0.204** ± 0.042 (122%)	>10 (40%)	>10 (12%)
154	MZ1413	CH_3		-	**0.151** ± 0.045 (103%)	>10 (18%)	>10 (36%)
155	MZ1437	CH_3		-	**0.0602** ± 0.0108 (111%)	>10 (47%)	>10 (30%)
156	MZ1438	CH_3		-	**0.127** ± 0.034 (110%)	>10 (29%)	>10 (-15%)
157	MZ1440	CH_3		-	**0.0532** ± 0.040 (45%)	>10 (-3%)	>10 (12%)
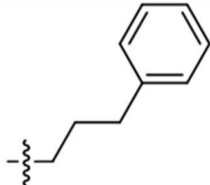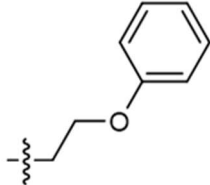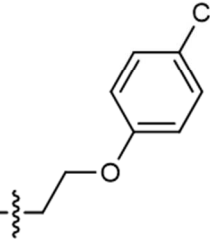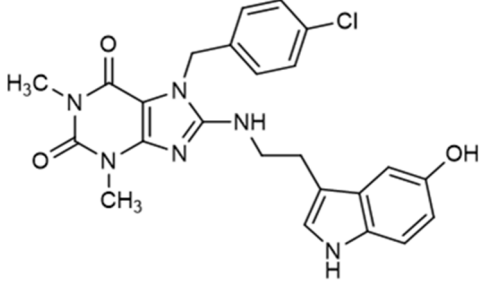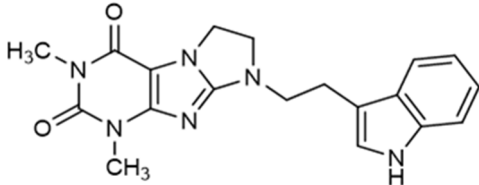
158	MZ1414	CH₃		-	**0.149** ± 0.056 (134%)	>10 (41%)	>10 (14%)
159	MZ1451	CH₃		-	**0.0246** ± 0.051 (117%)	>10 (35%)	>10 (-16%)
160	MZ1461	CH₃		-	**0.138** ± 0.013 (127%)	>10 (3%)	>10 (-22%)
161	MZ1445	CH₃		-	**0.0454** ± 0.081 (84%)	>10 (26%)	>10 (-3%)
162	MZ1415	CH₃		-	**0.0191** ± 0.0034 (141%)	>10 (43%)	>10 (8%)
163	MZ1446	CH₃		-	**0.0724** ± 0.547 (65%)	>10 (33%)	>10 (13%)

164	MZ1463	CH$_3$		-	**0.136** ± 0.017 (111%)	>10 (45%)	>10 (-6%)
165	MZ1457	CH$_3$		-	**0.0426** ± 0.0155 (98%)	>10 (31%)	>10 (-8%)
166	MZ1462	CH$_3$		-	**0.352** ± 0.096 (111%)	>10 (30%)	>10 (-10%)
167	MZ1448	CH$_3$		-	**0.0711** ± 0.0174 (85%)	>10 (13%)	>10 (33%)
168	MZ1456	CH$_3$		-	**0.101** ± 0.013 (134%)	>10 (34%)	>10 (-27%)
169	MZ1455	CH$_3$		-	**0.137** ± 0.032 (123%)	>10 (13%)	>10 (-8%)
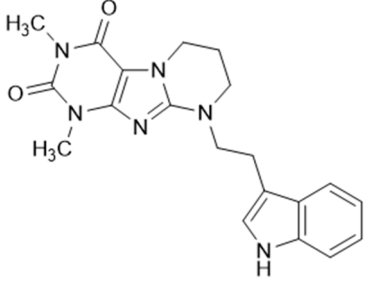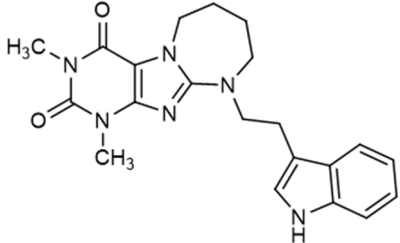
170	MZ1460	CH_3		-	**0.0604** ± 0.0122 (129%)	>10 (10%)	>10 (-43%)
171	MZ1454	CH_3		-	**0.189** ± 0.027 (148%)	>10 (23%)	>10 (-48%)
172	MZ1452	CH_3		-	**0.166** ± 0.024 (122%)	>10 (36%)	>10 (-24%)
173	MZ1442	CH_3		-	**0.347** ± 0.0136 (45%)	>10 (24%)	>10 (15%)
174	MZ1444	CH_3		-	**0.0642** ± 0.0308 (72%)	>10 (-4%)	>10 (-5%)
175	MZ1417	CH_3		-	**0.442** ± 0.152 (155%)	>10 (45%)	>10 (8%)
176	MZ1453	CH_3		-	**0.102** ± 0.024 (103%)	>10 (38%)	>10 (-48%)

177	MZ1418	CH₃		-	**0.120** ± 0.027 (176%)	>10 (45%)	>10 (4%)
178	MZ1429	CH₃		-	**0.229** ± 0.048 (64%)	>10 (11%)	>10 (-8%)
179	MZ1430	CH₃		-	**0.417** ± 0.173 (64%)	>10 (17%)	>10 (13%)
180	MZ1464			-	**0.340** ± 0.069 (114%)	>10 (30%)	>10 (-10%)
181	KD478			-	**5.68** ± 1.54 (146%)	>10 (20%)	>10 (27%)

| 182 | KD-107 | | - | 0.556 ± 0.126 (106%) | >10 (-5%) | >10 (20%) |
| 183 | KD477 | | - | 0.454 ± 0.156 (171%) | >10 (38%) | >10 (21%) |

[a] % inhibition of standard agonist induced luminescence signal (GPR18: 10 µM Δ^9-THC; GPR55: 1 µM LPI)
[b] % activation compared to standard agonist induced luminescence signal (GPR18: 10 µM Δ^9-THC; GPR55: 1 µM LPI)
[c] in comparison to 30 µM Δ^9-THC (maximal effect)

A series of 62 synthesized derivatives was investigated for their activity at the human GPR18 and GPR55 in both agonist and antagonist assays. The first compound set contained derivatives with different alkyl substitutions at the *N1*-position (R^1). In the lead compound **182**, this position is occupied by a methyl residue. Compound **121**, the only unsubstituted derivative (R^1 = H), showed no activity in the β-arrestin recruitment assay. Therefore, it can be concluded that a substituent is required. Compound **177** lacks the two methyl residues at the N1- and the N7-position. It also showed no activity at GPR18. This N1-substituent was consequently enlarged to ethyl (compound **124**), propyl (compound **125**), and butyl (compound **130)** but already the ethyl-substituted compound **124** showed no agonistic activity. More diverse substituents were introduced at this position, but only three compounds showed some activity at GPR18. Compounds **143**, **144** and **145** displayed an EC$_{50}$ value around 1-3 µM and an efficacy between 45-75%. Thus, they were weaker than the initial hit and did not exhibit full activation of GPR18 compared to Δ^9-THC. The three compounds share a structural component. Of all the N1 substitutions, these were the only phenylpropyl or phenoxyethyl residues. All other substituents were shorter in chain length and did not show any agonistic activity at 10 µM test concentration (compare the compounds **124** to **149**). Therefore, the weak activation was linked to the chain length and aromaticity of the N1 residue. The compounds also have been tested as GPR18 antagonists, but also failed to inhibit by 10 µM THC activated GPR18 receptors.

The initial hit compound **182** is a tricyclic xanthine derivative. As a first variation, the third ring was substituted by diazepane and an imidazolidine (compounds **183** and **181**). The seven atomic diazepane ring showed a slightly increased EC$_{50}$ value of **0.454** µM, compared to **182**. In contrast, the five atomic imidazolidine ring showed ten-fold less activity with an EC$_{50}$ value of **5.68** µM. Here, the two larger rings were clearly favored, indicating that a lipophilic interaction is important.

The basic tricyclic structure does not provide many substitution opportunities. Therefore, the structure has been kept on the base of the xanthine and varied widely on the N7 position. The first compound without basic tricyclic structure was **139**, with an indolylethylamino residue at C8 and a methyl substitution on the N7 nitrogen atom. With an EC$_{50}$ value of **0.902** µM, the activity was decreased when comparing to compound **182**. The N7 methyl residue was altered and the influence of different substitution investigated.
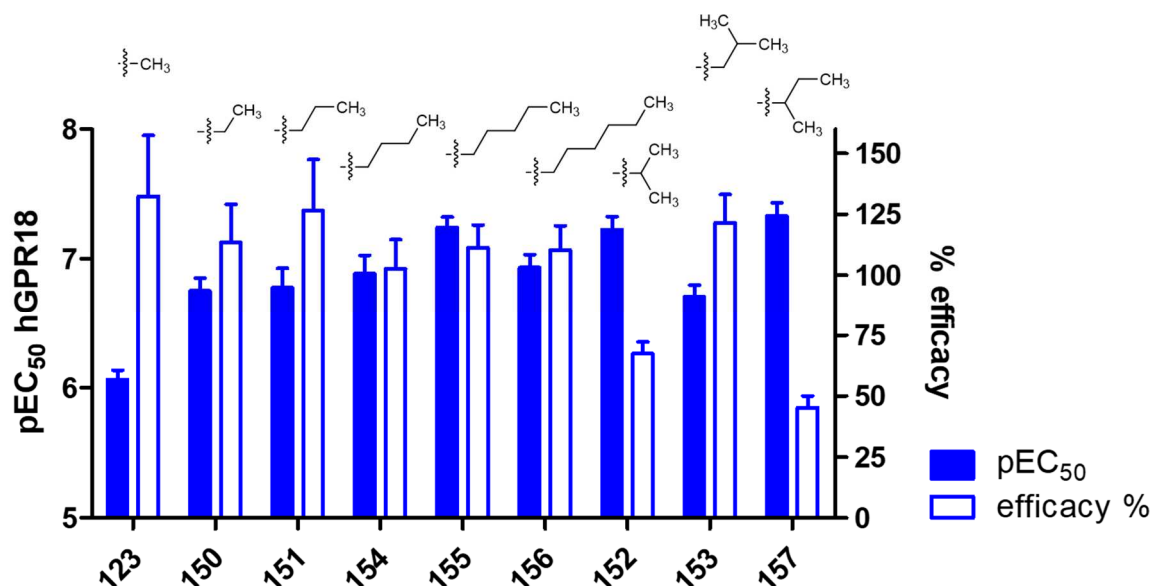
Figure 35: influence of the alkyl side chain substitution on GPR18 activation

As can be observed in Figure 35, the activity of the compounds increased up to a pentyl chain (compound **155**) with an EC_{50} value of **0.0602** µM. Compound **156** with a hexyl chain had a slightly reduced activity with an EC_{50} value of **0.127** µM. Branched alkyl chains were also evaluated. The isopropyl side chain (compound **152**) was comparably more activate than the n-propyl compound **151** with an EC_{50} value of **0.0623** µM. Further, there were two different isobutyl substituted compounds (**153** and **157**). The latter compound was with an EC_{50} value of **0.0532** µM more active than the unbranched alkyl-substituted compounds. However, compound **157** and also **152**, the isopropoyl derivative, showed a reduced efficacy. In total, it can be concluded that from the small methyl-substituent in compound **123** to the most potent compound **157** the activity increased from **0.902** µM to **0.0532** µM. This was a 17-fold change. Therefore, the lipophilic substitution can be regarded as a successful optimization concerning the potency.

In the next step, aromatic substitutions were evaluated. Compound **158** has a benzyl-ring at the N7 nitrogen and an activity of **0.149**. It is more potent than a compound with only a methyl residue (compare to **123**). In comparison to **154**, an aliphatic compound with a longer chain as butyl (EC_{50} = **0.151** µM) the activity is very similar. In Figure 36, different aromatic substitutions are plotted against the activity.
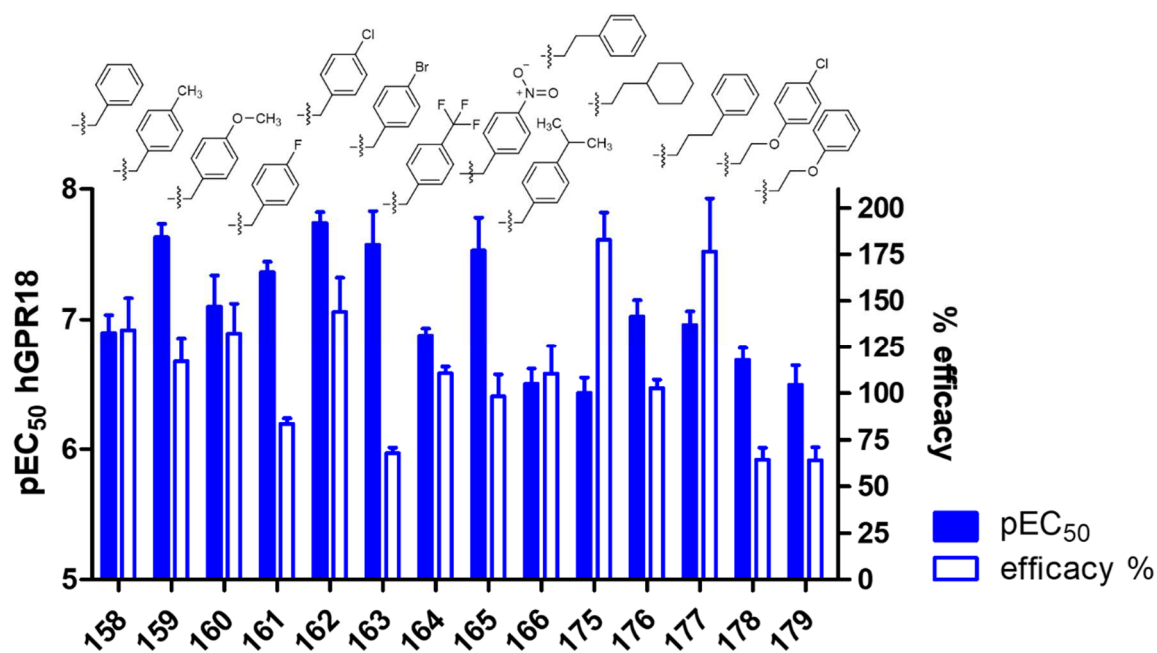
Figure 36: influence of the aromatic substitution at N7 on GPR18 activity, part I

The *para*-methylation of the benzyl-residue increases the activity significantly, compound **159** showed an EC$_{50}$ value of **0.0246** µM, which was a 6-fold increase in potency. The *para*-methoxy compound **160** with an EC$_{50}$ value of **0.138** µM was not as potent as **159**. It showed a quite comparable activation to **158**. With the *para*-fluoro-, chloro- and bromo- substitution the space was filled with a very lipophilic residue. All three compounds were more potent than the benzyl compound **158**. The *para*-chloro substituted compound **162** was the most potent compound of the whole compound set with an EC$_{50}$ value of **0.0191** µM. The *para*-bromo- and *para*-fluoro-compound **163** and **161** were both slightly less active with EC$_{50}$ values of **0.0724** µM and **0.0454** µM, respectively. Compound **165** with a *para*-nitro function also showed an EC$_{50}$ value of **0.0426** µM. These residues were comparably small and lipophil. Larger residues also have been investigated, e.g. compound **164**, with a trifluoromethyl- and **166** with an isopropyl residue in *para* position of the benzyl-substituent. They both showed a reduced potency when compared to **162** with EC$_{50}$ values of **0.136** µM and **0.352** µM. The space for this lipophilic interaction seemed to have an optimum with smaller lipophilic substitutions at the aromatic ring. Compound **175** with a phenylethyl-residue instead of the benzyl showed a further reduced activity with an EC$_{50}$ value of **0.442** µM. The corresponding saturated residue (**176**) was more potent with an EC$_{50}$ value of **0.102** µM. Compound **177**, where the residue has been prolonged to phenylpropyl, was with an EC$_{50}$ value of **0.120** µM also in the same range of potency. The phenyloxyethyl- and *para*-chlorophenyloxyethyl- compounds were even less potent. Altogether, this suggest that a lipophilic substitution at N7 is crucial for the high potency agonists. There seems to be an optimum for small but very lipophilic substitutions in *para*-position. If the residue gets too large, the activity decreases.

So far, only *para*-substituted compounds have been described. In Figure 37, results for *meta* and *ortho*-substituted benzyl-residues are depicted.
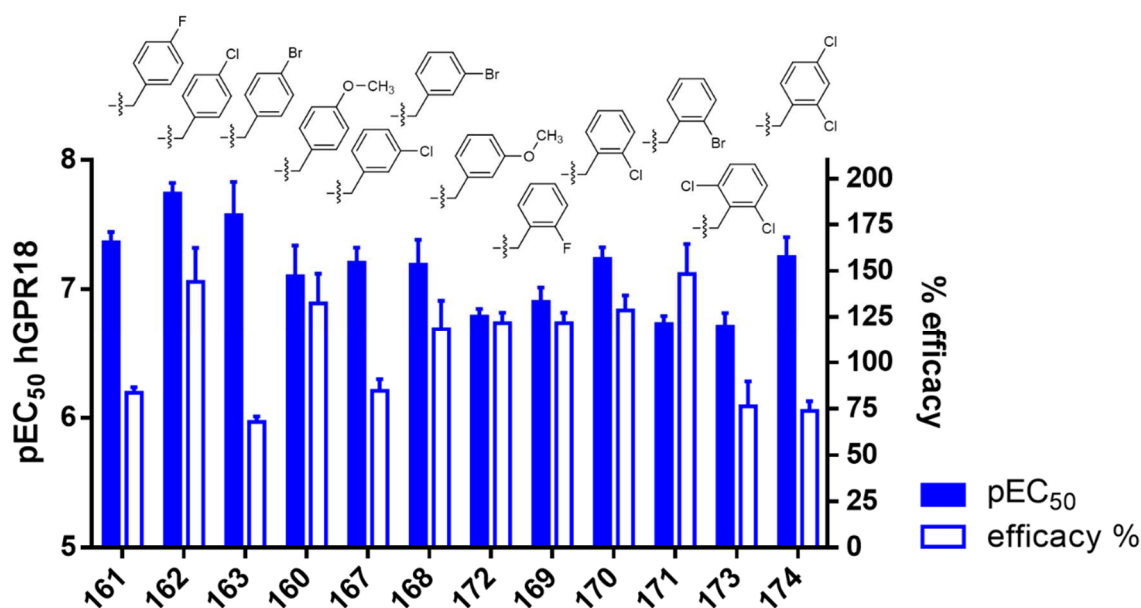
Figure 37: influence of the aromatic substitution at N7 on GPR18 activity, part II

If we compare the *meta*-substituted compounds to their corresponding *para*-substituted compounds (**162** and **167**, **161** and **168**, and **160** and **172**), it can be observed that the *meta*-substituted compounds were all less active. The *meta*-chloro compound **167**, for example, had an EC_{50} value of **0.0711** µM in comparison of the **0.0191** µM of the *para*-choro-benzyl compound **162**. For the halogen-substituted compounds, there were further *ortho*-compounds (compare **161** and **169**, **162** and **170**, and **163** and **171**) depicted in Figure 37. The *ortho*-substituted compounds were not as active as the *para*-substituted compounds. They showed very comparable activities in regard to the *meta*-substituted compounds. Further, the 2,6-dichloro-benzyl compound **171** can be explored. It showed an even reduced activity when compared to the 2-chloro-benzyl- substitution (**170**). The 2,4-dichloro-benzyl residue (**174**) showed an equal activation in regard to the *ortho*-chloro-compound **170**. There was no further activity increase through the *para*-chloro substitution.

Overall, in the N7 position an aromatic residue was preferred over the alkyl substitution. The most active compound was **162** with a *para*-chloro-benzyl residue with an EC_{50} value of **0.0191** µM. The structure-activity relationships described above show a clear favor for lipophilic substituents that do not exceed a certain size. The activity is reduced for larger lipophilic substitutions as *para*-isopropyl-benzyl- or hexyl-side chains.

The compound **122** resembles **162**, the most active compound, with only one exception: In the R^1 position the methyl residue is exchanged by a hydrogen. In the first part of this structure activity

compound **122** showed an EC_{50} value of **0.329** µM. This is a 17-fold reduction in activity and can be viewed at in Figure 38. This underlines the importance of the methylation of the N1 moiety.
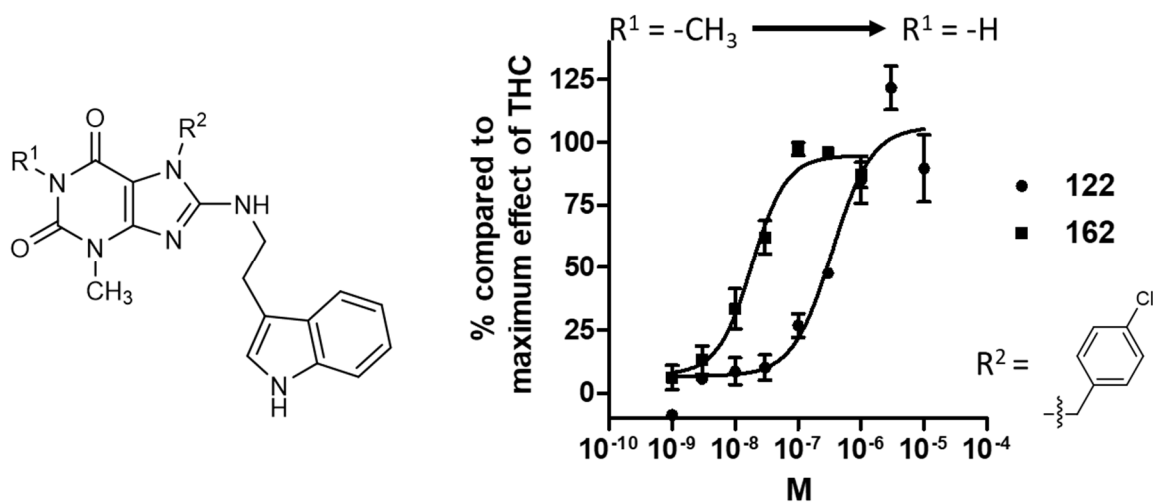
Figure 38: Concentration-response curve for compound **162** and **122**, which only differ in the R^1 substitution (**162:** R^1 = -CH$_3$; **122**: R^1 = -H)

Another substitution has been investigated: **180** is the only compound, where the indole-residue has been altered. The indolylethylamino moiety might recall the look of a tryptophan, one of the essential amino acids. Tryptophan is also part of many important signaling molecules, such as tryptamine (2-(Indol-3-yl-)ethylamine) and its derivatives. One of this derivatives is serotonin, an crucial interaction partner in neurotransmission, which can chemically be described as 5-hydroxy-tryptamine. In compound **180**, the indolylethylamine has been varied to a 5-hydroxy-indolyl-ethylamin. With an EC_{50} of **0.329** µM, it shows a reduced activity when compared to **162**, with whom it shares both R^1 as also R^2.
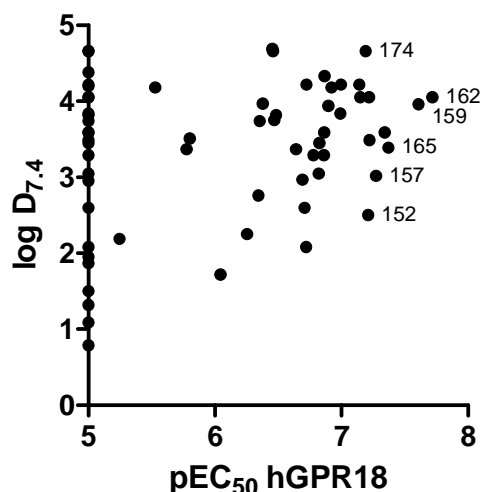
Figure 39: Correlation between log $D_{7.4}$ and pEC$_{50}$value of the human GPR18 potency, log D values were calculated with Marvin 17.4.3, ChemAxon (http://www.chemaxon.com)

The physicochemical parameter log $D_{7.4}$ was correlated with the agonistic potency at the human GPR18 to investigate a possible connection with the lipophilicity. The calculated log $D_{7.4}$ values ranged between 1.8 and 4.8 for the active compounds. Although the most active compounds showed log $D_{7.4}$ values of 4, there were also compounds with high potency which showed log $D_{7.4}$ values of 2.6 (compound **152**). For drug design, a value between 0-5 is necessary and our compounds were in the range of 1.7 to 4.7. The properties are regarded advantageous when the log D value is lower 3.5, as high lipophilicity is often combined with bad solubility. Therefore, our most potent compounds could be optimized regarding their physicochemical properties. However, all reported GPR18 ligands have been very lipophilic compounds indicating that a distinct lipophilicity is needed to target GPR18.
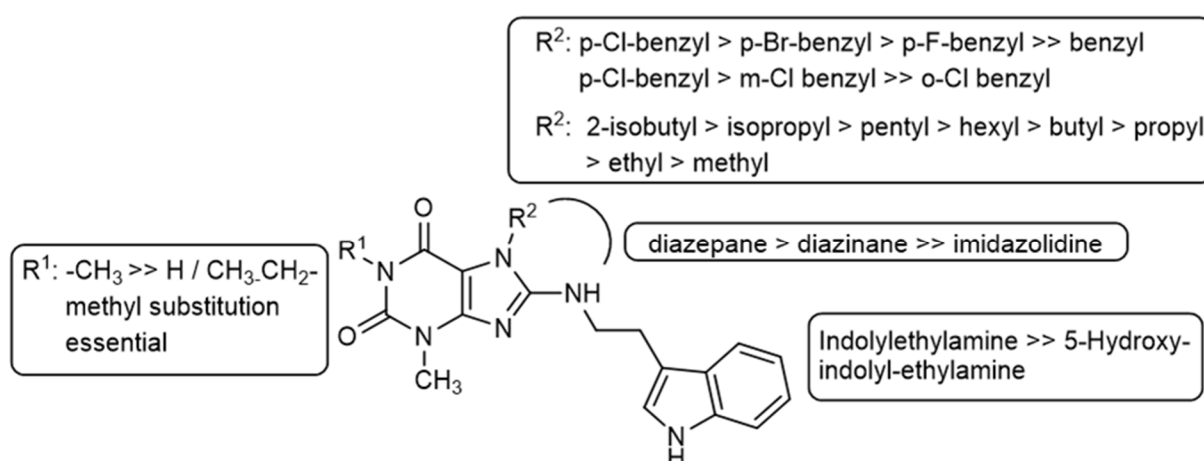
Figure 40: summary of the structure-activity relationships of 8-(indolyl-ethylamino)-xanthines

A summary of the structure-activity relationships for this newly discovered class of GPR18 agonists can be found in Figure 40. As can be seen the two positions at N1 and N7 have already been

investigated with a set of diverse substitutions. Whereby substitution of the N7 position with lipophilic aromatic groups proved to increase the activity. On the N1 position only a methylation is tolerated. With the 5-hydroxy-indolyl-ethylamine compound a first attempt to study the structure-activity relationships at the indolyl-residue has been made.

There are further positions, which also could be investigated, they are depicted in Figure 41.
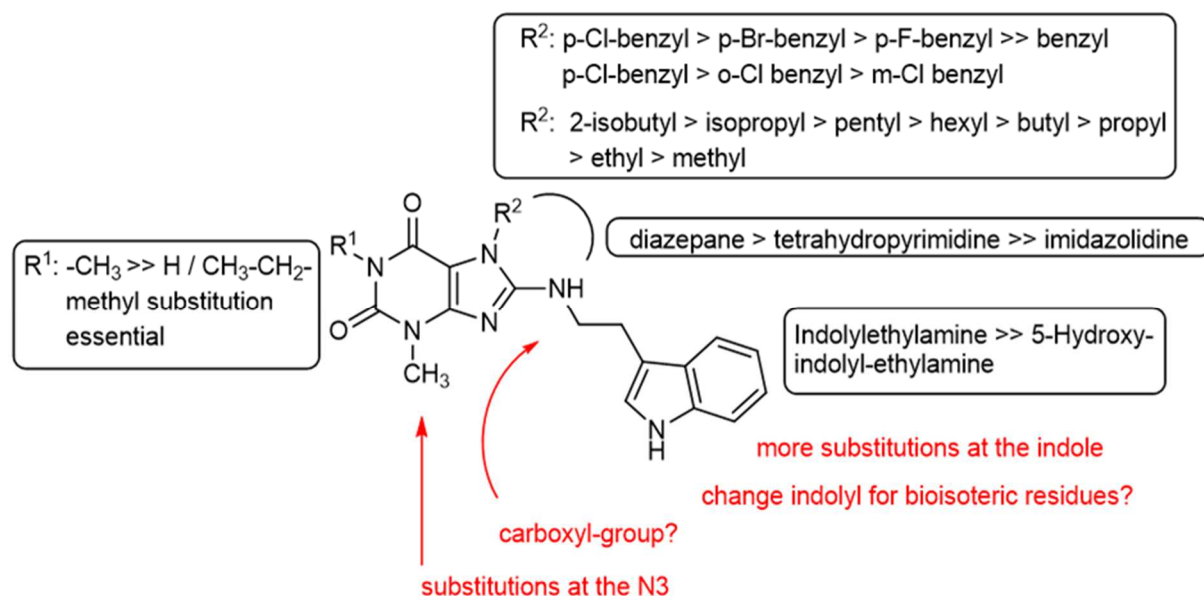
Figure 41: Further recommendations (in red) to study the structure-activity relationships

Overall, the study of the structure-activity relationships has been proven to be very successful. From the initial hit compound **182** with an EC_{50} value of **0.556** µM, it was possible to improve the potency up to **0.0191** µM for compound **162**. It is the most potent small molecule agonist for GPR18 known to date.

3.3.4. Selectivity versus the related orphan GPCR GPR55
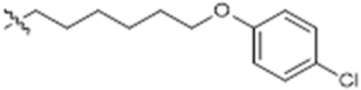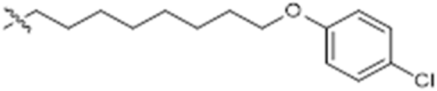
A first selectivity test was accomplished by testing the potency of the GPR18 agonists at the orphan GPR55. GPR55 was also expressed in the PathHunter™ test system (DiscoverX) and therefore the assay relies on the same principles as the GPR18 assay. This selectivity test serves as an important exclusion criteria. If a compound is nonselective acting at both cell lines in the same test system, it is either acting at both receptors or it interferes with the test system without even targeting a receptor. To exclude such possible false positive hits or artifacts, the compounds were tested simultaneously at GPR18 and GPR55 (for results, see Table 11). No activation or inhibition was observed for any compound at GPR55. Thus, the compounds showed complete selectivity for GPR18 versus GPR55 using the same test system.

3.3.5. Blockade of GPR18 agonists by antagonists

The newly developed class of GPR18 agonists was further evaluated in experiments with the already established GPR18 antagonists. The most important question was, whether the antagonists were able to block the signal of the agonists and if so, whether the IC_{50} values were similar as versus Δ^9-THC. Compound **162** and **182**were selected as agonists, in addition to Δ^9-THC. A series of antagonists (see section 3.2) was evaluated versus all three agonists, the lipid-like Δ^9-THC and the small peptide-like newly discovered agonists **182** and **162**. The results are summarized in Table 12. For comparability, the antagonists have all been evaluated against the EC_{80} of the respective agonist (for Δ^9-THC: 10 µM; **182**: 1 µM; **162**: 0.1 µM) and concentration-dependent inhibition of β-arrestin recruitment was determined.

Table 12: IC_{50} values of selected GPR18 antagonists versus different agonists

No.	Compd.	Chemical structure	Δ^9-THC[a] IC_{50} (µM) maximal inhibition (%)	KD-107[b] IC_{50} (µM) maximal inhibition (%)	MZ1415[c] IC_{50} (µM) maximal inhibition (%)
17	PSB-CB-5		**0.279** ± 0.111 (71%)	**11.3** ± 1.1 (100%)	**29.2** ± 12.4[d]
43	CB-4		**2.55** ± 0.71 (100%)	**17.2** ± 8.7 (100%)	>10 (25%)
69	CB-20		**1.73** ± 0.37	>10 (43%)	>10 (8%)
70	CB-22		**3.59** ± 2.25	**12.6** ± 2.6	>10 (10%)
71	CB-15		**1.65** ± 0.45	>10 (70%)	>10 (-33%)
74	CB-24		**1.49** ± 0.39	**6.34** ± 0.71	>10 (23%)
76	CB-25		**3.25** ± 1.22	**8.70** ± 4.59	>10 (-6%)
77	CB-28		**2.38** ± 1.15	**6.28** ± 3.13	>10 (20%)
78	CB-26		**1.14** ± 0.44	**6.35** ± 2.61	>10 (14%)

79	CB-27		**0.650** ± 0.134 (100%)	**2.21** ± 0.47 (65%)	**22.4** ± 5.9 (100%)
80	CB-29		**1.15** ± 0.17	**3.26** ± 1.43	>10 (-29%)

[a] 10 µM; [b] 1 µM; [c] 0.1 µM ([a,b,c] concentration corresponding to EC_{80} of agonist)
[d] extrapolated value

It can be observed that the antagonists were able to inhibit the compound **182**-induced signal, but most of them were not able to inhibit the **162**-induced signal or they were far weaker versus that agonist.

In Figure 42, the concentration-dependent inhibition of the three agonists Δ^9-THC, **182** and **162** by **PSB-CB-5** (**17**) is displayed. **PSB-CB-5** (**17**) was a partial antagonist of Δ^9-THC-induced GPR18 activation, with an IC_{50} value of **0.279** µM. Its inhibition curves were shifted to the right versus the new agonist, **182** and **162**. The IC_{50} value was **11.3** µM, 40-fold weaker versus **182**, but it reached full inhibition. **PSB-CB-5** (**17**) was even less potent against compound **162** (0.1 µM), and its IC_{50} value could only determined by extrapolation (**29.2** µM).
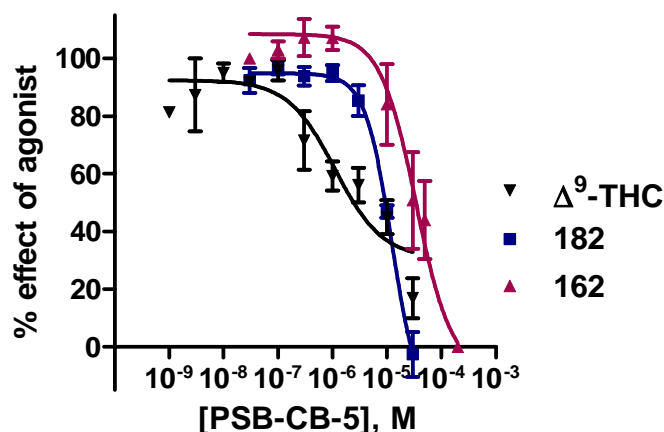
Figure 42: Concentration-dependent inhibition of GPR18 activation by **PSB-CB-5** (**17**). The agonists were employed at their EC_{80} concentrations (Δ^9-THC: 10 µM; **182**: 1 µM; **162**: 0.1 µM)

A competitive antagonist shifts the agonist curve to the right in a concentration-dependent manner, without lowering the maximal effect. Thereby, the EC_{50} value of the agonist increases. A non-competitive antagonist decreases the maximal effect concentration-dependently, but does not change the EC_{50} value.
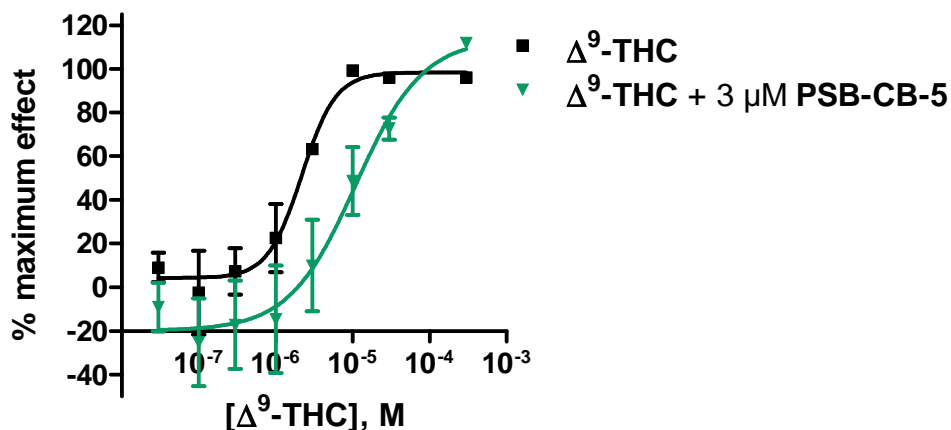
Figure 43: GPR18 activation with Δ^9-THC in the absence and presence of 3 µM PSB-CB5, data by Viktor Rempel[66]

(A)

	$EC_{50\,(\mu M)}$	E_{max} (%)
182	**1.31** ± 0.48	100
+ 3 µM PSB-CB-5	**0.508** ± 0.100	89
+ 10 µM PSB-CB-5	**0.338** ± 0.098	41
+ 15 µM PSB-CB-5	**0.293** ± 0.067	45

(B)

	EC_{50} (µM)	E_{max} (%)
182	**0.788** ± 0.143	100
+ 3 µM **79**	**0.554** ± 0.216	92
+ 10 µM **79**	**0.190** ± 0.058	75
+ 15 µM **79**	**0.171** ± 0.038	63
+ 20 µM **79**	**0.205** ± 0.034	53
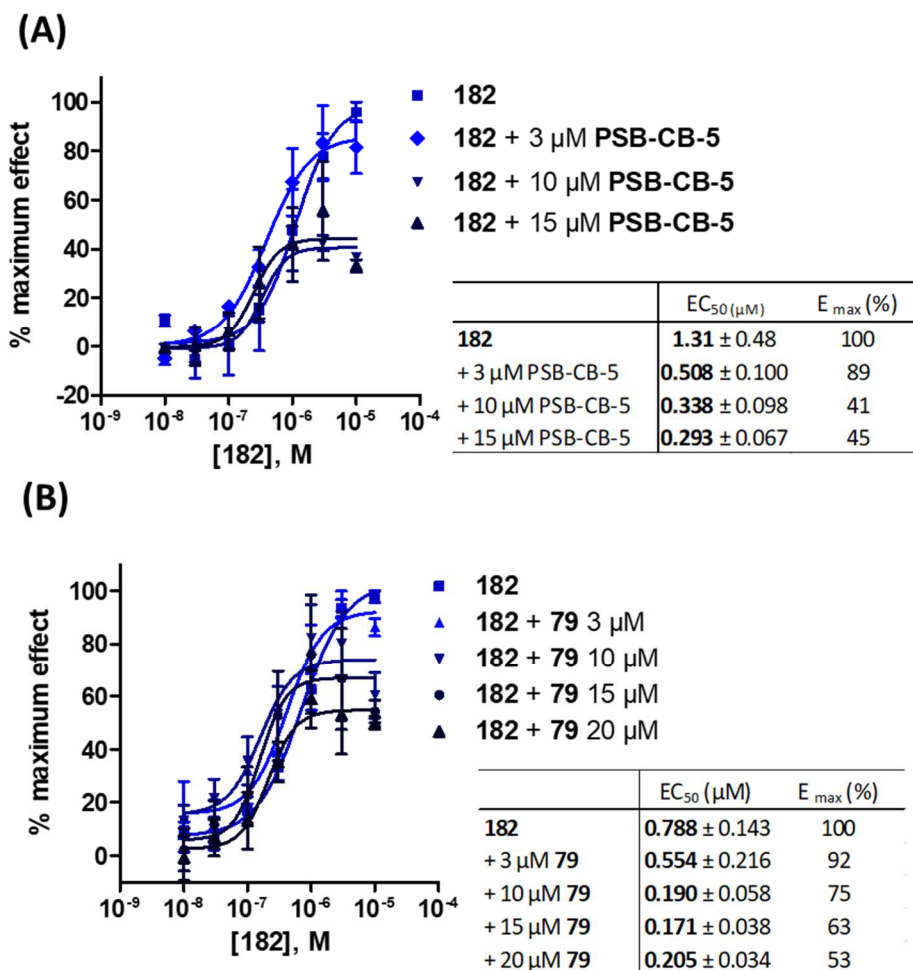
Figure 44: Agonist stimulation in the absence and presence of different antagonists at different concentrations; (A) **182** versus PSB-CB-5 (**17**); (B) **182** versus **79**

The behavior of the antagonists **PSB-CB-5** (**17**) and **79** was investigated versus the newly identified compound **182** (see Figure 44). Viktor Rempel determined the rightward shift of the concentration-effect curve of Δ^9-THC in the presence of **PSB-CB-5** (**17**); (see Figure 43).[66] It was concluded that **PSB-CB-5** (**17**) is a competitive antagonist versus Δ^9-THC. **PSB-CB-5** (**17**) inhibited the activation of compound **182** by lowering the maximum effect, while the curve was not shifted to the right. The effect was more pronounced for higher concentrations of **PSB-CB-5** (**17**) (10 µM and 15 µM), while a concentration of 3 µM showed no significant effect.
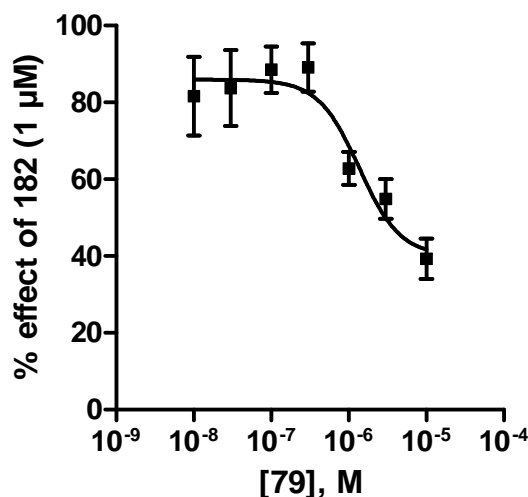
Figure 45: Concentration-dependent inhibition of **182**-induced GPR18 activation by compound **79**

Moreover, it can be concluded that none of the already established antagonists inhibited the effect of compound **162** significantly. Some of the antagonists were able to inhibit the effect of **182**, but the inhibition was weaker as compared to Δ^9-THC. In addition, it could be shown that the antagonists behaved as allosteric rather than competitive antagonists versus **182**, while they appeared to be competitive antagonist versus Δ^9-THC. It appears likely that the agonists do not share the same binding site. Δ^9-THC itself is a lipophilic compound similarly as the investigated GPR18 antagonists, while the newly discovered agonists display peptide-like properties.

3.3.6. Selectivity of GPR18 agonists versus cannabinoid receptors

The typical cannabinoid receptor ligand Δ^9-THC interacts with a GPR18. Therefore, the receptor had been proposed as a new "cannabinoid-like" receptor.[170] To investigate the selectivity of the newly discovered GPR18 agonist class, the compounds have been investigated at the classical cannabinoid receptors CB_1 and CB_2. For this purpose, a radioligand binding assay using membrane preparations overexpressing the receptor of interest was used and K_i values were determined (see Table 13).

Table 13: Affinities of identified GPR18 agonists at cannabinoid receptors determined in radioligand binding studies[a]

No.	Compd.	Human CB$_1$	Human CB$_2$
		K$_i$ (µM) vs. [^{3}H]CP55,940 (% inhibition of specific binding)	K$_i$ (µM) vs. [^{3}H]CP55,940 (% inhibition of specific binding)
120	MZ1458	>10 (34%)	>10 (18%)
121	KM-15-1	>10 (-6%)	>10 (13%)
122	MZ1459	>10 (16%)	**1.32** ± 0.17 (100%)
123	MZ1416	>10 (10%)	>10 (15%)
124	KM-15-3	>10 (29%)	>10 (16%)
125	KM-15-4	>10 (19%)	>10 (21%)
126	KM-15-5	>10 (20%)	>10 (22%)
127	KM-15-6	>10 (20%)	>10 (29%)
128	KM-15-7	>10 (9%)	>10 (10%)
129	KM-15-8	>10 (9%)	>10 (15%)
130	KM-15-9	>10 (-1%)	>10 (17%)
131	KM-15-10	>10 (6%)	>10 (29%)
132	KM-15-11	>10 (29%)	**1.42** ± 0.42 max. inhibition of radioligand-binding: 66%
133	KM-15-12	**0.867** ± 0.329 max. inhibition of radioligand-binding: 56%	**0.950** ± 0.272 max. inhibition of radioligand-binding: 54%
134	KM-15-13	>10 (24%)	>10 (31%)
135	KM-15-17	>10 (43%)	>10 (39%)
136	KM-15-14	>10 (48%)	>10 (46%)
137	KM-15-18	>10 (15%)	>10 (18%)
138	KM-15-15	>10 (42%)	**2.00** ± 0.43 max. inhibition of radioligand-binding: 64%
139	KM-15-16	**1.61** ± 0.60 max. inhibition of radioligand-binding: 58%	**1.14** ± 0.38 max. inhibition of radioligand-binding: 59%
140	KM-15-19	>10 (26%)	>10 (42%)
141	KM-15-20	>10 (49%)	>10 (31%)
142	KM-15-21	>10 (33%)	>10 (32%)
143	KM-15-22	**1.80** ± 0.63 max. inhibition of radioligand-binding: 57%	**1.40** ± 0.54 max. inhibition of radioligand-binding: 71%
144	KM-15-23	>10 (22 ± 10%)	>10 (31 ± 6%)
145	KM-15-24	>10 (42%)	>10 (38%)
146	KM-15-26	>10 (-11%)	>10 (24%)
147	KM-15-28	>10 (11%)	>10 (5%)
148	KM-15-29	>10 (12%)	>10 (-1%)
149	KM-15-30	>10 (-5%)	>10 (7%)
150	MZ1412	>10 (11%)	>10 (39%)
151	MZ1411	>10 (8%)	>10 (42%)
152	MZ1439	>10 (-8%)	>10 (29%)
153	MZ1441	>10 (42%)	>10 (44%)

154	MZ1413	>10 (18%)	**8.14** ± 2.58
			max. inhibition of radioligand-binding: 84%
155	MZ1437	>10 (47%)	**1.72** ± 1.08
			max. inhibition of radioligand-binding: 100%
156	MZ1438	**4.66** ± 1.09	**0.571** ± 0.148
		max. inhibition of radioligand-binding: 82%	max. inhibition of radioligand-binding: 88%
157	MZ1440	>10 (2%)	**9.65** ± 4.37
			max. inhibition of radioligand-binding: 100%
158	MZ1414	>10 (14%)	**3.06** ± 1.09
			max. inhibition of radioligand-binding: 100%
159	MZ1451	**3.91** ± 1.08	**0.827** ± 0.287
		max. inhibition of radioligand-binding: 58%	max. inhibition of radioligand-binding: 87%
160	MZ1461	>10 (34%)	**1.41** ± 0.38
			max. inhibition of radioligand-binding: 100%
161	MZ1445	>10 (40%)	>10 (48%)
162	MZ1415	**1.18** ± 0.44	**0.481** ± 0.104
		max. inhibition of radioligand-binding: 100%	max. inhibition of radioligand-binding: 100%
163	MZ1446	**1.08** ± 0.47	**0.749** ± 0.344
			max. inhibition of radioligand-binding: 77%
164	MZ1463	>10 (35%)	**1.15** ± 0.48
			max. inhibition of radioligand-binding: 85%
165	MZ1457	>10 (31%)	**4.89** ± 0.91
			max. inhibition of radioligand-binding: 81%
166	MZ1462	**6.28** ± 4.80	
		max. inhibition of radioligand-binding: 67%	
167	MZ1448	>10 (49%)	**0.896** ± 0.157
			max. inhibition of radioligand-binding: 100%
168	MZ1456	**3.48** ± 1.72	**0.344** ± 0.104
		max. inhibition of radioligand-binding: 100%	max. inhibition of radioligand-binding: 67%
169	MZ1455	>10 (40%)	**2.28** ± 0.89
			max. inhibition of radioligand-binding: 100%
170	MZ1460	>10 (16%)	>10 (47%)
171	MZ1454	>10 (34%)	**1.69** ± 0.91
			max. inhibition of radioligand-binding: 76%
172	MZ1452	>10 (36%)	**1.62** ± 0.46
			max. inhibition of radioligand-binding: 100%

173	MZ1442	>10 (45%)	**1.09** ± 0.24 max. inhibition of radioligand-binding: 79%
174	MZ1444	>10 (2%)	>10 (43%)
175	MZ1417	>10 (20%)	**2.16** ± 0.72 max. inhibition of radioligand-binding: 100%
176	MZ1453	>10 (47%)	**0.786** ± 0.045 max. inhibition of radioligand-binding: 100%
177	MZ1418	>10 (37%)	**1.79** ± 0.55 max. inhibition of radioligand-binding: 100%
178	MZ1429	>10 (7%)	>10 (30%)
179	MZ1430	>10 (9%)	>10 (44%)
180	MZ1464	**10.2** ± 3.7 max. inhibition of radioligand-binding: 78%	>10 (37%)
181	KD478	>10 (30%)	>10 (30%)
182	KD107	>10 (11%)	>10 (29%)
183	KD477	>10 (24%)	>10 (46%)

[a] Chemical structures are shown in Table 11

The most affine compound was **168** with a K_i value of **0.334** µM for the CB_2 receptor. It was also a quite potent GPR18 agonist with an EC_{50} **0.352** µM. The most potent GPR18 agonist **162** proved to be also active at both CB receptors. For the CB_2 receptor, it showed a K_i value of **0.481** µM and a K_i value of **1.18** µM for the CB_1 receptor. This corresponds to a 25-fold selectivity for GPR18 over CB_2 and a 62-fold selectivity over CB_1.
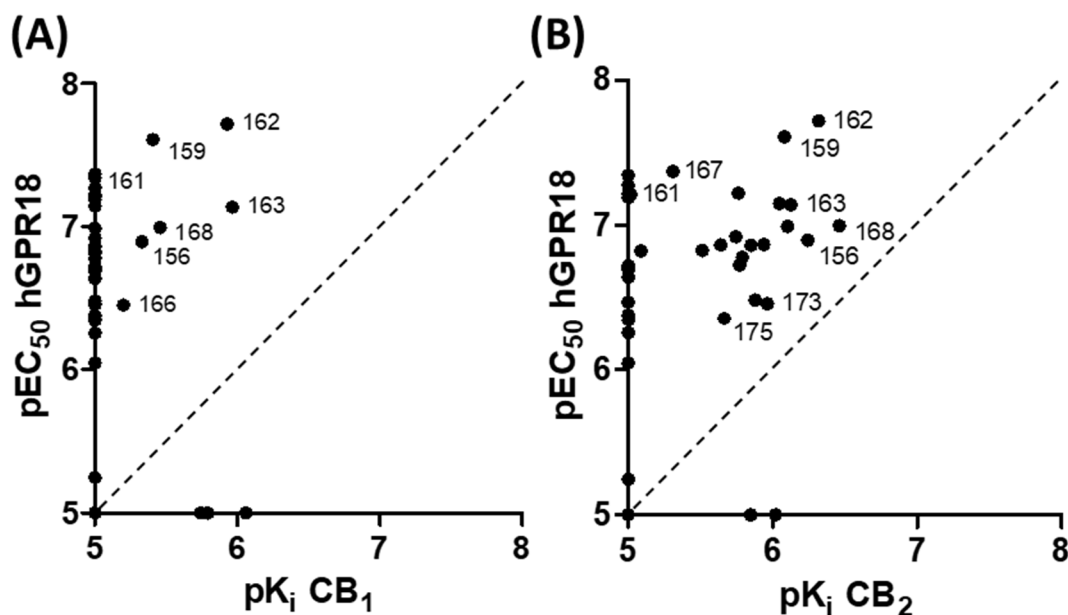
Figure 46: Selectivity of the newly discovered GPR18 agonists versus the cannabinoid receptors, (A) selectivity versus CB_1 receptor; (B) selectivity versus CB_2 receptor

In Figure 46, the affinity to the cannabinoid receptors was plotted against the activity at GPR18. From this graph, it is rather easy to identify the most selective compounds. The most selective compound was **161** with no affinity to the CB receptors up to concentrations of 10 µM and an EC_{50} value at GPR18 of **0.0454** µM. This result corresponds to a 220-fold selectivity for GPR18.
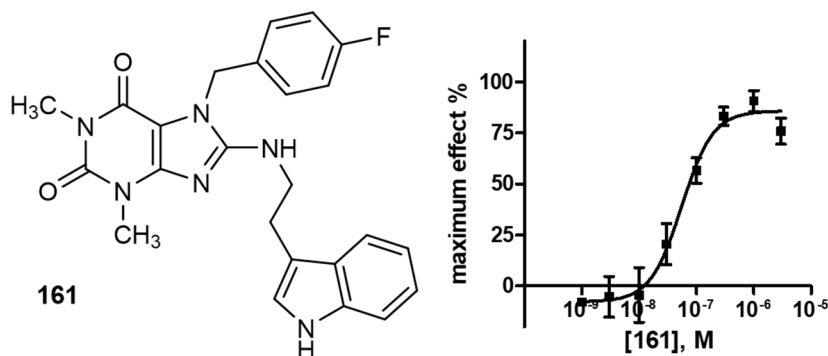
Figure 47: the most selective compound **161** of the indolylethylaminoxanthines
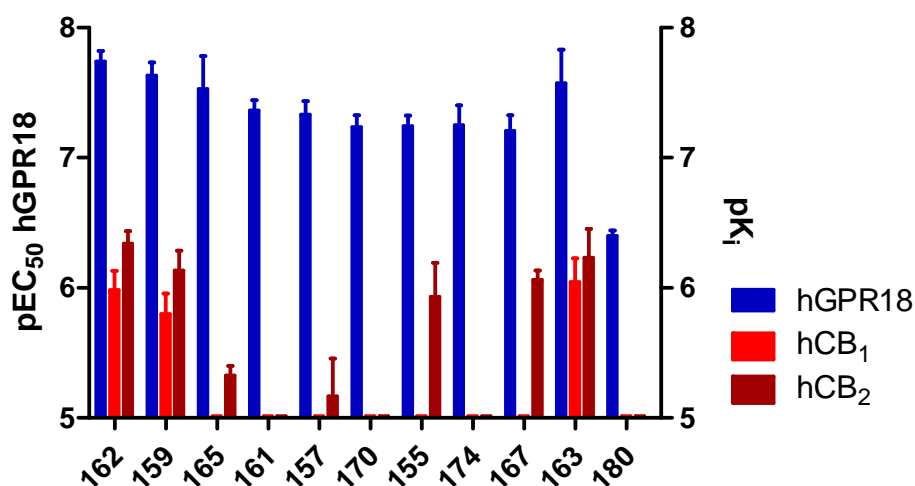
Figure 48: Selectivity profile of the ten most potent GPR18 ligands and compound **180**

When analyzing the affinity of the compounds for the CB- receptors, it can be observed that the same group of compounds were both the most potent at the CB_1 and to CB_2 receptor. From this, it can be concluded that the compounds do not have a selectivity between CB_1 and CB_2, although most of them were slightly more affine to the CB_2 receptors.
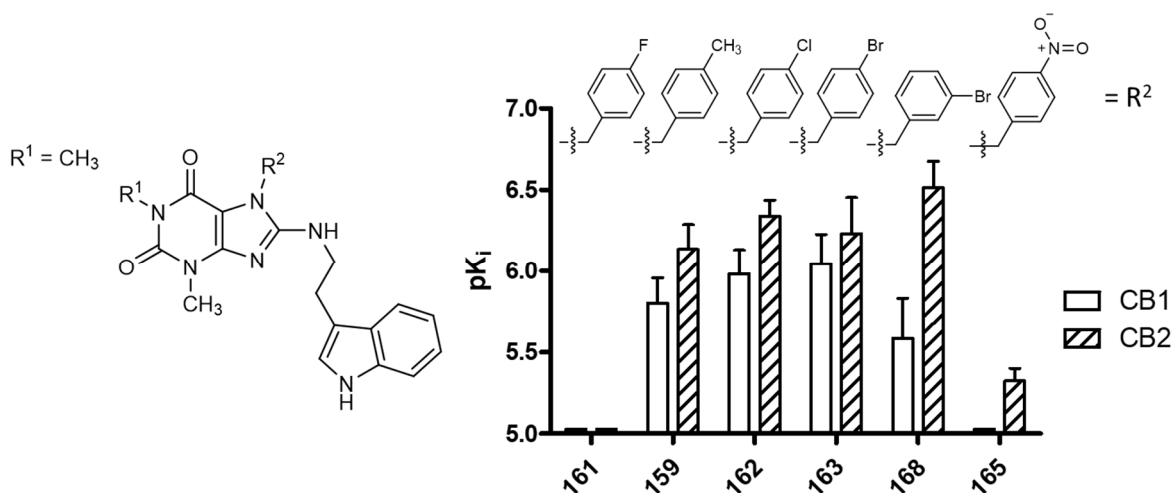
Figure 49: Structure-activity relationships for the affinity at the cannabinoid receptors

In Figure 49, the structure of some of the compounds are plotted with their R^2 residue. The compounds with a high affinity to the CB receptors showed a quite large lipophilic substitution, the *para*-chloro and *para*-bromo-derivatives being very potent. Interestingly, the smaller fluoro-substitution showed no affinity to the CB receptors up to 10 µM. For the *para*-nitro compound a low affinity to the CB_2 receptor can be observed, but no affinity to CB_1. With an EC_{50} value of **0.0462** µM for GPR18, it also belongs to the most potent compounds at this receptor.

One prominent result has to be mentioned: compound **180**, which resembles **162**, but differs only in the 5-hydroxy-group at the indole residue, showed no affinity to the CB_2 receptor. With a K_i value of **10.2** µM for CB_1 it was a rather weak ligand. Compound **180** was not as potent as compound **162** for GPR18, but still had an EC_{50} value of **0.340** µM.

Overall, it can be observed that some compounds of this new class of GPR18 agonists interact with CB receptors. The most potent compound **162** showed a 25-fold selectivity for GPR18 over CB_2 and a 62-fold selectivity over CB_1. With compound **161**, there was a compound that did not interact with the CB receptors up to a concentration of 10 µM. In general, compounds showed an affinity for the CB_2 receptor than for the CB_1 subtype and it was a typically higher at CB_2.

However, structure-activity relationships are still limited, and more data are required to fully analyze specific structure-activity relationships for each of these receptors.
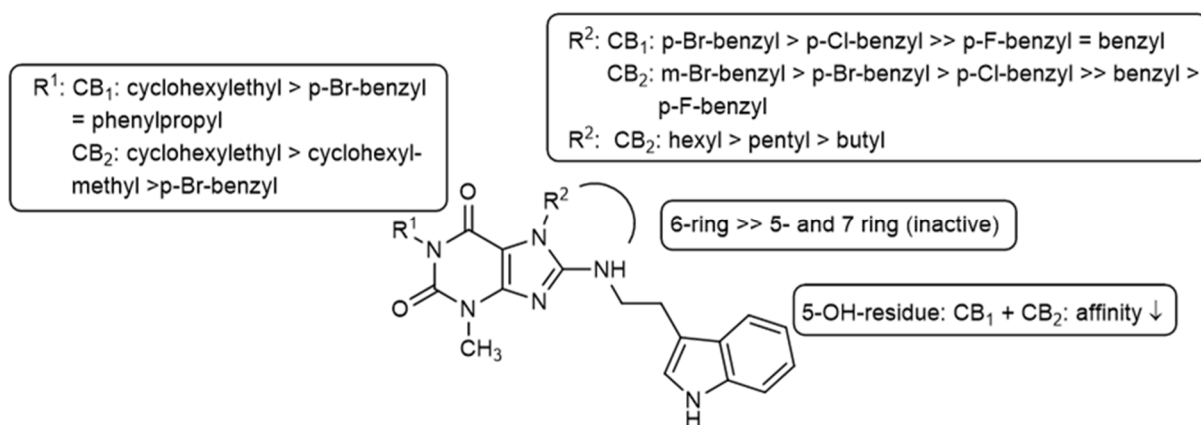
Figure 50: Structure-activity relationships for the cannabinoid receptors.

3.3.7. Selectivity of GPR18 agonists versus adenosine receptors

The compound group of pyrimidopurinediones was originally synthesized to study their structure-activity relationships at adenosine receptors. They have been investigated at A_1, A_{2A}, A_{2B} and A_3 receptors [171-175]

In the series of studies on this compound class at the adenosine receptors, the authors could observe some important structural features for adenosine receptor binding. For the A_{2A} receptor, phenylethyl-substituted compounds proved to be most potent.[174] Compound **182** has originally been synthesized in this set of compounds (compare Drabczyńska *et al.* **2007**). In the whole series, only two compounds exist with an indole residue. Compound **182** is one of them. The other one, compound **184**, has also been tested at GPR18, but showed no activity up to a concentration of 10 µM. As can be seen in Figure 51, it has a propyl residue in position R^1. In 3.3.3, we observed the importance of the methyl

substitution for R^1. Compound **184** with its propyl residue was not expected to be active and it fitted to the expectation.

182 $R^1 = CH_3$
$R^2 = CH_3$
184 $R^1 = CH_2\text{-}CH_2\text{-}CH_3$
$R^2 = CH_2\text{-}CH_2\text{-}CH_3$
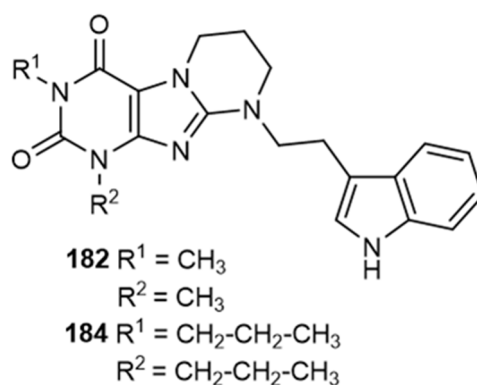
Figure 51: Chemical structures of compound **182** and **184**

In Table 14, the affinities of compound **182** and **184** are collected. Both compounds showed an affinity to the A_{2A} receptor. Compound **182** was more potent with a K_i value of **0.330** µM at the rat A_{2A} receptor.

Table 14: affinities of compound **182** and **184** at adenosine receptors, data were taken from Drabczyńska *et al.* **2007**.[174]

Compd.		**Radioligand binding**			
		K_i (µM) (% inhibition of specific binding)			
		rat A$_1$	**rat A$_{2A}$**	**human A$_{2B}$**	**human A$_3$**
182	KD-107	>25 (41%)[a]	**0.33** ± 0.07	~10 (56%)	>10 (21%)
184	KD-168	**1.79** ± 0.48	**0.90** ± 0.11	Nd[b]	>1 (9%)[c]

[a] tested at 25 µM
[b] nd, not determined
[c] tested at 1 µM

All compounds that were synthesized in this series were collected in a sublibrary. Many of these compounds show different substitutions instead of the indole residue. They were screened at the human GPR18 in β-arrestin assays (for results see Figure 53). The screen was performed for agonistic and antagonistic effects, and was repeated in case the initial screen was positive. In the first screen same few positive results could be detected. However, when they were retested three times none of the compounds showed any effects.
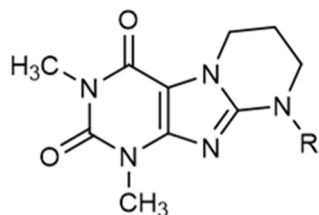
R = methyl, ethyl, propyl, butyl, pentyl, hexyl
R = isoproyl, isobutyl, 1-methyhexyl
R = cylylopropyl, -butyl, -pentyl, hexyl
R = adamantyl
R = phenyl, benzyl, naphthoyl
R = *p*-chloro-/methoxy-/ethoxy-/methyl-/ethylphenyl
R = *p*-fluoro-/chloro-/methoxy-/methyl-/ethylbenzyl
R = *m*-chloro-/trifluoromethylphenyl
R = *m*-methoxybenzyl
R = *p*-chloro-/*o,p*-methoxyphenylethyl
R = aminoethyl, diethylaminoethyl, hydroxy-*t*-butyl
R = 4-(1-hydroxyl-/1-methylcyclohexyl)
...

Figure 52: Lead structure of the compounds that had been synthesized for adenosine receptor ligand optimization.
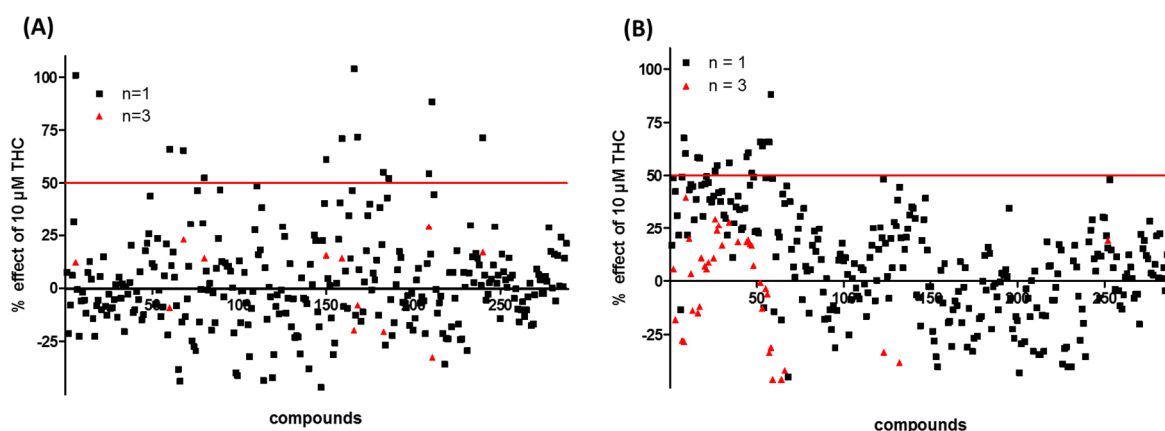
Figure 53: Screening result at GPR18. Initial screen with black labels, positive findings from the first screen were retested three times (red label). On the left side (A): screening of antagonists against 10 µM Δ^9-THC, on the right side (B): agonist screening, effects were compared to the activation of 10 µM Δ^9-THC.

From these results, it can be learned that the indole residue is very important for GPR18 activity. This sublibrary consists of many compounds with different substitution patterns at the 8-amino residue. Only compound **182** was a GPR18 agonist.

It should be further kept in mind that the initial hit compound **182** displays an affinity especially to the A_{2A} adenosine receptor. The newly synthesized compounds should also be tested for selectivity at the A_{2A} receptor.

3.3.8. Results and discussion

A new class of GPR18 agonists has been discovered and investigated in this study. The initial hit was found to be a moderately potent and selective agonist with an EC_{50} value of **0.556** µM. Its main structural feature was a pyrimido-purinedione ring system, substituted with an indolylethyl group.

Structure-activity relationship were subsequently investigated, which resulted in the optimized compound **162** with an EC_{50} value of **0.0191** µM. The indole residue proved to be crucial for GPR18 activation, as also the methylation of the N1-atom. Every attempt to change the N1-substitution resulted in a decrease in potency. At the N7-position, a lipophilic substitution was advantageous, with *para*-chloro-benzyl resulting in the most potent compound.

The selectivity of the compounds was assessed versus GPR55, a closely related orphan receptor in the same assay system, at which it showed no activity at all. Furthermore, the compounds were evaluated at the cannabinoid receptors, whereby compound **162** showed a 25-fold selectivity for GPR18 over CB_2 and a 62-fold selectivity over CB_1. Future studies should focus on modifications of the N3 and substitution of the indole ring.

Experiments with GPR18 antagonists led to the conclusion that Δ^9-THC and the new agonist class do not share the same binding site in the receptor. As a next step, we want to identify the binding site of compound **162** to understand the binding behavior and the generated data. This will be accomplished by site-directed mutagenesis studies. In this set-up, selected amino acids will be exchanged for other amino acids. If the selected amino acids are crucial for ligand binding, the EC_{50} value of the agonist will change. In order to know which amino acids may be important for ligand binding a homology model will be established. Based on docking studies, amino acids can be proposed that are predicted to interact with the ligand, and proposals for mutagenesis studies can be generated. The homology models were generated in cooperation during a three-month research stay in the laboratories of Prof. Jens Meiler, Vanderbilt University, Nashville, TN, USA, and continued in Bonn.

Compound **182** and **162** and all here investigated compounds share the indolyl residue, which is a preferred structure in nature. Especially, the amino acid tryptophan and its natural derivatives, for example, the tryptamines, contain such an indolyl residue. From a structural perspective compound **162** resembles more a peptide than a lipid. Aromatic substitution at N7 was beneficial for GPR18 activity. A possible overlay of the structures of a hypothetical dipeptide and compound **162** can be found in Figure 54. Other peptide-activated receptors can be found in relatively close phylogenetic relationship to GPR18, for example, the PAR1 receptor. There are also many related receptors, for which an endogenous ligand is not known. As long as the endogenous ligand has not been unambigously confirmed other hypotheses should also be considered and investigated.
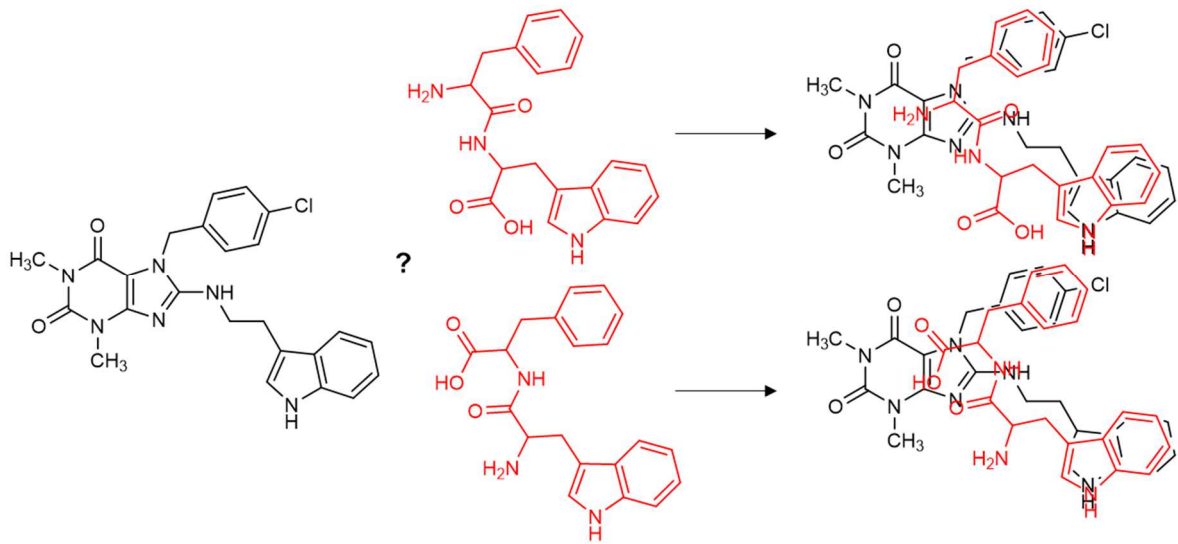
Figure 54: Structural similarity of compound **162** to peptides

3.4. GPR18 agonists: Evaluation at the mouse GPR18 receptor

3.4.1. Introduction

The newly described GPR18 agonists were evaluated at the mouse GPR18. GPCRs can share a high degree of conservation between related species, but there are also many examples, where the interspecies sequences are very different. There is no guarantee that a ligand developed and optimized for a human GPCR will also act in the same way or with the same potency at its mouse orthologue. Major species differences have been described for GPR35, which is closely related to GPR18. Kynurenic acid, which was identified in rat and proposed as an endogenous GPR35 agonist, acts only very weakly on human GPR35.[176,177] Therefore, it is now doubted that kynurenic acid could be the endogenous ligand.[178] Similarly, the human GPR35 radioligand [³H]PSB-13-253 binds with high affinities to the human GPR35 with an EC_{50} of **12.1** nM in β-arrestin assays[179] and a K_D of **5.27** nM[180] in radioligand binding experiments, but displays only a micromolar EC_{50} value at the mouse orthologue (Meyer and Thimm, unpublished results).

An important reason for investigating the activity of the ligands at mouse receptor is the fact that many experiments are conducted in mice. Especially, for target validation mice are of major importance. Knock-out mice, one of the most important pharmacological tools, exist for many genes (although none has been described for GPR18 so far). When working with a mouse model, it has to be ensured that the applied ligands are well characterized at the mouse receptor. Mouse studies are typically undertaken before a drug is delivered to humans for the first time. Therefore, a well-characterized pharmacological tool compound is needed for the mouse receptor.

3.4.2. Expression and establishment of a prolink1-mouse GPR18 cell line

The human and the mouse orthologues of GPR18 share a sequence identity of 86% (NCBI Blast). This reflects a high degree of homology. An alignment of the two sequences can be found in Figure 55.

```
mus   M A T L S N H N Q L D L S N G S H P E E Y K I A A L V F Y S C I F L I G L F V N V T A L W V F S C T T K K R T T V T I Y
homo  M I T L N N Q D Q P V P F N S S H P D E Y K I A A L V F Y S C I F I I G L F V N I T A L W V F S C T T K K R T T V T I Y

mus   M M N V A L L D L V F I L S L P F R M F Y Y A K G E W P F G E Y F C H I L G A L V V F Y P S L A L W L L A F I S A D R Y
homo  M M N V A L V D L I F I M T L P F R M F Y Y A K D E W P F G E Y F C Q I L G A L T V F Y P S I A L W L L A F I S A D R Y

mus   M A I V Q P K Y A K E L K N T G K A V L A C G G V W V M T L T T T V P L L L L Y E D P D K A S S P A T C L K I S D I T H
homo  M A I V Q P K Y A K E L K N T C K A V L A C V G V W I M T L T T T T P L L L L Y K D P D K D S T P A T C L K I S D I I Y

mus   L K A V N V L N F T R L I F F F L I P L F I M I G C Y V V I I H S L L R G Q T S K L K P K V K E K S I R I I M T L L L Q
homo  L K A V N V L N L T R L T F F F L I P L F I M I G C Y L V I I H N L L H G R T S K L K P K V K E K S I R I I I T L L V Q

mus   V L V C F V P F H I C F A V L M L Q G Q E N S Y S P W G A F T T F L M N L S T C L D V V L Y Y I V S K Q F Q A R V I S V
homo  V L V C F M P F H I C F A F L M L G T G E N S Y N P W G A F T T F L M N L S T C L D V I L Y Y I V S K Q F Q A R V I S V

mus   M L Y R N Y L R S V R R K S V R S G S L R S L S N M N S E M L
homo  M L Y R N Y L R S M R R K S F R S G S L R S L S N I N S E M L
```

predicted helix
typical conserved regions
disulfide

Figure 55: Alignment of the mouse (*Mus musculus*) and human (*Homo sapiens*) GPR18 sequences.

For pharmacological evaluation, the mouse receptor was expressed in a prolink1 vector from DiscoverX. The prolink1 vector contains the β-arrestin-galactosidase fusion protein. When ligated correctly into the plasmid, the receptor is expressed along with the enzyme complementation peptide, which is necessary for galactosidase activity. The purified plasmid will then be expressed via lipofection in CHO cells (DiscoverX®, suitable for β-arrestin assays), a cell line that already carries the gene for the β-arrestin-galactosidase fusion protein and a hygromycin resistance. The prolink1 vector contains a G418 resistance, which is used to select transfected cells. Non-transfected CHO-β-arrestin cells (DiscoverX) will be used as a control. After selection with G418, a first assay was conducted. If the first results were promising, a monoclonal selection would be undertaken, which ensures a high signal-to-noise ratio and a stable luminescence range.

(A) MZ1415 0.3 µM

(B) KD-107 3 µM

(C) Δ9-THC 10 µM

(D)

clone	Signal-to-noise-ratio		
	THC 10 µM	KD-107 3 µM	MZ1415 0.3 µM
clone 7	1.2	2.2	2.5
clone 14	0.8	1.3	1.3
clone 10	0.9	1.4	1.4
clone 16	1.2	1.9	2.3
clone 2	1.0	2.0	2.2
clone 8	1.2	2.2	2.5
clone 6	0.8	1.5	1.5
clone 13	1.0	1.7	1.4
polyclonal	1.1	1.5	1.7
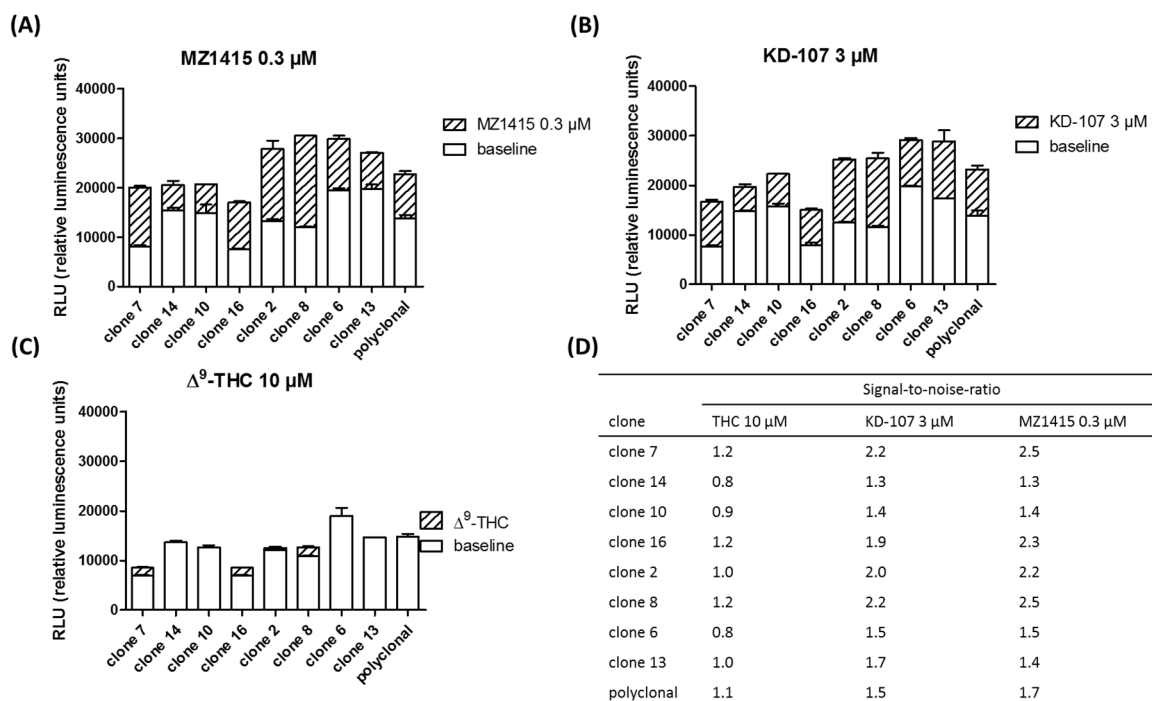
Figure 56: Signal-to-noise ratio for different mouse GPR18 clones.

95

In Figure 56, the signal-to-noise ratio for different mouse GPR18 cell line monoclones are depicted. The ratio can be found in the table in Figure 56 (D). Clone 7 and 8 performed equally well and showed the best signal-to-noise ratio higher than that of the polyclonal cell line. These were subsequently applied for further testing.

3.4.3. Standard ligands at the mouse GPR18

Some standard ligands have been investigated at the mouse GPR18 to characterize its pharmacology. First of all, the two agonists **162** and **182** were investigated. As can be seen in Table 15, the potencies of the standard agonists differ for both orthologue receptors.The compounds were more potent at the human as compared to the mouse GPR18. Compound **162** and **182**, the indole derivatives were 3-fold more potent at the human receptor.

Table 15: Potencies of standard agonists at the mouse and human GPR18

	EC_{50} (µM) mouse GPR18	EC_{50} (µM) human GPR18
KD-107	**1.78** ± 0.62	**0.556** ± 0.126
MZ1415	**0.0541** ± 0.0241	**0.0191** ± 0.0034
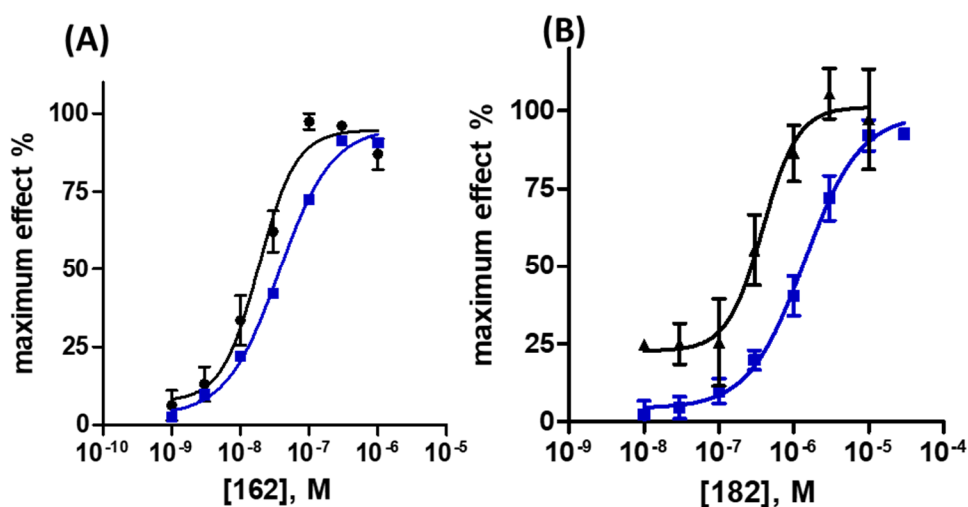
Figure 57: Concentration-dependent activation of the mouse GPR18 by selected agonists, (A) compound **162**, (B) compound **182**

In Figure 57, the concentration-dependent activation of GPR18 by the selected agonists can be observed. The maximum signal was obtained by applying 3 µM of compound **162** as a control. Compound **182** was also a full agonist compared to **162**.
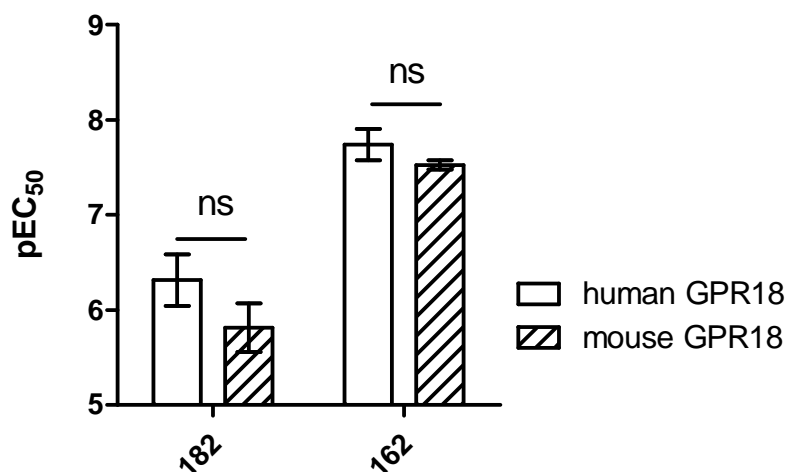
Figure 58: Potencies of Δ^9-THC, compound **182** and **162** at the human and the mouse GPR18 (ns= not significant; $p > 0.05$, pEC_{50} values with SD)

In Table 15, we could already see that compound **182** and **162** do not share the same EC_{50} value at both orthologous receptors. In Figure 58, the pEC_{50} values are compared for both species and a significance level was calculated. The pEC_{50} values of compound **162** and **182** were not significantly different (two-tailed t-test, $p > 0.05$). The compound class of indolylethylaminoxanthines was further investigated at the mouse GPR18 to get more information on the differences and similarities of the compound response. We also studied the effects of some cannabinoid compounds at the mouse GPR18.

3.4.4. Potencies of GPR18 agonists at the mouse GPR18

Here, all indolylethylaminoxanthines were tested to completely characterize their pharmacology at the mouse GPR18.

Table 16: Potencies of indolylethylaminoxanthines at the mouse GPR18

		mouse GPR18	
No.	Compd.[a]	antagonistic activity	agonistic activity
		$IC_{50} \pm SEM$ (µM)[b]	$EC_{50} \pm SEM$ (µM)[c] % efficacy[d]
120	MZ1458	>10 (-9%)	>10 (19%)
121	KM-15-1	>10 (-3%)	>10 (12%)
122	MZ1459	-	**0.527** ± 0.020 (79%)
123	MZ1416	-	**2.97** ± 1.02 (132%)
124	KM-15-3	>10 (-8%)	>10 (35%)
125	KM-15-4	>10 (3%)	>10 (23%)
126	KM-15-5	>10 (-8%)	>10 (11%)
127	KM-15-6	>10 (-3%)	>10 (17%)

128	KM-15-7	>10 (19%)	>10 (12%)
129	KM-15-8	>10 (11%)	>10 (12%)
130	KM-15-9	>10 (-3%)	>10 (19%)
131	KM-15-10	>10 (-6%)	>10 (16%)
132	KM-15-11	>10 (-6%)	>10 (24%)
133	KM-15-12	>10 (3%)	>10 (24%)
134	KM-15-13	>10 (-3%)	>10 (24%)
135	KM-15-17	>10 (-13%)	>10 (41%)
136	KM-15-14	>10 (6%)	~10 (52%)
137	KM-15-18	>10 (-13%)	>10 (36%)
138	KM-15-15	>10 (7%)	>10 (39%)
139	KM-15-16	>10 (8%)	>10 (13%)
140	KM-15-19	>10 (11%)	>10 (19%)
141	KM-15-20	>10 (9%)	>10 (39%)
142	KM-15-21	>10 (-6%)	>10 (21%)
143	KM-15-22	-	**1.69** ± 0.23 (106%)
144	KM-15-23	-	**1.67** ± 0.47 (115%)
145	KM-15-24	-	**3.15** ± 1.91 (75%)
146	KM-15-26	>10 (4%)	>10 (16%)
147	KM-15-28	>10 (-12%)	>10 (47%)
148	KM-15-29	>10 (-10%)	>10 (10%)
149	KM-15-30	>10 (-9%)	>10 (4%)
150	MZ1412	-	**0.379** ± 0.055 (85%)
151	MZ1411	-	**0.299** ± 0.109 (81%)
152	MZ1439	-	**0.129** ± 0.040 (85%)
153	MZ1441	-	**0.288** ± 0.055 (103%)
154	MZ1413	-	**0.207** ± 0.038 (111%)
155	MZ1437	-	**0.114** ± 0.024 (135%)
156	MZ1438	-	**0.156** ± 0.056 (120%)
157	MZ1440	-	**0.160** ± 0.066 (127%)
158	MZ1414	-	**0.194** ± 0.053 (116%)
159	MZ1451	-	**0.0463** ± 0.0058 (95%)
160	MZ1461	-	**0.171** ± 0.013 (96%)
161	MZ1445	-	**0.124** ± 0.056 (79%)
162	MZ1415	-	**0.0541** ± 0.0241 (100%)
163	MZ1446	-	**0.058** ± 0.008 (105%)
164	MZ1463	-	**0.216** ± 0.066 (112%)
165	MZ1457	-	**0.280** ± 0.194 (155%)
166	MZ1462	-	**0.150** ± 0.019 (87%)
167	MZ1448	-	**0.220** ± 0.062 (134%)
168	MZ1456	-	**0.180** ± 0.033 (101%)
169	MZ1455	-	**0.128** ± 0.018 (106%)
170	MZ1460	-	**0.157** ± 0.007 (96%)
171	MZ1454	-	**0.156** ± 0.013 (92%)
172	MZ1452	-	**0.245** ± 0.030 (108%)
173	MZ1442	-	**0.559** ± 0.050 (101%)
174	MZ1444	-	**0.244** ± 0.026 (104%)
175	MZ1417	-	**0.288** ± 0.071 (108%)
176	MZ1453	-	**0.127** ± 0.013 (100%)
177	MZ1418	-	**0.223** ± 0.043 (104%)
178	MZ1429	-	**0.334** ± 0.080 (88%)
179	MZ1430	-	**0.444** ± 0.084 (84%)
180	MZ1464	-	**0.638** ± 0.159 (114%)

181	KD478	>10 (37 ± 12%)
182	KD-107	**1.78** ± 0.62 (104%)
183	KD477	**0.583** ± 0.214 (111%)

[a] for chemical structures see Figure 27

[b] % inhibition of standard agonist induced luminescence signal, 0.3 µM compound **162**

[c] % activation compared to standard agonist induced luminescence signal, 0.3 µM compound **162**

[d] in comparison to 3 µM MZ1415

In Table 16, the potencies of all indolylethylaminoxanthines are collected. The two most potent compounds were **162** and **159**, the latter with an EC_{50} of **0.0463** µM. This resembles the results for the human receptor. Both compounds were slightly less active at the mouse receptor, but as we discussed above, this difference was not significant
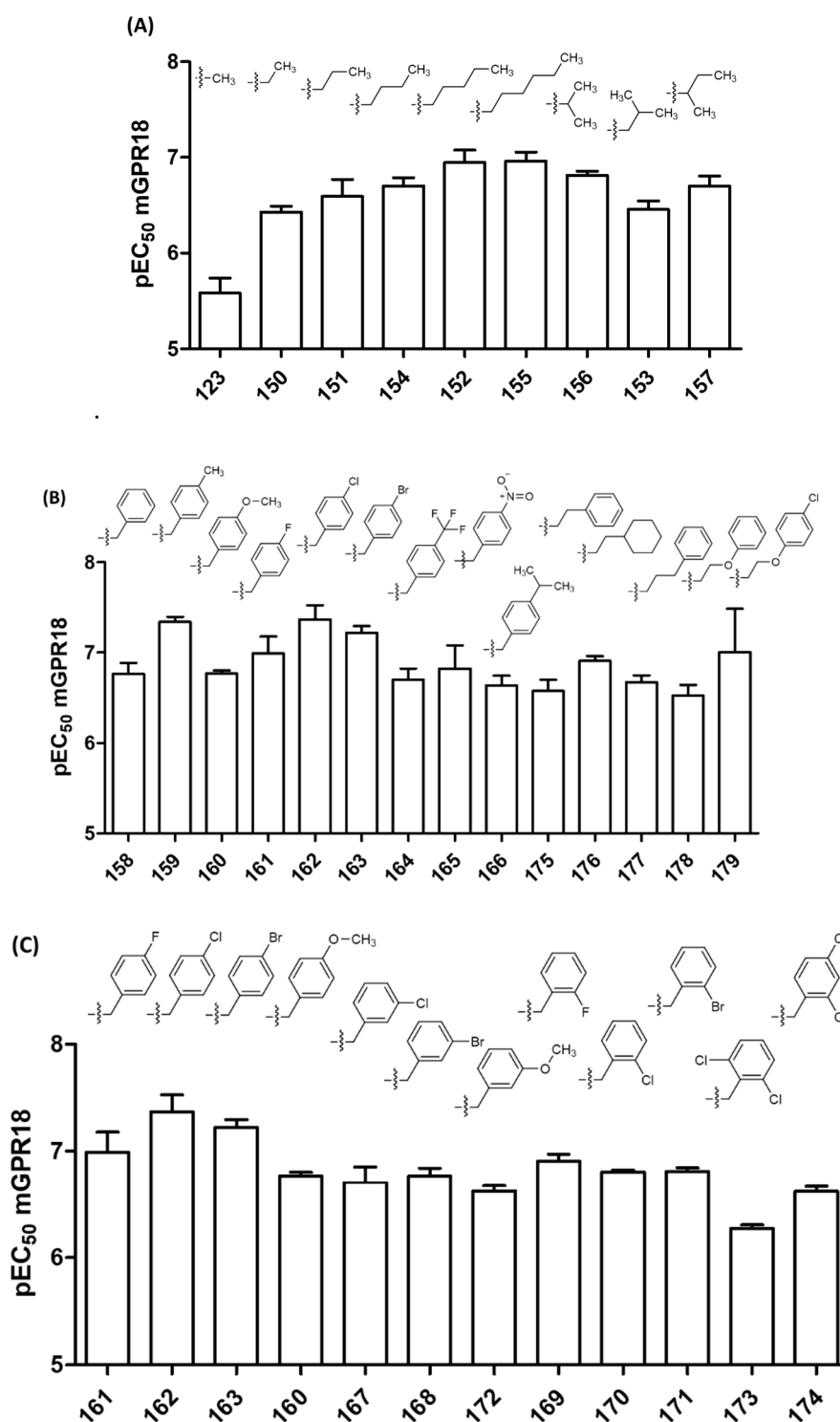
Figure 59: Structure-activity relationships for the mouse GPR18, (A) aliphatic substitutions at R^2; (B) *p*-substituted aromatic substitions at R^2; (C) other aromatic substitutions in R^2

Overall, the structure-activity relationships were equal to those of the human GPR18. A slight decrease in activity was observed at the mouse as compared to the human GPR18. This decrease was for some compounds larger, for example, for compound **165** or for **181**, which was not active up to 10 µM. But some compounds also displayed the same activity at both receptors. There was no clear pattern observable. When Figure 59 was compared to the results in 3.3.3, it can be concluded that the

structural elements defining GPR18 activation were preserved also for the mouse receptor. A correlation of the pEC_{50} values of the human and the mouse GPR18 is shown receptor in Figure 60.
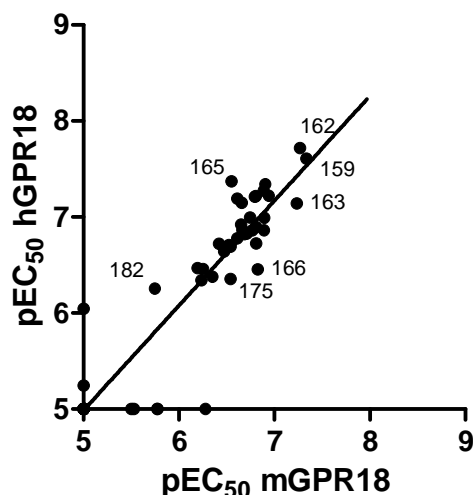
Figure 60: Potencies of indolylethylaminoxanthines at the human and mouse GPR18, r^2 = 0.8754

As can be seen above, the potencies laid on a straight line, indicating that the potency for both orthologues was linear. The slope of the straight line was 1.1, there was a slight preference for the human GPR18. Compound **165**, for example, was the compound with the strongest human GPR18 preference (compare human GPR18 EC_{50}: **0.0426** µM and mouse GPR18 EC_{50}: **0.280** µM) and compound **166** displayed the largest mouse GPR18 preference (compare human GPR18 EC_{50}: **0.352** µM and mouse GPR18 EC_{50}: **0.150** µM). The structure-activity relationships study and the selectivity plot both indicate that the GPR18 agonists were almost equipotent at both orthologues. This will be useful with regard to further studies in mice.

3.4.5. Evaluation of lipids and cannabinoids at the mouse GPR18

GPR18 has been described in the literature to be activated by several lipids, as for example AEA and NAGly (compare chapter 1.4.1). Rempel *et al*. could not observe any activation of the human GPR18 in β-arrestin assays by both lipids[66], although they have been reported to interact with GPR18 by Kohno *et al*.[60] and McHugh *et al*. [69,181] The latter group used a rat-derived cell line for their experiments, immortalized BV-2 microglia cells, which are employed as a model for microglial cells.[182] The most important lipids of this studies have also been investigated at the newly generated mouse GPR18 cell line. For this purpose, NAGly, AEA and AA-5-OH-HT have been chosen.

Table 17: Potencies of lipid compounds at the mouse GPR18

No.	compound	antagonistic activity	agonistic activity
		IC$_{50}$ ± SEM (μM)[a]	EC$_{50}$ ± SEM (μM)
1	AEA	>10 (8%)	>10 (4%)
10	NAGly	>10 (0%)	>10 (5%)
185	AA-5-HT	**14.6** ± 3.2[b]	>10 (-2%)

[a] 0.3 μM compound **162** was applied as agonist
[b] extrapolated

None of the lipids showed any activation of the mouse GPR18. **AA-5-HT** (arachidonoyl-serotonine) displayed weak inhibitory effects.

Cannabinoids also have been described to interact with GPR18, this has been investigated for the human receptor already in 3.1. Here, the potencies of the compounds have been evaluated for the mouse receptor.

Table 18: Potencies of phenolic cannabinoids at the mouse GPR18

	compound	antagonistic activity	agonistic activity
		IC$_{50}$ ± SEM (μM)[a]	EC$_{50}$ ± SEM (μM)
11	abn-CBD	**13.1** ± 1.7	>10 (8%)
12	CBD	**8.59** ± 1.77	>10 (14%)
13	O-1602	>10 (40%)	>10 (0%)
14	O-1918	**17.3** ± 4.2[b]	>10 (16%)

[a] 0.3 μM compound **162** were applied as agonist
[b] extrapolated

CBD, which was found to be an agonist at the human receptor of comparable potency to Δ^9-THC, acted as weak antagonist against compound **162** at the mouse receptor with an IC$_{50}$ value of **8.59** μM. **Abn-CBD** and **O-1918** also displayed weak inhibitory potency.

3.4.6. Discussion

The indolylethylaminoxanthines have been proven to be potent GPR18 agonists at the human orthologue of the receptor. In this chapter, they were also investigated at the mouse GPR18. This is important for their applicability in early target validation studies, which are typically conducted in mouse models. It could be shown that the agonists display a comparable activation at the mouse receptor. Only few compounds such as compound **182,** were slightly less active at the mouse receptor, but most other compounds showed no significant difference or were slightly more potent.

The GPR18 ligands described in literature such as anandamide (AEA) and arachidonoylglycine (NAGly) did not interact with the mouse GPR18 to recruit β-arrestin. Controversies regarding the reported activation data cannot be explained by interspecies differences. Nevertheless, further

investigation is necessary to understand the complex ligand behaviour of the endogenous lipids. For investigating GPR18 signalling, the newly developed compounds provide a reliable basis to study GPR18 pharmacology also in mice.

3.5. Molecular modeling of the human GPR18

3.5.1. Introduction

In section 3.3.5, it could be observed that the two agonists Δ^9-THC and the newly identified class of indolylethylxanthines probably interact with different sites of the receptor since antagonists behave differently when tested against each of the two agonist classes. While Δ^9-THC is a lipid-like compound the xanthines represent peptide-like structures. GPCR signaling can be modified by ligands in many ways. It has been known for a long time that so-called orthosteric and allosteric ligands can be differentiated. "Orthosteric" meaning the same binding site as the endogenous ligand and "allosteric" meaning a different binding site. As the GPCR receptor family consists of many diverse receptors, they also show very different binding sites for their endogenous ligands, thus reflecting the broad spectrum of very diverse endogenous ligands. The binding position of a large peptide consisting of hundreds of atoms and a small agonist with only dozens of atoms, will be completely different. Nevertheless, GPCRs all function in the same way and obey to the same rules.[183]

Especially in the δ-branch of class A GPCRs, this phenomenon has been observed before. When Zang *et al.* crystallized the P2Y$_1$ receptor, a nucleotide receptor and not too far relative of GPR18, in complex with a non-nucleotide antagonist, BPTU. This antagonist was found to probably approach its binding site at the very periphery of the helical bundle from the membrane side.[184] However, BPTU was an antagonist inhibiting the receptor. Kruse *et al.* crystallized the muscarinic M2 receptor not only in its inactive state, but also in its active state, using the superagonist iperoxo, which is more potent than the endogenous agonist acetylcholine, and additionally with a positive allosteric modulator. This positive allosteric modulator was shown to bind way up in the extracellular site of the receptor.[185] Recently, a binding site deep in the membrane and from the outside bending over helix VI has been reported for the glucagon receptor, a class B GPCR. Here, the antagonist captures the quite flexible helix VI, which is the major key player in receptor signal transduction towards the G protein.[186] But also, this compound was an antagonist. As it is much harder to get crystal structures of agonist-bound receptor states not so many crystal structures in the active state have been solved yet.

Which techniques are available to predict and understand ligand binding behavior? We used functional assays to characterize our newly designed agonists. A much more precise experiment, is to investigate the ligand binding in a radioligand binding experiment, in which the ability of a ligand to replace a labelled ligand is monitored. However, the design and establishment of a radioligand requires compound optimization, synthesis optimization and assay development. To fulfil the expectations on a radioligand, the corresponding compound has to have a high affinity (in the low nanomolar range) and suitable physiochemical properties, to reduce non-specific binding. Furthermore, there has to be

a suitable chemical structure that allows the labelling with a radioactive isotope in the last synthesis step. If a radioligand is replaced, the competing ligand and the radioligand likely share the same binding site. Allosteric modulation of radioligand binding can also be observed, but is much more challenging to interpret.[183]

Nevertheless, to know the exact binding partners of a ligand in a binding pocket, mutagenesis studies are necessary. An amino acid is exchanged for another one, which displays different functions. Most commonly, an amino acid is exchanged for a small amino acid such as alanine. Large changes can influence the protein topography, which can lead to non-functional receptors that may not be expressed on the cell surface. A receptor like a GPCR consists of many amino acids, and a binding pocket is formed by amino acids that can be positioned almost everywhere in the amino acid sequence. They do not even need to be neighboured since the folding of the protein generates an overall conformation, which is on the one hand defined by the arrangement of the amino acids direct next to each other, but also by amino acids from completely different parts of the sequence. Therefore, it is challenging to predict the amino acids that form a binding site if no crystal structure is available.

This kind of prediction is achieved with bioinformatic tools. To construct a model of a receptor a method called homology or comparative modeling is used, which is a so-called structure-based approach. This means, the gathered information is derived from a protein structure and corresponding models. First of all, it has to be checked, if a crystal structure of the target receptor exists. For the GPCRs it is rather hard to obtain crystal structures, because they are membrane bound proteins, that do not crystallize easily outside of lipophilic surroundings. When the first human GPCR was crystallized in 2007 by Brian Kobilka,[2] this was a breakthrough in the field. Nowadays, the number of crystallized GPCRs has been increasing, but still some GPCR families are unrepresented. In the δ-branch of class A GPCRs, only three receptors have been crystalized so far. For GPR18, there is no available crystal structure, so we used a homology modeling approach to construct a model of the receptor. The crystal structures of related receptors were used as templates. The sequences was compared and then a model was built based on the homology of the receptors. The less similarity between the receptors exists the more challenging is this approach. Several other conditions can also limit the success of the modeling performance: the number and states of the available templates, the resolution, the unique structural differences of the receptor of interest with the templates and the fitness of the method applied.[187] The basic principle of this method is depicted in Figure 61.
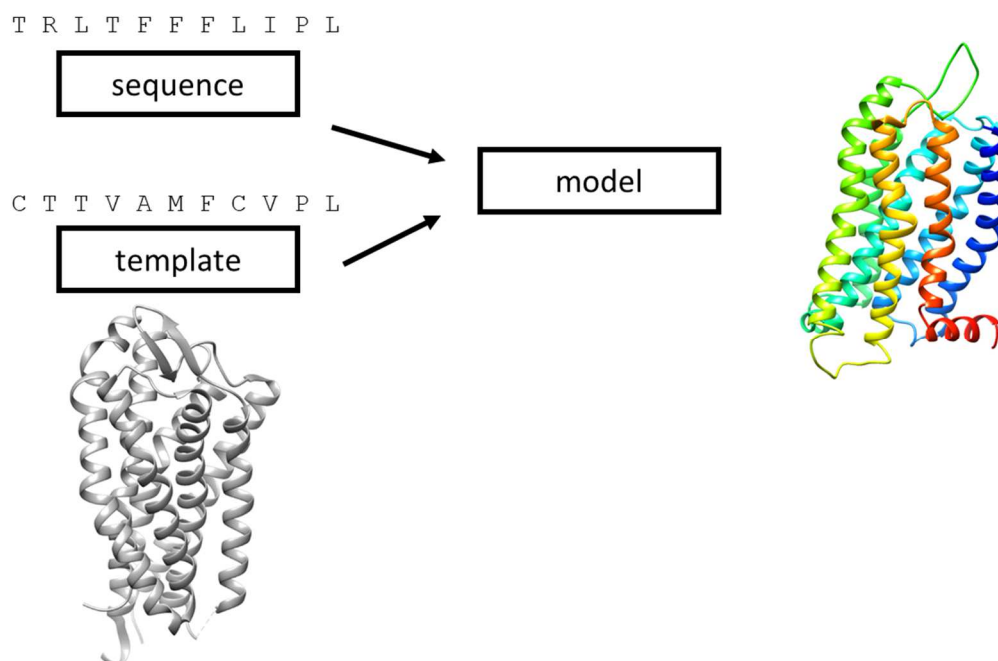
Figure 61: Structure-based molecular modeling approach

There exist different computational solutions to solve this task. In our study, we used the software Rosetta during a research stay in the laboratory of Prof. Jens Meiler the Vanderbilt University, Nashville, TN, USA. The Rosetta software suite, a command line driven application for Linux operating systems, has been developed and distributed by the labratory of Prof. David Baker from the University of Washington, Seattle, WA, USA. It works based on two major approaches: Rosetta takes on the one hand fragments out of the pdb library to obtain optimal conformations of the local peptide orientation and, on the other hand it optimizes the overall structure.[188] It uses Metropolis Monte-Carlo simulation algorithms. Rosetta was originally designed as a *de-novo* folding prediction tool for proteins that have no templates available. This means a construction from the primary structure directly to the correct conformation of a functional protein. However, this is a challenging task that has many limitations. *De-novo* folding reaches its limits at amino acid sequence lengths of 150. For larger proteins, the template-based approach is a much more productive way to circumvent the drawbacks of the *de-novo* predictions. In the Critical Assessment of Techniques for Protein Structure Prediction (CASP), Rosetta was able to solve one of the problems in *de-novo* folding almost perfectly.[189] Nevertheless, every modeling approach has its own challenges and difficulties.

The modeling undergoes a certain operational procedure, which is depicted below (Figure 62).
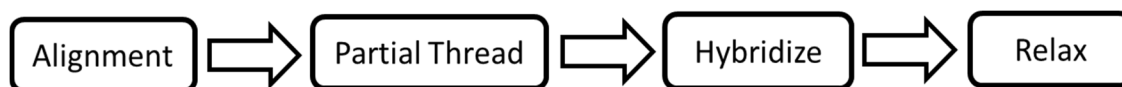
Figure 62: Workflow of by comparative modeling

All parts that involve modeling were done by this procedure, and each step was individually adapted to solve the arising problems. As a second step, the small molecule ligand was docked to the built model. Both procedures require selection processes. No prediction can produce a correct solution instantly. Every time, a large number of models were built, and out of this pool of models the most probable ones have been selected. The selection was based on a score that describes the energetic state of the model. The lower the value of the energy descriptor, the better the model is scored, the higher is the confidence in it. As the natural state is regarded as the energetically most favorable one, this is a rather straightforward kind of selection. But sometimes the best scoring model is not the natural state. Therefore, a second method is applied, which is called clustering. It ensures that not only the best scoring models will be taken forward, but also the models that are created most frequently. This is important to ensure a high degree of diversity, so that the final ensemble will most probably enclose models which resemble the natural state of the protein.[190]

One of the biggest challenges of this approach was to capture the loop conformations accurately. The transmembrane helical part of the GPCRs is quite well described and quite homologous in all known GPCR structures, and therefore, the confidence in the prediction of that part was higher. The major difference is found in the loop regions. GPCRs have three extracellular and three intracellular loops, which fulfill different functions. The outer loops can be involved in the ligand binding and activation processes, as for example in the PAR1 receptor (protease-activated receptor 1), where part of the *N*-terminal residues are cleaved by a protease and then activate the receptor.[191] On the intracellular site, the loops are involved in the G protein binding and activation. These loops will not be optimized in this project, because they presumably do not play an important role for ligand binding.

For GPCR comparative modelling, around 40 crystal structures are available. In some GPCR subfamilies, there are more solved structures than in others. GPCRs can be divided into different classes (in our case: class A rhodopsin-like GPCRs, the by far largest class), and further subdivided into subfamilies (in our case: δ-branch receptors). This already narrows down the available models. Normally, they are chosen by sequence identity. A sequence identity of less than 30% makes comparative modeling approaches more challenging. For GPR18 modeling, only class A GPCRS were taken as templates, class B receptors were already too different in sequence and structure. The largest number of known crystal structures exists for α-branch and γ-branch GPCRs. The γ-branch consists mainly of peptide receptors, and they all show some specific features, as for example, the occurrence of β-strands in their second extracellular loop (ECL2). The crystallization process in most cases requires a bound ligand (this minimizes the energy), but most of the receptors have been crystalized with an antagonist. Only very few models exist with an agonist bound. The first agonist state receptor that was crystallized by the Kobilka lab was the β_2-adrenergic receptor.[192]

The chosen models were taken forward to the next step of the modeling process, and either further modeling procedures or ligand docking were applied. Docking was executed by an application of Rosetta: RosettaLigand. Rosetta itself is designed as a software that can be easily adapted to specific scientific questions, by constructing applications in Rosetta via so-called xml-files. In these files, the special calculations and processes one wants the program to undertake, can be specified and adopted to one's needs. This gives the researcher a big freedom in the experimental set-up. RosettaLigand was designed as an xml-application, where key parameters can be adapted as required.[193,194]

To further evaluate the ligand position and to generate the right conformers the BCL (BiochemicalLibrary) was used, a software suite that is distributed by the laboratory of Jens Meiler. The BCL can construct quantitative structure-activity relationship models and be applied to ligand-based compound development.[195] In our case, it will be used to evaluate the docking procedure.

3.5.2. Alignment and template search

The sequence of the human GPR18 was downloaded in FASTA format from Pubmed protein sequence database (accession number: AAH66927, compare Figure 63). At first, suitable templates were identified and downloaded from the RCSB protein data bank. The NCBI Blast tool was used to search for appropriate structures. We specified to only search for amino acid sequences that have been crystallized (the so-called "pdb-search").[196] Structures were chosen according to their sequence homology in percent, the e-value (it describes the possibility to find random matches in large databases, the lower the value, the better, and the more significant is the match), the resolution of the crystal structure (the resolution in Ångstrom is a measure of the variability of the atom in space, it should be lower than 3 Å), and the conformational state of the model. All agonist state models were included, as we are going to dock an agonist to our models.

```
>hGPR18
MITLNNQDQPVPFNSSHPDEYKIAALVFYSCIFIIGLFVNITALWVFSCTTKKRTTVTIYMMNVALVDLIFIMTL
PFRMFYYAKDEWPFGEYFCQILGALTVFYPSIALWLLAFISADRYMAIVQPKYAKELKNTCKAVLACVGVWIMTL
TTTTPLLLLYKDPDKDSTPATCLKISDIIYLKAVNVLNLTRLTFFFLIPLFIMIGCYLVIIHNLLHGRTSKLKPK
VKEKSIRIIITLLVQVLVCFMPFHICFAFLMLGTGENSYNPWGAFTTFLMNLSTCLDVILYYIVSKQFQARVISV
MLYRNYLRSMRRKSFRSGSLRSLSNINSEML
```
Figure 63: sequence used for modeling, (accession number: AAH66927).

In total, a number of 18 crystal structures were chosen. They are briefly described in Table 19.

Table 19: Selected pdb templates.

Pdb-code	Receptor and description
3VWL	PAR1 receptor bound to the antagonist voraxapar, 2.2 Å, Zhang et al.[191], δ-branch receptor, 30% sequence identity
4XNV	P2Y$_1$ receptor bound to the allosteric ligand BPTU, 2.2 Å, Zhang et al.,[184] δ-branch receptor, nucleotide receptor, 23% sequence identity
4NTJ	P2Y$_{12}$ receptor bound to AZD1283, a non-nucleotide-antagonist, 2.62 Å, Zhang et al.[197], δ-branch receptor, nucleotide receptor, not listed by pdb-blast, but selected because of close phylogenetical relation
5DHG	Nociceptin/orphanin FQ receptor (NOP) in complex with C-35 (small molecule ligand), γ-branch receptor, peptide receptor, 3.0 Å, Miller et al.,[198] 25% sequence identity
4DJH	κ-Opioid receptor, in complex with JDTic (small molecule antagonist), 2.9 Å, Wu et al.,[199] γ-branch receptor, peptide receptor, 27% sequence identity
5C1M	μ-Opioid receptor with small molecule agonist BU72, 2.1 Å, Huang, et al.[200] γ-branch receptor, peptide receptor, 27% sequence identity
4N6H	δ-Opioid receptor in complex with naltrindole (small molecule antagonist), 1.8 Å, Fenalti et al.,[201] γ-branch receptor, peptide receptor, 26% sequence identity
4ZUD	Angiotensin receptor, in complex with the small molecule antagonist ZD7155, 2.8 Å, Zhang et al.,[202] γ-branch receptor, peptide receptor, 29% sequence identity
4MBS	CCR5 chemokine receptor bound to the small molecule antagonist maraviroc, 2.71 Å, Tan et al.,[203] γ-branch receptor, peptide receptor, 26% sequence identity
2LNL	CXCR1 chemokine receptor in phospholipid bilayers, NMR structure, Park et al.,[204] γ-branch receptor, peptide receptor, 26% sequence identity
3ODU	CXCR4 chemokine receptor in complex with the small molecule antagonist IT1t, 2.5 Å, Wu et al.,[205] γ-branch receptor, peptide receptor, 28% sequence identity
4XES	Neurotensin receptor in an active-like state bound to neurotensin, 2.6 Å, Krumm et al.,[206] β-branch receptor, peptide receptor, not listed by pdb-blast, but taken because of active state
2YDO	A$_{2A}$-receptor bound to adenosine, active state, 3.0 Å, Lebon et al.,[207] α-branch receptor, nucleotide receptor, 24% sequence identity
3PBL	Dopamine D$_3$ receptor bound to eticlopride (small molecule antagonist), 2.89 Å, Chien et al.,[208] α-branch receptor, biogenic amine receptor, not listed by pdb-blast, but taken to includediversity
4QKX	β$_2$-adrenergic receptor, agonist state bound to 35V, 3.3 Å, Weichert et al.,[209] α-branch receptor, biogenic amine receptor, 21% sequence identity
4IAR	5-HT$_{1B}$ serotonin receptor bound to ergotamine (small molecule antagonist), 2.7 Å, Wang et al.,[210] α-branch receptor, biogenic amine receptor, 20% sequence identity
3RZE	H1 histamine receptor in complex with the small molecule ligand doxepin, 3.1 Å, Shimamura et al.,[211] α-branch receptor, biogenic amine receptor, not listed by pdb-blast, but taken because of diversity
3UON	M$_2$ muscarinergic receptor bound to 3-quinuclidinyl-benzilat (small molecule antagonist), 3.0 Å, Haga et al.,[212] α-branch receptor, biogenic amine receptor, 23% sequence identity

In a first step, only the transmembrane domains were of major importance. The GPR18 protein sequence was aligned with ClustalOmega and transferred as textfile to Excel, where the alignment was adapted manually. The helix domains of each receptor were marked as determined visually in PyMOL. For GPR18, the transmembrane spanning domains were predicted with Octopus (http://octopus.cbr.su.se).[213] These domains were expected to be in the same range as the helix domains of the others. In this first step, the loop regions were not exactly aligned, they would be evaluated and eventually also modeled, when their performance was not good enough.

GPCRs are a big family of receptors that mediate quite comparable reactions – the transduction of a signal across the membrane to activate G proteins and recruit β-arrestins. Therefore, they also share some common structural sequences. Most of the receptors show two conserved motifs, the E/DRF motif at the end of the third helix, which maintains a hydrogen bond network that stabilizes the receptor. GPR18 shows this structural motif. Another common motif is the NPxxY motif at the end of the seventh helix, also establishing hydrogen bonds that are disrupted upon activation. Here, GPR18 is missing the conserved sequence, as can be observed in Figure 64.

Figure 64: Detail from the alignment: helix seven, hypothetical NPxxY motif, proline is numbered according to Ballesteros-Weinstein nomenclature.[214] Yellow: possible membrane spanning domains, beige: observed helix in crystal structure or model, magenta: conserved proline; h = human.

As can be seen in the detail of the alignment, GPR18 lacks the conserved proline and shows a valine instead. Proline is the only amino acid with a secondary amine – which means that the amine is not able to establish as many hydrogen bonds as a primary amine in the other amino acids. In the tertiary structure of proteins, it displays helix breaking properties. In many cases, the proline interrupts a straight helix and the amino acid chain bends at this point. Therefore, the exchange of conserved proline to a valine, as in this case, can be estimated to play a role in the formation of the tertiary structure. But not all GPCRs have this conserved proline, only around 90%.[215] Especially δ-branch GPCRs can show other motifs. All six depicted receptors (Figure 64) show an aspartate instead of an asparagine vicinal to the $P^{7.50}$, but the common opinion on that is, that both can maintain the same function in the hydrogen bond network. The two crystallized receptors, $P2Y_1$ and $P2Y_{12}$, both share the expected proline, but GPR55 and GPR35 have a valine or the related alanine, respectively. If and how

these lipophilic amino acids can contribute to the tertiary structure in comparison to proline still has to be evaluated, especially, as none of the already crystallized structures shows replacement of the proline $P^{7.50}$. This structural abnormality has to be taken into account, when judging the models.

Furthermore, it can be observed that GPR18 has one of the two "conserved disulfide bonds", between helix III and the extracellular loop 2, but not the other one that is present, for example, in P2Y$_1$ between the N-terminus and helix VII.[184]

Overall, GPR18 shows some of the common features of a GPCR, but also some specialties of the δ-branch receptors. In all further experiments, these will have to be evaluated in the context of the GPCR structures we already know.

The alignment for every step of homology modeling is always in construction and can be changed from one modeling round to the other quite fluently. Therefore, the presented alignments always refer to a certain problem and may not be true for every step.

3.5.3. Building the transmembrane domain

In the first approach of homology modeling, the transmembrane domains was built. Nevertheless, the whole receptor was constructed, but the orientation of the extracellular loops was of minor priority, as they were cleaved off and built individually when not performed correctly. For building the transmembrane domain, the RosettaCM application was used as described by the example material of the RosettaWorkshops, distributed by the laboratory of Prof. Dr. Jens Meiler (version: Rosetta 3.6 - 2016; and Rosetta 3.5 - 2015, http://www.meilerlab.org/index.php/rosetta-tutorials) and the protocols that were published by Bender *et al*.[216] with some adaptions to the system and problems of the present study.

In this first step, the transmembrane domains were aligned most tightly to avoid any holes in the transmembrane domains. This alignment was then used to generate so-called threaded templates – i.e. the alignment information was transferred into pdb coordinate information. With this and the applied information of transmembrane domains from Octopus-prediction, disulfide connection information and fragments RosettaCM constructed a large number of models. The models were refined by relax, and than evaluated by scoring and clustering. Out of 8800 models, 20 were chosen to be further proceeded. In Figure 65, the results of this first step can be observed, namely an ensemble of models, which were clearly different from each other. Subsequently, a single model is depicted.
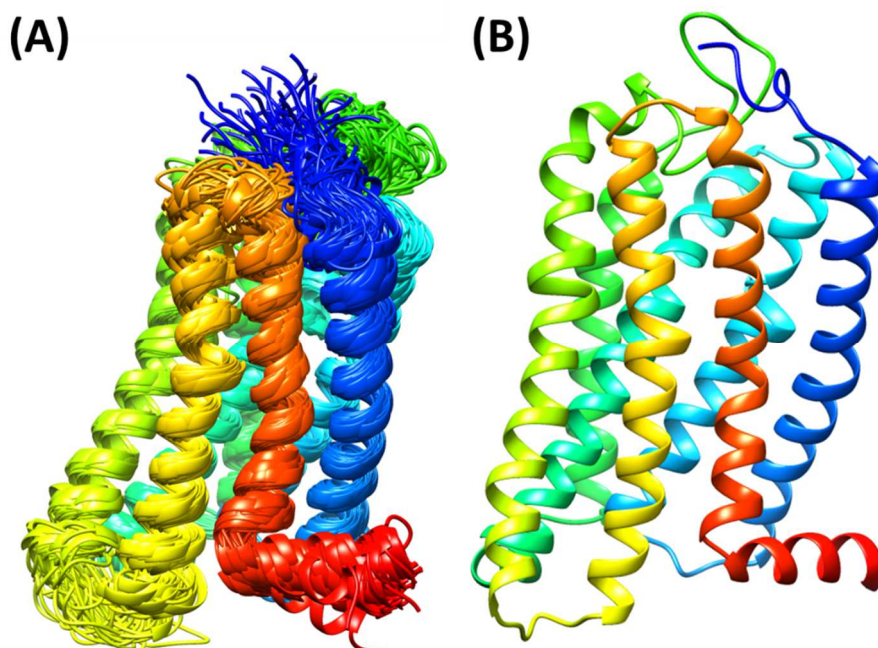
Figure 65: (A) Top scoring model ensemble, (B) a single model.

In this first step, the helices are judged based on visual examination. Important key issues are the kinking of helices, when a proline is present in the sequence. Also, the part of the model is examined, where the NPxxY motif is located. This can be observed in Figure 66.
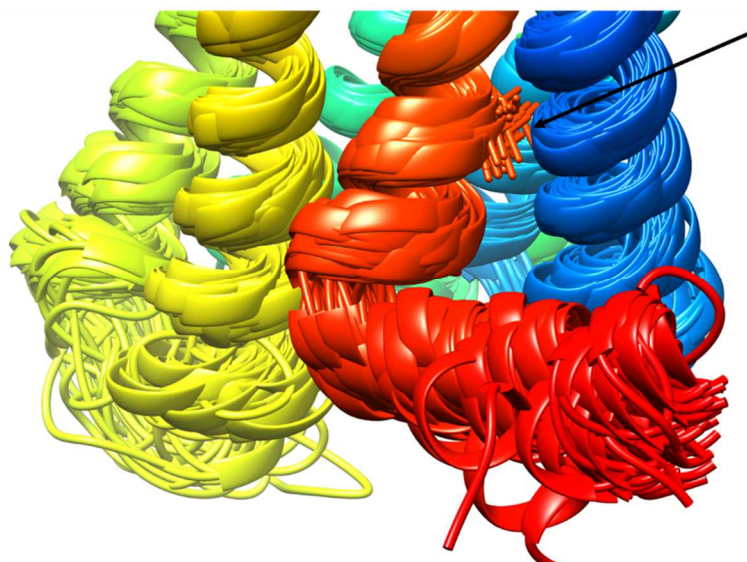
Figure 66: Detail from the ensemble: the arrow points to the position where GPR18 has a valine instead of the "conserved" proline.

Special attention was paid to capturing a broad diversity of models in this region. As no structure with such a motif exists every assumption could be misleading, and therefore models with the greatest

RMSD difference over this certain helix region were also included, when their overall performance was acceptable.

Interestingly, helix VIII was almost always completely built. There seemed to be a high degree of confidence in this secondary structural element, which does not exist in all GPCRs. For example, the P2Y$_{12}$ receptor also shows it, but not the P2Y$_1$ or the PAR1 receptor.[184,191,197] On the other hand, crystallization is always a non-natural state, because of the extreme conditions used in this procedure; more flexible regions will be impaired by crystallization more likely than rigid ones.
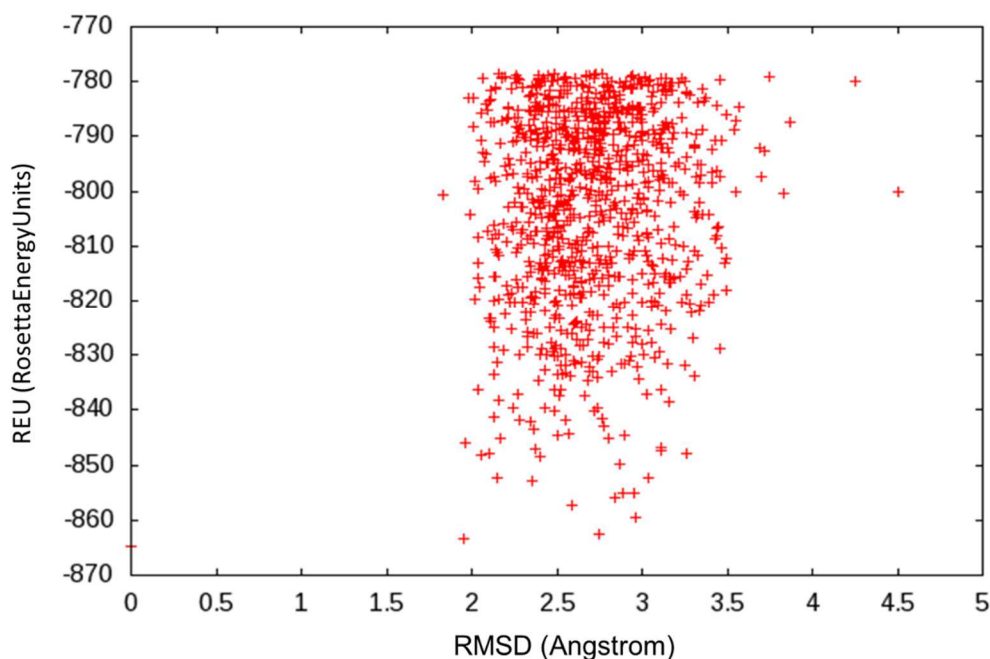
Figure 67: Top scores in RosettaEnergyUnits (REU) and RMSD (root mean square deviation) of the α-carbon atoms in comparison to the best scoring model

Only very few models have been completely disrupted or destroyed. In the Figure 68, the RMSD versus the top scoring energy units is pictured. The applied method should generate an ensemble of conformational diverse models, which can be measured by the RMSD (a measurement of the spatial similarity between proteins). Here, it can be seen that the best scoring model and all other models differ in the top scoring range between 2 to 4 Å RMSD, which can be regarded as an appropriate diversity.
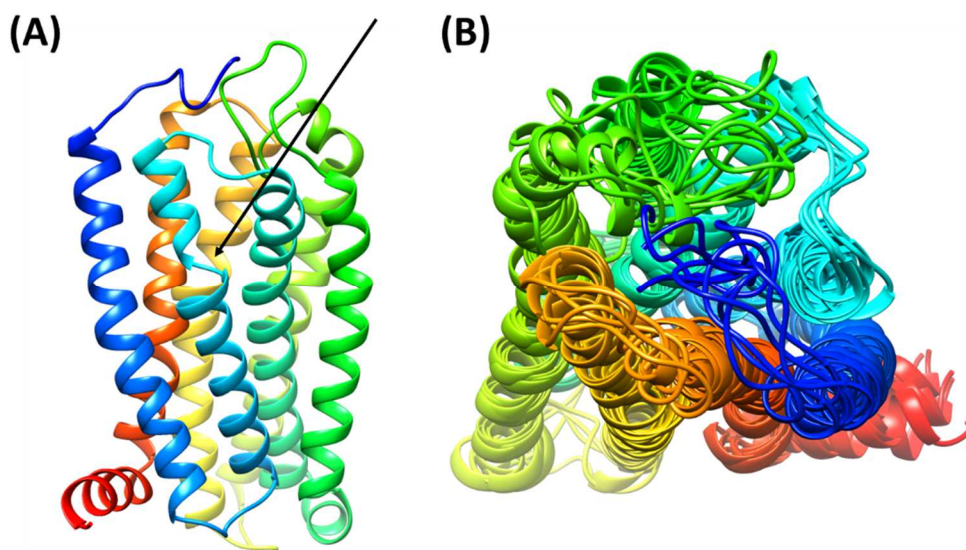
Figure 68: (A) One model out of the ensemble, the arrow points to an area that seems to be undefined in its secondary structure; (B) top view of the ensemble.

In Figure 68, the arrow points to a region, where the helix was not formed accurately. This must not be a sign of bad performance, especially in the case shown here. Whenever proline or glycine occurs in a helix, it will disrupt its straight orientation. By visual inspection, the best scoring models were selected when their helical orientation was accurate.

Nevertheless, the loop performance was not acceptable. The N-terminus was still too long and interacted with the protein structure to an extent that was not realistic (which is based on the assumption of the program to minimize surfaces). Therefore, it was chopped off. In the next chapter, we will discuss the orientation of the amino acids in the loops one by one, and there we will also see that the preliminary models did not capture the known side-chain orientations in an acceptable manner. This is the major reason for cutting the loops off and remodel them in a step-by-step procedure.

3.5.4. Loop building

There are three extracellular loops in a GPCR. ECL1 is a rather short and well-conserved loop, which was the reason to establish it first. ECL2 is long and curvy and can contain certain secondary structural elements, for example, β-strands, as in most of the γ-branch GPCRs (which are all peptide receptors). Therefore, it was built last. ECL3 is a little bit longer (5-9 amino acids), not so conserved but very well defined. A schematic overview is given in Figure 69. In contrast to the first modeling steps, the structure to be build comes with a template itself and additional sequence information. Moreover,

only the interesting parts of the template structures will be used to obtain models. We did not design the intracellular loops, as they do not play a significant role in ligand binding.

Subsequently, we tried to build the loops in the presence of the ligand. This should prevent the collapsing of the ligand binding pocket. This requires some adaptions to the protocol used for the hybridization step. To maintain an open conformation in the ligand binding pocket, the ligand MZ1415 will be docked in between.
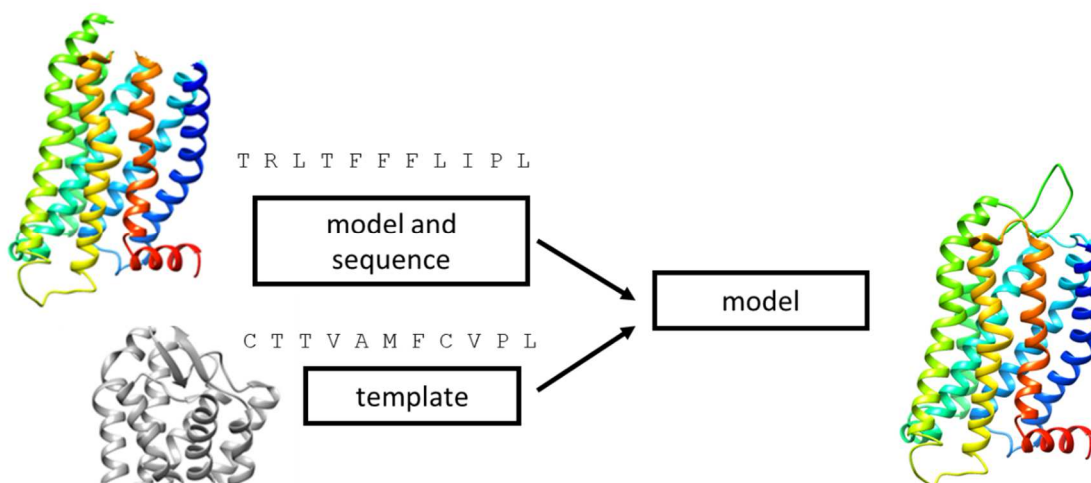
Figure 69: Procedure for loop modeling.

For the design of the loops, the alignments were adapted as necessary. For example, the A_{2A} receptor showed a completely different conformation in the ECL2, therefore, it will not be used as a template. By template selection and the alignment with the exactly matching amino acids, the loops were refined.

In total, the loop modeling will be pursued in the following sequence (compare Figure 70).
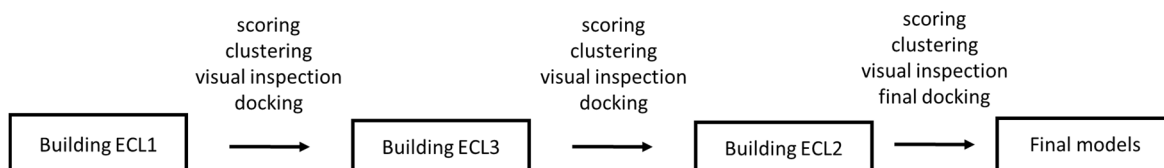
Figure 70: Workflow for loop modeling.

3.5.4.1. Extracellular loop 1

The extracellular loop 1 shows a highly conserved conformation in most of the GPCR subfamilies. With very few exceptions, it is characterized by a conserved tryptophan residue, which shows a very specific sidechain conformation (compare Figure 72 (A)); this has to be captured in a modeling

approach. As very good templates for modeling the peptide receptors of the γ-branch could be identified. They also contain the WPFG sequence that GPR18 shows. Therefore, we compared the sidechain orientation in these peptide receptors to evaluate our loop modeling results. The only receptor, that has no conserved tryptophan in that position, is the adenosine A_{2A} receptor. It shows a phenylalanine, which is also an aromatic amino acid (see alignment in Figure 71). The loop is located in light blue region. The conserved tryptophan is marked.

|			
hGPR18_begin of build	D L I F - I M T L P F R M F Y Y A -	K D - - - - - G E Y F	C Q I L G A L T V F Y
hGPR18_end of build	D L I F - I M T L P F R M F Y Y A -	K D - E W P F G E Y F	C Q I L G A L T V F Y
		ECL1	
3VWL_A	D V L F - V S V L P F K I S Y Y F -	S G S D W Q F G S E L	C R F V T A A F Y C N
4XNV_A	D F L Y - V L T L P A L I F Y Y F -	N K T D W I F G D A M	C K L Q R F I F H V N
4NTJ_A	- - - - - - - - - - - - - - - - -	- - - - - - - - - -	- - - - - - - - - -
5DHG_A	D T L V - L L T L P F Q G T D I L -	L G - F W P F G N A L	C K T V I A I D Y Y N
4DJH_A	D A L V - T T T M P F Q S T V Y L -	M N - S W P F G D V L	C K I V L S I D Y Y N
5C1M_A	D A L A - T S T L P F Q S V N Y L -	M G - T W P F G N I L	C K I V I S I D Y Y N
4N6H_A	D A L A - T S T L P F Q S A K Y L -	M E - T W P F G E L L	C K A V L S I D Y Y N
4ZUD_A	D L C F - L L T L P L W A V Y T A -	M E Y R W P F G N Y L	C K I A S A S V S F N
4MBS_A	D L F F - L L T V P F W A H Y A A -	A - - Q W D F G N T M	C Q L L T G L Y F I G
2LNL_A	D L L F - A L T L P I W A A S K V -	N - - G W I F G T F L	C K V V S L L K E V N
3ODU_A	D L L F - V I T L P F W A V D A V -	A - - N W Y F G N F L	C K A V H V I Y T V N
4XES_A	D L L I - L L A M P V E L Y N F I W	V H H P W A F G D A G	C R G Y Y F L R D A C
2YDO_A	D I L V G V L A I P F A I A I S - -	T G - - F C A A C H G	C L F I A C F V L V L
3PBL_A	D L L V A T L V M P W V V Y L E V -	T G G V W N F S R I C	C D V F V T L D V M M
4QKX_A	D L V M G L A V V P F G A A C I L -	T K - T W T F G N F W	C E F W T S I D V L C
4IAR_A	D L L V S I L V M P I S T M Y T V -	T G - R W T L G Q V V	C D F W L S S D I T C
3RZE_A	D L I V G A V V M P M N I L Y L L -	M S - K W S L G R P L	C L F W L S M D Y V A
3UON_A	D L I I G V F S M N L Y T L Y T V -	I G - Y W P L G P V V	C D L W L A L D Y V V

Figure 71: Alignment for modeling of ECL1. ECL1 in light blue, conserved tryptophan in blue and conserved cysteines, forming a disulfide bond, in turquoise.

The procedure for loop modeling resembles the procedure for the overall receptor modeling, with the difference, that the program is provided with template files, that only consist of the part of the receptor, which is shown in the alignment. In the beginning, it was almost impossible to capture conformations with tryptophan in a plausible orientation (compare Figure 72, (B)). The tryptophan tended to flip around. By exactly determining the pose of the tryptophan in the templates, certain defined key features could be noted, as, for example, the angles of the bonds between the C-α and C-β atom of the tryptophan. They were then constrained. A constraint in Rosetta means a defined specification that is provided to the program and has to be fulfilled. For this tryptophan, we constrained angles and distances to the neighboring atoms of different residues. With this addition to the protocol, the tryptophan could finally be located as it was supposed to, compare Figure 72, (C).
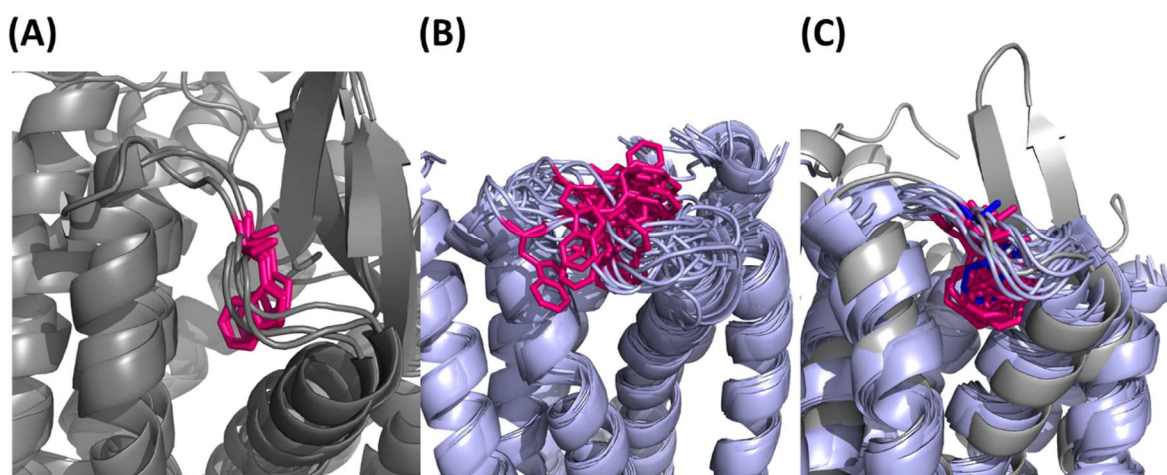
Figure 72: Conformation of the conserved tryptophan in ECL1 (pink residue): (A) templates (grey) 3VW7, 4N6H, 4XNV; (B) first modelling attempt (C) after constraining the conserved tryptophan; overlay of models (light blue) and the template structure 4MBS (grey).

3.5.4.2. Extracellular loop 3

The extracellular loop 3 contains five amino acids in GPR18. When aligning the templates to GPR18 based on the starting point of the helices, it became obvious, that ECL3 can have different lengths in different templates. In Figure 73, the amino acids that were aligned to the two last helix residues are highlighted.
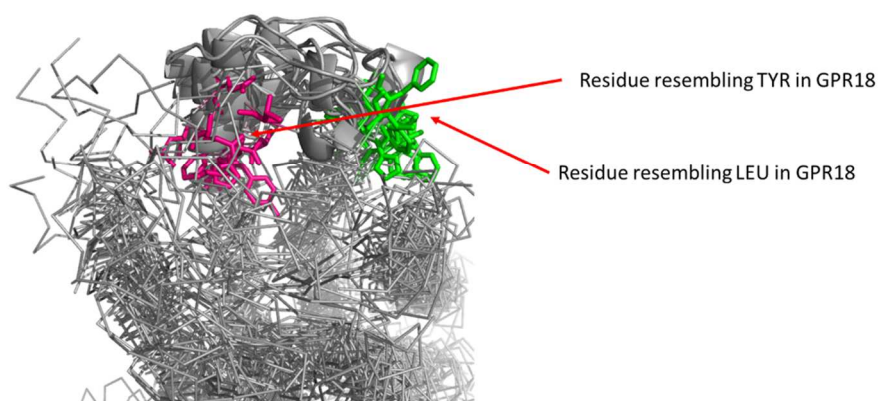
Figure 73: ECL3 – in pink the residues that resemble TYR in GPR18 and in green those that resemble LEU in GPR18 are shown.

In the alignment in Figure 74, it can be observed that the length of the ECL3 appears to be typical for each branch. The short ECL3 is shared by the α-branch receptors (many biogenic amine receptors). The peptide receptors of the γ-branch have the longest ECL3, or longer helices. The last amino acid of the helices were determined in the GPR18 models and in the aligned templates by visual inspection (pink and green residues in Figure 73). An additional grey helix turn can be observed for some

117

structures above the pink colored residue. This refers to the templates with more amino acids. To prevent Rosetta from applying helix turns in the models, the alignment shows a gap at this point.

The alignment of the structures and sequences further shows that the GPR18 ECL3 resembles more the α-branch receptors.

Figure 74: Alignment of ECL3 with the corresponding templates, green and pink border refer to the designated residues in Figure 73

In this step, we generated 4400 models. They were evaluated by visual inspection, and by scoring and clustering. When first inspecting the models, it became obvious that the arrangement of the side chains of the former models were altered again. This could be prevented by applying the former constraints also in this step, compare Figure 75.
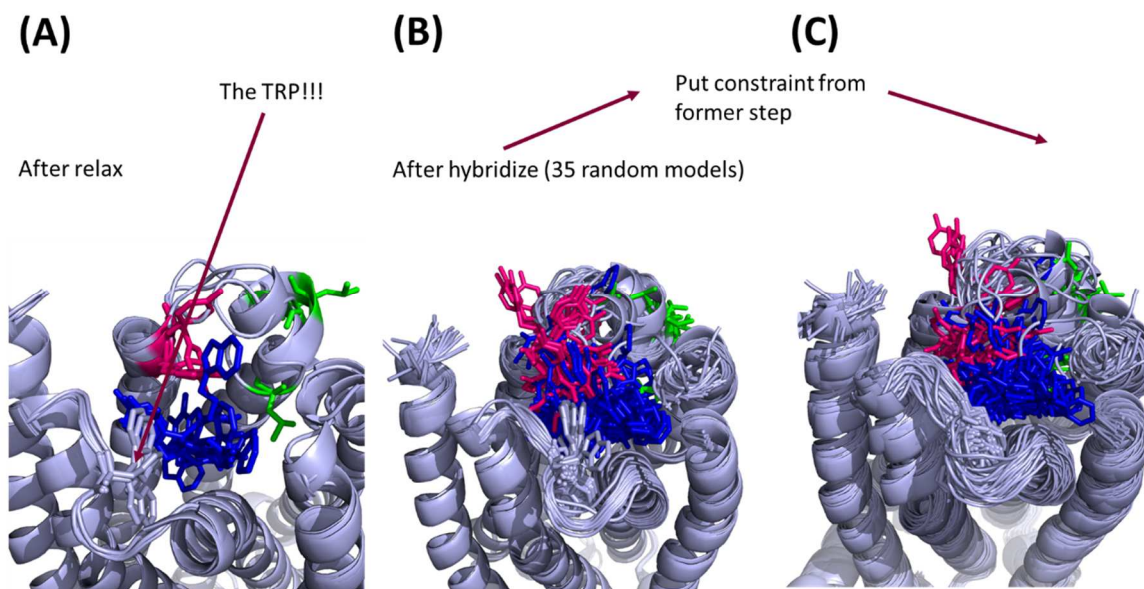
Figure 75: In each part of the picture are 35 random models; blue = the ligand, pink = tyrosine, green = leucine. (A) After the relax step (without constraints) the TRP that was carefully assigned in 3.5.4.1 is turned around again. (B) After the hybridize step, it can be seen that the TRP is already moved around. (C) putting the ECL1 constraint in the relay step prevents it from turning around.

When selecting appropriate models, one key issue was the tyrosine (pink in Figure 75), which should be pointing into the receptor inner space. Loops, where it bent far to the outside, did not resemble the template conformations so well.

ECL3 was the only loop, where it was possible to construct the loop in the presence of the ligand. This is the reason, why the ligand (blue) is visible in the pictures in Figure 75.

Overall, it can be concluded that the straightforward loop modeling of the ECL3 came rapidly to a plausible result. The first obstacle, the ECL1-TRP conformation, could be overcome easily by applying a logical constraint.

3.5.4.3.   Extracellular loop 2

The extracellular loop 2 is by far the longest missing structural element. When comparing the ECL2's of different templates some structural differences can be observed. There are receptors, as the γ-branch receptors, but also the δ-branch receptors, that have beta-strands in the ECL2. Another important feature, that has to be noticed, is the conserved disulfide bond, that forms between helix III and the ECL2. The most important goal of this approach is the reformation of this disulfide bond.
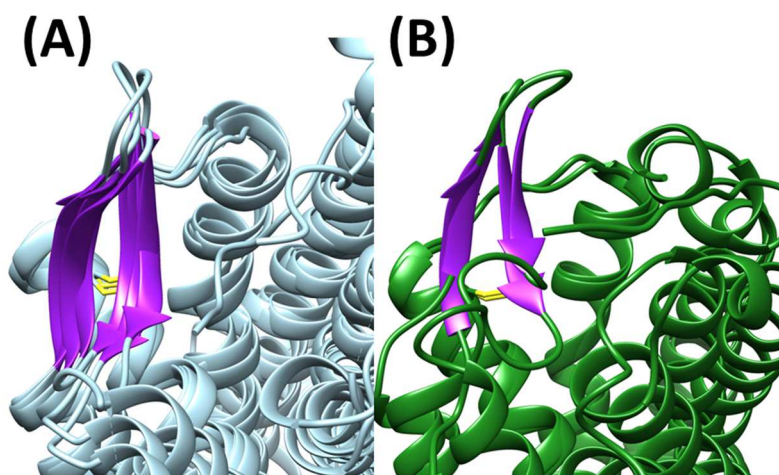
Figure 76: Comparison of ECL2 of (A) 4N6H/δ-opioid, 4ZUD/angiotensin, 5C1M/μ-opioid, 4DJH/κ-opioid and (B) δ-branch receptors (3VW7/PAR1, 4XNV/P2Y1).

In Figure 76, these two subfamilies can be compared. It can be observed, that all of the receptors show a disulfide bond. Nevertheless, there are differences. For example, the β-strand of the γ-branch receptor form directly the next helix, while the δ-branch receptors on the righthand side show an additional coil before forming the helix. Furthermore, the β-strand seems to be one residue longer in the γ-branch receptors, having the disulfide bond situated a little bit higher. In the alignment, this was

taken into account. Still, it has to be mentioned, that visualization is not without mistake and some differences might also be due to the visualization software.

Another aspect has to be pointed out: the GPR18 sequence in this region is quite unique. In contrast to the sequence observed in the template structures, it shows a proline in the region, where a β-strand could be expected (compare Figure 77). Proline cannot participate in as many hydrogen bonds as other amino acids. In β-strands, every amino group is part of the necessary hydrogen bonding - therefore, in this case, proline can be assumed to not favor β-strand formation. The two neighbor amino acids have to form the hydrogen bonds. GPR18 can form the conserved disulfide bond, as the templates also do.

Figure 77: Sequence alignment of the human GPR18 and chosen templates for ECL2.

When predicting the secondary structure for the ECL2 loop region with jufo_2 and psipred (depicted in Figure 78), the results were not completely clear, but showed a strong preference. Wherever an E can be observed in the third row, the program proposes a β-strand. As this is an anti-parallel β-strand, there have to be two parts of β-strand prediction, which was the case with psipred. Further, psipred predicted both strands with six amino acids, which can be critically assessed. In the models, a lysine forms the last helix amino acids, it is lysine with the pose number 142, which therefore will not be part of a possible β-strand. This prediction was more accurate with jufo_2. On the other hand, for jufo_2, there was only one region of Es to be observed, which is undecided on the possible formation of anti-parallel β-strands. As both at least indicate the later part of the β-strand, the full formation was with a high probability the right structural element to choose.

	Jufo_2					psipred		
Pos.-Nr. aa		coil	helix	β-strand	Pos.-Nr. aa		coil	helix	β-strand
139 L H		0.294	0.553	0.153	139 L H		0.147	0.764	0.099
140 L H		0.191	0.602	0.207	140 L H		0.026	0.749	0.259
141 L H		0.232	0.550	0.218	141 L E		0.009	0.433	0.722
142 L H		0.298	0.463	0.239	142 L E		0.047	0.150	0.754
143 Y C		0.410	0.383	0.207	143 Y E		0.136	0.059	0.621
144 K C		0.465	0.304	0.231	144 K E		0.324	0.038	0.426
145 D C		0.498	0.294	0.207	145 D E		0.474	0.020	0.394
146 P C		0.538	0.263	0.199	146 P E		0.284	0.041	0.602
147 D C		0.520	0.264	0.217	147 D E		0.202	0.017	0.706
148 K C		0.526	0.268	0.206	148 K C		0.745	0.042	0.225
149 D C		0.539	0.286	0.175	149 D C		0.945	0.014	0.033
150 S C		0.613	0.243	0.145	150 S C		0.980	0.010	0.016
151 T C		0.586	0.252	0.162	151 T C		0.911	0.009	0.070
152 P C		0.381	0.346	0.273	152 P E		0.399	0.007	0.543
153 A H		0.202	0.406	0.391	153 A E		0.078	0.003	0.873
154 T E		0.183	0.316	0.501	154 T E		0.012	0.003	0.962
155 C E		0.235	0.327	0.437	155 C E		0.013	0.005	0.952
156 L E		0.247	0.335	0.418	156 L E		0.078	0.009	0.836
157 K C		0.366	0.365	0.270	157 K E		0.295	0.007	0.678
158 I C		0.452	0.340	0.209	158 I C		0.898	0.007	0.108
159 S C		0.484	0.336	0.180	159 S C		0.973	0.007	0.018
160 D C		0.533	0.358	0.109	160 D C		0.896	0.048	0.015
161 I C		0.471	0.428	0.101	161 I H		0.166	0.834	0.002

Figure 78: Secondary structure predicition using the tools jufo_2[217] and psipred[218], in the first row the Rosetta pose number can be found, then the amino acid one letter code, the predicted secondary structure (H = helix, C = coil, E = β-strand) and the probabilities for each of these secondary structures.

When pursuing the ECL2 loop modeling, initial results were quite disappointing. There was a bad recovery of the disulfide bond and the loop was not built in the right place. Some adaptions to the original protocol were executed and led to an optimized performance, view Figure 79 (major optimization included: the template to model ratio in xml files, the alignment of 3D coordinates of templates and models for threading process, and the inclusion of far more template material in the threading process and deletion of the ligand).
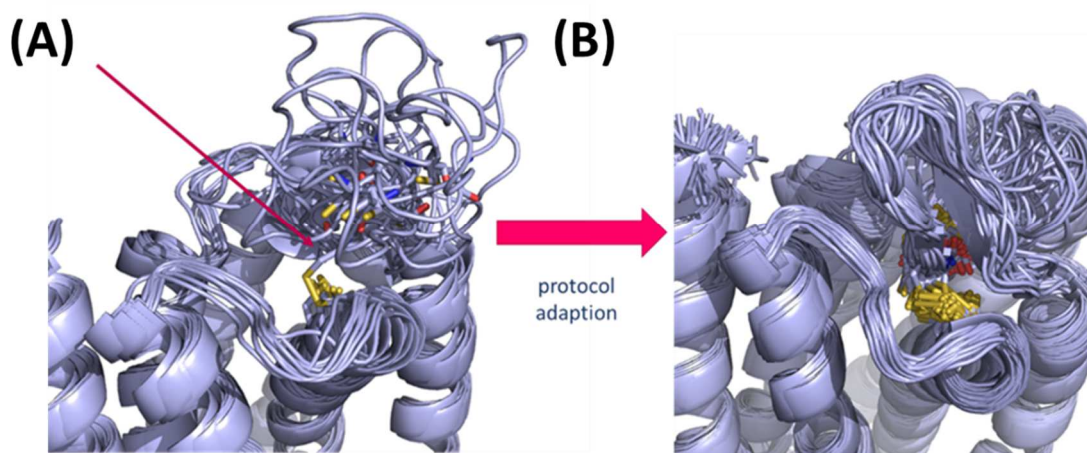

Figure 79: (A) First attempts to model ECL2, (B) the optimized protocol shows appropriate results.

After optimization, a satisfactory result was obtained. The disulfide was built in almost all models and the other loops stayed in a correct place. After the hybridize step, 62 out of 4335 models showed β-strands (1.43%) in PyMol. They could however not be preserved through the normal relax step.

For the docking of the ligand itself, the formation of β-strands was regarded as not so important, as long as the amino acids are located rationally. In order to save time for further protocol adaption and test runs, 85 models were selected based on scoring and clustering.

The formation of the β-strands in GPR18 will be further pursued in a project, optimizing the relax process to rescue the β-strand conformation from the hybridize step.

3.5.4.4. Evaluation of modeling in the presence of the ligand

For all loop building steps, we tried to perform them in the presence of the docked ligand to maintain a conformation suitable for ligand docking. The program generally tries to minimize surfaces towards the outside and therefore tries to close open space. Furthermore, the prospect of modeling the loop conformations in the presence of the ligand has the elegant aspect of complementarily optimizing receptor and ligand position.

We tried to perform the loop modeling in all three cases in the presence of the ligand. But in two out of three steps problems due to the ligand's presence arose. As the space of the loops is normally covered with atoms that are interacting with others, this possible space can be occupied by the ligand and block the space for the loop's sidechains.

Table 20: Evaluation of loop modeling in the presence of the ligand.

	POSSIBLE TO OBTAIN EXCEPTABLE RESULTS?	COMMENTS?
ECL1	No – ligand was discarded	Ligand was interfering with the space where the loop should be built
ECL2	No – ligand was discarded	Ligand was interfering with the space where the loop should be built
ECL3	Yes, modeling succeeded in the presence of the ligand	Probably possible because the ligand did not interact much with the necessary space

In total, it was only possible to model a loop in the presence of the ligand for ECL3. This could be possible because the ligand is not interfering with the space of ECL3 in most of the docking results. Also, when we take a look at the results in 3.5.5, we will see, that the ligand is interacting with amino acids both in ECL2 and ECL1. The missing interaction can also be a problem for the docking step. The results are summarized in Table 20.

In total, the objective of this approach can be regarded as promising and helpful to get an overall plausible receptor conformation, but the technical difficulties in interpreting the ligand in the comparative modeling step and the rather poor performance were certainly a drawback. There is definitively need for protocol optimization. This first approach shows that it is possible (ECL3) but afflicted with problems (ECL2 and ECL1) that need to be solved.

3.5.5. Docking

3.5.5.1. Docking procedure

We performed the docking of the agonist **162** with the RosettaLigand application.[193] The ligand was placed into the possible binding pocket and then its position was further optimized by so-called focused docking. The major read-out was the interface_delta, the energy gain of the system, through binding the ligand in that exact position. As this is an energy term, the lower the energy of the system, the better is the stability, and therefore, the probability increases. But, it has to be noted that this energy term is a rosetta-specific one which cannot be compared to other energy terms, for example, experimentally obtained binding energies. In the focused docking process, the angle and the space in which the ligand can move were narrowed down, until the docking score did not get any lower.

In this approach, the agonist **162** has been selected for docking, because it is the most potent ligand of the GPR18 receptor so far. Furthermore, structure-activity relationships for this compound class are already established and can be taken into account when examining the proposed poses. With the results from the docking procedure, hypotheses will be generated, to test the proposed binding sites by mutagenesis experiments. Naturally, docking results can be improved based on experimental data from mutagenesis studies. Therefore, the whole docking process can be regarded as a hypothesis that has to be experimentally proven. On the other hand, every experimental result can improve the model. Modeling is always a mutual process depending on experiments.

To start the docking procedure, a conformer library of the ligand is needed, which was acquired by using the bcl::ConformerGenerator.[219] The program calculates every possible conformation of a ligand, as depicted in Figure 80. The number of possible conformers depends on the flexibility of the ligand, especially its rotatable bonds. During the docking process, RosettaLigand will pick different conformers. In the sorting and scoring process, the best models will be selected, and certain conformers will be scoring higher than others.
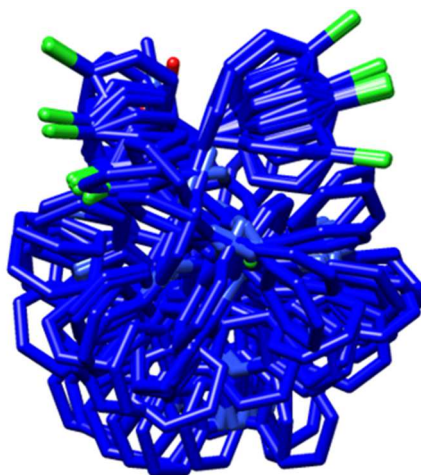
Figure 80: Conformer library of compound **162**.

One of the conformers was manually positioned in the starting models in PyMol. The first round of docking was carried out and from that, a large number of models was chosen (~500). This ensures a broad range of positions of the ligand in the possible binding pocket.

All models with a negative interface_delta (that means all models where the binding of the ligand showed an energy gain) were transferred to the second round of docking. There, the ligand was still allowed to rotate and move with in a quite large space (rotation = 360°, space to move = 4 Å). These docking rounds were evaluated by their docking score, and also by clustering and therefore sampling the most frequently observed conformations. Of course, this clustering was only be allowed up to a certain interface_delta value, that ensures reasonable conformations. By plotting the interface_delta as energy read-out against the ligand-RMSD an idea about the energy probability against the frequency of a certain position can be visualized. In the end, all of the interesting poses were visually evaluated. The docking was further focused by adapting the spacial movement and the rotation of the ligand. The docking was not further progressed when the interface_delta remained static and no improvement could further be achieved. In Figure 81 and Table 21, the progression of the docking procedure can be observed.
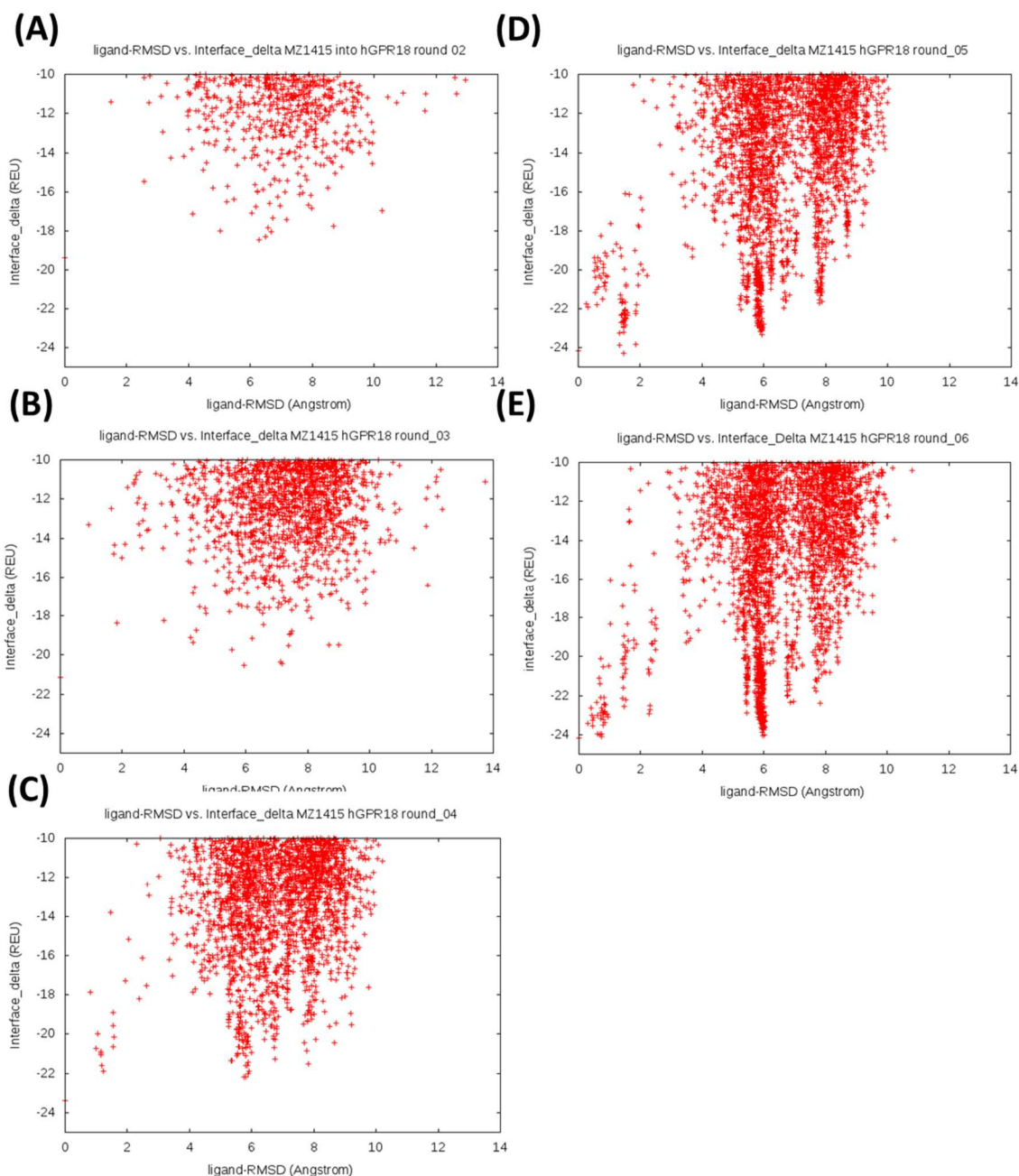
Figure 81: Focused docking: (A) first round, (B) second round, (C) third round, (D) fourth round, (E) fifth round; in each figure the interface_delta (REU) is plotted against the ligand-RMSD (Ångstrom) of the best scoring ligand.

Only models with a better interface_delta than -10 REU were plotted. The process was running from (A) to (E), and by comparing the lowest energy values, it can be tracked how the score improved in each round, beginning with (A) (interface_delta > -19 REU) to (D) and (E), where the best model scores with < -24 REU) were found. It can also be observed, that the number of negative models increases with every further round, compare Table 21.

From Figure 81, it can be further observed that certain positions of the ligand stand out of the point cloud. The Ligand-RMSD, which was taken as a measure for the diversity of the ligand poses, indicates

the difference compared to the best-scoring model, nevertheless it wa a good surrogate parameter to estimate the similarity of the poses.

Table 21: Focused docking: change of interface_delta over the different docking rounds

Round of Docking	Rotation	Spacial movement	Best interface delta (REU)	Number of negative scoring models
round_02	360°	4 Å	-19.355	5309
round_03	270°	3 Å	-21.141	7614
round_04	180°	2 Å	-23.368	8344
round_05	90°	1 Å	-24.288	8472
round_06	45°	0.5 Å	-24.187	8586

With the sixth round of docking, the interface_delta did not improve further. This set of models was further analyzed regarding the ligand position. From this ensemble, we will deduce proposals for mutagenesis studies.

3.5.5.2.   Evaluation and proposals for GPR18 mutagenesis experiments

In this section, we analyzed the models that have been generated by the docking procedure, and deduced proposals for further experimental studies. When taking a closer look at the ligand-RMSD vs. interface_delta plot, certain groups of models could already be identified that clustered together. In the case of this modeling approach, the best model (-24.187 REU) did not belong to the biggest cluster (the most often sampled conformation). In Figure 82, the ligand-RMSD is plotted against the best model of the biggest cluster (differently to the plots before, where it was just plotted against the best scoring model). It can now be observed that all other poses are 6 Å far away from this biggest cluster.
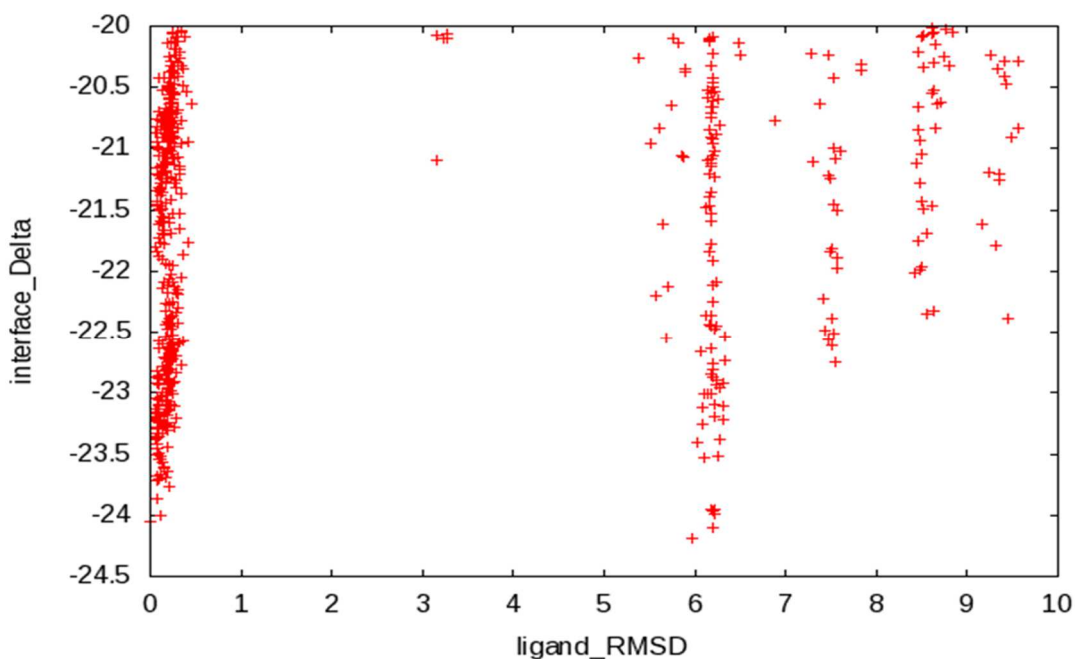
Figure 82: Interface_delta (>-20 REU), sixth docking round, plotted against the best model of the biggest cluster (which is not the best model overall).

With the help of the BCL, the models were clustered (only <-20 REU) and as can already be visually observed from the plot, the largest cluster was Cluster_1082. At a distance of 6 Ångstrom, the best scoring cluster can be found, which was rather small.
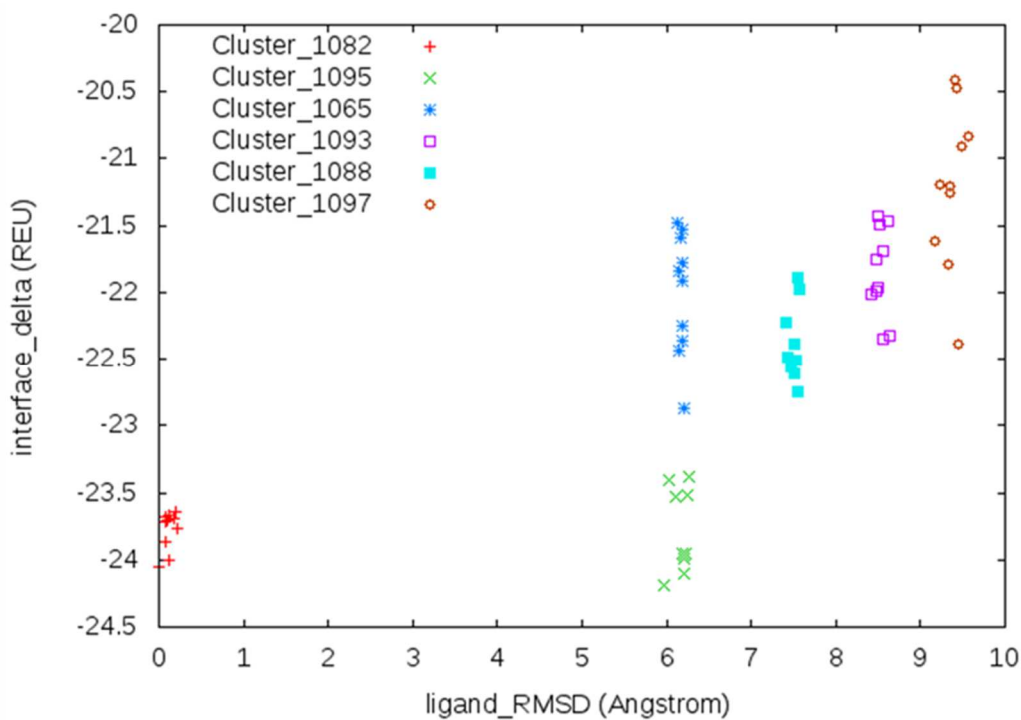

Figure 83: The best ten models of the best clusters.

In Figure 83, the best ten models out of the best clusters are shown. Cluster_1065 and Cluster_1095 obviously share the same difference in ligand-RMSD but not the same best-scoring interface_delta. The same ligand-RMSD does not necessarily has to mean the exact same position, it just indicates the difference compared to the selected model: here, the difference was 6 Å. By visually checking the pose of the ligand, the complex can be further investigated. Furthermore, it can be noted that two clusters scored better by 2 REU, namely Cluster_1082 and Cluster_1095.

For the mutagenesis proposals, Cluster_1065 was not used as it scored comparably less good than Cluster_1095 while having the same ligand-RMSD.

A summary of the results of the docking analysis is provided in Table 22 and Table 23. Some key issues were evaluated there, which provide an idea, whether the pose can be used for the prediction. One very important point was the ability of the models to capture the structure-activity relationships that were already established. In particular, a decrease in potency when prolonging the *N1*-alkyl chain was used for critical assessment.

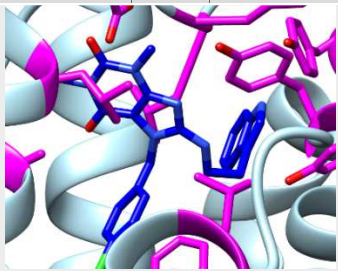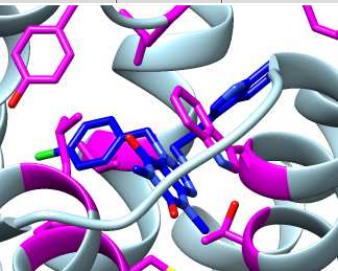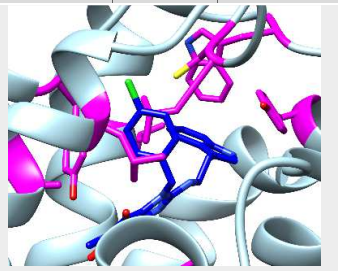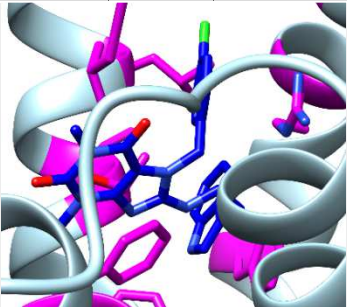Table 22: Characterization of the obtained clusters, part I.
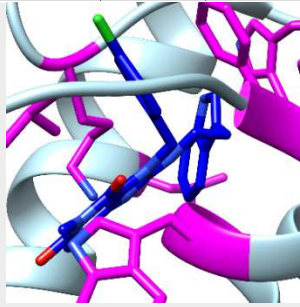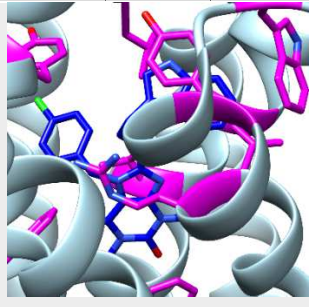
	Hypothesis I			Hypothesis II			Hypothesis IIb		
Cluster name	1082			1095			1065		
Linkage (RMSD)	0.453864			1.60199			0.299187		
Cluster size	377			57			39		
Interface_delta (REU)	-24.058			-24.187			-22.873		
Energy_breakdown: Top 10 aminoacids	Pose-Nr.	Aa	%	Pose-Nr.	Aa	%	Pose-Nr.	Aa	%
	235	PHE	22.19	250	TRP	22.88	235	PHE	22.77
	156	LEU	16.88	254	THR	11.39	156	LEU	20.89
	164	LEU	11.70	235	PHE	9.04	164	LEU	12.01
	64	TYR	11.41	143	TYR	6.69	64	TYR	8.21
	167	VAL	5.52	238	LEU	6.46	143	TYR	5.54
	238	LEU	5.37	156	LEU	6.31	70	TRP	4.33
	157	LYS	5.12	64	TYR	5.61	80	LEU	3.76
	247	TYR	4.76	85	VAL	5.23	167	VAL	3.17
	65	TYR	4.32	155	CYS	4.21	155	CYS	2.49
	145	ASP	3.31	234	CYS	3.57	231	PHE	2.32
Pose									
In accordance with SAR?	Yes *N1*-methyl blocked			Yes *N1*-methyl blocked			Yes *N1*-methyl blocked		
Hydrogen-bonds	TYR 64 – phenolic hydroxylgroup interacts with indole nitrogen			THR 254 – with secondary amine (acceptor) of the linker to the indole (as hydrogen bond donator)			ASN 171 (with C6-xanthine-oxygen (ketone))		

Table 23: Characterization of the obtained clusters, part II.

	Hypothesis III				Hypothesis IV				Hypothesis V			
Cluster name	1093				1088				1097			
Linkage (RMSD)	1.47901				0.619756				1.87483			
Cluster size	27				18				14			
Interface_delta (REU)	-22.352				-22.745				-22.389			
Energy_breakdown: Top 10 aminoacids	Pose-Nr.	Aa	%		Pose-Nr.	Aa	%		Pose-Nr.	Aa	%	
	156	LEU	20.87		247	TYR	21.99		64	TYR	19.98	
	235	PHE	19.01		70	TRP	13.76		84	THR	12.16	
	54	PHE	17.32		157	LYS	13.59		54	PHE	10.48	
	61	ARG	8.14		64	TYR	7.69		70	TRP	10.42	
	64	TYR	7.29		235	PHE	6.30		247	TYR	9.46	
	231	PHE	6.23		238	LEU	6.10		156	LEU	8.87	
	84	THR	5.76		251	GLY	4.46		80	LEU	6.29	
	83	LEU	3.79		80	LEU	3.59		61	ARG	5.18	
	80	LEU	3.74		250	TRP	3.42		231	PHE	5.08	
	251	GLY	3.46		158	ILE	3.38		252	ALA	4.19	
Pose												
In accordance with SAR?	No - *N1*-methyl has a lot of space…				Yes, *N1*-methyl blocked				Yes, *N1*-methyl blocked			
Hydrogen-bonds	weak – THR 84, to *N9* of the xanthine				LYS 157, to *N9* of the xanthine				THR 255 – with C6-keto group			
									ARG 61 – to *N9* of the xanthine THR 254 – C6-keto group			

The information provided in the tables can be summarized as follows: cluster_1082 was the by far biggest cluster with over 300 models included. Cluster_1095 was nevertheless the best-scoring cluster, but comparably infrequently sampled. There were three further clusters, which all scored 2 REU less well. They were also quite small with around 20 models each. Cluster_1082 was by all means the largest and also quite well-scoring. When checking the already established structure-activity relationships, the *N1*-substituent of the xanthine was located in an area, where an enlargement of the alkyl sidechain would not be further tolerated, which is in agreement with experimental data.
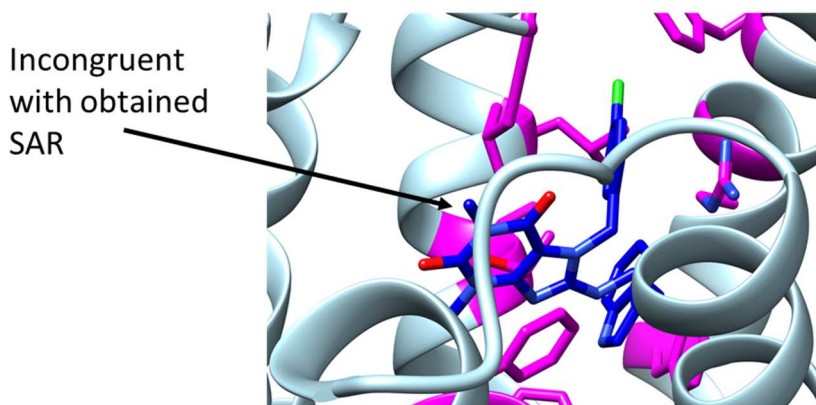

Figure 84: Pose of compound **162** in the model of Cluster 1093.

For cluster_1093, it can be observed (Figure 84) that the methyl residue in position *N1* was quite free in the space of the binding site. A methyl has been shown in our structure-activity relationships as the only residue to be tolerated, whereas larger substituents or the lacking of the substituent was detrimental. Therefore, the Cluster 1093 was not included in further analysis due to its lack to resemble experimental data.
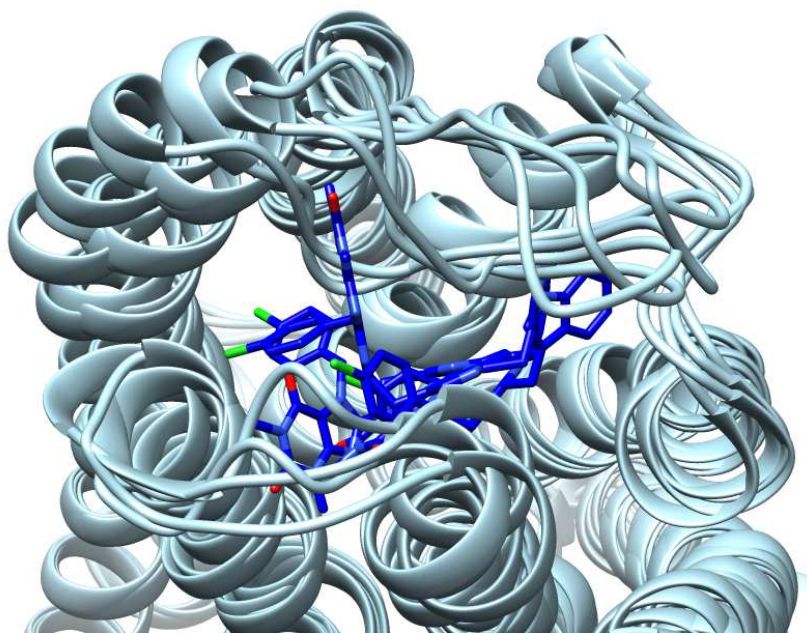

Figure 85: Overlay of the best-scoring model of the Clusters 1082, 1095, 1088 and 1097.

In Figure 85, out of the four reasonable clusters the best-scoring model can be observed. First of all, it can be noted that each model derived from a different original model, which shows that all attempts to ensure diversity were successful. The ligand was in all models quite similarly oriented, the indole residue pointed towards the ECL1. The conformation of the ECL2 also played a role. In some models the loop curved deeper down into the space of the binding pocket. If this was the case, the space could not be filled by the ligand. If the loop was a little bit more up towards the extracellular space either the xanthine or the *para*-chlorobenzyl residue could fit into this space. Only the cluster 1097 showed a somewhat different orientation of the ligand pose. Here, the xanthine reisdue pointed straight down into the receptor core. There can be different poses observed for ligands in GPCR binding sites, therefore, it is not easy to predict the correct orientation. The deeper pose was not as easily accessible as the other poses, and this might be a reason why it was not sampled that often. On the other hand, the large difference in the interface_delta together with the far less probable sampling led to the assumption, that it might not be preferable. These four poses also covered the obtained structure-activity relationships. Their possible interactions with amino acids in the binding pocket were evaluated and also their ability to form hydrogen bonds was studied. For all four poses, possible hydrogen bonds could be observed, but very different ones. For cluster 1082, a possible hydrogen bond of the indole nitrogen with a tyrosine of helix II was found, but for the clusters 1088 and 1096 the *N9* of the xanthines interacted with possible hydrogen bond donors.

Cluster_1082 served as a primary hypothesis as it was the best-scoring and most often sampled pose. As can be observed in Figure 86, the ligand was positioned quite high in helix V below the bow of the ECL2. In the other poses, this position could be blocked by the ECL2 bending further down, and therefore the xanthine moiety did not have the space to fill this position. The *para*-chlorobenzyl-residue pointed into a hydrophobic pocket, where valine and isoleucine created a suitable surrounding. The indole was stabilized through a hydrogen bond from a tyrosine of helix II. The position of the ligand was in total rather high up in the pocket, towards the extracellular space. Further experiments will have to prove this hypothesis.
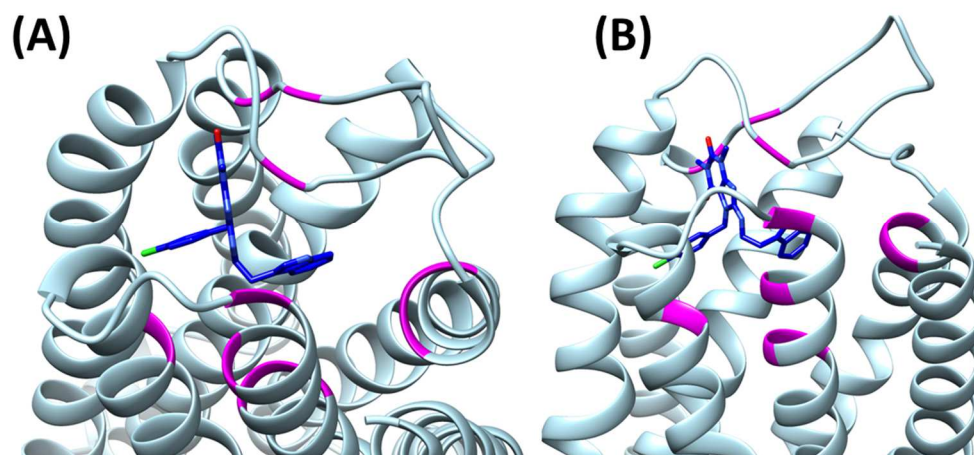
Figure 86: Pose of the ligand in cluster_1082, (A) from the top, (B) from the side.

As asummary of this evaluation, the four clusters 1082, 1095, 1088 and 1097 were further investigated and their interaction with the amino acid residues of the receptor wiere examined. Due to the probability and strength of this interaction the best ten interactions were selected and then a proposal was provided for subsequent mutagenesis studies. In this approach, the cluster 1082 served as the primary hypothesis. If this hypothesis would fail, the others can also be considered. In total, ten point mutations will be made, seven were predicted from cluster 1082, and in addition from each other cluster a crucial interaction was picked as well.

In chapter 3.4, we already investigated the ability of the identified potent agonist of the human GPR18 to activate the mouse GPR18. In the next section, these results were compared to the predicted interactions to corroborate our hypothesis of the proposed binding site.

3.5.6. Proposals for mutagenesis

Proposals for mutagenesis were generated by analyzing the possible interaction partners of the ligand in the hypothetical binding pocket. This was done on one hand with Rosetta and on the other hand by visually determining the nature of the interaction. The Rosetta tool used to calculate the energy gain of ligand binding, is called energy_breakdown. It breaks up the total sum of interactions of all residues in the model with each other into the interaction between each of the residues– but here, we only took the interactions with the ligand into account. This was not only done for one model, but for the best ten models of each cluster. The total energy scores were summed up and the ratio of each residue was determined in percentage. Whenever the possibility was detected that a hydrogen bond could be formed this was also be inspected (and can also be viewed in Table 22 and Table 23).

At first, we analyzed the ten highest impact interactions of every cluster and collected the results in Table 24. In Table 25, the collected interactions were transferred into rational proposals for the mutagenesis studies.

Table 24: Overview of all involved amino acids, their type of interaction and proposals for mutagenesis experiments; bold text for amino acids involved in hydrogen bonding (note: pose numbers refer to Rosetta pose numbering and not to the total sequence).

	Total involved amino acids		Cluster	Type of interaction	Mutagenesis proposals
1	235	PHE	1082, 1088	1082:π-π-interaction with benzyl residue 1088: interaction less pronounced	ALA (LEU is observed in nature)
2	65	LEU	1082	nonpolar interaction, with indole core	GLY or PHE
3	164	LEU	1082	nonpolar interaction, with methyl group	GLY, or change to polar, like SER
4	**64**	**TYR**	1082, 1095,1088, 1097	is a conserved YY-feature in δ, but in other GPCRs D,V,N etc.	PHE, ALA
5	167	VAL	1082	nonpolar interaction with methyl, forms outer border for methyl residue, in fish GPR18=ASP	GLY, ASP
6	238	LEU	1082	part of a lipophilic pocket, probably no big impact	ILE?
7	**157**	**LYS**	1082, 1088	in this model backbone interaction, in other models it is a hydrogen bond donor (alternative hypothesis); loop region	ALA
8	247	TYR	1082, 1088	here more of a backbone interaction, but in other models also involved in binding , anchor point for ECL3	ALA
9	65	TYR	1082	π-π-interaction, but part of conserved YY-motif, ILE in other GPCRs observed	ALA
10	145	ASP	1082	loop region, in no other hpyothesis	ALA
11	250	TRP	1095, 1088	interacting with xanthine	ALA
12	**254**	**THR**	1095	hydrogen bond aceptor!	VAL/ALA
13	143	TYR	1095	lipophilic pocket/π-π-interaction	ALA
14	238	LEU	1095, 1088	interacting with methylgroup	ALA
15	156	LEU	1095, 1097	no clear result	ALA
16	85	VAL	1095		
17	155	CYS	1095	close to indole, lipophilic part, disulfide bridge	no exchange
18	234	CYS	1095	next to methyl group	ALA
19	54	PHE	1097		
20	**61**	**ARG**	1097	frames xanthine	ALA
21	80	LEU	1088		
22	247	TYR	1097	π-π-interaction	ALA

23	70	TRP	1088, 1097	π-π-interaction, highly conserved TRP -?	no
24	251	GLY	1088	backbone interaction	ALA/VAL
25	158	ILE	1088	frames the *p*-chlorobenzyl residue	ALA
26	231	PHE	1097	frames the xanthine residue with both methyl residues	ALA
27	84	THR	1097	interaction not completely clear	GLY/ALA
28	252	ALA	1097	backbone interaction	no
29	**255**	**THR**	1088	possible hydrogen bond in Cluster 1097	ALA/VAL

Eleven proposals were made for further experimental conformation in mutagenesis studies. We will ude the results of the mutagenesis studies subsequently to optimize the modeling performance by feeding the data back into the process. Such proposals will be regarded as rational that have a high probability of making a difference to the ligand binding. Therefore, it does not make sense to change a leucine to an alanine, because there is not enough difference in the amino acids. However, exchanging a tyrosine for a phenylalanine, when a hydrogen bond has been proposed, should make a large impact on ligand binding (for example, Tyr 64). From the ten proposals, seven were from cluster_1082 and also include amino acids that have been found in other clusters to interact with the ligand. Three additional proposals were selected from the other poses8 (seeTable 25).

Table 25: Proposals for mutagenesis (note: pose numbers refer to Rosetta pose numbering and not to the total sequence).

Entry	Amino acids		Cluster	Mutagenesis proposals
1	235	PHE	1082, 1088	ALA (LEU is observed in nature)
2	**64**	**TYR**	1082, 1095,1088, 1097	PHE
3	**64**	**TYR**	1082, 1095,1088, 1097	ALA
4	**157**	**LYS**	1082, 1088	ALA
5	247	TYR	1082, 1088	ALA
6	65	TYR	1082	ALA
7	145	ASP	1082	ALA
8	143	TYR	1095	ALA
9	250	TRP	1095, 1088	ALA
10	**254**	**THR**	1095	ALA
11	**255**	**THR**	1088	ALA

In total eleven proposals will be evaluated in mutagenesis studies.

3.5.6.1.   Comparison of the human and mouse receptor for docking evaluation

In the previous chapter, it was already mentioned that the mouse GPR18 data will be compared to the human receptor data, to further evaluate the possible predictions for the mutagenesis. The sequence of the human and mouse receptor share a high degree of identity; nevertheless, there are also differences. Further, the sequences of GPR18 for different species will be compared to know if the residues proposed for mutagenesis are conserved and if not, to which amino acids they were converted during evolution.

When the activation data were compared, compound **162** showed an EC_{50} for the human receptor of **19.1** nM and of **54.1** nM for the mouse receptor. To get an idea, whether this meant a significant difference a two-tailed t-test was performed, as can be seen in Figure 87 and Figure 88.
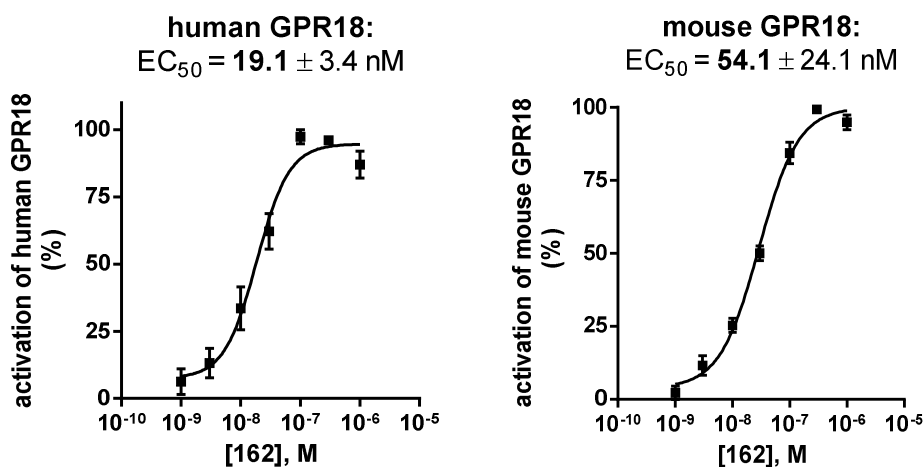
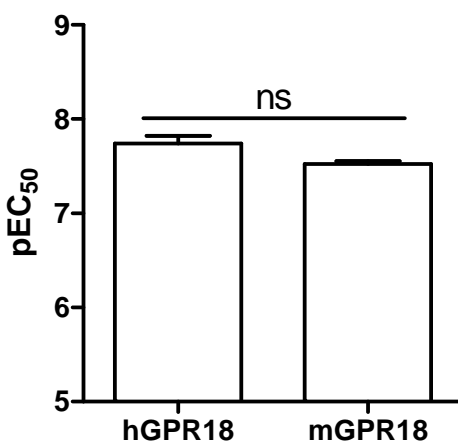Figure 87: Activation curve of compound **162** in β-arrestin recruitment assays, 100% = maximum effect.

Figure 88: human vs. mouse GPR18: two-tailed t-test, p>0.05, ns = not significant.

The EC_{50} value of the mouse receptor was not significantly different from that at the human GPR18, (two-tailed t-test, p > 0.05). The difference can therefore not be regarded as more than a trend. This means that the amino acids involved in ligand binding probably do not differ significantly between the two species. The predicted amino acids will be compared (see Figure 89).

Sequences of all species were aligned for which a confirmed GPR18 sequence was available in pubmed (https://www.ncbi.nlm.nih.gov/pubmed). It turned out to be the mammalian species mouse (*Mus musculus,* NP_877958.1), rat (*Rattus norvegicus*, NP_001073178.1), chimpanzee (*Pan troglodytes*, NP_001233295.1), cattle (*Bos taurus*, NP_001029861.1), horse (*Equus caballus,*

NP_001296104.1), and the two fish species catfish (*Ictalrus punctatus*, NP_001187728.1) and atlantic salmon (*Salmo salar*, ACN10695.1).

First of all, none of the predicted amino acids (black frame), was different between human and mouse – which was in accordance with the experimental data. When comparing the known sequences of all eight species, some interesting effects could be observed. Residue 143, which was a tyrosine in the human and mouse receptor, was an aspartate in rat and salmon, and a glutamate in catfish. Nevertheless, these are all amino acids that can form hydrogen bonds. The other predicted amino acids, where a difference can be observed, was residue 235 which was a phenylalanine in all species except for salmon, which showed a leucine, also a lipophilic but not an aromatic residue.

In conclusion, GPR18 is a very well conserved receptor in the analyzed species. The largest differences exist between the two fish species and the mammalian receptor, as can be expected. The two fish receptors, for example, show a shorter N-terminus. All of the sequences show a modified "NPxxY" motif, as discussed for the human receptor in 3.5.2. It is not always exactly the same: the human sequence is DVILY, whereas the two fish species are DIILY and the two murine receptors contain DVVLY (see Figure 89).

Overall, the most frequent changes existed in the small lipophilic residues. The sequences most commonly varied between valine, isoleucine, methionine and leucine, which should not generate a big difference in ligand binding.

It can be noted that there were no differences between the mouse and the human receptor, which could effect ligand binding and subsequent receptor activation. This was in accordance with the experimental obtained data. From this analysis, there was no reason to discard any of the poses that were modeled.

Figure 89: Multi-species alignment. ECL= extracellular loop, ICL = intracellular loop, species only from complete mRNA from pubmed..

3.5.7. Discussion and outlook

In the modeling approach, compound **162**, the most potent compound we developed so far, was docked to a modeled receptor. The modeling of the receptor required information about templates, the unique sequence of GPR18 and the applied techniques to generate models with the Rosetta protein design software. The models were established using Rosetta Comparative Modeling based on information from multiple sequence alignments of GPCR templates with GPR18. It could be learned that GPR18 has some unique features that only exist in the δ-branch of the class A GPCRs, for example, it lacks the NPxxY motif conserved in the majority of GPCRs. Which impact this has on receptor activation and signaling has yet to be elucidated. Furthermore, the extracellular loops of GPR18 were closely examined and modelled step by step to ensure an optimal performance. In this process, the conformation of the ECL2 was predicted as β-strand, which, however, could not be rescued into the final models. For the docking itself, this does not make a big difference, but there is further need to evaluate and adapt these results.

Compound **162**, the most potent ligand of GPR18 known to date, was docked to the receptor model and the docking pose was optimized by a procedure called focused docking. Compound **162** was chosen due to its high potency. Other potent compounds were structurally very similar to **162**, so that there would probably not be a great difference in the positioning of the ligand. Another ligand, Δ^9-THC, not potent enough to give a confident feedback on the docking pose. It is likely that compound **162** and Δ^9-THC bind to different sites since their structure are very different, compound **162** being more peptide-like, and Δ^9-THC being lipid-like.

For compound **162**, different docking poses could be observed and which were analyzed. The most often sampled and best-scoring positions were selected. To verify the proposed docking pose, the interaction of the residues of the receptor and the ligand were predicted and suitable proposals for mutagenesis studies were developed. The alternative docking poses were kept as back-up possibilities, if the predicted interactions should not be confirmed experimentally. The modeling approach can subsequently be adapted to be in accordance with the mutagenesis results, and the ligand position can then be optimized.

4. NATURAL PRODUCTS AS LIGANDS FOR CANNABINOID AND CANNABINOID LIKE RECEPTORS

4.1. Introduction

Naturally occurring chemical substances are a major source of biologically active drugs. More than 75% of all marketed drugs are directly or indirectly derived from natural products.[220] For drug development, the use of plant-derived scaffolds is a promising way to enlarge the chemical space and develop new tool compounds. Some of the most famous drugs from nature are morphine, derived from the seeds of *Papaver somniferum*, atropine from the fruits of *Atropa belladonna* or taxol from *Taxus brevifolia*.[221; 222] In 2015 the Nobel prize was awarded to William C. Campbell and Satoshi Omura for their discovery of avermectin from *Streptomyces avermitilis*, which is used against parasites such as round worm infections, and to Youyou Tu for the identification of the antimalarial drug artemisinin from *Artemisia annua*, a traditional chinese herbal medicine.[223] The first compound known to target the cannabinoid receptors and later on GPR18 has been Δ^9-THC, also a plant derived drug. This shows the significance of natural products for medicinal chemistry and also for our project.

Although the techniques for drug development have undergone major changes towards more rational and computer-based approaches, drugs derived from natural products still give a high impact in research.[224] Therefore, natural products have also be part of our approach to identify and investigate new ligands for cannabinoid and cannabinoid-like receptors.

In the first part of this chapter, we present the continuation of a project, in which the natural product tetrahydromagnolol (**186**) is used as a lead structure for the development of CB_1- and CB_2 receptor agonists and potential ligands for the orphan GPR55. In the second part, the test results for a group of compounds is presented, which are similar in structure to the recently published CB_1 receptor antagonist amauromine[225], that was also shown to inhibit the orphan GPR18. Moreover, screening results of a natural product library will be presented.

4.2. Magnolol and honokiol derivatives as cannabinoid receptor ligands

4.2.1. Introduction to magnolol and honokiol derivatives as cannabinoid receptor ligands

The two lignans magnolol (**187**)and honokiol are constitutional isomers; both can naturally be found in the leaves and bark cones of the herbal drugs *Magnolia officinalis* and *Magnolia grandifolia* of the *Magnoliaceae* plant family. They are established in the traditional herbal medicine of Japan and China, especially in the so-called Kampo medicine. Honokiol (**188**) has been known for its pleiotropic effects,

for example, it has been described to display antimicrobial activity, especially against methicillin-resistant *Staphylococcus aureus*.[226] Also anti-cancer applications due to antiangiogenetic effects have been described.[227] Magnolol shares some of the pharmacological properties of honokiol. Both have been reported to produce central depressant effects as sedation, ataxia, muscle relaxation and a loss of the righting reflex in mice.[228] Furthermore, they were anxiolytic[229] and displayed neuroprotective and antidepressant effects.[230,231] Magnolol further showed antiepileptic and protective effects against Alzheimer's disease.[232]
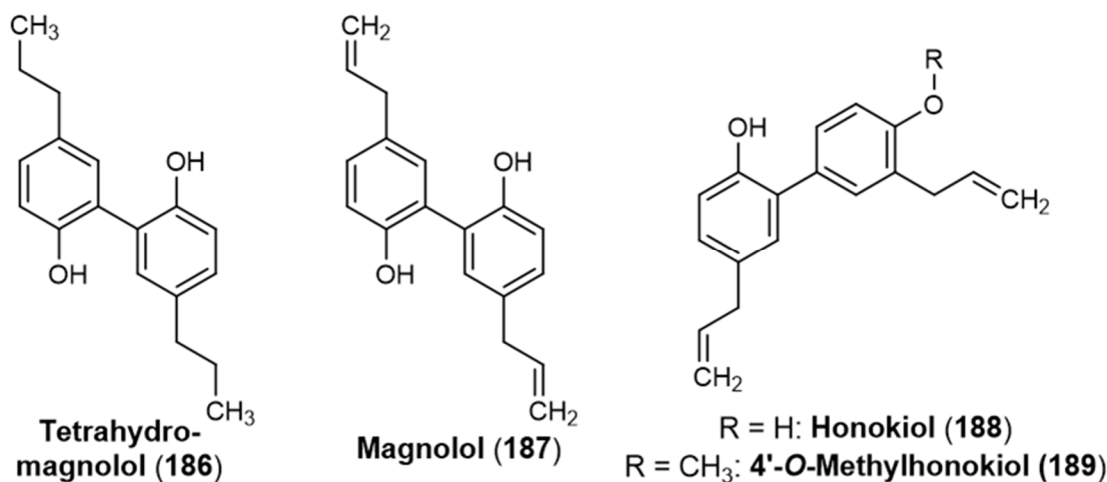
Figure 90: Chemical structure of tetrahydromagnolol (**186**) and magnolol (**187**) and honokiol (**188**)

However, a specified target mediating these effects is still in discussions one of their main mechanism of action, antioxidative properties have been proposed and investigated.[233] For example, Chuang *et al.* showed that both compounds inhibited NMDA receptor induced superoxide production in microglial cells.[234] Both, honokiol and magnolol have been reported to act on the metabolic regulator PPARγ with EC_{50} values in the low micromolar range in reporter-gene assays.[235]

Later, it could be shown that the binding behavior of ligands of the $GABA_A$ receptor channel was increased in the presence of honokiol (**188**) or reduced in the presence of magnolol (**187**).[236] An allosteric mode of action was hypothesized. The antiepileptic effects of magnolol (**187**) were attenuated by the $GABA_A$ channel antagonist flumazenil.[237] In the presence of the $GABA_A$ receptor activator pentobarbital magnolol (**187**) enhanced the sleeping behavior in mice.[238] In the brain many different $GABA_A$ receptor isoforms are present, distinguishable in their subunit composition (α_{1-5}, β_{1-3}, γ_{1-3}, δ, π, ε, θ, ρ_{1-3}).which defines function and selectivity. Five of these subunits are located around an inwardly rectifying Cl⁻channel, which upon activation leads to a hypopolarization of the synapse. It has been reported that magnolol (**187**) or honokiol (**188**) either interact with receptors containing the α_2[239] or with the δ subunit.[240] Baur *et al.* further investigated this, and expressed different $GABA_A$ receptor isoforms in *Xenopus oozytes* to compare the effect of an equimolar concentration in patch-

clamp experiments, with the conclusion, that different α and β subunits show effects, but no other subunit. They further showed that 4-*O*-methylhonokiol (**189**) potentiated currents more strongly in their system than honokiol (**188**). With different pharmacological tools they tried to block the potentiation of 4-*O*-methylhonokiol (**189**), but could not identify a binding site for this compound.[241] 4-*O*-methylhonokiol (**189**) is a natural product, it can be extracted from the seed oil of *Magnolia grandiflora*.[242]

Lee *et al.* investigated the protective effects of *Magnolia officinalis* extracts against Alzheimer's disease and showed that lipopolysaccharide-induced memory deficiencies can be attenuated by feeding Magnolia extract.[232] Their main conclusion was that the extract prevents a neuroinflammatory process in the brain. Later on, 4-*O*-methylhonokiol (**189**) was shown to act as a selective CB_2 receptor inverse agonist in osteoclasts.[243] The authors argue that CB_2 receptor-mediated effects may also be responsible for the observed neuroprotection.[244] CB_2 is the more broadly distributed receptor in the immune system, CB_1 is a major regulator of GABAergic and glutamatergic signaling. Both can be involved in neuroinflammatory processes.

Previously, Rempel *et al.* from our group investigated the other constituents of *Magnolia officinalis* - mainly magnolol (**187**) and honokiol (**188**) - at both cannabinoid receptors. In this study, magnolol (**187**) showed a higher affinity to the CB_2 receptor than honokiol (**188**), which was unselective. Both showed K_i values in the low micromolar range. Magnolol (**187**) acted as partial agonist in functional cAMP studies. Honokiol (**188**) as well as *magnolia officinalis* extract proved to act as inverse agonists at the CB_2 receptor, while they act as agonists at the CB_1 receptor. Furthermore, one of the main metabolites of magnolol (**187**) was investigated: tetrahydromagnolol (**186**), which showed to have an even higher affinity for the CB_2 receptor than magnolol (**187**) with a K_i value of **0.416** µM. It could be characterized as an agonist at the CB_1 receptor and as a partial agonist at CB_2. From these findings it was hypothesized that magnolol (**187**) undergoes bioactivation. Tetrahydromagnolol (**186**) also showed antagonistic effects in β-arrestin assays at the orphan GPR55 with an IC_{50} value of **13.3** µM.[245,133] Tetrahydromagnolol (**186**) can be regarded as a promising lead compound for cannabinoid receptor ligand development. CB_2 receptor agonists are of interest as drugs for treating neuropathic and chronic pain, as well as inflammatory diseases such as arthritis and multiple sclerosis.

4.2.2. Structure-activity relationships of tetrahydromagnolol derivatives at cannabinoid receptors and GPR55

The tetrahydromagnolol (**186**) structure bears some resemblance to other plant-derived cannabinoid ligands, especially to Δ^9-THC, which also features a phenolic structure, with a lipophilic

substituent and a second ring system. Fuchs *et al.* subsequently investigated the structure-activity relationships of tetrahydromagnolol derivatives by changing the *para-* positioned lipophilic side chain and by methylation of the phenyl residues.[133]

It could be observed that symmetrical substitution with alkyl chains *para*-positioned to the phenolic hydroxyl group led to CB_2 receptor-preferring compounds, with an affinity optimum for the propyl-substitution. Whenever one of the phenolic groups was methylated - leading to an unsymmetrical compound - CB_2 receptor preference was lost resulting in potent unselective agonists for both CB receptor subtypes. By removing one lipophilic side chain and by varying the other one, an optimal length could be determined. By keeping this length fixed the other lipophilic side chain was investigated. This proved to be crucial for CB_2 receptor affinity. Thus, the affinity could be increased from methyl to propyl, but was reduced upon further enlargement of the alkyl chain. Now this optimal side chain was fixed and the other one was investigated. The highest affinities for both receptors were observed for a hexyl substitution. Subsequently, one phenolic group was methylated, but as this compound is unsymmetrical two possibilities arise. When the *para*-positioned phenolic group to the large hexyl residue was methylated the CB_2 affinity significantly decreased. When the *para*-positioned phenolic group to the propyl residue was methylated the CB_1 affinity strongly increased (compound **191**; K_i CB_1: **0.00957** µM and K_i CB_2: **0.0238** µM).[133]
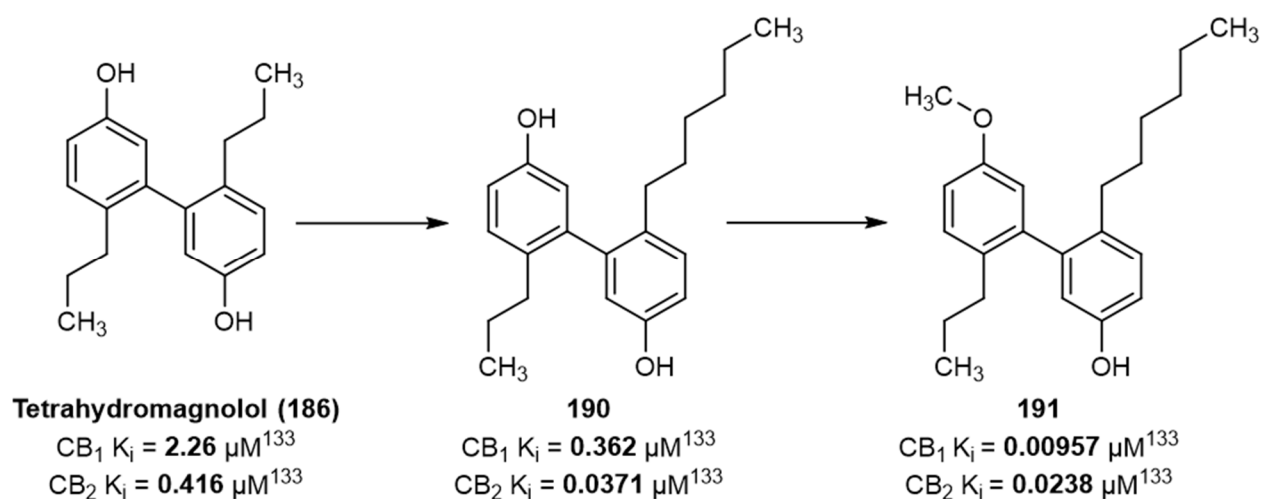
Figure 91: Improvement of compound affinities through subsequent investigation of the alkyl moieties: compound **186**, **190** and **191**

Further, Fuchs *et al.* also investigated 4'-*O*-methylhonokiol (**189**), for which they could show similar affinities in radioligand binding as described before, but not an inverse agonistic effect in functional assays. They reported an agonistic effect – in contrast to the data of Schuehly *et al.*[243] Additionally, Fuchs *et al.* tested the activity of their tetrahydromagnolol derivatives also at GPR55, a cannabinoid-

144

like orphan GPCR, which has been described to interact with different CB receptor ligands, for example the phenolic compound CP55,940. Typically, GPR55 is inhibited by CB receptor agonists, while it is activated by CB antagonists (inverse effects).[106,132] For the tetrahydromagnolol derivatives, which are all agonists at the CB receptors, only antagonistic effects at the orphan GPR55 could be found. The antagonistic potency could be markedly increased, when the phenolic hydroxyl group *para* to the hexyl moiety was methylated. The most potent compound of this series showed an IC_{50} value of **3.25** µM.[133]

192
$CB_1 K_i = 0.313$ µM[133]
$CB_2 K_i = 0.281$ µM[133]
GPR55 $IC_{50} = 3.25$ µM[133]
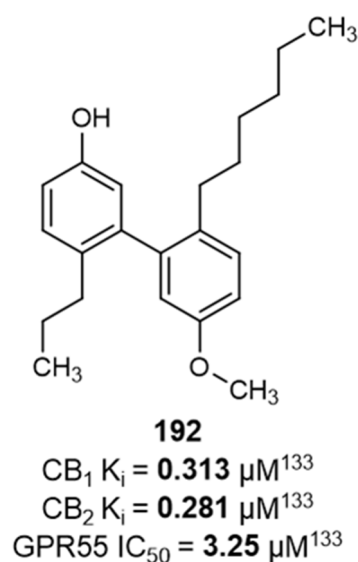
Figure 92: Chemical structure of the most potent GPR55 antagonist of the tetrahydromagnolol series compound **192**

The structure activity-relationshipsknown sofar can be summarized up as follows:

methylation CB_1-affinity ↑

alkyl substitution:
hexyl > pentyl > butyl > *t*-butyl > heptyl > octyl

alkyl substitution:
propyl > ethyl > methyl > H

methylation: CB_2 affintiy ↓

mono-methoxy compounds: unselective
unmethylated compounds: CB_2 receptor preference

Figure 93: Summary of established structure-activity relationships for tetrahydromagnolol derivatives[133]
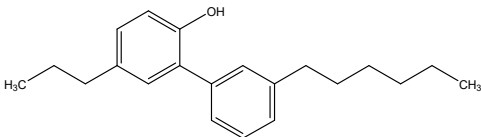
In this study, we further investigated the structure-activity relationships substituents in different positions. The length of the ether sidechain was varied and an optimal length was determined. In

another approach, the biphenylic core structure was replaced by a phenylaminophenol. All compounds were synthesized by Dr. Alexander Fuchs and pharmacologically evaluated in the present study.

4.2.3. Results for tetrahydromagnolol derivatives for the cannabinoid receptor

The already established structure-activity relationships were completed by two additional compound sets. In the first group, we varied the alkyl substitution of the ether in chain length (from ethyl to propyl and isopropyl to compare these modifications to the methylated compounds). This has been done for both possible phenolic substitutions. We determined the affinity of the compounds in the same radioligand binding experiment versus 0.1 nM [3H]CP55,940. The results are listed in Table 26.

Table 26: Affinities of magnolol derivatives with varying lipophilic substitutions on the ether residue at the cannabinoid receptors

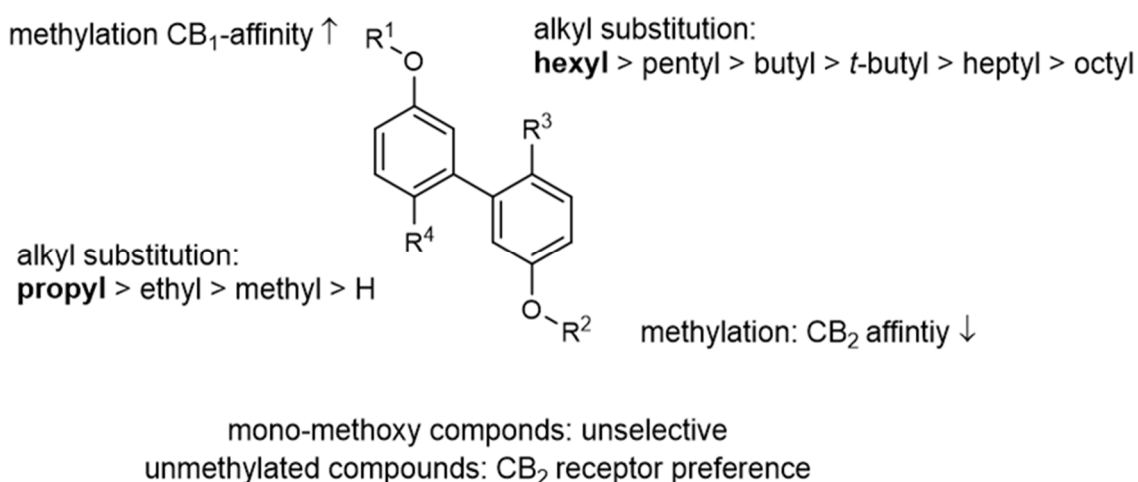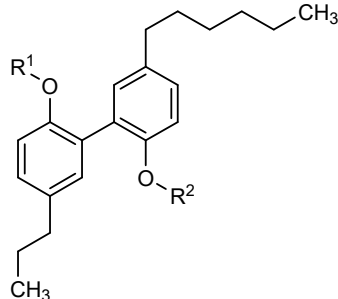| No.	Compd.	Chemical structure		Radioligand binding	
				Human CB$_1$	Human CB$_2$
		R^1	R^2	K_i (µM) vs. [3H]CP55,940	K_i (µM) vs. [3H]CP55,940
193	AF097	H	ethyl	**0.882** ± 0.369	**1.36** ± 0.77
194	AF098	H	propyl	>10 (40%)	**1.184** ± 0.64
195	AF099	H	isopropyl	>10 (26%)	**0.599** ± 0.115
196	AF100	ethyl	H	**0.291** ± 0.100	**0.412** ± 0.172
197	AF101	propyl	H	**0.175** ± 0.052	**0.132** ± 0.058
198	AF102	isopropyl	H	**0.189** ± 0.079	**0.178** ± 0.101
199	AF105			**0.163** ± 0.039	**0.0673** ± 0.0082

The first group (compound **193**, **194** and **195**) is characterized by an alkylated phenolic hydroxyl group in the *para*-position to the hexyl residue. Their potencies can be compared to compound **192**, which has a methoxy residue.
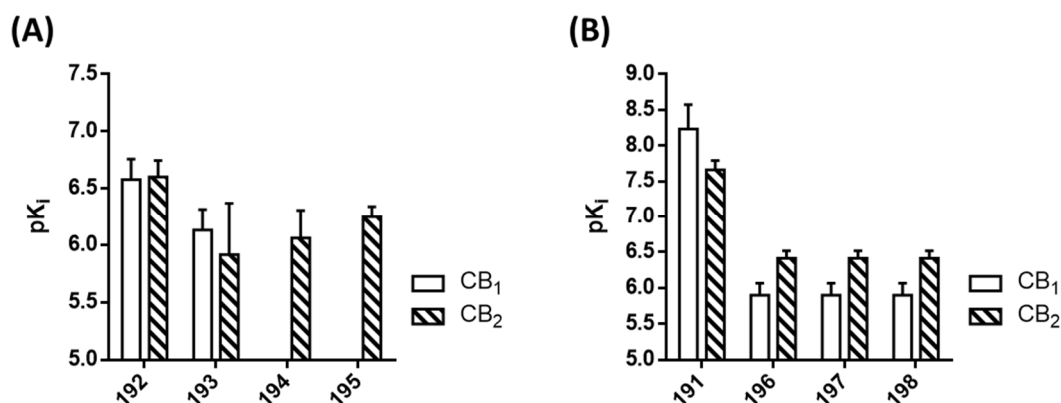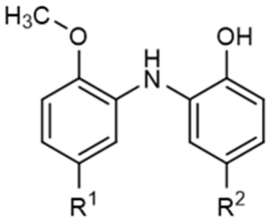
Figure 94: Cannabinoid receptor affinities. A: 5'-hexyl-2'-alkyloxy derivatives, B: 5'-propyl-2'-alkyloxy derivatives

As can be seen in Figure 94, the lead compounds for either variation, compound **192** and **191**, displayed in both cases higher affinities, thus the enlargement of the alkyl function was not favorable. For both cases, the methoxy compound was the most potent one. Notably, the CB_1 affinity was lost for the 5'-hexyl-2'-alkyl-oxy derivatives when a chain length of propoxy or isopropxy was reached, although the CB_2 affinity was preserved. For the 5'-propyl-2'-alkyloxy derivatives the decrease in affinity was rather large, only showing K_i values around 1 μM – in contrast to the highly potent methoxy compound **191**. Larger moieties were not tolerated here.

Furthermore, a compound was synthesized that lacks the second phenolic group: **199**. It showed a slightly higher K_i value for CB_2, than compound **190**, which has a phenolic group. The CB_1 receptor K_i value was slightly lower.

In a second compound set, the biphenylic core of the compounds was exchanged for a phenylaminophenol (see Table 27).

Table 27: Affinities of diphenylamine derivatives at cannabinoid receptors

No.	Compd.	Chemical structure		Radioligand binding	
				Human CB$_1$	Human CB$_2$
		R^1	R^2	K_i (µM) vs. [^{3}H]CP55,940	K_i (µM) vs. [^{3}H]CP55,940
200	AF128	methyl	propyl	**14.1 ± 4.2**	**5.01 ± 2.56**
201	AF127	methyl	butyl	**2.55 ± 0.20**	**1.55 ± 0.23**
202	AF126	methyl	pentyl	**1.48 ± 0.28**	**0.258 ± 0.032**
203	AF125	methyl	hexyl	**1.42 ± 0.13**	**0.295 ± 0.018**
204	AF132	propyl	propyl	**10.8 ± 2.3**	**1.65 ± 0.793**
205	AF135	propyl	pentyl	**2.34 ± 0.16**	**0.509 ± 0.143**
206	AF137	pentyl	propyl	**4.01 ± 0.61**	**2.11 ± 1.33**
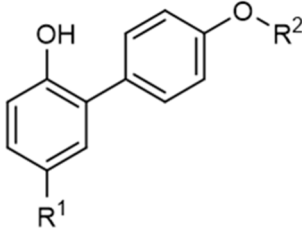
For these compounds, it was found that the CB$_1$ affinity always ranged in the low micromolar range. Three compounds showed a nanomolar K$_i$ value for CB$_2$. None of them was as potent as **191**, the most potent compound of the series. In general, the compounds showed a slightly higher affinity for CB$_2$ than for CB$_1$. Some of the already for the biphenylic compounds oberserved structure-activity relationships could also be found in this compound set. The three best CB$_2$ ligands had a pentyl or hexyl residue in the *para*-position to the phenolic hydroxyl group. The shorter this chain the higher the K$_i$ value. The exchange of the 5'-alkyl chain from methyl to propyl was not beneficial for affinity. The most potent compounds were the 5'-methyl-5-pentyl **202** and 5'-methyl-5-hexyl derivatives **203**. Overall, the biphenylic core was superior to the diphenylamine.

4.2.4. Cannabinoid receptor affinities of honokiol-like compounds

As already mentioned above, 4'-*O*-methylhonokiol (**189**) has been reported to act as a positive allosteric modulator of the GABA$_A$ receptor.[241] The group of Dr. Erwin Sigel investigated a group of honokiol and magnolol derivatives in patch-clamp experiments, which were synthesized by Dr. Alexander Fuchs. In the present study, these compounds have further been investigated at the CB receptors to determine their selectivity. 4'- *O*-methylhonokiol (**189**) itself showed a K$_i$ values of **8.43** µM for CB$_1$ and **0.0432** µM for CB$_2$ receptors. In the study of Fuchs *et al.* honokiol-like compounds turned out to be very potent in current potentiation at the GABA$_A$ receptor, especially compound **209**, **210** and **212** showed an >1000 % allosteric potentiation at 3 µM test concentration in the presence of 0.5 µM GABA. The compounds were found to probably interact with the β-subunit. The benzodiazepine

binding site could be excluded.[246] Recently, an additional binding site has been described for the endogenous cannabinoid 2-arachidonoylglycerol (2-AG) on the β_2 subunit of the GABA$_A$-receptor.[247] The honokiol derivatives might also bind to this newly characterized site.[246] Data of CB receptors affinities are shown in Table 28.

Table 28: Cannabinoid receptor affinities of honokiol-like compounds with variations in length of the lipophilic chain.

No.	Compd.	Chemical structure		Radioligand binding	
				Human CB$_1$	Human CB$_2$
		R^1	R^2	K$_i$ (µM) vs. [³H]CP55,940	K$_i$ (µM) vs. [³H]CP55,940
207	AF114	methyl	methyl	**2.97** ± 0.52	**0.834** ± 0.074
208	AF085	ethyl	methyl	>10 (22%)	**2.40** ± 0.952
209	AF083	propyl	methyl	>10 (49%)	**0.472** ± 0.178
210	AF115	butyl	methyl	**8.07** ± 1.84	**0.549** ± 0.116
211	AF116	pentyl	methyl	**2.73** ± 0.80	**0.134** ± 0.029
212	AF084	hexyl	methyl	**0.339** ± 0.135	**0.642** ± 0.383
213	AF112	heptyl	methyl	**3.69** ± 1.48	**0.591** ± 0.255
214	AF113	octyl	methyl	**1.95** ± 0.80	**1.66** ± 0.49
215	AF117	hexyl	ethyl	**0.125** ± 0.015	**0.595** ± 0.127
216	AF118	hexyl	propyl	**0.205** ± 0.177	**0.453** ± 0.177
217	AF119	hexyl	isopropyl	**2.57** ± 0.73	**0.243** ± 0.082

Compared to the lead structure 4'-*O*-methylhonokiol (**189**), the affinity to the CB$_2$ receptor was reduced, while the affinity to the CB$_1$ receptor was constant or even increased. The most potent compounds **209**, **210** and **212** differ in the length of the R^1 moiety increasing from propyl and butyl to hexyl. The compounds with the two smaller chains had no affinity to the CB$_1$ receptor up to 10 µM or were rather weak with **8.07** µM. For compound **208** the CB$_1$ affinity was with **2.73** µM in the low micromolar range and therefore also moderate. The hexyl-substituted derivative **212** on the other hand showed an increased affinity for CB$_1$ with a K$_i$ value of **0.339** µM. The longer lipophilic residue seemed to be beneficial for CB$_1$ affinity – the compounds **215** and **217**, which both share the hexyl residue, showed comparable K$_i$ values. For the CB$_2$ receptor, the affinity could be overall reduced in comparison to 4'-*O*-methylhonokiol (**189**). The three most potent compounds showed affinity between **0.472** µM to **0.642** µM – thus a ten-fold decrease in affinity. Nevertheless, the CB$_2$ affinity was still high. The most potent CB$_2$ ligand of this series was the pentyl-substituted compound **211**. This resembles the already described correlation for the magnolol derivatives, where a chain length of

pentyl and hexyl was also favoured. The affinity decreases when the chain was too long, see compound **214**, or when the chain was too short, see compound **208**.

Overall, it can be concluded that the 4'-*O*-methylhonokiol derivatives are a promising lead structures for the further development of positive allosteric potentiators for the $GABA_A$ receptor. They still show affinities for the CB receptors, more pronounced for the CB_2 receptor.

4.2.5. Activity of magnolol and honokiol derivatives at the cannabinoid-like receptors GPR18 and GPR55

It was already mentioned, that tetrahydromagnolol derivatives have been shown to act as antagonist at the orphan GPR55. The most potent compound with an IC_{50} value of **3.25** µM was **192**.[133] Here, we investigated all newly synthesized compounds at the two orphan GPCRs GPR18 and GPR55 to analyze these structure-activity relationships.

The already described magnolol derivatives, which varied in their ether substitution, are listed below in Table 29.

Table 29: Potencies of magnolol derivatives with varying lipophilic substitutions at the ether residue, at human GPR18 and GPR55

No.	Compd.[a]	human GPR18		human GPR55	
		Antagonistic activity	Agonistic actvity	Antagonistic activity	Agonist activity
		$IC_{50} \pm$ SEM (µM)	EC_{50} (µM)	$IC_{50} \pm$ SEM (µM)	EC_{50} (µM)
193	AF097	>10 (29%)	>10 (-5%)	**6.03** ± 1.38	>10 (-36%)
194	AF098	>10 (8%)	>10 (9%)	**8.55**± 1.13	>10 (20%)
195	AF099	>10 (21%)	>10 (9%)	**9.13**± 2.26	>10 (17%)
196	AF100	>10 (16%)	>10 (17%)	**7.24**± 1.44	>10 (23%)
197	AF101	>10 (3%)	>10 (9%)	>10 (37%)	>10 (12%)
198	AF102	>10 (15%)	>10 (9%)	**6.08** ± 0.98	>10 (35%)
199	AF105	>10 (15%)	>10 (19%)	**9.01** ± 1.29	>10 (40%)

[a] for chemical structures see Table 26

As can be seen almost all of the compounds, except **197**, showed a moderate inhibition in the micromolar range, but none of them was more active then **192**. They also did not differ much in their inhibitory strength, so explicit structure-activity relationships could not be deduced. In the first group (the 5'-hexyl-2'-alkyloxy derivatives), there seemed to be a tendency, that the smaller ether substitutions were favored. In the second group a clear dependency could not be determined.

Further the phenylanilin derivatives were investigated, the results can be found in Table 30.

Table 30: Potencies of diphenylamine derivatives for human GPR18 and GPR55

No.	Compd. [a]	human GPR18		human GPR55	
		Antagonistic activity $IC_{50} \pm$ SEM (μM)	Agonistic actvity EC_{50} (μM)	Antagonistic activity $IC_{50} \pm$ SEM (μM)	Agonist activity EC_{50} (μM)
200	AF128	>10 (10%)	>10 (19%)	>10 (36%)	>10 (19%)
201	AF127	>10 (25%)	>10 (26%)	>10 (25%)	>10 (30%)
202	AF126	>10 (17%)	>10 (42%)	>10 (31%)	>10 (34%)
203	AF125	>10 (23%)	>10 (25%)	>10 (45%)	>10 (18%)
204	AF132	>10 (25%)	>10 (-3%)	>10 (41%)	>10 (1%)
205	AF135	>10 (24%)	>10 (13%)	>10 (43%)	>10 (20%)
206	AF137	>10 (18%)	>10 (-7%)	~10 (53%)	>10 (18%)

[a] for chemical structures see Table 27

All of the diphenylamine derivatives turned out be inactive at both receptors, indicating that an intact biphenyl core structure is necessary to achieve inhibitory effects of GPR55. Furthermore, the 4'-*O*-methylhonokiol compounds have been investigated – the results can be found in Table 31.

Table 31: Potencies of honokiol-like compounds for human GPR18 and GPR55

No.	Compd. [a]	human GPR18		human GPR55	
		Antagonistic activity $IC_{50} \pm$ SEM (μM)	Agonistic actvity EC_{50} (μM)	Antagonistic activity $IC_{50} \pm$ SEM (μM)	Agonist activity EC_{50} (μM)
207	AF114	>10 (15%)	>10 (8%)	>10 (-32%)	>10 (3%)
208	AF085	~10 (52%)	>10 (23%)	>10 (33%)	>10 (-20%)
209	AF083	>10 (22%)	>10 (25%)	>10 (36%)	>10 (-15%)
210	AF115	>10 (18%)	>10 (2%)	>10 (29%)	>10 (-8%)
211	AF116	>10 (35%)	>10 (-4%)	>10 (22%)	>10 (12%)
212	AF084	~10 (60%)	>10 (4%)	>10 (-9%)	>10 (-15%)
213	AF112	>10 (36%)	>10 (-16%)	>10 (-18%)	>10 (21%)
214	AF113	>10 (24%)	>10 (12%)	>10 (0%)	>10 (7%)
215	AF117	>10 (29%)	>10 (-11%)	>10 (20%)	>10 (9%)
216	AF118	>10 (22%)	>10 (-19%)	>10 (34%)	>10 (13%)
217	AF119	>10 (25%)	>10 (-12%)	>10 (34%)	>10 (6%)

[a] for chemical structures see Table 28

The 4'-*O*-methylhonokiol derivatives also were all inactive at both investigated receptors. These results clearly show, that only tetrahydromagnolol derivatives were able to inhibit GPR55 activation. It can be concluded that tetrahydromagnolol derivatives should be further investigated, while honokiol derivatives are inactive

4.2.6. Summary of the structure-activity relationships for magnolol and honokiol derivatives as cannabinoid receptor ligands

The obtained results complete our efforts to study the structure-activity relationships of the tetrahydromagnolol and honokiol derivatives. As has been discussed above, we investigated the substitution of both phenolic hydroxyl groups by different lipophilic residues, also diephenylamine derivatives in contrast to the already established biphenylic compounds and different derivatives of 4'-O-methylhonokiol were examined. All of them have been studied at the cannabinoid receptors CB_1 and CB_2 and at orphan GPCRs GPR18 and GPR55.

The structure-activity relationships for the cannabinoid receptors can be summarized as follows:
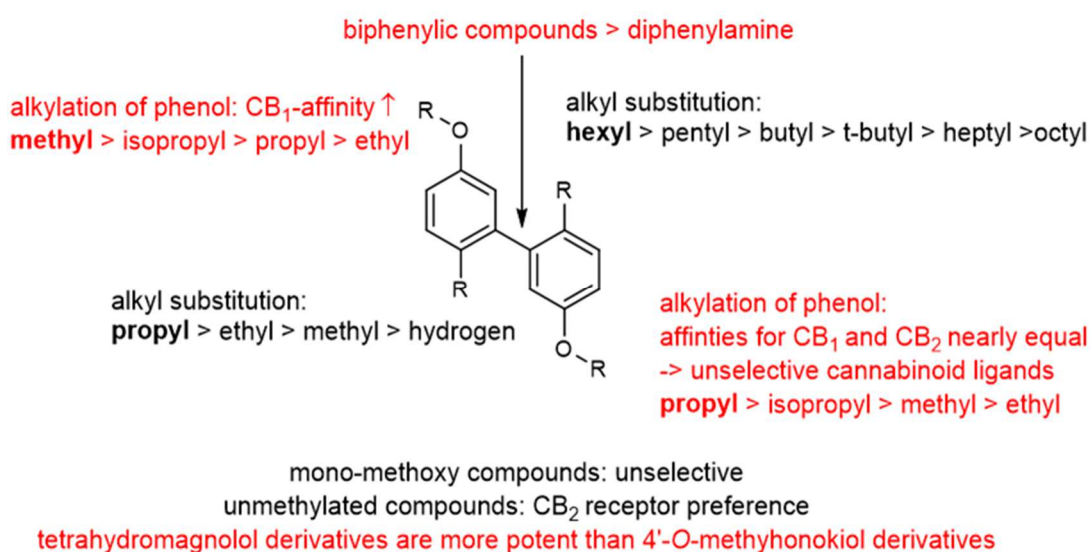
Figure 95: Updated structure-activity relationships for tetrahydromagolol derivatives at the cannabinoid receptors, new results in red

For the orphan GPR55 it can be summarized, that the realized variations were not superior to the already established compound **192**. The tetrahydromagnolol derivatives showed some inhibitory effects, while the 4'-O-methylhonokiol derivatives and the diphenylamine were inactive. Tetrahydromagnolol (**186**) could be confirmed as a lead structure, whereas the other two compound classes were less suitable.
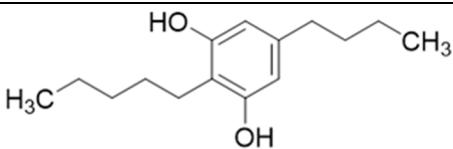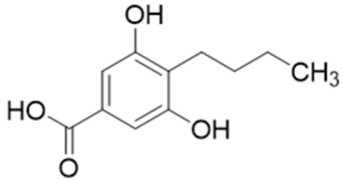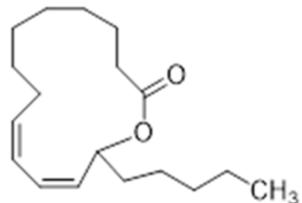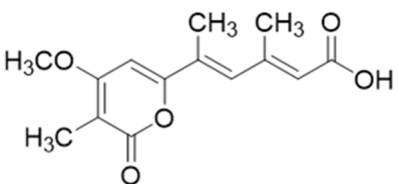
Thus, the investigations that were carried out further helped to analyze the structure-activity-relationships of this compound class.

4.3. Stemphol derivates

We further investigated a class of different natural products that was isolated by the research group of Prof. Dr. Gabriele König, especially by Dr. Jan Schroer and Dr. Mahmoud Elsebai (see Table 32). A

phenolic compound named stemphol (**218**) was obtained from the fungus *Stemphylium globuliferum*, which belongs to the sooty molds. Normally, this fungus causes crop damage, because it lives on fruits and vegetables. However, the group of Prof. König was able to isolate this fungus from algae. Stemphol (**218**) already has been described to display some mycotoxic effects in its vegetable hosts.[248] We wanted to investigate stemphol due to its lipophilic properties and because of its phenolic structure on cannabinoid and cannabinoid-like receptors. Other compounds were 4-butyl-3,5-dihydroxy benzoic acid (**219**), coriolide (**220**) – a macrolide, that was discussed to play a role in the chemoattraction of Costa Rica longwing butterflies[249], and infectopyrone (**221**), which has been described to occur in *Stemphylium* genera which grow on rotten tomatoes.[250] The group of Prof. König found all these compounds in marine fungi, which had not been known before. Another group of phenolic compounds was investigated, they belong to the paniceines, and were isolated by Dr. Mahmoud Elsebai. These group of compounds were already identified in the marine sponge *Reniera fulva* before.[251]

Table 32: Affinities of stemphol (**218**) and other lipophilic natural products at the cannabinoid receptors

No.	Compd.	Chemical structure	Radioligand binding	
			Human CB$_1$	**Human CB$_2$**
			K_i (µM) vs. [^{3}H]CP55,940	K_i (µM) vs. [^{3}H]CP55,940
218	Stemphol		**6.65** ± 1.61	**2.92** ± 0.27
219	4-Butyl-3,5-dihydroxy-benzoic acid		>10 (18%)	> 10 (3%)
220	Coriolide		>10 (11%)	>10 (9%)
221	Infectopyrone		>10 (7%)	>10 (8%)

222	Panicein C (RmF-36)		>10 (46%)	>10 (38%)
223	Panicein B3 (RmF-37)		>10 (33%)	>10 (27%)
224	Panicein B2 (RmF-82)		>10 (38%)	>10 (25%)
225	Panicein hydrochinon (RmF-83)		>10 (38%)	>10 (23%)
226	Panicein A (RmF-84)		>10 (21%)	>10 (11%)

As can be seen in Table 32, the compound stemphol (**218**) showed weak affinity in the low micromolar range to the CB receptors. This might not be surprising, because the compound contains a phenolic group and a lipophilic pentyl side chain, as already observed in the magnolol derivatives. The lack of the second aromatic moiety might also explain why it only displayed weak affinity. The other compounds, including the paniceins, had no affinity towards the CB receptors. Further, the compounds were also tested at the orphan GPR55 and GPR18 (see Table 33).

Table 33: Potency of stemphol (**218**) and other lipophilic natural products at GPR18 and GPR55

		Human GPR18		Human GPR55	
No.	Compd.[a]	Antagonistic activity	Agonist activity	Antagonistic activity	Agonistic activity
		$IC_{50} \pm SEM$ (µM)	EC_{50} (µM)	$IC_{50} \pm SEM$ (µM)	EC_{50} (µM)
218	Stemphol	n.d.	n.d.	>10 (37%)[b]	>10 (32%)[c]
219	4-Butyl-3,5-dihydroxy-benzoic acid	n.d.	n.d.	>10 (-26%)[b]	>10 (43%)[c]
220	Coriolide	n.d.	n.d.	>10 (-18%)[b]	>10 (41%)[c]
221	Infectopyrone	n.d.	n.d.	>10 (-21%)[b]	>10 (37%)[c]

222	Panicein C (RmF-36)	**11.1** ± 0.4	>10 (23%)[c]	**1.68** ± 0.35	>10 (-9%)[c]
223	Panicein B3 (RmF-37)	>10 (41%)[b]	>10 (-34%)[c]	**2.13** ± 0.91	>10 (-12%)[c]
224	Panicein B2 (RmF-82)	>10 (16%)[b]	>10 (9%)[c]	**5.39** ± 1.33	>10 (1%)[c]
225	Panicein hydrochinon (RmF-83)	>10 (44%)[b]	>10 (-37%)[c]	**8.52** ± 1.41	>10 (-14%)[c]
226	Panicein A (RmF-84)	>10 (18%)[b]	>10 (-4%)[c]	>10 (36%)[b]	>10 (-8%)[c]

[a] for chemical structures see Table 32.

[b] % inhibition of standard agonist induced luminescence signal (GPR18: 10 µM Δ^9-THC; GPR55: 1 µM LPI)

[c] % activation compared to standard agonist induced luminescence signal (GPR18: 10 µM Δ^9-THC; GPR55: 1 µM LPI)

The paniceins showed some inhibitory activity for the orphan GPR55 in the low micromolar range. Compound **222** was the most potent one with an IC_{50} value of **1.68** µM. This compound is also the most polar one, all its phenolic groups are not methylated compared to in the other paniceins. The second most active compound **223** lacks the 3-phenolic hydroxyl group but showed almost the same IC_{50} value of **2.13** µM. The potency decreases the more phenolic groups are substituted – compare compound **224** and **225**. The last compound **226**, which has no free hydroxyl group, was not active.

It has to be mentioned, that the paniceins contain aromatic aldehyde functions. Aldehydes are reactive and might form covalent bonds. Some of the compounds contain hydroquinone or quinone structures, which are also known to be reactive due to their oxidizing properties. Even if these compounds would reach their desired site of action in the body metabolic enzymes could rapidly inactivate them. Therefore, they can probably not be considered as good lead structures for further development.

4.4. Amauromine derivatives

Amauromine (**18**) is an alkaloid derived from the fungus *Auxarthron reticulatum* that lives together with the marine sponge *Ircinia variabilis* and was isolated by Dr. Mahmoud Elsebai. It is a symmetric diketopiperazine. The chemical structure arises from two tryptophan units, which are both prenylated.[225] Amauromine (**18**) was originally isolated from *Amauroascus sp.*, which lives in the Japanese woods and has been reported to act as vasodilatator when superperfusing rat aortic strips.[252]

It was further shown by Elsebai *et al.* to act as a CB$_1$ receptor antagonist with a high binding affinity showing a K$_i$ value of **0.178** µM. In cAMP accumulation assays the compound could further be described as a neutral antagonist.[225] No affinity to the CB$_2$ receptor could be observed, thus,

amauromine is a selective CB_1 receptor antagonist. In further experiments it could be shown, that amauromine (**18**) is also a moderate inhibitior of Δ^9-THC induced β-arrestin recruitment at human GPR18 with an IC_{50} value of **3.74** μM.[225]
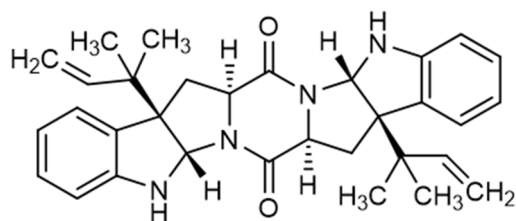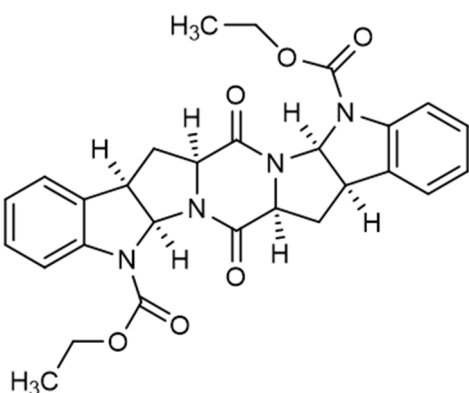
amauromine (18)
CB_1 K_i = 0.178 μM
hGPR18 IC_{50} = 3.74 μM
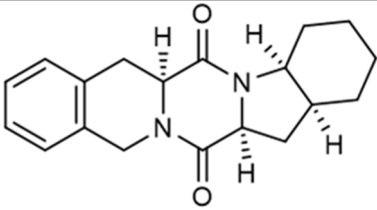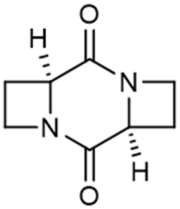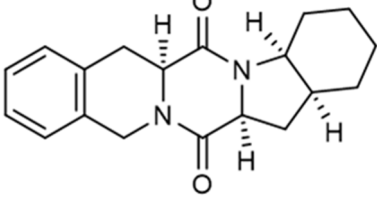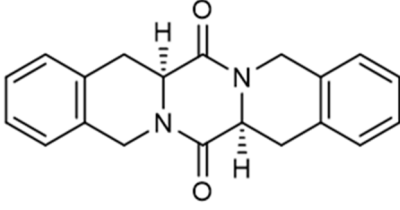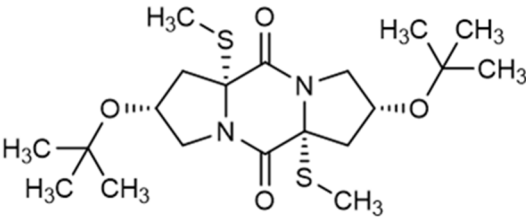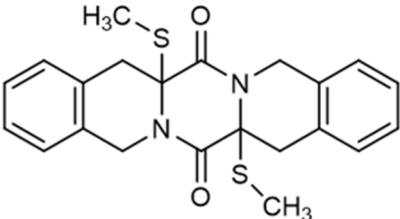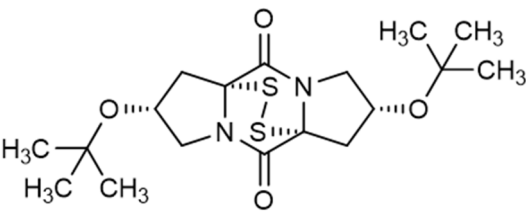
Figure 96: Chemical structure of the natural product amauromine (**18**)
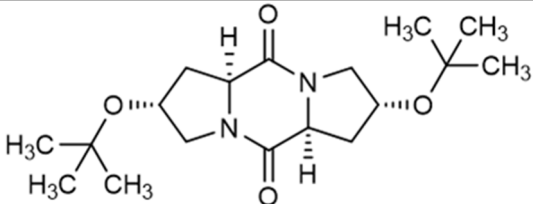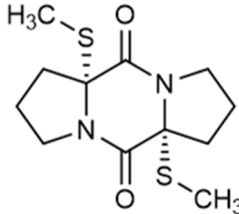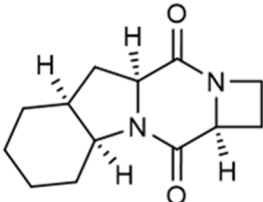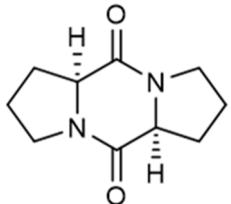
We wanted to get more insight in this structurally new class of CB receptor antagonists and investigated twelve diketopiperazine synthezised by the research group of Prof. Dr. Stefan Bräse. Originally, these compounds were synthesized because they belong to a group of biological active mycotoxines.[253]

To further investigate this compounds class the following compounds were screened at both CB receptors and the two orphan receptors GPR18 and GPR55.

Table 34: Affinities of diketopiperazines at human cannabinoid receptors

			Radioligand binding	
No.	Compd.	Chemical structure	Human CB$_1$	Human CB$_2$
			K_i (μM) vs. [^{3}H]CP55,940	K_i (μM) vs. [^{3}H]CP55,940
227	SZ **47**		>10 (8%)	>10 (19%)

228	SZ **85**		>10 (6%)	>10 (24%)
229	SZ **65**		>10 (-1%)	>10 (19%)
230	SZ **85** F3		>10 (4%)	>10 (17%)
231	SZ **66**		>10 (18%)	>10 (23%)
232	SZ **87**		>10 (3%)	>10 (17%)
233	SZ **67** (racemat)		>10 (36%)	>10 (25%)
234	SZ **88**		>10 (11%)	>10 (-1%)

235	SZ **69**		>10 (3%)	>10 (2%)
236	MSS **22** (scalemic)		>10 (9%)	>10 (2%)
237	SZ **83**		>10 (13%)	>10 (6%)
238	MSS **20**		>10 (5%)	>10 (2%)

None of the investigated compounds showed any effect in radioligand binding at both CB receptor subtypes. Thus, the structural similarity to amauromine has to be greater to get more ideas, which residues are important to achieve CB_1 receptor antagonism.

Table 35: Potencies of diketopiperazines at human GPR18 and GPR55 in β-arrestin recruitment[a]

	compound	**human GPR18**		**human GPR55**	
		Antagonistic activity IC$_{50}$ ± SEM (µM)	Agonist activity EC$_{50}$ (µM)	Antagonistic activity IC$_{50}$ ± SEM (µM)	Agonistic activity EC$_{50}$ (µM)
227	SZ **47**	>10 (10%)0	>10 (16%)	>10 (8%)	>10 (4%)
228	SZ **85**	>10 (8%)	>10 (-5%)	>10 (4%)	>10 (-1%)
229	SZ **65**	>10 (17%)	>10 (14%)	>10 (8%)	>10 (-1%)
230	SZ **85** F3	>10 (3%)	>10 (13%)	>10 (1%)	>10 (2%)
231	SZ **66**	>10 (-6%)	>10 (21%)	>10 (-32%)	≈10 (56%)
232	SZ **87**	>10 (43%)	>10 (33%)	>10 (19%)	>10 (8%)
233	SZ **67**	>10 (51%)	>10 (6%)	**9.77 ± 2.41**	>10 (9%)
234	SZ **88**	(64%)[b]	>10 (-100%)	(64)%[b]	>10 (-23%)
235	SZ **69**	>10 (2%)	>10 (9%)	>10 (3%)	>10 (10%)
236	MSS **22**	>10 (-20%)	>10 (21%)	>10 (7%)	>10 (7%)
237	SZ **83**	>10 (16%)	>10 (50 %)	>10 (3%)	>10 (13%)
238	MSS **20**	>10 (-8 %)	>10 (34%)	>10 (-8 %)	>10 (13%)

[a] for chemical structures see Table 34; [b] no concentration-dependent inhibition could be observed

The most closely related compound to amauromine **227** showed no inhibitory or activatory effects. Compared to amauromine (**18**) and also the agonists described in section 3.3 the indole nitrogen was substituted to a carbamin. This further strengthens the hypothesis of the necessity of an indole residue. But also, this compound lacks the prenylated side chains, which also can be of certain importance as lipophilic substituents. All other compounds lack the indole. Compound **234** showed promising results in the screens, but no curve was obtained at neither receptor. As these compounds have been synthesized because they are mykotoxins, a toxic effect on the cells may be possible. Even the small compounds **238** and **236**, which contains the diketopiperazine structure, displayed no effects. Thus suggesting that a certain size is necessary and that this core structural motif is not sufficient for inhibition of Δ^9-THC induced β-arrestin signaling.

For further investigations, it would be interesting to test derivatives that are more related to amauromine. As a necessary structural component the indole residue should be present.

4.5. Summary on natural products as ligands for cannabinoid and cannabinoid-like receptors

In this section, we showed our results on the study of natural products as cannabinoid receptor ligands, and also the approach to further investigate these compounds at the two cannabinoid-like orphan receptors GPR55 and GPR18.

Magnolol and honokiol-derived compounds as CB receptor ligands were introduced by Fuchs *et al.*[133] Here, we expanded the structure-activity relationships for this compound class (see Figure 97).
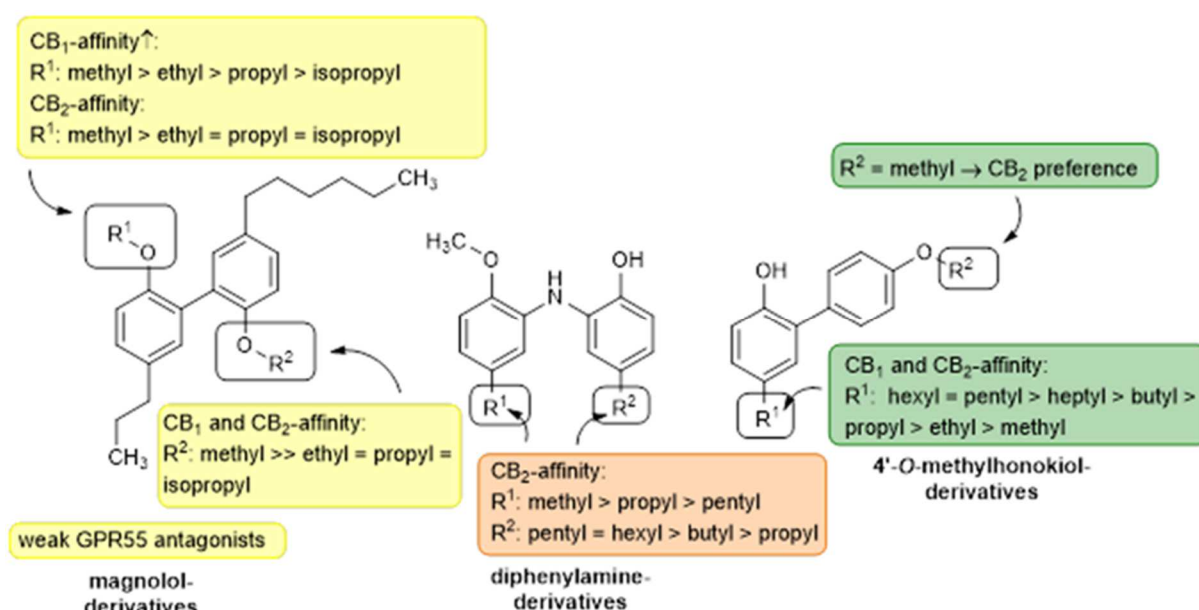
Figure 97: Structure-activity relationships of the magnolol and honokiol-derived CB ligands

The magnolol-derived compounds were the more potent than the diphenylamines and 4'-*O*-methylhonokiol-derived compounds. However, we were not able to develop a more potent ligand than compound **192**, which was the most potent compound of this compound class before. The magnolol-derivatives proved to be GPR55 antagonists with IC_{50} values in the low micromolar range. Most of the diphenylamines showed a preference for the CB_2 receptor, especially **compounds 202** and **203** were potent CB_2 ligands with K_i values of **0.258** and **0.295** µM, respectively, and a 6-and 5-fold preference of the CB_2 receptor, respectively. The 4'-*O*-methylhonokiol derivatives were potent CB_2 ligands, especially compound **211** with a K_i value of **0.134** µM and a 20-fold preference for CB_2.

Different phenolic natural products were investigated at the CB receptors and the orphan GPR18 and GPR55. Some so-called paniceins showed a moderate inhibition of GPR55 in the low micromolar range. The most potent was compound **222** with an IC_{50} value of **1.36** µM. However, these compounds were chemically not preferable as they contain reactive aldehydes.

We further investigated compounds with a similar scaffold as amauromine (**18**), a CB_1 and GPR18 antagonist. However, the here investigated compounds were inactive at both receptor.

5. CHROMEN-4-ONES AS AGONISTS AT GPR55

5.1. Chromen-4-ones as lead structure for GPCR ligands

Chromen-4-ones have been shown to be a privileged structure for the development of drugs. Many compounds can be found in natural products that contain a chromenone core structure, for example, the large group of flavonoids.

Chromenones have already been described as useful lead structures for the development of ligands for GPCRs. Pranlukast (**239**) is a marketed drug for asthma; it blocks the cysteinyl-leukotriene receptor 1 (CysLT$_1$ receptor),[254] which is a δ-branch class A rhodopsin-like GPCR. Pranlukast has been shown to also act as a weak antagonist at GPR17.[255] This confirms the utility of chromenone derivatives as GPCR ligands being suitable lead structures for drug development.

Furthermore, chromen-4-ones were extensively investigated by Funke *et al*. and optimized as GPR35 agonists.[179] The authors were able to design a radioligand for GPR35, a useful tool to study the (patho)physiology of this orphan receptor.[179] In their study, chromen-4-ones were also tested at the orphan GPR55 to prove the selectivity of their compounds. This is of primary interest, because GPR35 is closely related to GPR55. From this study, it was already known that some of the compounds were able to inhibit LPI-induced β-arrestin signaling in GPR55-expressing CHO-β-arrestin cells with moderate potencies in the low micromolar range. [179; 180] Chromen-4-ones have also been designed and optimized to act at the orphan receptors GPR17 and GPR84.[256]
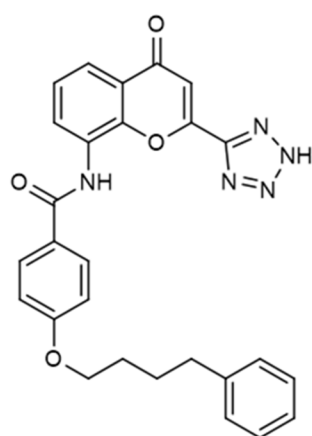
Pranlukast (239) - CysLT$_1$ Antagonist
CysLT1: IC$_{50}$ = **0.0043** µM (radioligand binding)[254]
hGPR17: IC$_{50}$ = **2.69** µM (Ca^{2+} mobilization assay)[255]
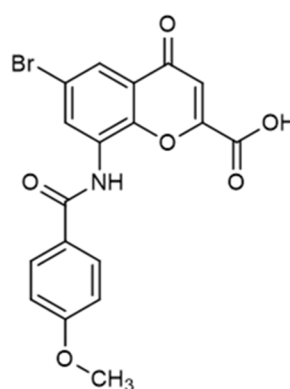
PSB-13253 (240)
hGPR35: EC$_{50}$ = **0.0121** µM (β-arrestin-assay)[179]

Figure 98: Pranlukast and **PSB-13253** (**240**), chromenone ligands that are used in pharmacological research[255,257; 258]

In the present study, a large in-house library of chromen-4-ones was investigated for interaction with GPR55. We analyzed structure-activity relationships including previous as well as new data. This

will provide a better understanding of the potencies of the compounds at GPR55 and a clear selectivity profile for the GPR35 agonists of this series.

5.2. Chromen-4-ones as GPR55 agonists

5.2.1. Previous results of chromen-4-ons at GPR55

All compounds were synthesized by Anne Meyer (ANM-compounds), Mario Funke (MF-compounds) and Thomas Blaschke (THB-compounds). The investigated compounds differ in many positions and cover a broad range of structural diversity. Funke *et al.* discovered that chromen-4-ones can be moderate antagonists of GPR55, while being very potent GPR35 agonists. An acidic functionality proved to be mandatory for GPR35 activation, because GPR35 contains positively charged amino acids, mainly arginines, in the binding pocket, which form ionic interactions with the negatively charged acidic function.[259] Another crucial structural feature for GPR35 activation is the bromo-substitution in position 6 of the chromenone core, together with relatively small substitutions at the 8-benzamido-residue in the *para*-position.[257]

The most potent GPR55 antagonists of this series so far have been compound **241** and **242** with IC$_{50}$ values of **2.65** µM and **4.34** µM, respectively (see Figure 99). All compounds that have been shown to act at GPR55 display some common features. Most of them have rather small or no substitutions at position 6. In contrast to GPR35 agonists, there have to be bulky lipophilic residues in the *para*-position of the benzamido moiety to achieve high GPR55 potency. Compound **242**, for example, contains a *para*-fluorobenzyloxy residue, and compound **241** an even longer *para*-phenylbutoxy residue. This pattern confirms previously obtained results for GPR55 antagonists (data not shown).[256]

(A)
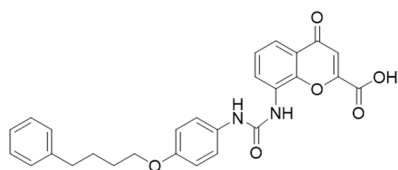
241
GPR17: IC$_{50}$ = **5.35** µM (Ca^{2+}-assay)[a]
GPR35: EC$_{50}$ = >10 µM; IC$_{50}$ = **46.6** µM (β-arrestin-assay)[b]
GPR84: IC$_{50}$ = **2.33** µM (cAMP-assay); IC$_{50}$ = **52.8** µM (β-arrestin-assay)[c]
GPR55: IC$_{50}$ = 2.65 µM[b]

(B)
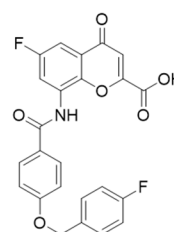
242
GPR84: IC$_{50}$ = **2.60** µM (cAMP-assay); IC$_{50}$ = **6.59** µM (β-arrestin-assay)[c]
GPR55: IC$_{50}$ = 4.34 µM[b]

Figure 99: The most potent chromen-4-one antagonists at GPR55, [a] data by Stephanie Weyer and Dr. Aliaa Abdelrahman, [b] data by Dr. Dominik Thimm, [c] data by Katharina Sylvester and Dr. Meryem Köse [256; 261; 260]

The GPR35 agonists were subsequently further optimized and in this context investigated at the GPR35 orthologues. To further enhance the selectivity profile of these compounds, we also monitored
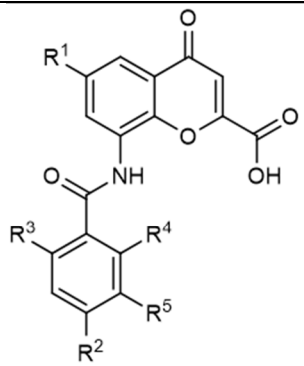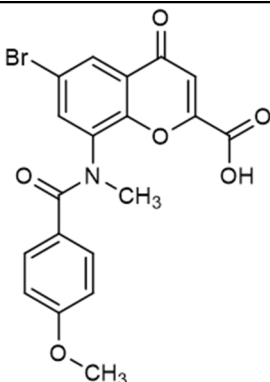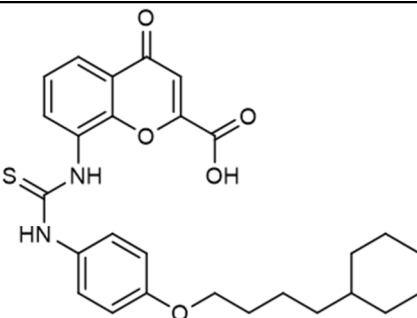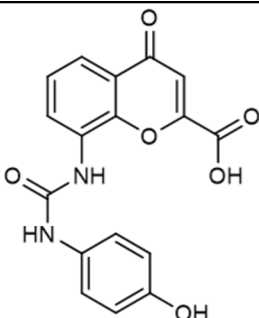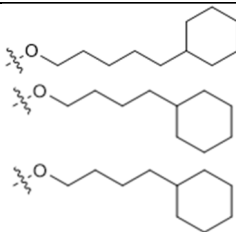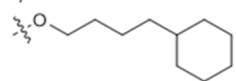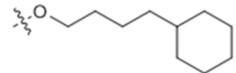
them at GPR55 and analyzed the structure-activity relationship. The results of this study can be found in the following parts of this chapter.

5.2.2. Activities of chromen-4-ones at GPR55

The investigated compound set can roughly be subdivided in three different classes. The first group of compounds is primarily substituted in the *para-* or *ortho-*position at the benzamido residue and can also be substituted in an additional position at the benzamido-residue. The second group consists of compounds that are modified in the *meta-*position. In the fourth group, compounds are described which do not fit into anyone of the three groups described before.

The *para-*substituted compounds have previously been shown to act as weak GPR55 antagonists by Funke *et al.*[179] In Table 36, more compounds with comparable substitutions are investigated as GPR55 antagonists and agonists.

Table 36: Potencies of *para*- and *ortho*- substituted chromen-4-one derivatives at the human GPR55

277 **278** **279**

No.	Compd.	Chemical structure					Human GPR55	
							antagonistic activity	agonistic activity
		R^1	R^2	R^3	R^4	R^5	$IC_{50} \pm SEM$ (µM)	EC_{50} (µM)
243	ANM158	H		H	H	H	**8.34** ± 1.16	>10 (7%)
244	ANM177	F		H	H	H	**3.26** ± 0.14	>10 (0%)
245	ANM170	Cl		H	H	H	**23.6** ± 10.6	>10 (-2%)
246	ANM6	Br	OCH_3	F	H	H	>10 (45%)	>10 (9%)
247	ANM7	Br	OCH_3	F	F	H	>10 (44%)	>10 (-4%)
248	ANM47	Br	OCH_3	OCH_3	H	H	>10 (8%)	>10 (-9%)
249	THB10	Br	SCH_3	H	H	H	**12.9** ± 1.7 (56%)[a]	>10 (-18%)
250	ANM190	Br	$-CH_2-CH_3$	H	H	H	**17.4** ± 6.4 (53%)[a]	>10 (-10%)
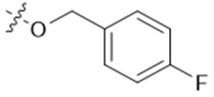
251	THB47	Br	[O-pentyl-phenyl]	H	H	H	**11.7 ± 0.8 (54%)[a]**	>10 (-1%)
252	ANM34	CH_3	OCH_3	H	H	H	>10 (18%)	>10 (7%)
253	ANM27	CH_3	OCH_3	H	H	F	>10 (27%)	>10 (-15%)
254	ANM59	CH_3	[O-CH₂-(4-F-phenyl)]	H	H	H	>10 (6%)	>10 (11%)
255	ANM173	CH_3	[O-propyl-cyclohexyl]	H	H	H	**4.54 ± 1.63**	>10 (2%)
256	ANM172	$-CH_2-CH_3$	OCH_3	H	H	H	>10 (8%)	>10 (-8%)
257	ANM97	$-CH_2-CH_3$	[O-CH₂-(4-F-phenyl)]	H	H	H	>10 (29%)	>10 (0%)
258	ANM217	$-CH_2-CH_3$	[O-pentyl-cyclohexyl]	H	H	H	>10 (23%)	>10 (-10%)
259	ANM40	OCH_3	OCH_3	H	H	H	>10 (4%)	>10 (12%)
260	ANM58	OCH_3	[O-CH₂-(4-F-phenyl)]	H	H	H	>10 (5%)	>10 (-3%)
261	ANM123	OCH_3	[O-propyl-cyclohexyl]	H	H	H	>10 (31%)	>10 (-5%)
262	ANM68	OCF_3	OCH_3	H	H	H	>10 (17%)	>10 (-14%)
263	ANM77	[phenyl]	OCH_3	H	H	H	>10 (-16%)	>10 (7%)
264	THB28	[phenyl]	OCH_3	F	F	H	>10 (28%)	>10 (0%)
265	ANM98	[phenyl]	[O-CH₂-(4-F-phenyl)]	H	H	H	>10 (1%)	>10 (-1%)
266	THB27	[phenyl]	[O-CH₂-(4-F-phenyl)]	H	H	F	**16.2 ± 6.0 (46%)[a]**	>10 (-13%)

		R1	R2					
267	ANM139	phenyl	O-CH2-(4-F-phenyl)	H	H	Cl	>10 (21%)	>10 (10%)
268	ANM130	phenyl	O-CH2-(3,4-diF-phenyl)	H	H	H	>10 (0%)	>10 (8%)
269	ANM141	4-F-phenyl	O-CH2-(4-F-phenyl)	H	H	H	>10 (35%)	>10 (-2%)
270	ANM151	4-F-phenyl	O-CH2-(3,4-diF-phenyl)	H	H	H	>10 (13%)	>10 (-15%)
271	ANM152	4-F-phenyl	O-CH2-(3,4-diF-phenyl)	H	H	Cl	>10 (5%)	>10 (7%)
272	ANM196	4-Cl-phenyl	OCH3	H	H	H	>10 (46%)	>10 (-5%)
273	ANM138	4-Cl-phenyl	O-CH2-(4-F-phenyl)	H	H	H	>10 (-4%)	>10 (3%)
274	ANM143	4-CH3-phenyl	O-CH2-(4-F-phenyl)	H	H	H	>10 (13%)	>10 (16%)
275	ANM203	4-OH-phenyl	O-CH2-(4-F-phenyl)	H	H	H	>10 (31%)	>10 (4%)
276	ANM142	4-OCH3-phenyl	O-CH2-(4-F-phenyl)	H	H	H	>10 (1%)	>10 (4%)
277	ANM78		See above	H	H	H	>10 (-6%)	>10 (1%)
278	ANM182		See above	H	H	H	**12.8 ± 1.3 (47%)**[a]	>10 (0%)
279	THB22		See above	H	H	H	>10 (11%)	>10 (10%)

| 280 | ANM26 | Br | H | | H | H | **8.54** ± 0.55 | >10 (6 ± 7%) |

^a percent inhibition at 10 µM test compound concentration

From the results in Table 36, it can be learned that small substituents in position R^1 are favorable for GPR55 inhibition. R^1 has been varied from very small substituents such as hydrogen to halogens including fluorine, chlorine and bromine and to alkyl groups such as methyl, ethyl, as well as aromatic residues. The active compounds contained hydrogen, small halogens or a methyl group. Ethyl or phenyl-substituted compounds were all inactive. Next, R^2 has been varied from very small methoxy goups to large lipophilic substituents such as cyclohexylalkyloxy groups with different chain lengths and corresponding aromatic derivatives. The most potent antagonists in this series were compound **255** and **244** with IC_{50} values between 3-4 µM. Both of them feature a cyclohexylbutoxy residue for R^2, but differ in R^1. Compound **244** has a fluorine in position R^1, while compound **255** contains a methyl residue, thus both have rather small residues in the R^1 position. The corresponding chlorine-substituted compound **245** and the methoxy-substituted **261** were inactive at a concentration of 10 µM.
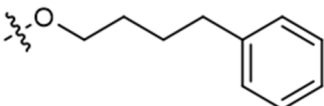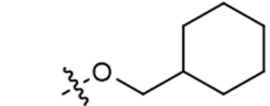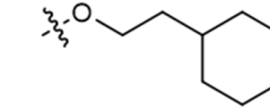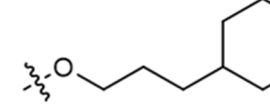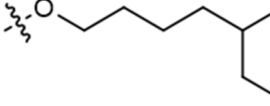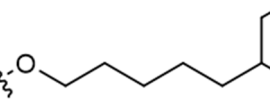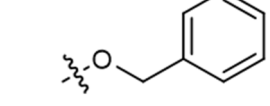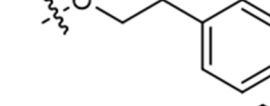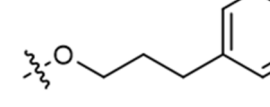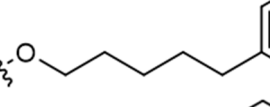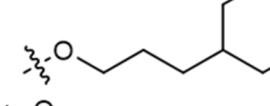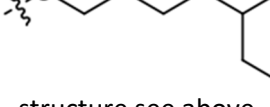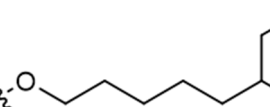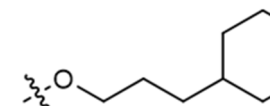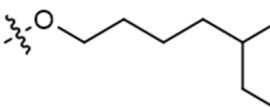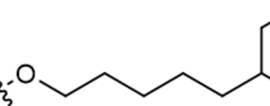
Only one *ortho*-substituted compound **280** displayed weak antagonistic activity versus GPR55, as has been observed for similar residues in position R^2 with *para*-substituted compounds.
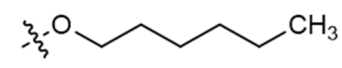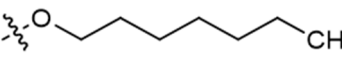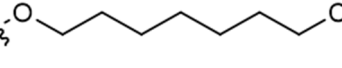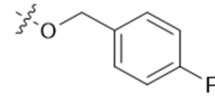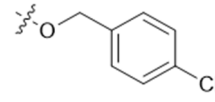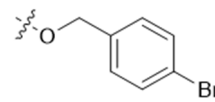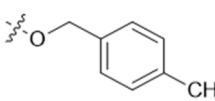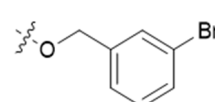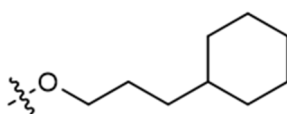
The most favorable R^2 residue for GPR35 activation (a methoxy residue) resulted in a completely inactive GPR55 ligand. This crucial structural feature of GPR35 activation therefore proves to be not tolerated at GPR55. The active GPR55 antagonists all show a large lipophilic side chain.

A second group of chromen-4-ones has been investigated at GPR55 (see Table 37).

Table 37: Potencies of compounds with *meta*-substituted benzamido-residues at the human GPR55.

No.	Compd.	Chemical structure		Human GPR55	
				antagonistic activity	agonist activity
		R^1	R^2	$IC_{50} \pm$ SEM (µM)	EC_{50} (µM) (% efficacy)
281	ANM234	H		>10 (45%)	>10 (20%)
282	ANM236	H		**6.30** $\pm$ 2.05	>10 (-3%)

			Structure		
283	THB49	H		**4.41** ± 0.28	>10 (2%)
284	ANM263	H		**1.48** ± 0.38	>10 (16%)
285	ANM267	H		>10 (38 %)	>10 (25%)
286	THB75	H		>10 (46%)	**0.111** ± 0.042 (29%)
287	ANM178	H		>10 (-51%)	**0.474** ± 0.099 (73%)
288	ANM250	H		>10 (-21%)	**0.202** ± 0.048 (52%)
289	ANM264	H		**6.88** ± 1.70	>10 (10%)
290	ANM270	H		**3.96** ± 0.82	>10 (14%)
291	ANM265	H		>10 (38%)	>10 (18%)
292	ANM280	H		>10 (21)	>10 (45%)
293	THB73	F		>10 (8%)	**0.117** ± 0.034 (29%)
294	THB71	F		>10 (-93%)	**0.373** ± 0.038 (71%)
295	ANM346		structure see above	>10 (-70%)	>10 (-9%)
296	ANM252	F		>10 (36%)	**0.263** ± 0.074 (58%)
297	THB74	Cl		>10 (-23%)	**0.323** ± 0.121 (40%)[d]
298	THB72	Cl		>10 (-115%)	**0.342** ± 0.039 (57%)
299	ANM251	Cl		>10 (-39%)	**0.196** ± 0.041 (86%)

300	ANM334	Cl		>10 (36%)	>10 (39%)
301	ANM337	Cl		>10 (9%)	**0.0400** ± 0.006 (39%)
302	ANM335	Cl		>10 (-11%)	**0.113** ± 0.064 (65%)
303	ANM20	Br		**10.6** ± 1.2 (87%)[a]	>10 (-2%)
304	ANM22	Br		>10 (36%)	**0.507** ± 0.033 (39%)
305	ANM21	Br		>10 (-87%)	**0.597** ± 0.137 (53%)
306	ANM235	Br		>10 (-15%)	**0.481** ± 0.84 (31%)
307	ANMDOT6	Br		**18.1** ± 7.1 (59%)[a]	>10 (16%)
308	ANM26	Br		>10 (18%)	>10 (6%)
309	ANM277	structure see above		>10 (31%)	>10 (27%)

When testing this compound series, some compounds such as **287** were found to act as <u>agonists</u> at GPR55.
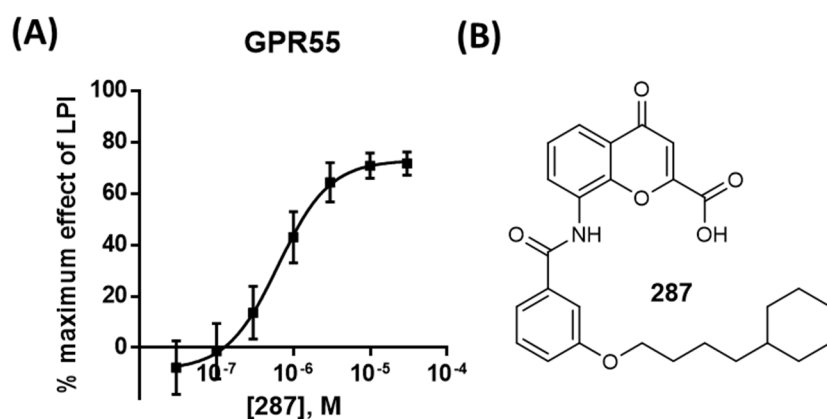
Figure 100: Concentration-dependent activation of compound **287** at the human GPR55, an EC_{50} value of **0.474** µM and an efficacy of 73% were determined

Although all chromen-4-ones investigated before had acted as antagonists, compound **287** displayed agonistic activity at GPR55 with high potency and an efficacy of 73% (compared to the full activation by 10 µM LPI, Figure 100). To further study this effect, a series of compounds were

170

synthesized that share different *meta*-substitutions. The results can be found in Table 37. The cyclohexylbutoxy residue of compound **287** was exchanged for smaller residues and for aromatic substituents or the alkyl chain length was reduced. In position 6, R^2 was exchanged for comparably small halogen atoms. This was done according to the former results described above, where small halogens proved to be preferred.
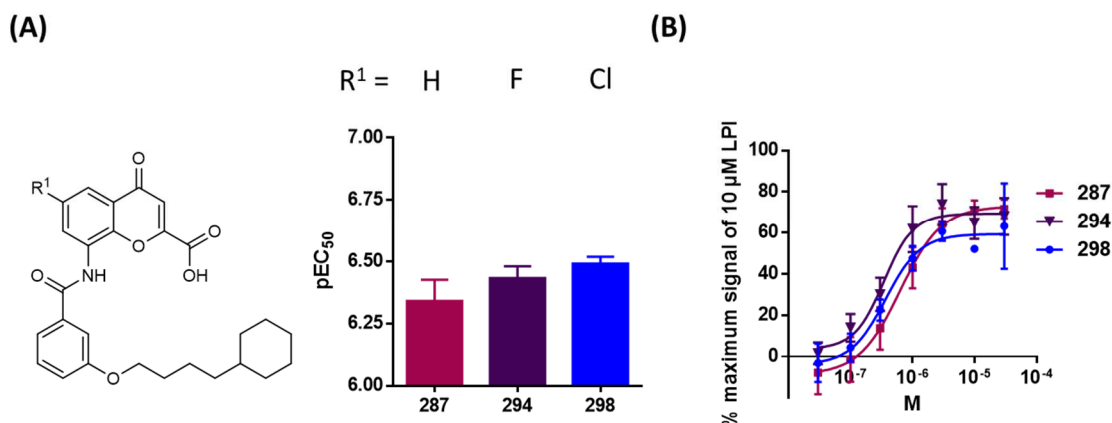
Figure 101: Potencies of 8-(3-cyclohexylbutoxy)benzamidochromen-4-one-2-carboxylic acids with different substitutions at position 6

In Figure 101, the effects of differently substituted derivatives of compound **287** are shown. Compound **294** and **298** have a fluorine or a chlorine at position 6. The activity increased slightly, which can be observed in Figure 101 (A), while the efficacy stayed unaltered (in Figure 101 (B) the maximum of the GPR55 activation did not change). Altogether, there was an insignificant advantage of a chlorine residue in position 6.

The R^2 residue was also intensively studied. First of all, the chain length of the cyclohexylalkyloxy group was varied. This was done for different R^1 substituted compounds.
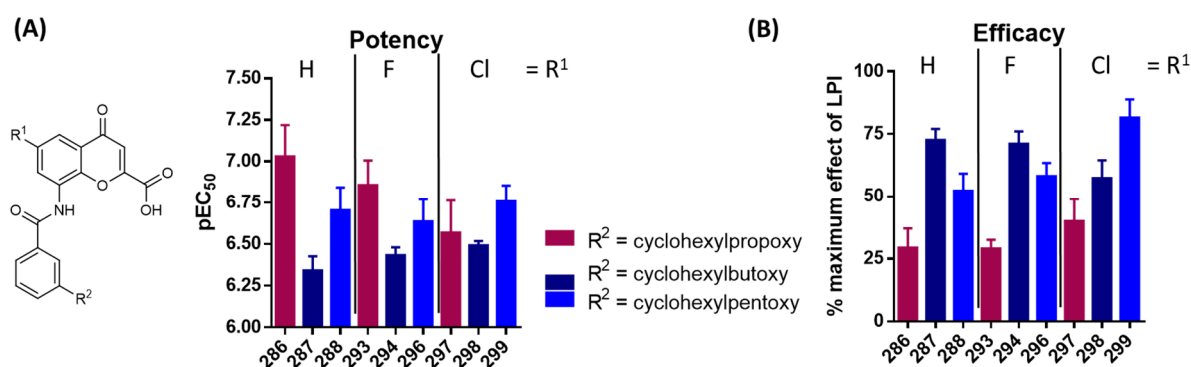
Figure 102: Influence of different alkyl chain length of the cyclohexylalkyloxy residue on GPR55 activation

In Figure 102, the cyclohexylalkyloxy residue for R^2 was investigated. The alkyl chain length of the first hit compound **287** was a butyloxy moiety. With compound **286** and **288**, propoxy and pentoxy moieties were also investigated. Compound **286** showed an EC_{50} value of **0.111** µM, but an efficacy of only 29%. Compound **288** was equally potent as **287**, with a slightly reduced efficacy. These three R^2 side chains have also been combined with derivatives with a fluorine or chlorine atom in R^1 position. For fluorine-substituted compounds, the same dependency could be observed as for the unsubstituted compounds. Compound **293** was the most potent compound of the fluorinated series with an EC_{50} value of **0.117** µM and an efficacy of 29%. Compound **294**, the cyclohexylbutoxy compound, was less potent but comparable to **287**, also regarding the efficacy. Compound **296**, the cyclohexylpentoxy derivative, was similar to **288**. Furthermore, a set of chlorinated compounds was investigated. In this series, the cyclohexylpentoxy derivative **299** was the most potent compound with an EC_{50} value of **0.196** µM and a high efficacy of 89%. Compound **297**, the cyclohexylpropoxy derivative, was the weakest compound of the three, both in potency as and efficacy. Out of these nine compounds, **299** was the most efficacious with the highest GPR55 activation.

The R^2 residue was varied to cyclohexylethoxy and cyclohexylmethoxy in compound **285** and **284**. Both compounds were not active at a concentration of 10 µM.
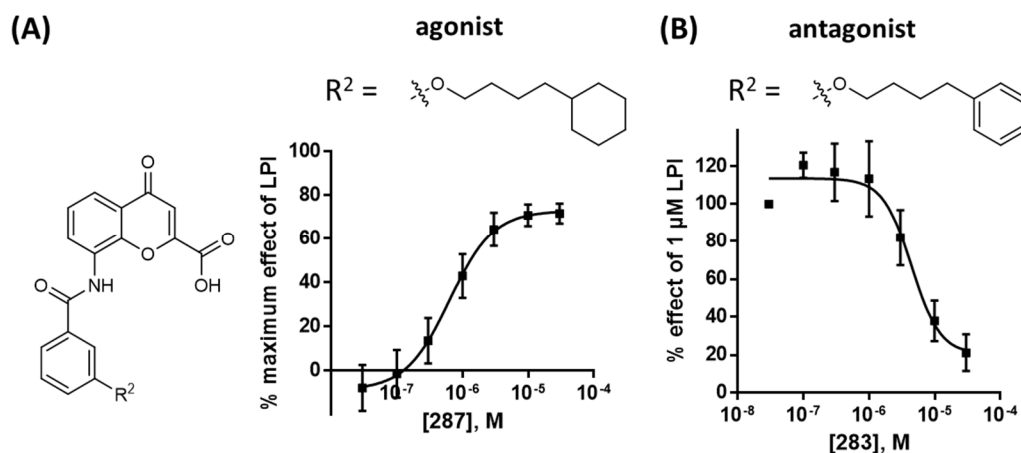
Figure 103: Functional difference between aliphatically and aromatically substituted compounds
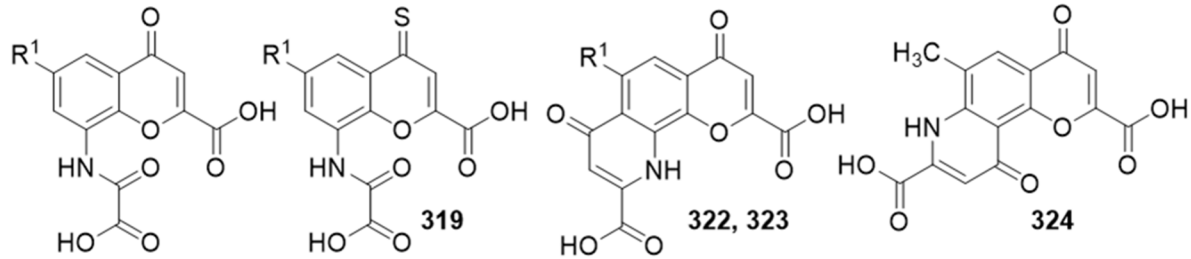
Aromatic substitutions have also been tested in the *meta*-position of the benzamido residue. Compound **283** is corresponding to **287**. Surprisingly, compound **283** showed no activating potency, but acted as antagonist versus LPI with an IC_{50} value of **4.41** µM. Further, the compounds **289** and **290** - both of them share aromatic substituents attached by different lengths of alkyl linkers - acted as weak antagonists at GPR55. Thus, aromatic residues prevent GPR55 activation. Aliphatic substitutions are necessary to activate the receptor, while aromatic substitutions lead to receptor blockade.

It has been shown before that *para*-substituted bulky lipophilic residues can lead to a moderate GPR55 inhibition, for both aliphatic and aromatic residues. In the *meta*-position, there is a switch between agonistic and antagonistic functionality for aliphatic and aromatic substitutions, especially when R^1 is a hydrogen or fluorine atom. However, there is a restriction: For compounds with a bromine atom in position 6, some benzyloxy residues (the *para*-chloro-, bromo- and methylbenzyloxy substituted compounds **304**, **305** and **306**) showed a quite potent activation with EC_{50} values of around 500 nM. However, they all displayed a very low efficacy (between 31-53% of the maximum effect of LPI). The only aliphatic brominated compound **280** showed no activation of GPR55. For fluorinated and unsubstituted compounds with aromatic residues in the *meta*-position no agonistic potency could be detected. They were inactive or had a moderate antagonistic effect.

A compound lacking the acidic function of the chomen-4-ones, such as compound **309**, did not activate or inhibit GPR55 signaling at all. The acidic function seemed to be necessary for GPR55 inhibition and activation.

The 8-benzamido-chromen-4-ones had been unfavorable for the mouse orthologue of GPR35. When the benzamido moiety was exchanged for an oxalic acid monoamide, which also introduced a second acidic function, the potency at the mouse receptor increased significantly. These compounds have now also been investigated at GPR55.

Table 38: Potencies of compounds with an additional acidic function at GPR55.

compound		Chemical structure	Human GPR55	
			antagonistic activity	agonist activity
		R^1	$IC_{50} \pm$ SEM (µM)	EC_{50} (µM)
310	THB12	H	>10 (-8%)	>10 (-14%)
311	ANM295	F	>10 (9%)	>10 (34%)
312	ANM296	Cl	>10 (6%)	>10 (27%)
313	ANM183	Br	>10 (1%)	>10 (3%)
314	ANM298	-CH$_3$	>10 (11%)	>10 (29%)
315	ANM297	-OCH$_3$	>10 (-1%)	>10 (27%)
316	ANM299	-CH$_2$-CH$_3$	>10 (27%)	>10 (19%)
317	ANM383	-CH$_2$-CH$_2$-CH$_2$-CH$_3$	>10 (2%)	>10 (48%)
318	ANM287		>10 (17%)	>10 (46%)
319	ANM300	structure see above	>10 (34%)	>10 (15%)
320	ANM379	-CH$_3$	>10 (14%)	>10 (4%)
321	ANM367	Br	>10 (11%)	>10 (-4%)-
322	ANM365	structure see above	>10 (22%)	>10 (16%)

It could be seen that none of these compounds was active at GPR55 at a concentration of 10 µM. This confirms their selectivity for GPR35.

Overall, the structure-activity relationships for the chromen-4-ones at GPR55 can be described as being very complex. While aliphatic *meta*-substitutions at the benzamido residue led to GPR55-agonistic activity, aromatic residues at the same position resulted in compounds with antagonistic effects. Aromatic and large aliphatic substitutions in *para*-position at the benzamido residue resulted in weak antagonistic activity. In position 6 of the chromen-4-one, agonists require small lipophilic substituents such as fluorine or chlorine. Larger residues were not tolerated. The acidic function of the chromen-4-ones appears to be required for interaction with GPR55.
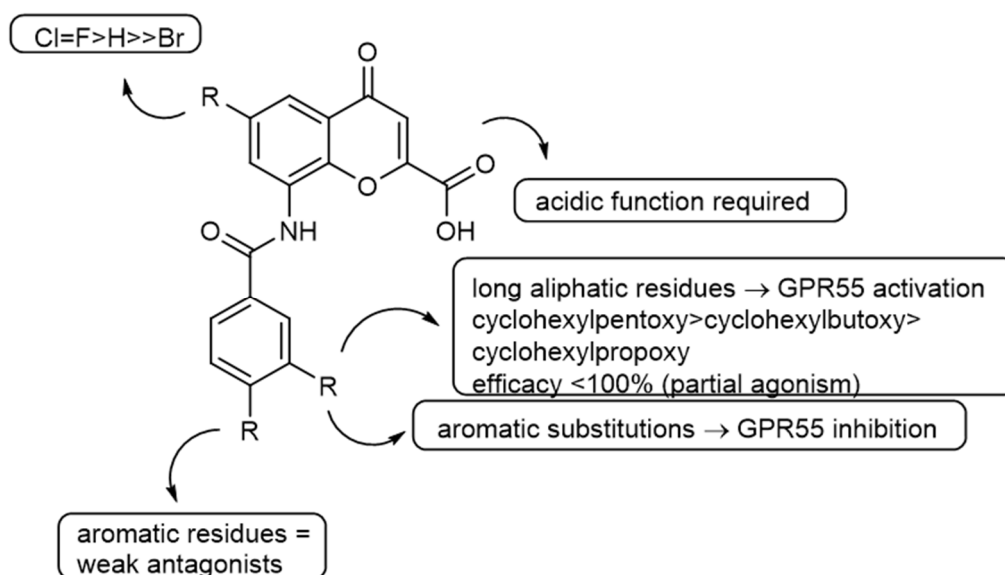
Figure 104: Structure-activity relationships of chromen-4-ones at the human GPR55

Several agonists for GPR55 have been described in the literature, as discussed in 1.4.2. We compared the newly investigated GPR55 chromen-4-one agonists to those previously identified structures. Chemical structures and potencies can be viewed in Figure 16.

Heynen-Genel et al. described three structural related GPR55 agonists by using a β-arestin assay with a fluorescence read-out (Transfluor® from Molecular Devices) and detected a 100% efficacy compared to the activation by LPI.[121] When comparing the new chromen-4-one agonists with these agonists some structural similarities but also differences are evident. All structures, including the chromen-4-ones, show an amide bond in the center of the molecule. This functional group might form hydrogen bonds. **ML-186** (**23**) and **ML-184** (**24**) both contain sulfonamide groups, whereas our chromen-4-ones contain a carboxylic acid residue. Both structures are bioisoteres and might bind to the same binding site. The GPR55 agonists GSK522373A (**25**) described by Brown et al. is structurally very similar to the agonists described by Heynen-Genel et al.[120] It also features an amide bond and a sulfonamide. The agonists **27** and **28** described by Yrjölü et al. have a comparable thiourea moiety in the center of the molecule.[126]

None of the reported GPR55 agonists has an acidic function, although this might be an important interaction partner in the biding site. For the compounds described by Heynen-Genel et al. and also for compound **299** and derivatives, a certain spacial arrangement between the "head group" with the polar functions and the lipophilic residue can be observed. Kotsikorou et al. proposed an L-shaped topology for GPR55 agonists. They investigated possible binding modes in homology modeling approaches, by which they created the hypothesis, that the long aliphatic tail of the 2-AG-PI or LPI binds deep down into the cavity of the transmembrane domain helix bundle, whereas the polar head groups point to the surface and show interactions with the extracellular loops.[262] For the compounds

investigated by Heynen-Genel *et al.* they proposed similar poses of the ligands. The chromen-4-one derivatives are also able to form analogous conformations (see Figure 106).

The physicochemical properties of the known GPR55 agonists described are quite comparable to the new GPR55 agonists identified in the present study. All compounds name a molecular weight of around 500 g/mol, which is at the limit defined by the Lipinski Rule of Five for peroral bioavailability.[263] However, the natural ligand LPI also shows a high molecular weight of 572.63 g/mol. Due to its charged phosphate group and the polar sugar moiety, LPI has a very low log D value both at pH 2.0 and also at pH 7.4. The described ligands however show comparably high log D values. Especially, the thiourea derivatives described by Yrjölä *et al*. are highly lipophilic. The advantage of our newly identified GPR55 agonists, is the reduced log $D_{7.4}$. The acidic function is deprotonated at a pH value of 7.4 and reduces the lipophilicity compared to an acidic environment. The only compound with less lipophilicity is the agonist **26** described by Morales *et al*. However, it only shows an activation of 51% and has no acidic character.

Table 39: Physicochemical properties of different GPR55 agonists (logD values were calculated with Marvin 17.4.3, ChemAxxon).

	Compound[a]	molecular weight (g/mol)	Log $D_{2.0}$	Log $D_{7.4}$
19	LPI	572.63	1.68	-0.30
22	ML-185	461.56	3.24	3.24
23	ML-186	436.54	1.58	3.60
24	ML-184	470.63	4.37	4.34
25	GSK522373A	516.56	4.37	4.38
26	22 Morales	440.24	-1.44	2.02
27	17b Yrjölä	519.61	5.95	5.95
28	17l Yrjölä	491.58	4.87	4.87
299	ANM251	512.00	6.32	3.13

[a] for structure see Figure 16

Especially, when comparing the chromen-4-ones to the possible endogenous ligand LPI, many of the discussed features become meaningful.

A possible endogenous agonist for GPR55 might be 2AG-PI, which is the 1-lyso-arachidonoylphosphatidylinositol, described by Oka *et al.*[264] The molecule contains the fatty acid arachidonic acid, a very lipophilic group, which is linked via glycerol to a negatively charged phosphate group, bound to the inositol. The latter two groups represent polar structures (see Figure 105).
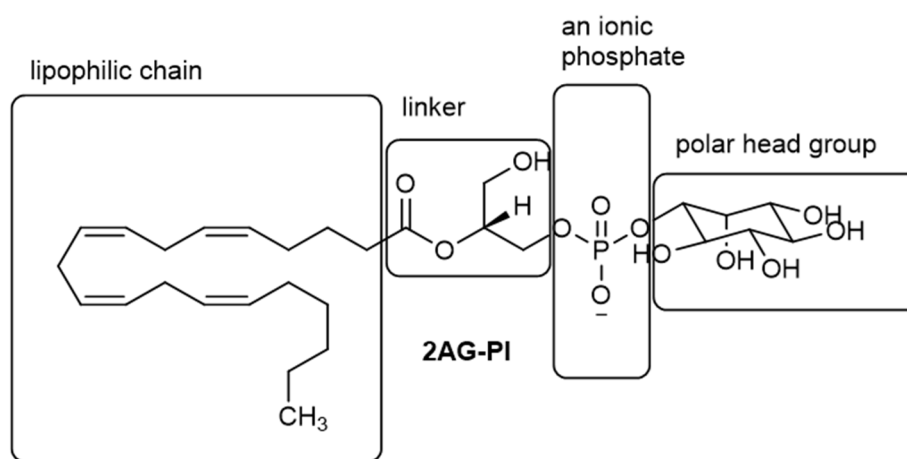
Figure 105: Chemical structure of 2AG-PI, a possible endogenous ligand for GPR55

When we compare this structure to our newly identified GPR55 agonists, especially to compound **299**, some common features can be determined (see Figure 106). The carboxylic acid of compound **299** will be negatively charged at physiological pH values, similarly to the phosphate group of 2AG-PI and LPI. The 4-carbonyl function of compound **299** and derivatives is located in a similar position as the hydroxyl function of 2AG-PI. The ester function and the amide of compound **299** are superimposable. The arachidonic acid is a polyunsaturated fatty acid and contains four double bonds, which are *cis*-configurated. It matches well with the long lipophilic side chain of compound **299**.

The two molecules are congruent in their topology regarding the lipophilic part, the linker and the negative charge, but 2AG-PI contains further a polar head group, inositol, which is lacking in compound **299**. This might be one reason for the partial agonism of the chromen-4-one derivatives compared to LPI. Exploration of the inositol binding pocket should be further explored.
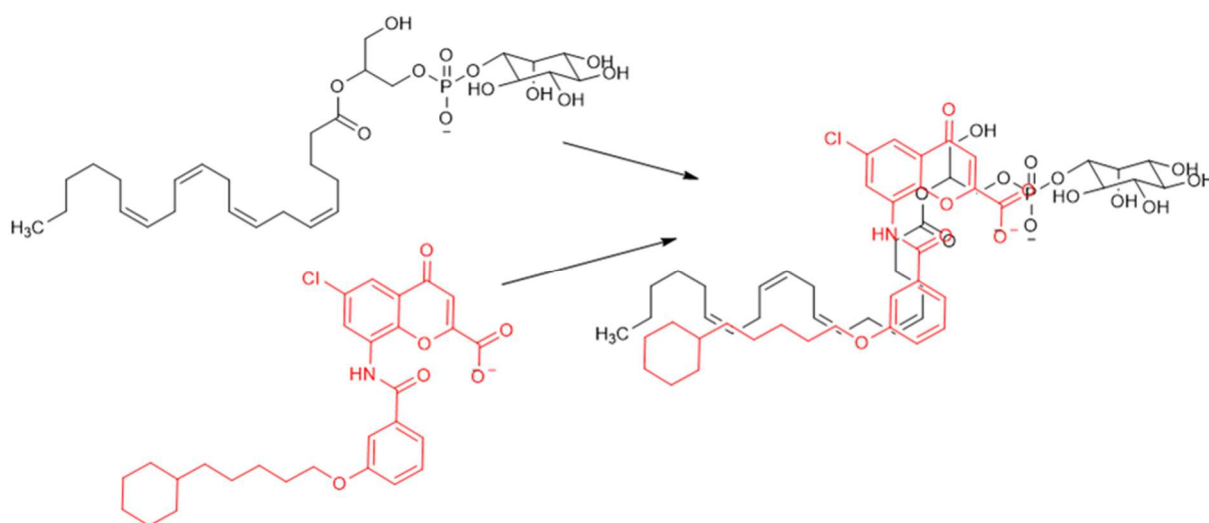
Figure 106: Superimposition of compound **299** and 2AG-PI

The results for GPR55 have been generated in β-arrestin assays only. To confirm the obtained results, the compounds should be tested in an additional assay system. GPR55 has been described to activate $G_{12/13}$ signaling, which results in the activation of small GTPases such as RhoA, and the phosphorylation of ROCK kinases.

Furthermore, the selectivity of the compounds has to be studied. The structure-activity relationships that have been established by Funke *et al.* suggest already a high degree of selectivity for GPR55, because GPR35 activation required a bromine at position 6.[257] The selectivity of the compounds versus GPR35, GPR18 and the cannabinoid receptors will be discussed in subsequent chapters.

5.3. Selectivity of GPR55 ligands versus GPR35, GPR18 and cannabinoid receptors

5.3.1. Selectivity of GPR55 ligands versus GPR35

The selectivity of the chromen-4-ones was investigated by testing them against the most closely related receptor, GPR35.

Assays have been performed by Dr. Dominik Thimm in the same test system as used for GPR55.[261]

Table 40: Potencies of chromen-4-ones at the human GPR35 in β-arrestin recruitment assays

		Human GPR35
No.	**Compd.**	**agonist activity**
		EC$_{50}$ ± SEM (µM)[a]
243	ANM158	>10 (12%)
244	ANM177	>10 (-2%)
245	ANM170	>10 (3%)
246	ANM6	**0.00446** ± 0.00030
247	ANM7	**0.00554** ± 0.00029
248	ANM47	**0.0162** ± 0.0009
249	THB10	**0.0150** ± 0.0009
250	ANM190	**0.0570** ± 0.0055
251	THB47	>10 (22%)
252	ANM34	**0.0377** ± 0.0036
253	ANM27	**0.00437** ± 0.00048
254	ANM59	>10 (22%)
255	ANM173	>10 (31%)
256	ANM172	**0.0306** ± 0.0074
257	ANM97	**7.47** ± 1.38
258	ANM217	**0.791** ± 0.228
259	ANM40	**0.0255** ± 0.0027
260	ANM58	>10 (33%)
261	ANM123	>10 (35%)
262	ANM68	**0.0104** ± 0.0017
263	ANM77	**0.00548** ± 0.00089
264	THB28	**0.00108** ± 0.00011
265	ANM98	>10 (40%)
266	THB27	**0.381** ± 0.021

267	ANM139	>10 (48%)
268	ANM130	>10 (8%)
269	ANM141	>10 (13%)
270	ANM151	>10 (1%)
271	ANM152	>10 (2%)
272	ANM196	**0.00821** ± 0.00189
273	ANM138	>10 (4%)
274	ANM143	>10 (5%)
275	ANM203	**0.583** ± 0.002
276	ANM142	>10 (20%)
277	ANM78	>10 (28%)
278	ANM182	**1.87** ± 0.08
279	THB22	**1.87** ± 0.08
280	ANM26	>10 (-2%)
281	ANM234	>10 (40%)
282	ANM236	>10 (27%)
283	THB49	>10 (22%)
284	ANM263	>10 (23%)
285	ANM267	>10 (8%)
286	THB75	>10 (-7%)
287	ANM178	>10 (-3%)
288	ANM250	>10 (-2%)
289	ANM264	**4.20** ± 0.57
290	ANM270	>10 (40%)
291	ANM265	>10 (14%)
292	ANM280	>10 (11%)
293	THB73	>10 (-4%)
294	THB71	>10 (-6%)
295	ANM346	>10 (2%)
296	ANM252	>10 (-9%)
297	THB74	>10 (-5%)
298	THB72	>10 (-6%)
299	ANM251	>10 (-8%)
300	ANM334	>10 (5%)
301	ANM337	>10 (-1%)
302	ANM335	>10 (-1%)
303	ANM20	>10 (7%)
304	ANM22	>10 (16%)
305	ANM21	>10 (6%)
306	ANM235	>10 (35%)
307	ANMDOT6	>10 (4%)
280	ANM26	>10 (20%)
309	ANM277	n.d.
310	THB12	**0.264** ± 0.017
311	ANM295	**0.106** ± 0.011
312	ANM296	**0.0293** ± 0.0015
313	ANM183	**0.0118** ± 0.0015
314	ANM298	**0.104** ± 0.003
315	ANM297	**0.0938** ± 0.0087
316	ANM299	**0.0275** ± 0.0025
317	ANM383	**0.0318** ± 0.0025
318	ANM287	**0.00968** ± 0.00048
319	ANM300	**0.00547** ± 0.00072

320	ANM379	**0.0295** ± 0.0046
321	ANM367	**0.037** ± 0.0021
322	ANM365	**0.0214** ± 0.0021

[a] for structures see Table 36, Table 37 and Table 38

[b] Effects were normalized to the signal induced by 30 µM zaprinast
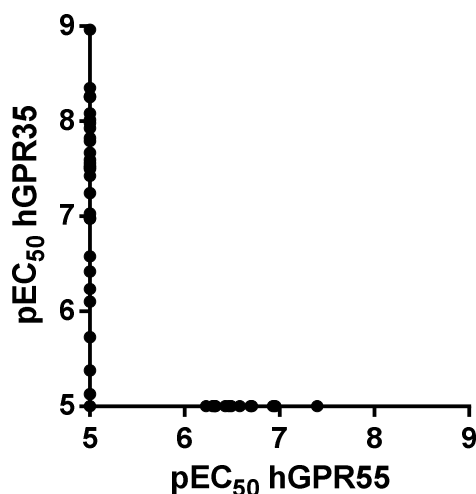
Figure 107: Correlation of EC_{50} values of chromen-4-ones for human GPR35 and human GPR55

In Table 40 and in Figure 107, the potencies of the compounds at the human GPR35 are shown. The chromen-4-one series contains many very potent GPR35 agonists, but the structure-activity relationships are very different from those at GPR55. GPR35 requires a bromine atom at position 6 and small lipophilic substitutions at the benzamido ring, preferably fluorine in the *ortho*-position and a methoxy group in the *para*-position for high potency. In contrast, GPR55 does not tolerate bromine substitutions in position 6 of agonists. On the other hand, GPR35 cannot be activated by chromen-4-ones with long aliphatic residues in the *meta*-position of the benzamido ring. In Figure 107, it can be observed that selectivity is obtained. Compounds, that activate GPR55, do not activate GPR35.

5.3.2. Selectivity of versus GPR18

GPR18 is another receptor that is closely related to GPR55. In contrast to GPR35 it can interact with cannabinoids like GPR55 (compare chapter 1.4.1). Therefore, we studied the selectivity of the identified GPR55 ligands at GPR18 (see in Table 41).

Table 41: Potencies of the chromen-4-one derivatives at the human GPR18

No.	Compd.[a]	Human GPR18	
		antagonistic activity	agonist activity
		IC$_{50}$ ± SEM (µM)	EC$_{50}$ (µM)
243	ANM158	>10 (36%)	>10 (5%)
244	ANM177	>10 (29%)	>10 (-15%)
245	ANM170	>10 (6%)	>10 (-24%)
246	ANM6	>10 (-28%)	>10 (12%)
247	ANM7	>10 (11%)	>10 (10%)
248	ANM47	>10 (7%)	>10 (18%)
249	THB10	>10 (18%)	>10 (-10%)
250	ANM190	>10 (22%)	>10 (-9%)
251	THB47	>10 (30%)	>10 (-7%)
252	ANM34	>10 (-10%)	>10 (34%)
253	ANM27	>10 (20%)	>10 (-3%)
254	ANM59	>10 (10%)	>10 (-24%)
255	ANM173	>10 (22%)	>10 (-33%)
256	ANM172	>10 (2%)	>10 (-23%)
257	ANM97	>10 (16%)	>10 (-13%)
258	ANM217	>10 (23%)	>10 (-10%)
259	ANM40	>10 (-20%)	>10 (15%)
260	ANM58	>10 (-12%)	>10 (11%)
261	ANM123	**28.1** ± 16.4	>10 (-57%)
262	ANM68	>10 (-1%)	>10 (18%)
263	ANM77	>10 (24%)	>10 (-8%)
264	THB28	>10 (15%)	>10 (4%)
265	ANM98	>10 (8%)	>10 (-47%)
266	THB27	>10 (17%)	>10 (-9%)
267	ANM139	>10 (19%)	>10 (26%)
268	ANM130	>10 (26%)	>10 (-33%)
269	ANM141	>10 (26%)	>10 (-50%)
270	ANM151	>10 (30%)	>10 (-1%)
271	ANM152	>10 (28%)	>10 (41%)
272	ANM196	>10 (-1%)	>10 (17%)
273	ANM138	>10 (38%)	>10 (-9%)
274	ANM143	>10 (10%)	>10 (25%)
275	ANM203	>10 (22%)	>10 (16%)
276	ANM142	>10 (10%)	>10 (-16%)
277	ANM78	>10 (-17%)	>10 (29%)
278	ANM182	>10 (31%)	>10 (16%)
279	ANM26	>10 (4%)	>10 (1%)
280	THB22	>10 (16%)	>10 (-4%)
281	ANM234	>10 (-2%)	>10 (2%)
282	ANM236	>10 (23%)	>10 (25%)
283	THB49	>10 (18%)	>10 (-1%)
284	ANM263	>10 (-2%)	>10 (9%)
285	ANM267	>10 (28%)	>10 (5%)
286	THB75	>10 (14%)	>10 (13%)
287	ANM178	>10 (3%)	>10 (14%)
288	ANM250	>10 (34%)	>10 (-16%)
289	ANM264	>10 (-17%)	>10 (1%)
290	ANM270	>10 (-7%)	>10 (-4%)
291	ANM265	>10 (1%)	>10 (-5%)

292	ANM280	>10 (23%)	>10 (0%)
293	THB73	>10 (3%)	>10 (17%)
294	THB71	>10 (22%)	>10 (13%)
295	ANM346	**13.1** ± 3.0	>10 (-51%)
296	ANM252	>10 (8%)	>10 (6%)
297	THB74	>10 (11%)	>10 (12%)
298	THB72	>10 (16%)	>10 (14%)
299	ANM251	>10 (25%)	>10 (-4%)
300	ANM334	>10 (3%)	>10 (10%)
301	ANM337	**9.24** ± 2.39	>10 (12%)
302	ANM335	>10 (32%)	>10 (19%)
303	ANM20	>10 (15%)	>10 (6%)
304	ANM22	>10 (26%)	>10 (11%)
305	ANM21	>10 (27%)	>10 (18%)
306	ANM235	>10 (-13%)	>10 (26%)
307	ANMDOT6	>10 (4%)	>10 (4%)
280	ANM277	>10 (2%)	>10 (15%)
309	ANM23	>10 (26%)	>10 (4%)
310	THB12	>10 (1%)	>10 (-4%)
311	ANM295	>10 (11%)	>10 (23%)
312	ANM296	>10 (32%)	>10 (25%)
313	ANM183	>10 (-22%)	>10 (14%)
314	ANM298	>10 (8%)	>10 (15%9
315	ANM297	>10 (9%)	>10 (16%)
316	ANM299	>10 (16%)	>10 (17%)
317	ANM383	>10 (-3%)	>10 (11%)
318	ANM287	>10 (17%)	>10 (36%)
319	ANM300	>10 (8%)	>10 (12%)
320	ANM379	>10 (0%)	>10 (0%)
321	ANM367	>10 (-1%)	>10 (-4%)
322	ANM365	>10 (-12%)	>10 (14%)

[a] for structures see Table 36, Table 37 and Table 38

The chromen-4-one derivatives showed no potency at the human GPR18, with only four exceptions. Three compounds displayed a weak inhibition of Δ^9-THC-induced β-arrestin recruitment mediated by GPR18. Compound **261** showed with an IC_{50} value of **28.1** µM very weak potency and did also not activate the human GPR18. This was also true for compound **295**, which displayed an IC_{50} value of **13.1** µM, at GPR18. Compound **301** had an IC_{50} value of **9.24** µM, a compound that contains a heptoxy side chain in the *meta*-position at the benzamido moiety. It is one of the low efficacy GPR55 agonists (EC_{50} = 0.040 µM, efficacy = 39%). Thus, a high degree of selectivity of the GPR55 compounds against GPR18 was confirmed.

5.3.3. Selectivity of GPR55 ligands versus the cannabinoid receptors

GPR55 can interact with by cannabinoids, for example the potent cannabinoid receptor agonist CP55,940 is a moderately potent antagonist at GPR55.[265] We determined the affinity of selected potent GPR55 agonists in radioligand binding against tritiated CP55,940 (seen Table 42).

Table 42: Affinities of selected GPR55 agonists at cannabinoid receptors

No.	Compd.[a]	Radioligand binding	
		Human CB$_1$ K_i (µM) vs. [^{3}H]CP55,940 (% inhibition of specific binding)	Human CB$_2$ K_i (µM) vs. [^{3}H]CP55,940 (% inhibition of specific binding)
286	THB75	**6.46** ± 2.06	>10 (23 ± 11%)
287	ANM178	**13.0** ± 7.1	**36.7** ± 16.6
293	THB73	**7.21** ± 1.15	**20.2** ± 6.1
294	THB71	**8.92** ± 2.05	**21.4** ± 5.1
299	ANM251	**14.6** ± 2.2	**16.0** ± 7.0

[a] for structures see Table 37

The compounds showed weak displacement of the radioligand binding. All K_i values ranged from around 5 to 40 µM. Therefore, they can be regarded as weak cannabinoid receptor ligands. The affinity of compound **299** with K_i values of **14.6** µM and **16.0** µM correlates to a 75-fold selectivity for GPR55 versus the CB$_1$ and 82-fold selectivity versus CB$_2$ receptors.

In further compound optimization studies the selectivity versus CB receptors has to be monitored. So far it appears to be no problem to achieve selectivity for GPR55 agonists.

Some of the chromen-4-one derivatives have also been investigated as ligands for the orphan receptors GPR17 and GPR84. The results of these studies for selected compounds are collected in Table 43. The potencies are in the low micromolar range. Compound **299**, which was inactive at hGPR84, was active at hGPR17 with an IC$_{50}$ of **1.58** µM. It still displayed an 8-fold selectivity for the human GPR55.

Table 43: Potencies of selected GPR55 agonist at the two orphan GPCRs GPR17 and GPR84[a]

| | Compound | Antagonistic activity | |
		Human GPR84	**Human GPR17**
		IC_{50} (μM)[b] cAMP accumulation assay	IC_{50} (μM)[c] Ca^{2+} mobilization assay
286	THB75	>3 (29%)	**4.28** ± 0.49
287	ANM178	**6.36** ± 1.94	**1.71** ± 0.04
293	THB73	**1.68** ± 0.57	**4.63** ± 0.60
294	THB71	**1.03** ± 0.04	**2.67** ± 0.49
299	ANM251	>3 (33%)	**1.58** ± 0.49
293	THB73	**1.68** ± 0.57	**4.63** ± 0.60

[a]data kindly provided by Katharina Sylvester and Dr. Meryem Köse (hGPR84) and Stepfanie Weyer and Dr. Aliaa Abdelrahman (hGPR17) [b]cAMP accumulation assay in CHO β-arrestin hGPR84 cells, in the presence of 100 μM Forskolin, activation with decanoic acid. [c]Ca^{2+}-mobilization assay in 1321N1 astrocytoma cells stably expressing GPR17, activation with MDL29,951.

5.4. Discussion and Outlook

A series of chromen-4-one derivatives has been investigated and optimized for the human GPR55. Those derivatives that have been developed as GPR35 ligands bromine in position 6 and a *para*-substituted benzamido residue in position 8, showed only weak inhibitory potency against GPR55 or were inactive. In this study, it was discovered that long aliphatic residues in *meta*-position of the benzamido moiety led to GPR55 activation. Different substitutents were investigated: cyclohexylalkyloxy residues displayed the highest potencies at the human GPR55, and the resulting compounds were partial agonists. The compound with the highest potency and efficacy was compound **299** (6-chloro-8-(3-((5-cyclohexylpentyl)oxy)benzamido)-4-oxo-4*H*-chromene-2-carboxylic acid) with an EC_{50} value of **0.196** μM and an efficacy of 86%. When the alkyl chain length was reduced the efficacy decreased. Chloro-substitution in position 6 of the chromen-4-one proved to be superior to other halogen atoms or a hydrogen atom.

Comparing compound **299** to other published GPR55 agonists, it displays similar potency, bit lower efficacy according to published data. All known GPR55 agonists show some molecular features, e.g. shape and functional groups.

Whenever the aliphatic moiety was exchanged for an aromatic substituent, the agonist properties were lost and weak antagonists potency was observed instead (agonist-antagonist-switch).

For further investigation, compounds with a polar group linked to the carboxylic function should be explored. Of major importance would be the confirmation of the agonism of the chromen-4-one derivatives in a second assay system, as well as investigation of potential species differences in rodents as compared to humans.

6. PHARMACOLOGICAL EVALUATION OF SYNTHETIC CANNABINOIDS IDENTIFIED AS CONSTIUENTS OF SPICE

6.1. Introduction

Many cannabinoids have been consumed because of their psychoactive effects. First of all, the herbal derived Δ^9-THC, which is found in marihuana (the flower and flower near leafs of the *Cannabis sativa* plant) or as hashish, then meaning the highly Δ^9-THC-rich resin of the female hemp, has been used to generate favorable psychic effects. These effects of hashish and marihuana have been known for many centuries. The main active chemical compound could be identified, isolated and synthesized in the 1960ies by Raphael Mechoulam from the Hebrew University.[266,267] They further investigated the biosynthesis of Δ^9-THC and some other cannabinoid compounds in the hemp plant, and established the structure-relationships of this compound group, at a time when the pharmacological target of the cannabinoids was not known.[268,269] In 1988, a cannabinoid receptor binding site in rat brain membrane preparations was identified by binding experiments with the tritiated ligand CP55,940, a compound that was developed by Pfizer as an antinociceptive drug.[12] Devane *et al.* proposed the CB receptor to be a G protein-coupled receptor,[10] Matsuda *et al*. could verify this in 1990 by cloning the cannabinoid receptor 1 for the first time.[11]

Δ^9-THC containing plant material, hashish and marihuana, have been known for a long time. First mentioning of the use of hemp for medicinal and recreational purpose dates back to the early Chinese and Assyrian civilizations[270] Although used for many purposes, cannabis effects have been discussed controversially. Following the legal drugs tobacco and alcohol, it is probably the most abundantly abused substance in the world. Nevertheless, till now the use of marihuana and hashish is regarded as rather safe, as no direct lethal effects of overdoses have been reported. An LD_{50} was determined for rat and mice (29 mg/kg and 43 mg/kg, respectively, when administered intravenous, 666 mg/kg and 482 mg/kg when given perorally).[271,272] The chronic administration, which can cause psychotic effects, is therefore more dangerous, as it comes along with tolerance and withdrawal symptoms.[273] But even here it should be noted that measurable neurotoxic effects occur in rodents after chronic administration of cannabis smoke for three month with some changes in the hippocampal pyramidal neurons. In rhesus monkeys these effects could not be observed after chronic treatment for a full year.[274] Therefore, the chronical toxic effects are still not clearly characterized.

Today, the use of cannabis is controlled in most of the countries in the world. In Germany, cannabis plant material and also Δ^9-THC as a purified substance are part of the controlled substances act, meaning that owning, consuming, buying and selling is restricted to the public authorities. Δ^9-THC itself can also be prescribed under these restrictions by medical doctors for certain indications such as cachexia and chronic pain.

Cannabis in its various dosage forms is the most sold, consumed and seized illegal drug in the European Union. Cannabis plant material and hashish resin still represent the major amount of consumed cannabinoids in Europe. Nevertheless, the amount of synthetic cannabinoids is increasing.[275] They are sold as "harmless" but effective alternatives to the restricted plant materials and resins of cannabis, as so-called 'legal highs'. Normally, they are labeled as 'not for human consumption' to circumvent medicinal and nutritional specifications. They are normally found to be mixed with plant material and also declared as such. These synthetic cannabinoids in plant material appeared in Europe in 2006 under the trademark 'Spice' or 'K2'. They are normally sold in colorful small plastic bags with an eye on the front. Many different types and tastes exist. In the early days of 'Spice' the true ingredients were not known, and the herbal plant material was declared to be the main component. Two groups later on identified nearly simultaneously synthetic cannabinoids in these "legal highs".[276,277] The two major identified compounds were JWH-018 and CP47,497 (see Figure 108), and derivatives of the latter. CP47,497 and derivatives are very similar to the well-known CP55,940. Both of these compound groups have been known for long times in medicinal chemistry as potent cannabinoid receptor agonists. Compounds with the compound identifier JWH have been developed by John W. Huffman as cannabinoid receptor ligands in the mid 90s,[278] and the CP compound identifier refers to Carl Pfizer and to the pharmaceutical company Pfizer, which developed cannabinoid receptor ligands in the late 80s and early 90s as antinociceptive drugs.[279]

3 CP55,940
CB_1: K_i = 0.5 - 5.0 nM[30]
CB_2: K_i = 0.69 - 2.8 nM[30]

4 Δ^9-THC
CB_1: K_i = 5.05 - 80.3 nM[30]
CB_2: K_i = 3.13 - 75.3 nM[30]

5 JWH-018
CB_1: K_i = 9 nM[30]
CB_2: K_i = 2.9 nM[30]
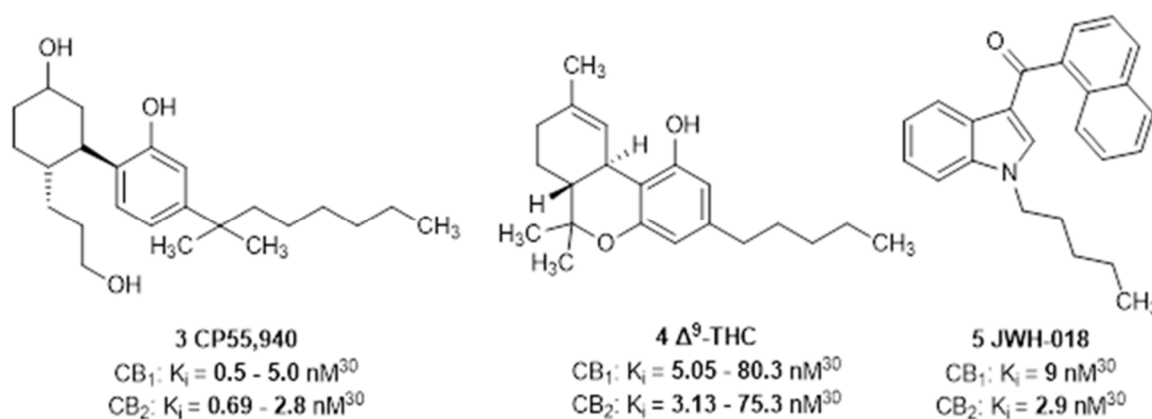
Figure 108: Δ^9-THC and the two synthetic cannabinoids CP55,940 and JWH-018 with their affinity to the CB receptors. [30,278]

These synthetic cannabinoids are more potent than the partial agonist Δ^9-THC, which can be referred to as a typical dirty drug – a compound that not selectively interacts with one target, but shows effects on various other targets. These synthetic cannabinoids are mostly highly potent cannabinoid receptor ligands, and their effects and also side-effects are more severe than those of Δ^9-THC itself. CP55,940 shows antinociceptive, antiemetic, anticonvulsive and anti-inflammatory effects via the CB receptors, and has been proposed for many indications, including Parkinson's disease

and cancer therapy-induced emesis, but never marketed as such.[280,281,282] CP55,940 nevertheless is the standard cannabinoid ligand that has been used in research for decades.

JWH-018, which has been developed to study the structure-activity relationships of the aminoalkylindoles and was only one compound out of many synthesized ones mainly to understand CB_2 receptor selectivity has had its inglorious revival as an abused drug in 'spice' blends. Upon discovery, it was restricted by law to the Narcotic Drug Act (BtMG in Germany), especially as these compounds are more potent and therefore can cause more severe side effects than Δ^9-THC. The most common side effects reported in context with JWH-018 have been an increased risk to induce psychosis[283] and direct toxic effects on the heart: tachycardia and arrhythmias.[284,285] More recently identified compounds such as **5-F-PB-22** (**375**) have been reported in context with lethal consumptions.[286] A climax was the reported "zombie-outbreack" in Brooklyn, Manhattan, USA, when around 30 unresponsive or slowly responsive persons staggered through their neighborhood. Later on, the synthetic compound **AMB-FUBINACA** (**323**) was identified to have caused these effects.[287]
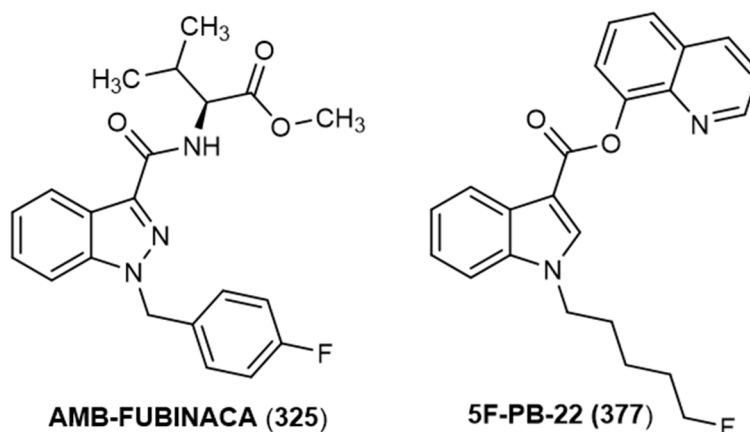
Figure 109: Chemical structure of **AMB-FUBINACA** (**323**) and **5F-PB-22** (**375**)

The severity and frequency of side-effects caused by synthetic cannabinoids is increasing and brought them intto the focus of the health care systems. One of the few studies on the hospitalization caused by synthetic cannabinoid intake was conducted in Anchorage, Alaska, from July 2015 to March 2016. They identified over 1000 ambulance transports in that time and a regular hospitalization with severe side-effects. Around 40% of the patients were homeless.[288] The increasing endangerment potential and the criminal intention of the sellers has accelerated the compounds restriction by law.

In 2009, only JWH-018 and CP47,497 and derivatives were restricted, but from that time on more and more synthetic cannabinoids have been appeared on the illicit drug market. The total number of restricted compounds has increased each year (compare Figure 110).
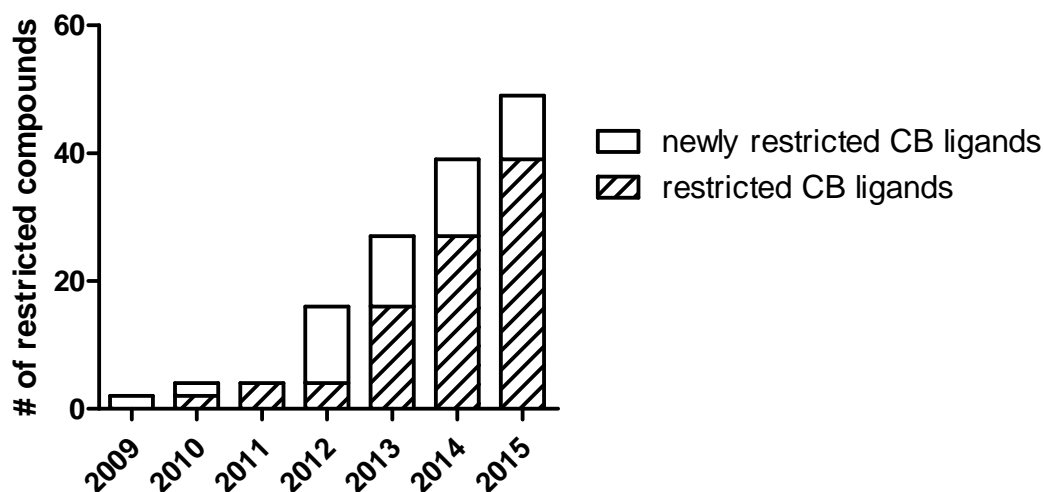
Figure 110: Newly restricted synthetic cannabinoids in the BtMG (Narcotic Drug Act in Germany) per year

Restriction by law can be circumvented by modifying the structure of the compounds. Due to the nature of the Narcotic Drug Act only clearly defined chemical compounds with an evidence to be abused can be restricted. There are many known cannabinoid compounds in the scientific literature, completely reported with synthesis and bioactivity data. Moreover, the already restricted synthetic compounds could also be altered in their chemical structure with the purpose of preserving bioactivity and circumventing the restriction by law.[289] Forensic researchers have to analyze the new compounds and investigate their chemical structure, compare these to known compounds, collect case studies until enough evidence exists to restrict them. As consumption of illegal compounds and of 'legal highs' is often associated with criminal behavior, clear facts are necessary to judge these cases correctly.

The EMCDDA (European Monitoring Centre for Drugs and Drug Addiction) defines a scaffold common to all of the synthetic cannabinoids. Their main constitution remains quite preserved, only the residues are exchanged. As most of these compounds have adventurous names on the illicit drug market, most often to enhance the sales, the EMCDDA also agreed on a common labeling system to describe each emerging compound uniquely.
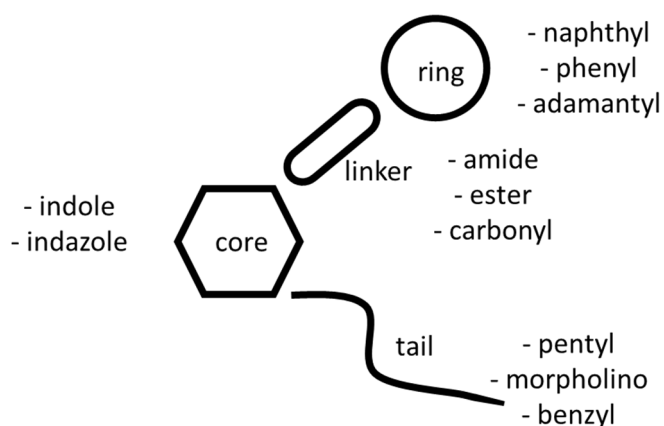
Figure 111: Scaffold of the synthetic cannabinoids as defined by the EMCDDA[290]

To circumvent restriction the residues that can be found in the 'tail' part and the 'ring' part of this scaffold are varied most commonly. Also, the substitutions have been combined in almost every possible way. There are three different types of 'linkers': amides, esters or carbonyl residues. These structure-activity relationships had already been established by Huffman *et al*.[291] and also by researchers from Abbott.[292] The main purpose of changing the chemical structure of the compounds is to circumvent restriction but maintaining bioactivity. Therefore typical bioisoteric groups are introduced into the main scaffolds. In 6.2, we will describe the different groups and how the affinity to the cannabinoid receptors is altered.

In November 2016, a new law was put into force in Germany that restricts compound classes based on their structure-activity relationships. Two groups of compounds were described in the enforcement, the synthetic cannabinoids and the cathinones (amphetamine-like compounds). However, clandestine chemists already launched compounds, which are not restricted by the New Psychotic Drugs Act.
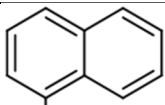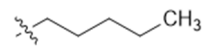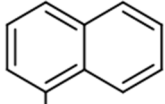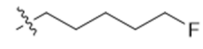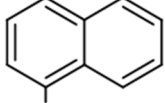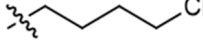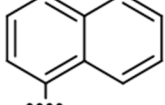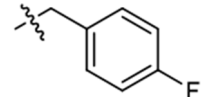
In the present study we investigated a series of compounds – collected by the Institute of Forensic Toxicology and Medicine, University of Bonn, based on the analysis of forensic samples – in radioligand binding assays for their interaction with both CB receptor subtypes, CB_1 and CB_2. Subsequently, the compounds were investigated for their functional properties in cAMP accumulation assays. Moreover, the potential of potent CB receptor agonists to cross the blood-brain barrier was estimated *in silico*. The compounds were additionally investigated for their ability to interact with the CB-like orphan receptors GPR18 and GPR55. The analysis of structure-activity relationships of the investigated compounds will help in predicting properties of novel derivatives.

6.2. Affinity to the cannabinoid receptors

In this study we investigated the CB receptor binding affinities and functional properties of different classes of compounds structurally related to known CB receptor agonists. These compounds had been identified in "spice" preparations suspected to be commercialized for drug abuse (unpublished data).
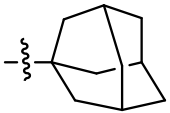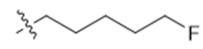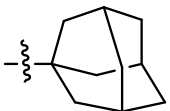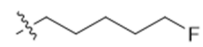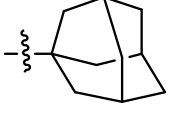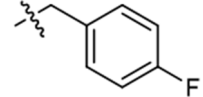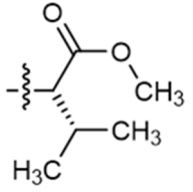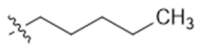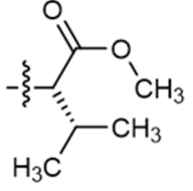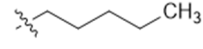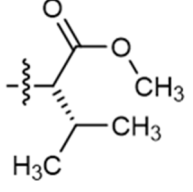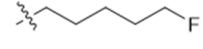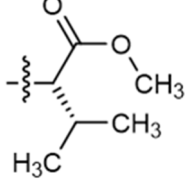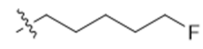
Table 44: Affinities of spice constituents to the cannabinoid receptors.

Compd. No.	Compd. Name	R¹	R²	X	$K_i \pm$ SEM (nM)	
					human CB$_1$	Human CB$_2$
3	CP55,940	for structure see figure 1			1.28 ± 0.44	1.42 ±0.75
4	THC	for structure see figure 1			3.87 ± 0.91	71.6 ± 2.4
5	JWH-018	for structure see figure 1			1.51 ± 0.67	2.24 ± 1.20

3-Amidoindoles and –indazoles (A)

Compd. No.	Compd. Name	R¹	R²	X	human CB$_1$	Human CB$_2$
324	NNEI			CH	1.82 ± 0.35 (K_i=1.25 Blaazer et al.[293])	21.9 ± 5.5 (K_i=100 Blaazer et al.[293])
325	5F-NNEI			CH	3.69 ± 1.97	13.4 ± 1.6
326	5Cl-NNEI			CH	10.2 ± 2.2	32.8 ± 10.8
327	FDU-NNEI			CH	7.42 ± 2.51	64.0 ± 15.0

328	5F-NNEI-2-naphthyl-isomer		CH	235 ± 15	226 ± 24[b]
329	MN-18		N	3.86 ± 0.90	3.47 ± 0.89
330	5F-MN-18		N	1.65 ± 0.26	2.50 ± 0.86
331	THJ		N	103 ± 25	12.7 ± 4.1
332	5F-THJ		N	22.6 ± 7.5	2.75 ± 0.99
333	SDB-006		CH	53.0 ± 1.1 (*EC$_{50}$ = 134* Banister et al.[294])	188 ± 38 (*EC$_{50}$ = 19* Banister et al.[294])
334	5F-SDB-006		CH	71.9 ± 13.5 (*EC$_{50}$ = 50* Banister et al.[294])	430 ± 73 (*EC$_{50}$ =123* Banister et al.[294])
335	SDB-006-N-phenyl-analog		CH	163 ± 17	275 ± 25
336	APICA		CH	6.52 ± 3.73 (*EC$_{50}$ = 128* Banister et al.[294])	1.22 ± 0.14 (*EC$_{50}$ = 29* Banister et al.[294])
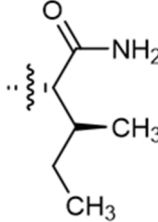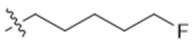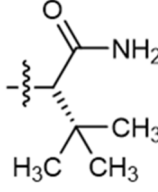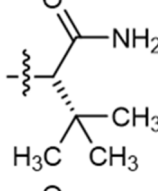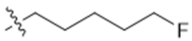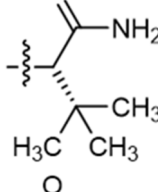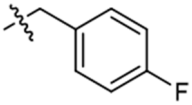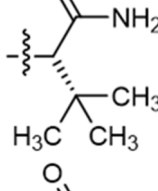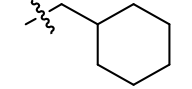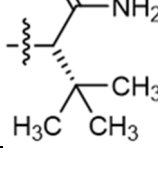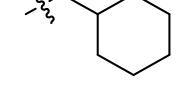
337	STS-135 (5F-APICA)			CH	**2.51** ± 0.35 (EC_{50} = 51 Banister et al. [294])	**0.794** ± 0.071 (EC_{50} = 13 Banister et al. [294])
338	5F-APINACA (5F-AKB48)			N	**1.94** ± 0.55	**0.266** ± 0.041
339	FUB-AKB-48			N	**1.06** ± 0.29	**0.174** ± 0.018
340	MMB-018			CH	**15.1** ± 5.9	**14.0** ± 0.8
341	AMB			N	**0.866** ± 0.057	**0.973** ± 0.104
342	MMB-2201			CH	**15.2** ± 5.0	**19.8** ± 4.2
343	5F-AMB			N	**1.13** ± 0.48 (EC_{50} = 1.9 Banister et al.[295])	**1.38** ± 0.22 (EC_{50} = 10 Banister et al.[295])
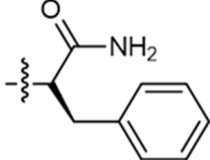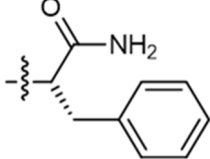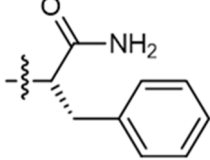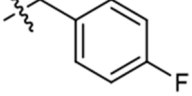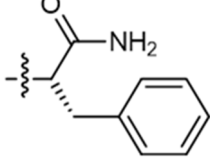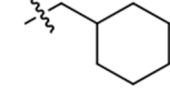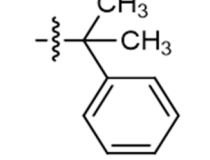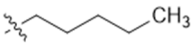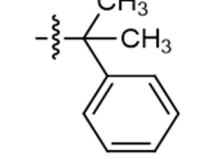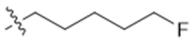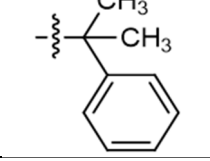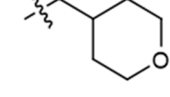
344	FUB-AMB			N	**0.387** ± 0.135 (EC_{50} = 2.0 Banister et al.[295])	**0.536** ± 0.115 (EC_{50} = 18 Banister et al.[295])
345	MDMB-CHMICA			CH	**0.410** ± 0.141 (EC_{50} = 10 Banister et al.[295])	**0.354** ± 0.050 (EC_{50} = 71 Banister et al.[295])
346	MA-CHMINACA			N	**0.339** ± 0.073 (EC_{50} = 5.1 Banister et al.[295])	**0.301** ± 0.092 (EC_{50} = 29 Banister et al.[295])
347	5-F-ADB			N	**23.3** ± 10.2 (EC_{50} = 0.59 Banister et al.[295])	**5.99** ± 2.47 (EC_{50} = 7.5 Banister et al.[295])
348	MDMB-FUBINACA			N	**0.0985** ± 0.0291 (EC_{50} = 3.9 Banister et al.[295])	**0.130** ± 0.010 (EC_{50} = 55 Banister et al.[295])
349	MDMB-CHMINACA			N	**0.135** ± 0.028 (EC_{50} = 10 Banister et al.[295])	**0.222** ± 0.034 (EC_{50} = 128 Banister et al.[295])
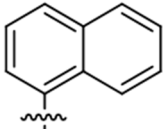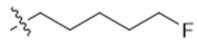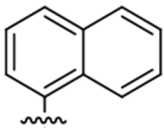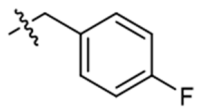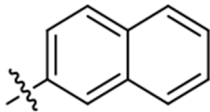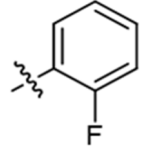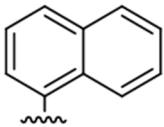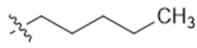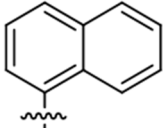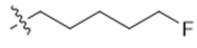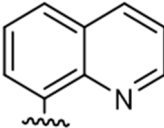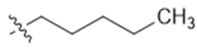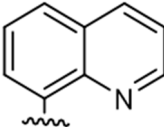
350	5F-ABPICA		CH	**35.0** ± 7.7 (*EC$_{50}$ = 12* Banister et al.[295])	**89.0** ± 33.2 (*EC$_{50}$ = 12* Banister et al.[295])
351	5F-AB-PINACA		N	**4.96** ± 1.37 (*EC$_{50}$ = 0.48* Banister et al.[296])	**3.77** ± 0.25 (*EC$_{50}$ = 2.6* Banister et al.[296])
352	5-Cl-AB-PINACA		N	**4.06** ± 1.95	**12.0** ± 1.7
353	AB-FUBINACA (3-F-benzyl-isomer)		N	**12.6** ± 0.7 (*EC$_{50}$ = 51.1* Buchler et al.[297])	**52.2** ± 10.2
354	AB-FUBINACA (2-F-benzyl-isomer)		N	**6.91** ± 3.42 (*EC$_{50}$ = 4.69* Buchler et al.[297])	**25.0** ± 6.1
355	AB-CHMINACA		N	**1.72** ± 0.14 (*EC$_{50}$ = 0.78* Wiley et al.[298])	**1.91** ± 0.20 (*EC$_{50}$ = 0.45* Wiley et al.[298])

356	5-F-ADB-PINACA-isomer 2		N	3.10 ± 1.53		4.28 ± 2.86
357	5F-ADBICA		CH	2.72 ± 0.35 (*EC$_{50}$ = 0.77* Banister et al.[296])		1.83 ± 0.11 (*EC$_{50}$ = 1.2* Banister et al.[296])
358	5F-ADB-PINACA		N	1.43 ± 0.69 (*EC$_{50}$ = 0.24* Banister et al.[296])		0.694 ± 0.078 (*EC$_{50}$ = 2.1* Banister et al.[296])
359	ADB-FUBINACA		N	0.360 ± 0.002 (*EC$_{50}$ = 1.2* Banister et al.[296])		0.339 ± 0.059 (*EC$_{50}$ = 3.5* Banister et al.[296])
360	ADB-CHMICA		CH	1.24 ± 0.360		0.628 ± 0.231
361	MAB-CHMINACA		N	0.333 ± 0.059 (*EC$_{50}$ = 0.289* Buchler et al.[297])		0.331 ± 0.048
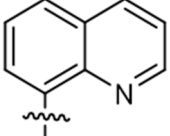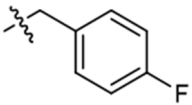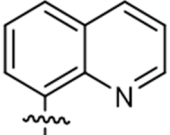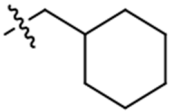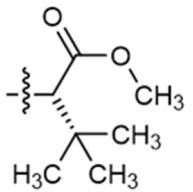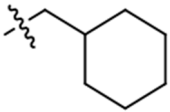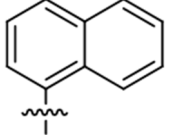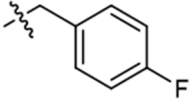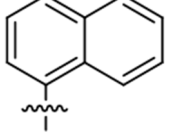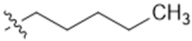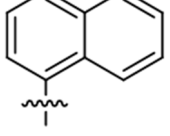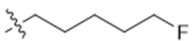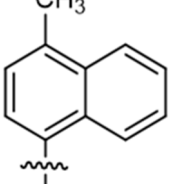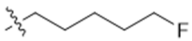
362	PX-2			CH	**127** ± 43	**17.4** ± 1.4
363	PX-1			CH	**485** ± 117	**164** ± 17
364	APP-FUBINACA			N	**56.3** ± 19.8 ($EC_{50} = 47.6$ Buchler et al.[297])	**58.1** ± 17.3
365	APP-CHMINACA			N	**9.81** ± 4.56 ($EC_{50} = 708$ Buchler et al.[297])	**4.39** ± 0.59
366	Cumyl-PICA			CH	**3.27** ± 0.32 ($EC_{50} = 0.66$ Bowden et al.[299])	**24.0** ± 8.8 ($EC_{50} = 13$ Bowden et al.[299])
367	5F-Cumyl-PICA			CH	**1.37** ± 0.26 ($EC_{50} = <0.1$ Bowden et al.[299])	**29.1** ± 2.4 ($EC_{50} = 0.37$ Bowden et al.[299])
368	Cumyl-THPINACA			N	**1.23** ± 0.20 ($EC_{50} = 0.1$ Bowden et al.[299])	**1.38** ± 0.86 ($EC_{50} = 0.59$ Bowden et al.[299])

3-Oxycarbonylindoles and –indazoles (B)
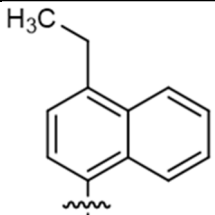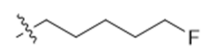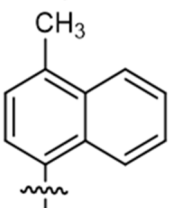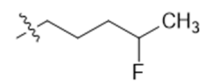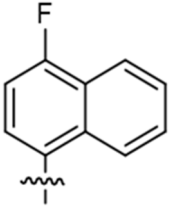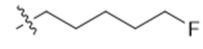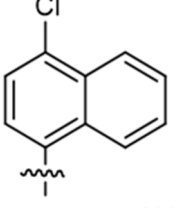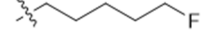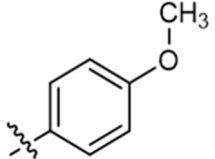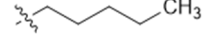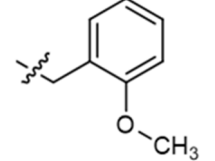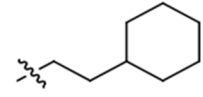
369	NM-2201			CH	**0.332** ± 0.107	**0.732** ± 0.174
370	FDU-PB-22			CH	**1.19** ± 0.39	**2.43** ± 0.92
371	3-CAF			CH	~**10,000** (48%)	**423** ± 106[c]
372	SDB-005			N	**3.59** ± 0.89 (*EC*$_{50}$ = 116 Banister et al.[294])	**2.61** ± 1.07 (*EC*$_{50}$ = 140 Banister et al.[294])
373	5F-SDB-005			N	**2.58** ± 1.09 (*EC*$_{50}$ = 148 Banister et al.[294])	**3.41** ± 1.34 (*EC*$_{50}$ = 136 Banister et al.[294])
374	PB-22			CH	**0.318** ± 0.071 (*EC*$_{50}$ = 5.1 Banister et al.[294])	**0.433** ± 0.106 (*EC*$_{50}$ = 2.8 Banister et al.[294])
375	5F-PB-22			CH	**0.468** ± 0.069 (*EC*$_{50}$ = 148 Banister et al.[294])	**0.633** ± 0.058 (*EC*$_{50}$ = 136 Banister et al.[294])
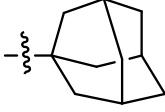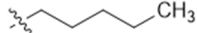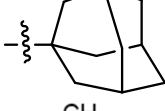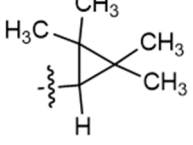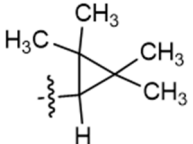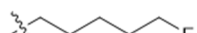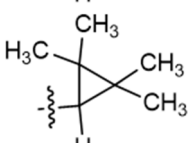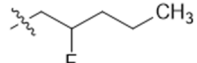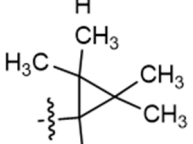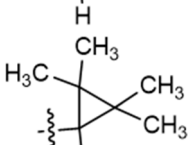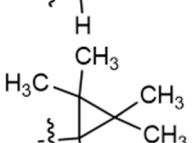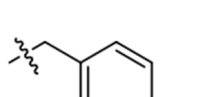
No.	Name	Core	Tail	X		
376	FUB-PB-22			CH	**0.386** ± 0.117	**0.478** ± 0.124
377	BB-22			CH	**0.217** ± 0.056	**0.338** ± 0.045
378	MO-CHMINACA			N	**10.4** ± 7.4	**1.11** ± 0.14

3-Carboxyindoles and -indazoles (C)

No.	Name	Core	Tail	X		
379	FUB-JWH-018			CH	**3.27** ± 1.76	**1.34** ± 0.48
380	THJ018			N	**5.84** ± 1.32	**4.57** ± 0.28
381	THJ2201			N	**1.34** ± 0.54	**1.32** ± 0.39
382	MAM-2201			CH	**1.58** ± 0.76	**0.582** ± 0.123
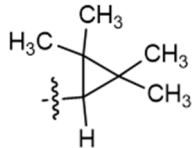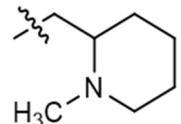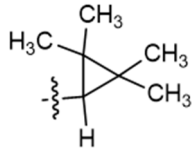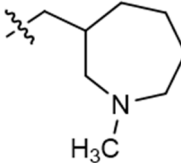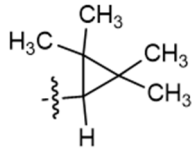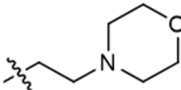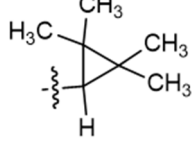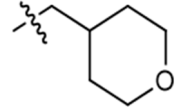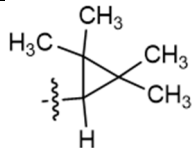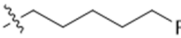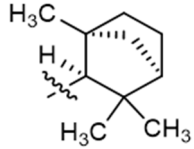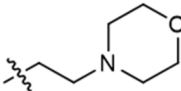
383	EAM-2201			CH	0.380 ± 0.111	0.371 ± 0.052
384	MAM-2201-4-fluorpentyl-isomer			CH	3.23 ± 1.56	0.808 ± 0.057
385	F-2201			CH	0.852 ± 0.192	1.89 ± 0.57
386	Cl-2201			CH	0.772 ± 0.101	1.18 ± 0.19
387	RCS-4			CH	26.6 ± 6.6 (*EC$_{50}$ = 145* Banister et al.[300])	2.86 ± 0.39 (*EC$_{50}$ = 145* Banister et al.[300])
388	RCS-8			CH	81.3 ± 15.8	14.6 ± 6.1
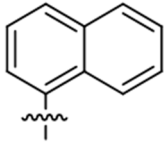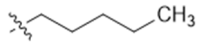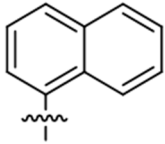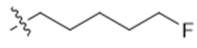
389	AB001			CH	**33.0** ± 7.42 (*EC$_{50}$ = 35* Banister et al.[301])	**1.72** ± 0.15 (*EC$_{50}$ = 45* Banister et al.[301])
390	5F-AB001			CH	**12.3** ± 3.0	**1.47** ± 1.03
391	UR-144			CH	**55.9** ± 6.5 (*K$_i$ = 150* Frost et al.[302])	**1.49** ± 0.25 (*K$_i$ = 1.8* Frost et al.[302])
392	XLR-11			CH	**29.4** ± 11.0 (*EC$_{50}$ = 98* Banister et al.[294])	**0.608** ± 0.151 (*EC$_{50}$ = 83* Banister et al.[294])
393	XLR-11-2-fluorpentyl-isomer			CH	**59.5** ± 16.9	**1.83** ± 0.47
394	FAB-144			N	**17.5** ± 1.1	**0.450** ± 0.111
395	XLR-12			CH	**43.7** ± 5.9 (*K$_i$ = 15* Frost et al.[302])	**0.831** ± 0.331 (*K$_i$ = 0.09* Frost et al.[302])
396	FUB-144			CH	**14.0** ± 2.7	**0.846** ± 0.209

397	AB005			CH	**59.4** ± 13.1 (K_i = 5.5 Frost et al.[302])	**1.04** ± 0.11 (K_i = 0.48 Frost et al.[302])
398	AB005-azepane-isomer			CH	**>10,000** (13%)	**212** ± 55
399	A-796,260			CH	**738** ± 142 (K_i = 845 Frost et al.[292])	**8.02** ± 0.77 (K_i = 4.4 Frost et al.[292])
400	A-834,735			CH	**25.0** ± 6.8 (K_i = 12 Frost et al.[292])	**0.566** ± 0.153 (K_i = 0.21 Frost et al.[292])

2-Methyl-3-carboxyindoles (D)

| 401 | M-144 | | | CH | **19.4** ± 7.8 | **4.59** ± 1.48 |

7-Methoxy-3-amidoindole (E)

| 402 | MN-25 | | | CH | **780** ± 66 (K_i = 245 Wroblenski et al.[303]) | **2.77** ± 1.59 (K_i = 11 Wroblenski et al. [303]) |

3-Carboxy-carbazol (F)

403	EG-018		CH₃	-	**7.17** ± 1.27	**2.27** ± 0.383
404	EG-2201		F	-	**22.4** ± 12.8	**4.36** ± 2.91

AM2201-benzimidazol (G)

405	FUBIMINA	-	-	-	**502** ± 181 ($K_i = 296$ Wiley et al.[299])	**99.0** ± 28.4 ($K_i = 23.5$ Wiley et al.[299])

All compounds were investigated in radioligand binding experiments at CHO cell membrane preparations stably expressing the human CB_1 or CB_2 receptor using [^{3}H]CP55,940 as a radioligand. K_i values are presented in Table 44. CB_1 or CB_2 selectivity of compounds was calculated based on the K_i values, and can be found in Table 45. All of the investigated compounds share a common core structure): (aza)indole. The only exceptions are **EG-018** (**403**), **EG-2201** (**404**) and **FUBIMINA** (**405**). Three different types of linkers between the (aza)indole ring system and a bulky, lipohilic residue are observed: an amide, an ester or a shorter carboxy linker. The most potent compounds for the CB_1 receptor were found among the ester-linked subgroup (**BB22** (**377**), **PB-22** (**374**) and **5F-PB-22** (**375**), **NM2201** (**369**)) with K_i values ranging from **0.217** to **0.468** nM. The only exception is the carboxy-linked compound **EAM-2201** (**383**), with a similarly low K_i value of **0.380** nM and the amido-linked **MDMB-FUBINACA** (**348**) with a K_i value of **0.0985** nM for CB_1 and a K_i value of **0.130** nM for CB_2.

In all three subgroups compounds with typical bioisosteric exchanges are found. Three features of the molecule are varied: the *N1*-substituent, which was originally a pentyl moiety in the lead compounds of the JWH group [291]; in the current compounds it is fluorinated or exchanged for a *para*-fluorobenzyl residue. The effect of fluorination on binding affinity was moderate: in the nine examples included in our study binding affinity for the CB_1 receptor was slightly enhanced for fluorinated compounds (compare **MN-18** (**329**) and **5F-MN-18** (**330**); **THJ** (**331**) and **5F-THJ** (**332**); **APICA** (**336**) and **STS-135** (**337**); **SDB-005** (**372**) and **5F-SDB005** (**373**); **THJ018** (**380**) and **THJ2201** (**381**) and **AB001** (**389**) and **5F-AB001** (**390**)) or slightly decreased (compare **NNEI** (**324**) and **5F-NNEI** (**325**); **SDB-006** (**333**) and **5F-SDB-006** (**334**); **PB-22** (**374**) and **5F-PB-22** (**375**)). Banister *et al.* investigated the effects of fluorinated compounds and found that although the EC_{50} value of the investigated compounds were lower *in vitro*, this was not translated to higher *in vivo* potencies, leading to the assumption that pharmacokinetic effects play a role.[294] In their study they investigated, amongst others, the pairs **UR-144** (**391**) and **XLR-11** (**392**), **PB-22** (**374**) and **5F-PB-22** (**375**), and also **APICA** (**336**) and **STS-135** (**337**). They performed membrane potential measurements using a FLIPR assay kit (Molecular Devices) and determined slightly higher EC_{50} values for the compounds compared to the radioligand binding data obtained in the present study. **XLR-11** (**392**), a derivative with a 2-fluoropentyl side chain, is the only compound in this series with a fluorine introduced at position 2 of the pentyl side chain. In comparison to the non-fluorinated analogue **UR-144** (**391**) the affinity at the CB_1 receptor was almost the same, but it was not as potent as **XLR-11**, the 5-fluoinated derivative. **MAM-2201** (**384**), a 4-fluoropentyl-substituted isomer, showed also slightly higher K_i values than the 5-fluoropentyl derivative **MAM-2201** (**382**). In this series only one compound contains of a 5-chloro-substitution: 5Cl-NNEI (**326**), which displayed 10-fold lower affinity for the CB_1 receptor than the unsubstituted derivative NNEI (**324**). Another bioisosteric replacement of the 5-fluoropentyl side chain is a *para*-fluorobenzyl residue. This variation is observed in four compounds of the present series (compare: **5F-AKB48** (**338**) and **FUB-**

AKB48 (**339**); **NM2201** (**342**) and **FDU-PB-22** (**370**); **5F-PB-22** (**375**) and **FUB-PB-22** (**376**); **XLR-11** (**392**) and **FUB-144** (**396**)). The affinity for both CB receptors was almost identical in three of the four pairs, only **FDU-PB-22** (**370**) was not quite as potent as **NM2201** (**369**). Thus, a *para*-fluorobenzyl residue appears to be an optimal bioisosteric exchange for obtaining compounds with a similarly high affinity as the 5-fluoropentyl-substituted parent compound.

Other side chains have been introduced at the indole nitrogen atom. Huffmann *et al.* who established alkylindoles as cannabinoid receptor ligands already performed a comprehensive structure-activity relationship study introducing different side chains. They showed that a five-carbon-side chain is preferred.[291] Thus, pentyl side chains and their bioisosteric analogs confer high potency and activity at the CB_1 receptor. Whenever the size is decreased, affinity for the CB_1 receptor is largely reduced. As this structural feature is crucial for high CB_1 affinity, it had previously been modified to design CB_2-selective compounds.[292]

Another frequently observed variation is the replacement of the indole core by an indazole ring system. In the group of compounds with an amide linker (**A**) it could be observed that the affinity for the CB_1 receptor was quite similar for indoles and indazoles, while the affinity for the CB_2 receptor was slightly increased in indazole derivatives (compare **NNEI** (**324**) and **MN-18** (**329**); **5F-NNEI** (**325**) and **5F-MN-18** (**330**); **STS-135** (**337**) and **5F-APINACA** (**338**)). In the group of compounds with an ester linkage (**B**) the indole derivative **NM-2201** (**369**) showed lower K_i values at CB_1 and CB_2 receptors than the corresponding indazole derivative **5F-SDB-005** (**373**). In group **C** compounds containing a keto-group as a linker, **XLR-11** (**392**) and its indazole analogue **FAB-144** (**394**) displayed almost identical binding affinities. Thus, a variation of the heterocyclic core from indole to indazole is widely tolerated.

One other common feature of this group of compounds is the bulky lipophilic residue in position R^1. Huffman *et al.* introduced mainly naphthyl residues in that position.[304] A variation of this structural element represents the introduction of a quinolone found in some compounds such as **THJ** (**331**) and **PB-22** (**374**).[305] In group **A** compounds with an amide linker the introduction of a quinolone led to 14- and 27-fold higher K_i values at CB_1 receptors, respectively (compare **MN-18** (**329**) with **THJ** (**331**), and **5F-MN-18** (**330**) with **5F-THJ** (**332**)), while the affinity for CB_2 receptors remained unaltered in the low nanomolar range. In the ester-linked compounds (**B**) the quinolone-substituted analogue of **NM2201** (**369**), **5F-PB-22** (**375**), showed comparable affinities for both receptors. **FUB-PB-22** (**376**) is a quinolone derivative with somewhat higher affinity at CB_1 and CB_2 receptors compared to its analogue **FDU-PB-22** (**370**). The most potent compound in this series of cannabinoid ligands, **BB-22** (**377**) – sometimes referred to as QUCHIC – is also a quinolone derivative, which was first described in illicit drug material in 2013 in Japan.[305] This compound has a cyclohexylmethyl residue in position R^2, which imitates the length of a pentyl chain that was previously described to be important for CB potency,[291] and which was beneficial for CB_1 receptor affinity also in a series of magnolol derivatives.[133]

Compounds **MAM-2201 (382)** and **EAM-2201 (383)** display substitution of the naphthyl residue, containing a methyl (**MAM-2201 (382)**) or an ethyl (**EAM-2201 (383)**) group in position 4 of the naphthyl ring. **EAM-2201 (383)** was highly potent at the CB_1 receptor with a K_i value of 0.380 nM without preference for any of the CB receptor subtypes. **MAM-2201 (382)**, which had been described to cause severe toxicity in the cerebellum of rats [306], was found to be four times less potent at the CB_1 receptor. Further, **F-2201 (385)** and **Cl-2201 (386)**, which are the respective fluoro- and chloro-derivatives, both display comparable subnanomolar potencies at CB_1 and very low nanomolar potencies at CB_2.

The only compound which is not linked in the 1-position of the naphthyl residue but in the 2-position, **5F-NNEI-2-naphthyl-isomer (328)**, was a much weaker CB_1 receptor ligand and showed only partial inhibition of radioligand binding at the CB_2 receptor. **NNEI (324)**, which was first described by Blaazer *et al*. 2011, showed a pK_i value of 8.9 in their binding experiments at the CB_1 receptor,[293] which we have now confirmed. The authors also synthesized a non-fluorinated derivative of compound **328** (**5F-NNEI-2-naphthyl-isomer**) which displayed a lower pK_i value of 7.2 for the CB_1 receptor. The same relation could be shown in the present study (compare **5F-NNEI (325)** and **5F-NNEI-2-naphthyl-isomer (328)**): if the naphthyl residue is linked in *meta*-position to the amide the affinity was decreased by 100-fold.

Huffman *et al*. investigated effects of substituting the naphthyl ring by smaller aromatic residues, which reduced affinity to the CB_1 receptor.[291] This could also be observed for the benzyl-substituted compounds **SDB-006 (333)** and **5F-SDB-006 (334)** investigated in the present study. They showed much lower affinity for both CB receptors as compared to the napththyl-substituted compounds with K_i values in the high nanomolar range. The phenyl-substituted derivative **SDB-006-N-phenylanalog (335)** displayed even higher K_i values. In group **C** compounds **RCS-4 (387)** and **RCS-8 (388)** also feature a phenyl or a benzyl residue. Wiley *et al*. described that the substitution in the *ortho*-position is crucial for high affinity, which is realized in both compounds.[307] **RCS-8 (388)**, first described in 2012 in the United States,[308] is benzyl-substituted in position 1 and has a cyclohexylethyl residue in position 2; it shows weaker affinity for both CB receptors than **RCS-4 (387)**. **RCS-4 (387)** and isomers were investigated by Banister *et al*. who found that **RCS-4 (387)** displayed EC_{50} values of 145 nM for CB_1 and 46 nM for CB_2, respectively.[300] In the present study **RCS-4 (387)** with K_i values of 26.6 nM for CB_1 and 2.86 nM for CB_2 displayed higher binding affinities.

The aromatic residue R^1 may be replaced by a more bulky lipophilic group, namely an adamantyl or a tetramethylcyclopropyl residue. Comparing the naphthyl derivatives **NNEI (324)** and **5F-NNEI (325)** with the adamantyl derivatives **APICA (336)** and **STS-135 (337)** it can be observed that CB_2 affinity was increased. Also the tetramethylcyclopropyl derivatives of group C displayed, independently of the side chain variations, a CB_2 preference. Compounds **UR-144 (391)**, **A-796,260 (399)**, **A-834,735 (400)** and **XLR-12 (395)** were first described by Frost *et al*. in the search for selective CB_2 agonists.[292] We could

confirm the reported K_i values, only **XLR-12** (**395**) displayed a 10-fold higher K_i value in our hands as compared to the literature data. From this group of compounds some derivatives emerged on the illicit drug market, mainly in Sweden.[309,310] **FAB-144** (**394**), the indazole and 5-fluoropentyl analogue of **UR-144** (**391**), showed slightly increased affinity for both CB receptors, and **FUB-144** (**394**), the *para*-fluorobenzyl derivative displayed similar affinity. Also, compound **M-144** (**401**) which is substituted in position 2 of the indole ring system with a methyl group, displayed a similar profile. **AB-005** (**397**), a chimeric compound with the CB_2 selectivity-increasing tetramethylcyclopropyl residue for R^1 and *N*-methyl-2-piperidinylmethyl substitution as R^2 which retains CB_1 affinity, was first introduced by Frost *et al.* in 2010.[292] A derivative with an azepane ring (**398**) appeared on the illicit drug market but as we found it displayed no affinity for the CB_1 receptor at concentrations up to 10 μM. If it should exert any psychotropic effect, that would not be mediated via this receptor. At CB_2 receptors a moderate affinity was observed for **398**. A structurally related but more potent compound is **MN-25** (**402**), which was introduced by Wrobelenski *et al.* that also has been reported to be abused in previous years.[303]

We further investigated compounds, which showed substitutions with amino acids as *t*-leucinate and *t*-valinate. These type of compounds was described in a patent of Pfizer, who developed this compound class as pain therapeutic and studied their structure-activity relationship extensively.[297] However, they always introduced an aryl or heteroaryl residue in R^2 and coupled the amino acid in R^1 with an amine.[297] The here presented compounds show a pentyl or 5-fluoropentyl side chain. **MMB-018** (**340**), the indole derivative with a valine methyl ester, was active in the low nanomolar range with a K_i value of **15.1** μM at CB_1. The corresponding indazole **AMB** (**341**) showed a subnanomolar affinity to the both CB receptors. The 5-fluoropentyl derivatives MMB-2201 and **5F-AMB** (**343**) were comparably active. The *p*-fluorobenzyl residue and the bioisosteric cyclohexylmethyl residue showed for both, indoles and indazoles, affinities in the subnanomolar range (**FUB-AMB** (**344**), **MDMB-CHMICA** (**345**) and **MA-CHMINACA** (**346**)). Banister *et al.* had already investigated these compounds and also **5F-AMB** (**343**) in a FLIPR membrane potential assay system from Molecular Devices. Their potencies were in the nanomolar range (EC_{50} values ranging from 1.9 nM to 71 nM). Our radioligand binding assay showed a higher potency here.

Three *t*-valine methyl ester compounds were investigated: **5F-ADB** (**347**), **MDMB-FUBINACA** (**348**) and **MDMB-CHMINACA** (**349**), which also have been substituted with 5-fluoropentyl, *p*-fluorobenzyl and cyclohexylmethyl residues. **MDMB-FUBINACA** (**348**) was the most potent compound of this set with a K_i value of 0.0985 nM for the CB_1 receptor and a K_i value of 0.130 nM for the CB_2 receptor. Banister *et al.* reported here an EC_{50} value of 3.9 nM for CB_1 and of 55 nM for CB_2.[296]

Furthermore, the compounds with a valine amide in R^1 were studied. The valinamide showed to be less potent then the valine methylester (compare **5F-ABPICA** (**350**) with **MMB-2201** (**342**); **AB-CHMINACA** (**355**) and **MA-CHMINACA** (**346**) or comparably potent (**5F-AB-PINACA** (**351**) and **5F-AMB**).

5F-ABPICA (350), which is the 5-F-pentyl indole, showed affinities of 35.0 nM and 89.0 nM for CB_1 and CB_2, the corresponding indazole **5F-ABPINACA (351)** displayed affinities in the low nanomolar range. We further investigated the 5-Cl-pentyl derivative, **5-Cl-ABPINACA (352)**, which showed comparable K_i values of 4.06 nM for CB_1 and 12.0 nM for CB_2. The *m*-fluorobenzyl and *o*-fluorobenzyl derivatives showed similar affinities at CB_1, as also reported by Buchler *et al* in radioligand binding assays.[297] **AB-CHMINACA (355)** also showed comparable potencies as reported by Wiley et al in radioligand binding assays.[298]

5-F-ADB-PINACA Isomer 2 (356) contains another structural isomer of isoleucineamide with a differently substituted side chain. However, this did not alter the binding affinity as compared to **5F-AB-PINACA (351)**, the corresponding valinamide. Furthermore, *t*-valineamides have been investigated. The 5-fluoropentyl substituted indole **5F-ADBICA (357)** showed low nanomolar affinities with a K_i of **2.72** nM for CB_1 and **1.83** nM for CB_2. This corroborates the data from Banister *et al.*, who reported similar potencies in a FLIPR membrane potential assay.[296] We found the corresponding indazole to be slightly more potent at the CB_2 receptor with a K_i value of 0.694 nM. Here, Banister *et al.* found a higher potency concerning CB_1 with an EC_{50} value of 0.24 nM, whereas we obtained a K_i value of **1.43** nM. The *p*-fluorobenzyl-substituted indazole **ADB-FUBINACA (359)** showed even lower K_i values of **0.360** nM for CB_1 and **0.339** nM for CB_2. The indole **ADB-CHMICA (360)** was substituted in R^1 with cyclohexylmethyl and showed a K_i value of **1.24** for CB_1 and **0.628** nM for CB_2. The corresponding indazole **MAB-CHMINACA (346)**, which was introduced by Buchler *et al.*, was even more potent with a K_i value of **0.333** nM for CB_1 and 0.331 nM for CB_2, which fits well with data reported by Buchler *et al.* in radioligand binding assay.[297]

PX-1 (363) and **PX-2 (362)** are the two enantiomers of the phenylalaninamide derivatives. **PX-1 (363)** is the *R*-enantiomer, while **PX-1 (363)** is the *S*-enantiomer. **PX-2 (362)** showed a K_i value for CB_1 of **127** μM and was less potent than a comparable valinamide derivative as **5F-ADBICA (357)**. The K_i value for CB_2 (17.4 nM) was in the lower than the K_i value of **1.83** nM for **5F-ADBICA (357)**. The *S*-enantiomer **PX-1 (363)** however displayed a K_i value of **485** nM for CB_1, which means a 4-fold decrease in affinity compared to the *R*-enantiomer. The K_i value of CB_2 (**164** nM) was 10-fold higher. This shows that the phenylalanineamides behave differently depending on the configuration at the α-carbon atom. However, we do not have any other example to investigate this effect further. The two other phenylalanineamides **APP-FUBINACA (364)** and **APP-CHMINACA (365)** were introduced by Buchler *et al.*[297] They contain both an indazole and vary in position R^1. The *p*-fluorobenzyl derivative **APP-FUBINACA (364)** showed potencies for both CB receptors of around 50 nM and the corresponding cyclohexylmethyl derivative **APP-CHMINACA (365)** was more potent displaying a K_i value of **9.81** nM.

Instead of an amino acid, R^1 can also be substituted with a cumyl-residue. This type of compounds was first described by Bowden *et al.* and was often found in illicit drug material in 2016. We could show

for all three derivatives affinities in the low nanomolar range for CB_1. Bowden *et al*. reported subnanomolar EC_{50} values in their homogeneous time resolved fluorescence (HTRF) based cAMP assay. **Cumyl-PICA (366)** and **5-F-Cumyl-PICA (367)** displayed potencies of around 25 nM for CB_2 in our hands.

In this series of compound, we only had one compound with a 3-Oxycarbonyl linker: **MO-CHMINACA (378)**, which is an indazole with a cyclohexylmethyl residue in R^1 and a *t*-valine methylester for R^2. It displayed a K_i value of **10.4** nM at CB_1 and **1.11** nM at CB_2. The only other cyclohexylmethyl compound we investigated was **BB-22 (377)**, however this is substituted with a quinolone at R^2 and contains an indole core. It showed a K_i value of **0.217** nM. However, we cannot conclude from this that valinamidemethlesters are less potent.

We further investigated three structural dissimilar compounds, which contain a carbazol core. This carbazol is substituted in position 3 with residues we observed in the former compounds. **EG-018 (403)** and **EG-2201 (404)** show a carboxy linker and a naphthoyl residue. **EG-018 (403)** displayed low nanomolar potencies with a K_i value of **7.17** nM for CB_1. We can compare **EG-018 (403)** to **JWH-018**, which showed similar potencies. **EG-2201 (404)** was less potent at CB_1 with a K_i value of **22.4** nM, but similar potency at CB_2. The here observed switch from indoles and indazoles to carbazols can be interpreted as reaction to the NpSG and similar regulations in other countries that restricted the whole class of indoles and indazoles based on the known structure-activity relationships.

We further investigated the only benzimidazol **FUBIMINA (405)**, which was also described by Wiley *et al*. We obtained a K_i value of **502** nM for the CB_1 receptor, which is perfectly in the same range as the reported K_i value of **296** nM from Wiley *et al*. in radioligand binding assays.[298]

Table 45: Selectivity index of selected compounds

No.	Compd	CB_1 selectivity $K_i CB_2/K_i CB_1$	CB_2 selectivity $K_i CB_1/K_i CB_2$
3	CP55,940	1.1	
4	THC	18.5	
324	NNEI	12.0	
325	5F-NNEI	3.6	
326	5Cl-NNEI	3.2	
327	FDU-NNEI	8.6	
328	5F-NNEI-2-naphthyl-isomer	1.0	1.0
329	MN-18	0.9	1.1
330	5F-MN-18	1.5	
331	THJ		8.1
332	5F-THJ		8.2
333	SDB-006	3.5	
334	5F-SDB-006	6.0	

335	SDB-006-N-phenyl-analog	1.7	
336	APICA		5.3
337	STS-135 (5F-APICA)		3.2
338	5F-APINACA (5F-AKB48)		7.3
339	FUB-AKB-48		6.1
340	MMB-018	1.1	
341	AMB	1.1	
342	MMB-2201	1.3	
343	5F-AMB	1.2	
344	FUB-AMB	1.4	
345	MDMB-CHMICA	1.2	
346	MA-CHMINACA		1.1
347	5F-ADB		3.9
348	MDMB-FUBINACA	1.3	
349	MDMB-CHMINACA		1.2
350	5F-ABPICA	2.5	
351	5F-AB-PINACA		1.3
352	5-Cl-AB-PINACA	3.0	
353	AB-FUBINACA (3-F-benzyl-isomer)	4.1	
354	AB-FUBINACA (2-F-benzyl-isomer)	3.6	
355	AB-CHMINACA	1.1	
356	5-F-ADB-PINACA-isomer 2	1.4	
357	5F-ADBICA		1.5
358	5F-ADB-PINACA		2.1
359	ADB-FUBINACA		1.1
360	ADB-CHMICA		2.0
361	MAB-CHMINACA	1.0	1.0
362	PX-2		7.3
363	PX-1		3.0
364	APP-FUBINACA	1.0	1.0
365	APP-CHMINACA		2.2
366	Cumyl-PICA	7.3	
367	5F-Cumyl-PICA	21.2	
368	Cumyl-THPINACA		1.1
369	NM-2201	2.2	
370	FDU-PB-22	2.0	
371	3-CAF		23.6
372	SDB-005		1.4
373	5F-SDB-005	1.3	
374	PB-22	1.4	
375	5F-PB-22	1.4	
376	FUB-PB-22	1.2	
377	BB-22	1.6	
378	MO-CHMINACA	10.0	
379	FUB-JWH-018		2.44
380	THJ018		1.3
381	THJ2201	1.0	1.0

382	MAM-2201		2.7
383	EAM-2201	1.0	1.0
384	MAM-2201-4-fluorpentyl-isomer		4.0
385	F-2201	2.2	
386	Cl-2201	1.5	
387	RCS-4		9.3
388	RCS-8		5.6
389	AB001		19.2
390	5F-AB001		8.4
391	UR-144		37.5
392	XLR-11		48.4
393	XLR-11-2-fluorpentyl-isomer		32.5
394	FAB-144		38.9
395	XLR-12		52.6
396	FUB-144		16.5
397	AB005		57.1
398	AB005-azepane-isomer		47.2
399	A-796,260		92.0
400	A-834,735		44.2
401	M-144		4.2
402	MN-25		282
403	EG-018		3.2
404	EG-2201	5.1	
405	FUBIMINA	5.1	
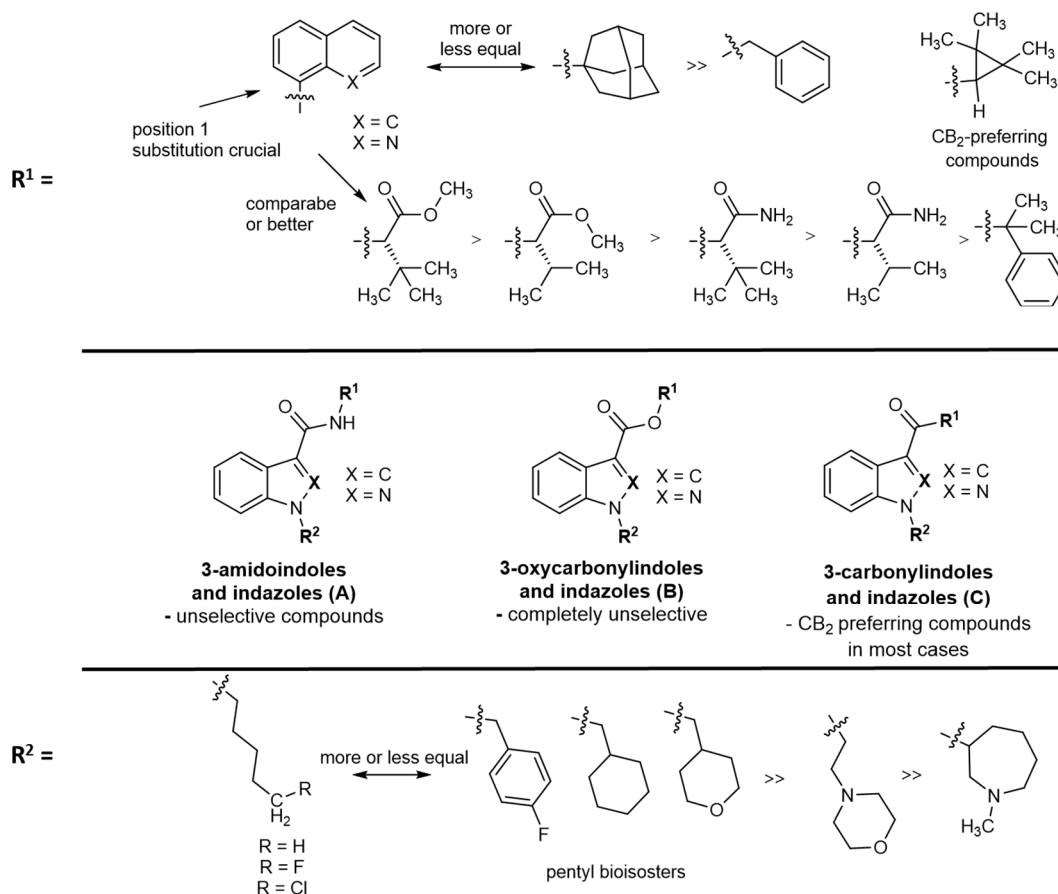
Figure 112: Summary on the investigated structure-activity relationships

In summary, almost all investigated compounds showed high affinity for CB receptors. Some compounds displayed K_i values in the subnanomolar range and thus are many times more potent than the psychoactive drug Δ^9-THC. Of special interest to public might be the here observed scaffold hopping. Carbazol derivatives circumvent restriction by law up to now and display a completely new lead structure for CB receptor ligands.

6.3. Functional properties of investigated compounds

To investigate the functional properties of the compounds cAMP accumulation assays were performed. Both CB receptors are G_i-coupled receptors, whose activation results in decreased cAMP levels in the cell. For comparison the full agonist CP55,940 and the partial agonist Δ^9-THC were investigated and results were normalized to maximal receptor activation by the full agonist CP55,940 (see Figure 2). Compounds were tested at a concentration where maximal binding was observed, either at 1 µM for the more potent compounds (K_i below 10 nM) or at 10 µM for the less potent compounds (K_i higher than 10 nM).
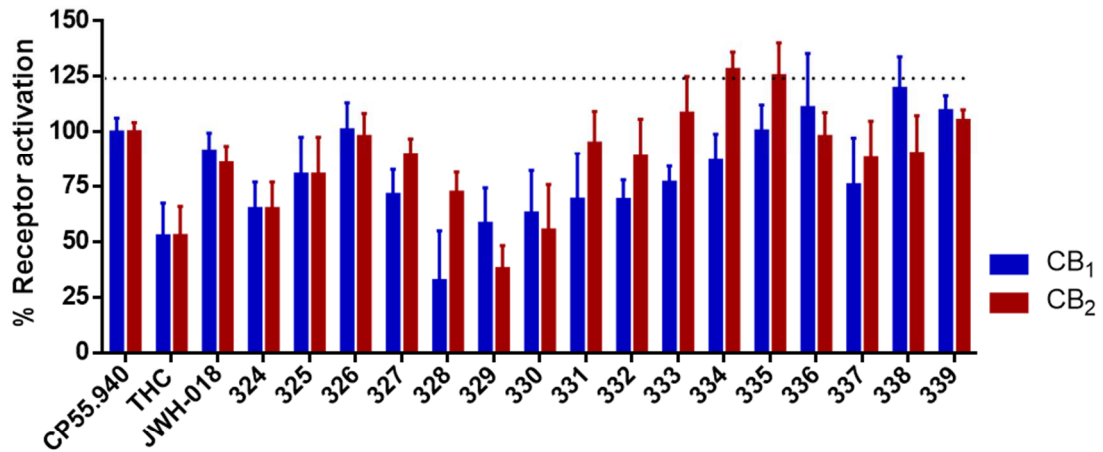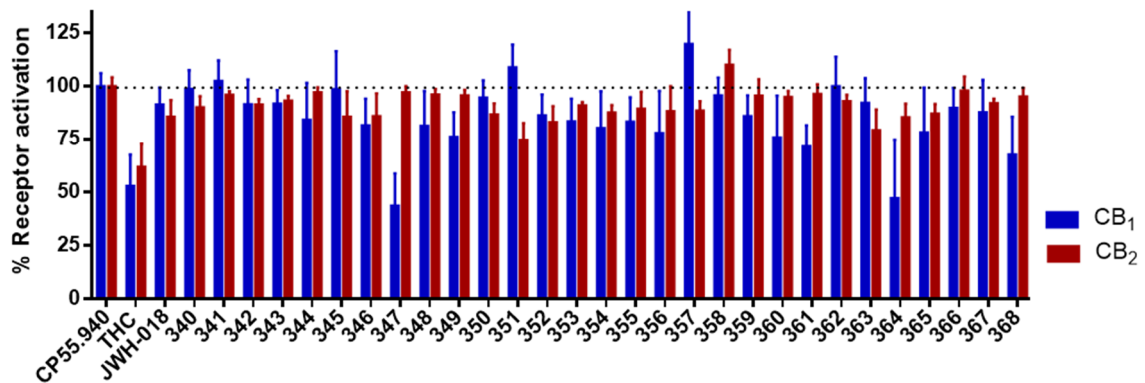
Figure 113: Functional properties of investigated compounds determined in cAMP accumulation assays, in the presence of forskolin (10 µM). Compounds were applied at 10 µM concentration in case their K_i value was > 10 nM and at 1 µM concentration when their K_i value was < 10 nM. All results were normalized to maximal receptor activation by the full agonist CP55,940 (1 µM); (A) compounds **324** to **339**; (B) compounds **340** to **368**

(A)

(B)

(C)
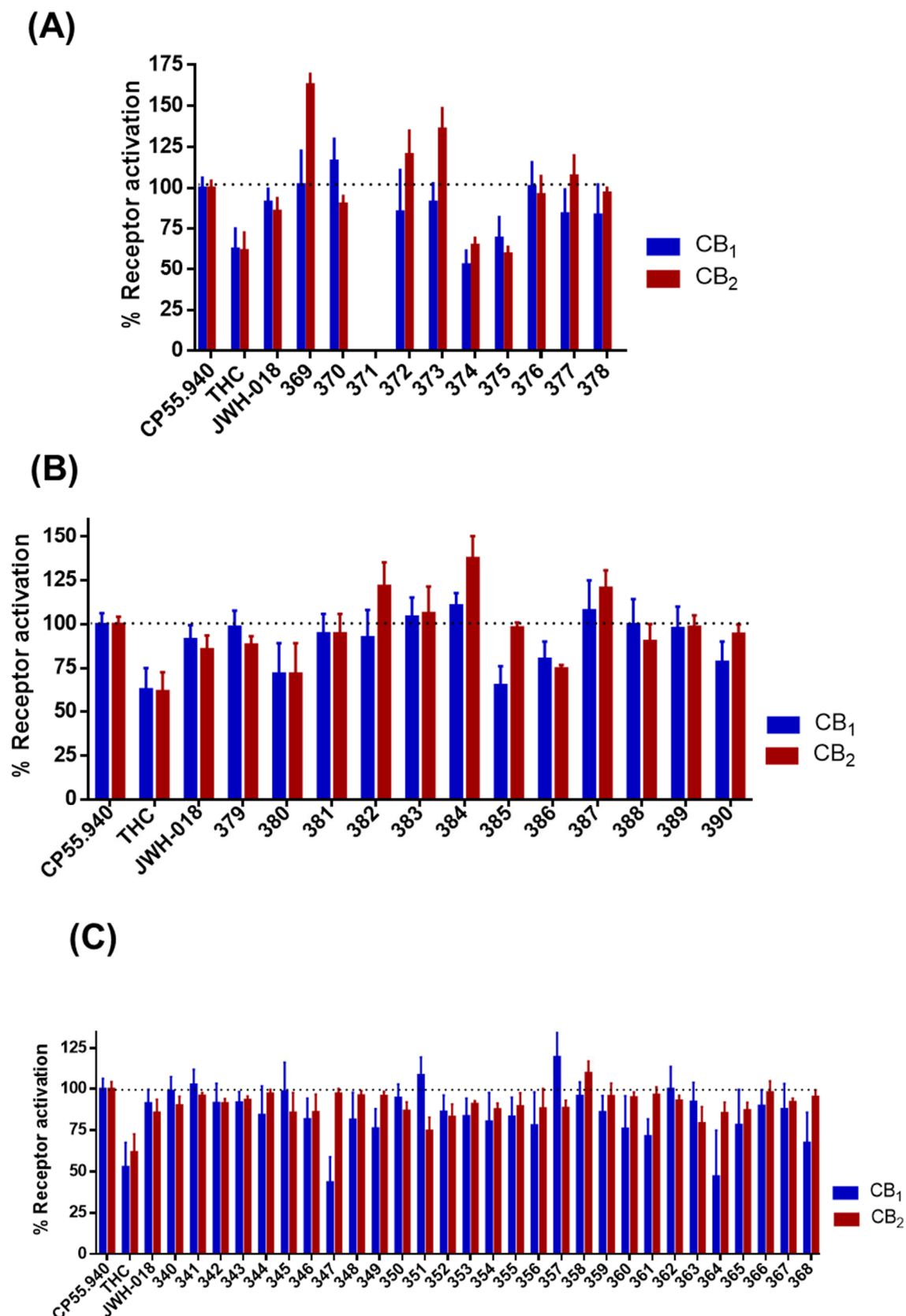
Figure 114: Functional properties of investigated compounds determined in cAMP accumulation assays, in the presence of forskolin (10 µM). Compounds were applied at 10 µM concentration in case their K_i value was > 10 nM and at 1 µM concentration when their K_i value was < 10 nM. All results were normalized to maximal receptor activation by the full agonist CP55,940 (1 µM); (A) compounds **369** to **378**; (B) compounds **379** to **390**; (C) compounds **391** to **405**

In the utilized recombinant cell lines, Δ^9-THC behaved as a partial agonist, at both CB_1 and CB_2 receptors, with 60% - 70% activation compared to the full CB_1/CB_2 agonist CP55,940. Almost all compounds showed a high degree of activation of both receptor subtypes. Exceptions were **3-CAF** (**371**), **FUBIMINA** (**405**) and **AB-005 azepane isomer** (**398**), which did not activate the CB receptors at all. As **3-CAF** (**371**) and **AB-005 azepane isomer** (**398**) showed affinity for the CB_2 receptor they may be characterized as moderately potent, CB_2-selective antagonists. The only agonistic compounds with lower efficacy than THC were **NNEI-2-naphthyl isomer** (**328**), **MN-18** (**329**), **XLR-12** (**395**) and **AB005** (**397**). Most of the compounds had similar efficacies at both receptor subtypes, only **5F-APINACA (351)** activated CB_1 receptor more efficaciously than CB_2.

For the CB_2-selective derivative **XLR-12** (**395**) full concentration response curves were recorded and EC_{50} values were determined (Figure 115). It showed a 30 times lower EC_{50} value of 0.391 nM at the CB_2 receptor than at the CB_1 receptor, thus the compound's preference could also be observed in functional assays.

(A)

CB$_1$ K$_i$ = **43.7** $\pm$ 5.9 nM
CB$_1$ K$_i$ = **0.831** $\pm$ 0.209 nM

CB$_1$: EC$_{50}$ = **11.7** $\pm$ 6.5 nM
CB$_2$: EC$_{50}$ = **0.391** $\pm$ 0.297 nM

(B)

CB$_1$: K$_i$ = **0.0985** $\pm$ 0.0291 nM
CB$_2$: K$_i$ = **0.130** $\pm$ 0.0100 nM

CB$_1$: EC$_{50}$ = **0.0641** $\pm$ 0.0364 nM
CB$_2$: EC$_{50}$ = **0.756** $\pm$ 0.578 nM
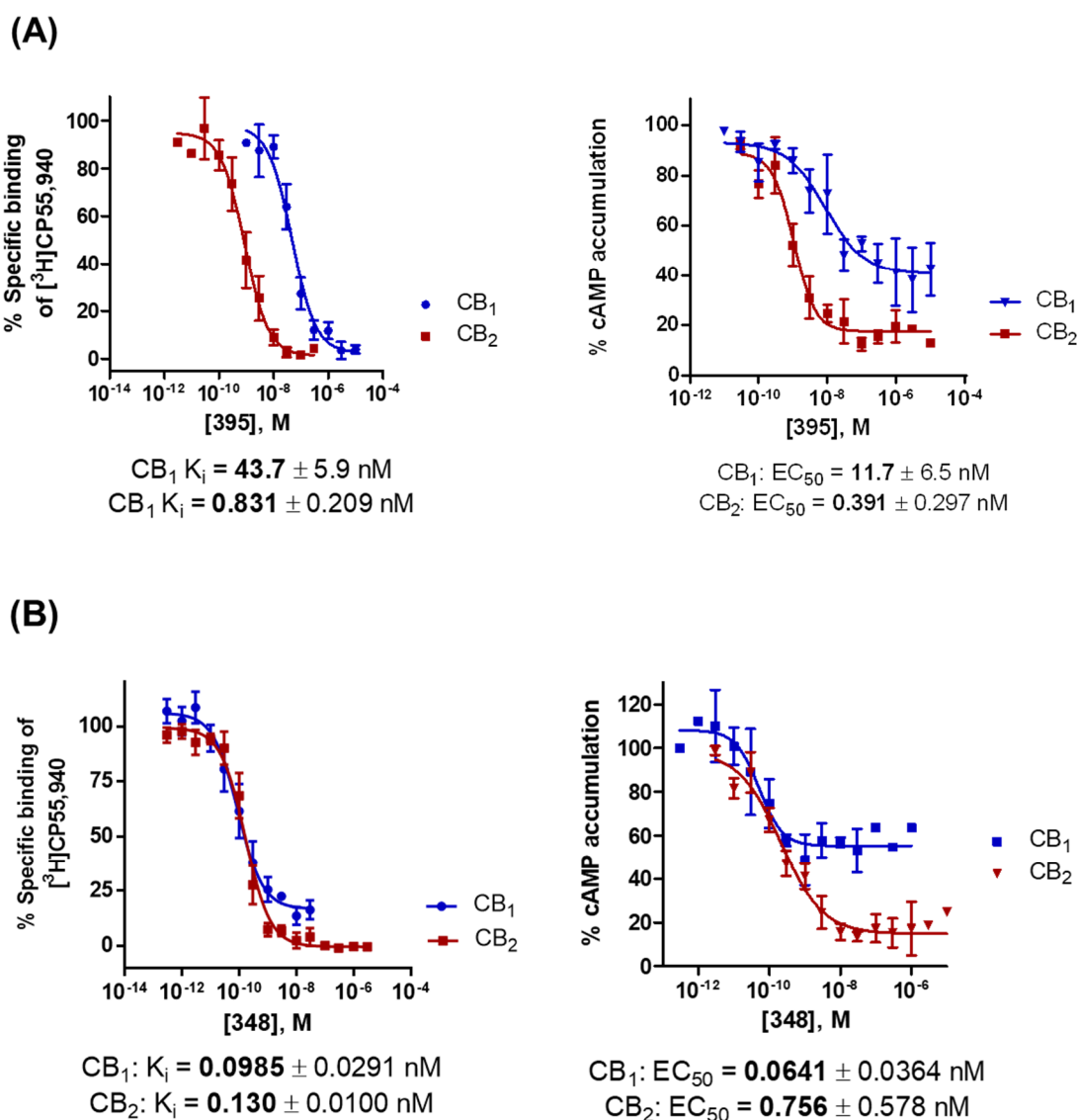
Figure 115: Concentration-dependent inhibition of radioligand binding (left side) and cAMP accumulation (right side); (A) by **XLR-12 (395)**; (B) by **MDMB-FUBINACA (348)**

K$_i$ values measured in radioligand binding in many cases correlated quite well with reported and the EC$_{50}$ values deterimined in cAMP accumulation assays. CB$_2$-selectivity of compound **XLR-12 (395)** could be confirmed, but in our hands it was lower (only 30-fold) than previously reported (167-fold[302]). It should be emphasized that EC$_{50}$ values depend on receptor expression levels while radioligand binding data are independent of receptor density or G protein expression. They directly reflect the affinity of compounds for the binding site on the receptors.

Moreover, we determined the EC$_{50}$ values of **MDMB-FUBINACA (348)** by measuring full concentration-inhibition curves, because it had shown very low K$_i$ values in radioligand binding assays (see Figure 115). With an EC$_{50}$ value of **0.0641** nM for CB$_1$ and **0.756** at CB$_2$ **MDMB-FUBINACA (348)** confirmed its high potency.

Compounds that activate the CB_1 receptor to a comparable extent as Δ^9-THC and that can cross the blood-brain barrier will likely cause similar psychotropic effects as Δ^9-THC. Some compounds showed even higher efficacy than the full agonist CP55,940, including the very potent compounds **EAM-2201** (**383**), **NM-2201** (**369**) and **BB-22** (**377**). Their toxicity may be much higher than that of Δ^9-THC due to their high potency and full efficacy. **PB-22** (**374**), a CB_1/CB_2 partial agonist with similar efficacy as Δ^9-THC but with higher, subnanomolar affinity, had previously been reported to even cause lethal intoxications.[286,311]

6.4. Prediction of *in-silico* drug properties

As a precondition to achieve psychoactive effects brain penetration of the compounds is required. This property can be determined in animal studies. Alternatively, an *in silico* prediction based on established data sets can be used to gain an idea whether a set of compounds is able to cross the blood-brain barrier. For the investigated compounds (compound **324**-**339**, **369**-**377**, **380**-**402**) this was accomplished using the QSAR software Stardrop 5.4 (Optibrium). In Figure 116, affinities of the investigated compounds were compared to their lipophility, which is one of the major determinants for crossing biomembranes. As can be observed all compounds share a rather high logP value between 3 and 7. All highly potent compounds exceeded a log P of 4.5. The standard CB agonists displayed similarly high logP values of 6.50 (Δ^9-THC), and 5.36 (CP55,940), respectively. The compounds' potency is not directly correlated with their lipophilicity (see Figure 116). Based on calculations to estimate lipophilicity (logP), topographical polar surface area (tPSA) and other parameters a prediction whether compounds are able to cross the blood-brain barrier (log BBB) is made by the program. The compounds could thus be divided into two groups, blood-brain barrier-penentrant and non-penetrant compounds. **THJ** (**331**) and **5F-THJ** (**332**), both of which are 3-(8-quinolonyl)amido-indazoles, were predicted not to cross the blood-brain barrier. Based on *in silico* predictions it is, however, likely that the majority of the investigated compounds has the ability to cross the blood brain barrier.

(A)

(B)
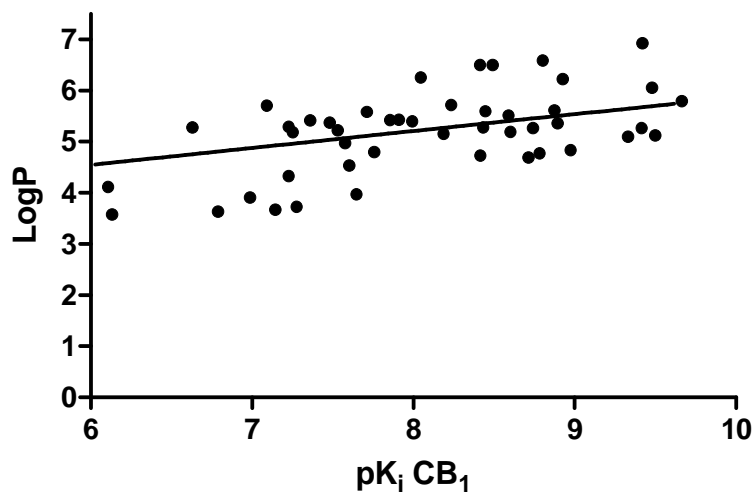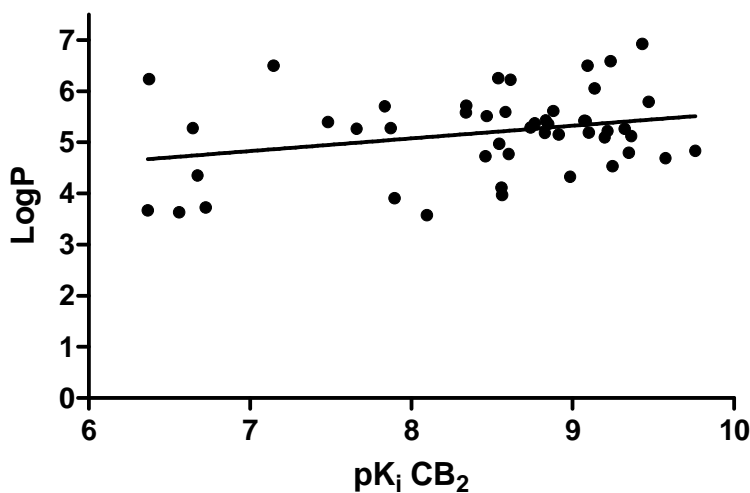
Figure 116: (**A**) Affinities of investigated compounds at the CB_1 receptor plotted against logP values. (**B**) Affinities of investigated compounds at the CB_2 receptor plotted against logP values.
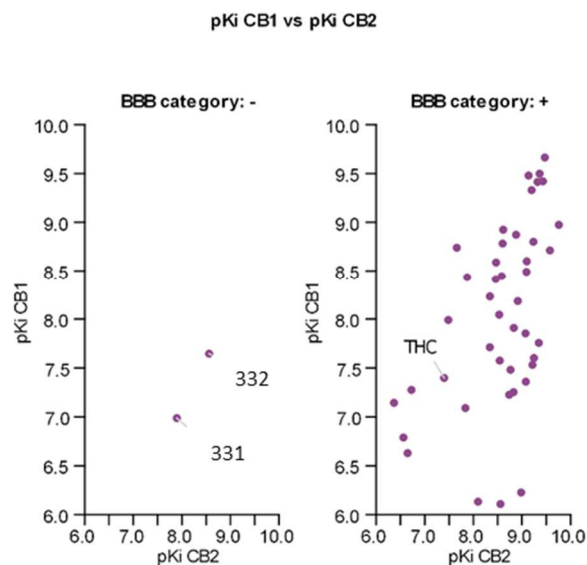
Figure 117: Blood-brain barrier category. Two groups of compounds were defined according to their predicted blood-brain barrier penetration. Stardrop 5.5 (Optibrium) defines scores based on established QSAR models. The prediction of the BBB category returns a binary prediction of penetration of the blood-brain barrier (+ : accuracy and specifity is 91%; - : accuracy and specificity is 83%)

6.5. Effects on the orphan GPR18 and GPR55

The orphan GPCRs GPR18 and GPR55 have been shown to be targeted by a range of cannabinoid receptor ligands.[106,245,132] Therefore we investigated whether the investigated spice constituents also interact with those cannabinoid-related receptors (Table 2). None of the compounds was able to activate GPR18 or to inhibit GPR18 activation up to a concentration of 10 µM. At GPR55 some compounds were found to be moderate antagonists, namely, APICA (**336**) and STS-135 (**337**) with IC_{50} values of 3-4 µM, as well as several compounds from group **C**. EAM-2201 (**383**) was the most potent GPR55 antagonists of this series with an IC_{50} value 1.86 µM. Interestingly, none of the ester compounds (**B**) showed any inhibitory effect, and most of the active compounds were tetramethylcyclopropyl-substituted derivatives containing the CB_2-preferring structure. UR-144 (**391**), XLR-11-2-fluorpentylisomer (**393**) and XLR-12 (**395**), which feature a lipophilic aliphatic or fluoropentyl side chain, were more potent than A-769,260 (**399**) or A834,735 (**400**) with a morpholino or pyran substituent. A typical functional behavior of cannabinoids at GPR55 can also be observed here: Although all of the identified GPR55 ligands were agonists at the CB receptors, they showed inhibitory effects at GPR55. The same had been demonstrated for the CB-agonist CP55,940 as well as other CB receptor agonists.[66; 132] On the other hand, CB_1 receptor antagonists, such as rimonabant, are agonists of GPR55.[54,103,66,103] Both receptors, CB_1 and GPR55, were reported to be co-localized in the brain, and receptor heteromerization has been postulated.[114; 112,114]
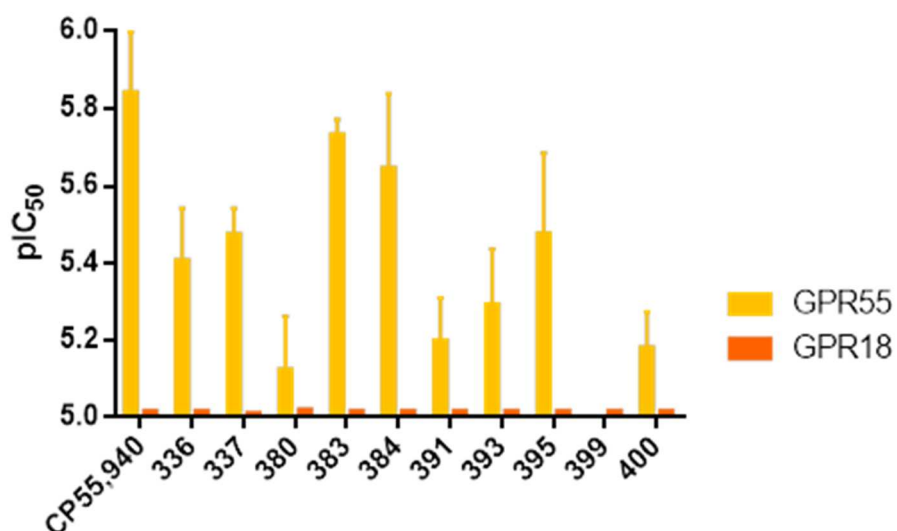
Figure 118: Inhibitory potency of selected compounds at the two orphan receptors GPR18 and GPR55.

Table 46: Results for spice constituents in β-arrestin recruitment assays at GPR55 and GPR18.

No.	Compd.	Human GPR55		Human GPR18	
		EC_{50} (μM) (% activation)	IC_{50} (μM) (% inhibition)	EC_{50} (μM) (% activation)	IC_{50} (μM) (% inhibition)
4	THC	-	**14.2**[129]	**4.61**[132]	-
3	CP55,940	-	**1.61**[245]	-	**5.99**[245]
3-Amido-indole and –indazoles (A)					
324	NNEI	**>10** (26%)	**>10** (30%)	>10 (42%)	>10 (-15%)
325	5F-NNEI	**>10** (25%)	**>10** (-8%)	>10 (-3%)	>10 (-17%)
326	5Cl-NNEI	**>10** (28%)	**>10** (5%)	>10 (1%)	>10 (-13%)
328	5F-NNEI-2-naphthyl-isomer	**>10** (19%)	**>10** (20%)	>10 (9%)	>10 (5%)
329	MN-18	**>10** (27%)	>10 (35%)	>10 (2%)	>10 (37%)
330	5F-MN-18	**>10** (38%)	>10 (-5%)	>10 (-26%)	>10 (23%)
331	THJ	**>10** (11%)	>10 (50%)	>10 (4%)	>10 (30%)
332	5F-THJ	**>10** (28%)	>10 (10%)	>10 (-17%)	>10 (44%)
333	SDB-006	**>10** (-5%)	>10 (36%)	>10 (-9%)	>10 (22%)
334	5F-SDB-006	**>10** (-3%)	>10 (11%)	>10 (13%)	>10 (-24%)
335	SDB-006-N-phenyl-analog	**>10** (20%)	>10 (1%)	>10 (9%)	>10 (-13%)
336	APICA	**>10** (11%)	**4.77** ± 1.69	>10 (8%)	>10 (44%)
337	STS-135 (5F-APICA)	**>10** (1%)	**3.41** ± 0.47	>10 (-2%)	>10 (30%)
339	FUB-AKB-48	**>10** (-11%)	(83%)	>10 (-27%)	(69%)

3-Oxycarbonylindoles and -indazoles (B)

369	NM-2201	>10 (17%)	>10 (23%)	>10 (-8%)	>10 (32%)
370	FDU-PB-22	>10 (11%)	>10 (30%)	>10 (30%)	>10 (-4%)
371	3-CAF	>10 (26%)	>10 (41%)	>10 (4%)	>10 (10%)
372	SDB-005	>10 (8%)	>10 (23%)	>10 (15%)	>10 (24%)
373	5F-SDB-005	>10 (21%)	>10 (47%)	>10 (21%)	>10 (24%)
374	PB-22	>10 (15%)	>10 (-12%)	>10 (-18%)	>10 (26%)
375	5F-PB-22	>10 (5%)	>10 (-10%)	>10 (-5%)	>10 (-5%)
376	FUB-PB-22	>10 (5%)	>10 (24%)	>10 (15%)	>10 (8%)
377	BB-22	>10 (9%)	>10 (34%)	>10 (2%)	>10 (18%)

3-Carboxylindoles and -indazoles (C)

380	THJ018	>10 (6%)	8.20 ± 2.11	>10 (33%)	>10 (-5%)
381	THJ2201	>10 (-1%)	>10 (47%)	>10 (18%)	>10 (21%)
383	EAM-2201	>10 (-24%)	1.86 ± 0.16	>10 (14%)	>10 (4%)
384	MAM-2201-4-fluorpentyl-isomer	>10 (-41%)	3.07 ± 1.48	n.d	n.d
389	AB001	>10 (-14%)	~10 (56%)	>10 (-12%)	~10 (62%)
390	5F-AB001	>10 (19%)	~10 (48%)	>10 (-6%)	~10 (18%)
391	UR-144	>10 (-5%)	6.70 ± 1.65	>10 (17%)	>10 (14%)
393	XLR-11-2-fluorpentyl-isomer	>10 (-8%)	5.69 ± 1.95	>10 (24%)	>10 (29%)
394	FAB-144	>10 (5%)	~10 (77%)	>10 (2%)	~10 (57%)
395	XLR-12	>10 (-5%)	4.56 ± 1.97	>10 (27%)	>10 (13%)
396	FUB-144	>10 (-3%)	~10 (62%)	>10 (-12%)	~10 (74%)
397	AB005	>10 (16%)	>10 (39%)	>10 (-38%)	>10 (-2%)
398	AB005-azepane-isomer	>10 (21%)	>10 (18%)	>10 (11%)	>10 (-6%)
399	A-796,260	>10 (-1%)	14.3 ± 2.5[a]	>10 (20%)	>10 (-10%)
400	A-834,735	>10 (8%)	6.88 ± 1.51[a]	>10 (6%)	>10 (6%)

2-Methyl-3-carboxyindole (D)

401	M-144	>10 (-5%)	~10 (86%)	>10 (-7%)	~10 (67%)

7-Methoxy-3-amidoindole (E)

402	MN-25	>10 (-8%)	>10 (47%)	>10 (-12%)	>10 (30%)

6.6. Conclusion

In conclusion we determined the binding affinity of a large number of synthetic compounds suspected to be constituents of spice herbal blends. Our results confirm that the majority of the investigated compounds behave as highly potent CB receptor ligands with affinities in the low nanomolar to subnanomolar concentration range. Furthermore we could show that they behave as agonists with high efficacy. In an *in-silico* approach all except for two derivatives from a selected set were predicted to cross the blood-brain barrier, and therefore are likely to produce psychoactive effects. The main structural variations of the compounds represent typical bioisosteric exchanges altering the structure of the compounds in order to circumvent restriction by law, but to retain the intended psychoactive effects. Knowledge of classical medicinal chemistry provides in these cases powerful strategies to bypass controlled substances. In our study we provide a comprehensive analysis of the structure-activity relationships of spice constituents including 41 compounds of previously unknown potency and efficacy. The obtained data were compared to those of established CB receptor ligands. In the future this may help to predict pharmacological behavior of novel compounds that appear on the illicit drug market.

The compounds were further investigated at the CB receptor-related orphan GPCRs GPR18 and GPR55. While no interaction with GPR18 was detected, some derivatives behaved as weak antagonists of GPR55. Since knowledge about these newly discovered orphan receptors is still very limited our results contribute to a better understanding of their ligands' structural requirements. Moreover, we have identified novel GPR55 antagonists that could be used as starting points for future optimization.

7. SUMMARY

7.1. Cannabinoid and cannabinoid-like receptors

The family of G protein-coupled receptors (GPCRs) represents one of the largest membrane-bound protein families, which are targeted by approximately 30% of all approved drugs. However, out of the ca. 800 human GPCRs more than 100 receptors remain *orphan*, i.e. their endogenous agonists have not been identified or confirmed yet. Orphan GPCRs likely represent future drug targets. Reliable and well-characterized tool compounds are required to study the receptors' functions and their effects.

In this study, we developed tool compounds for the orphan receptors GPR18 and GPR55. These belong to the δ-branch of the class A subfamily of GPCRs, to which nucleotide- and lipid-activated receptors belong among others. GPR18 and GPR55 interact with cannabinoids, although they are relatively unrelated to the classical cannabinoid receptors CB_1 and CB_2. GPR18 can be activated by Δ^9-tetrahydrocannabinol (Δ^9-THC). *N*-arachidonoylglycine (NAGly) has been proposed as an endogenous ligand of GPR18, which is, however, controversially discussed in the literature. GPR18 is predominantly expressed in cells of the immune system and plays a role in inflammation and pain. GPR55 is more widely expressed, activated by lysophosphatidylinositol (LPI), and has been proposed as a potential drug target in inflammation, metabolic dysfunctions and neuronal diseases.

7.2. Development of GPR18 and GPR55 antagonists based on an imidazothiazinone scaffold

Rempel *et al*. developed **PSB-CB-5** (**17**), a benzylidene-imidazothiazinone derivative, as the first potent GPR18 antagonist with an IC_{50} value of **0.279** μM determined in β-arrestin recruitment assays. However, this compound only showed partial inhibition of the Δ^9-THC-induced GPR18 activation and may therefore be described as an allosteric antagonist with respect to the agonist Δ^9-THC. In this study, we varied the substitution pattern of the benzylidene residue either by introducing large lipophilic substituents to target GPR18 or by small lipophilic substituents to target GPR55. Furthermore, we varied the heterocycle and the position of the substituents at the benzylidene residue. Structure-activity relationships are summarized in Figure 119.

Compounds with a *p*-chlorobenzyloxyalkyoxy residue in the *meta*-position of the benzlidene residue with different alkyl chain length were investigated. They proved to fully inhibit the effect of Δ^9-THC, with compound **79** being the most potent derivative with an IC_{50} value of **0.650** μM. Some of the *p*-chlorobenzyloxyalkyoxy-substituted derivatives showed ancillary inhibition of GPR55. For GPR55, the structure-activity relationships could be extended. Small halogen- and methyl-substituents

at the benzylidene residue resulted in increased inhibitory potency. The best GPR55 antagonist of the present series was **63** with an IC_{50} value of **2.93** µM. The developed antagonists displayed high selectivity as shown in Figure 120.
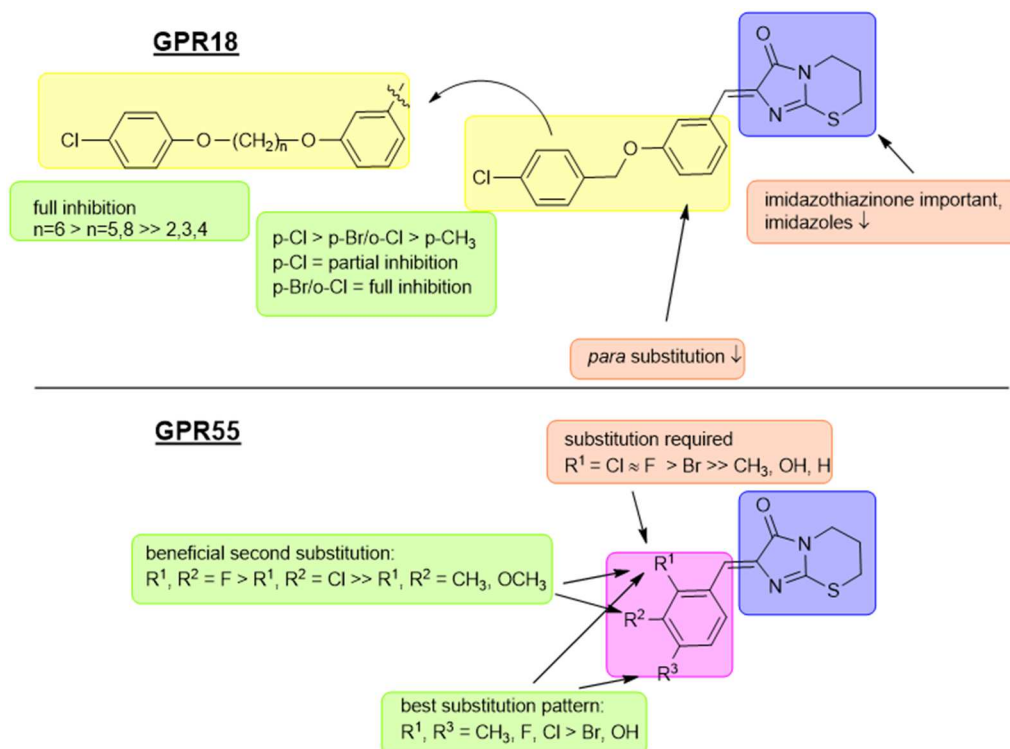
Figure 119: Structure-activity relationships of imidazothiazinones as GPR18 and GPR55 antagonists.

GPR18 antagonists

GPR18 IC$_{50}$ = **0.279 ± 0.111** µM

GPR55 IC$_{50}$ > 10 µM
CB$_1$ K$_i$ > 10 µM
CB$_2$ K$_i$ > **4.03 ± 0.51** µM

PSB-CB5 (16)

GPR18 IC$_{50}$ = **0.650 ± 0.134** µM

GPR55 IC$_{50}$ > 10 µM
CB$_1$ K$_i$ > 10 µM
CB$_2$ K$_i$ > 10 µM

79

GPR55 antagonists

GPR55 IC$_{50}$ = **2.93 ± 0.30** µM

GPR18 EC$_{50}$ > 10 µM; IC$_{50}$ > 10 µM
CB$_1$ K$_i$ > 10 µM
CB$_2$ K$_i$ > 10 µM

63
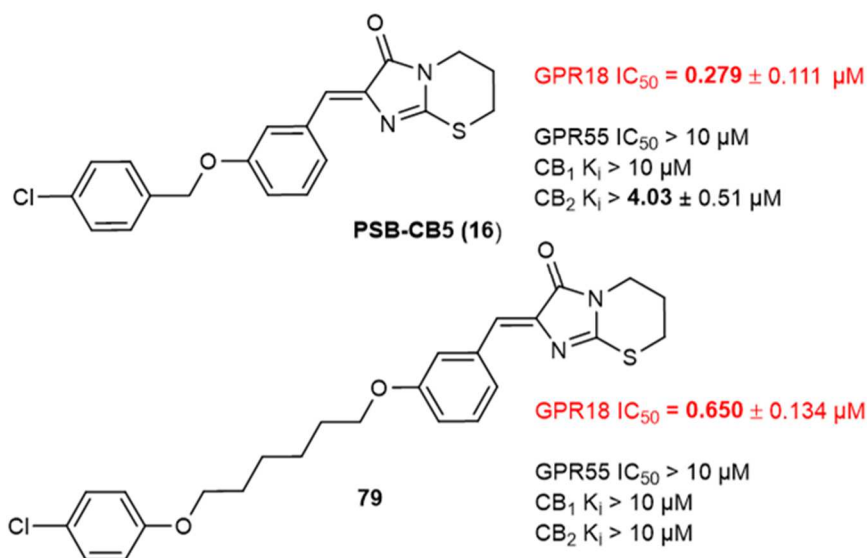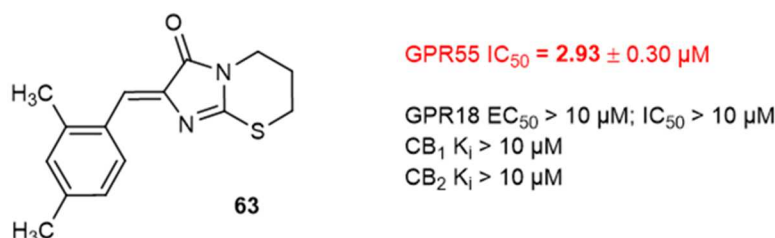
Figure 120: Chemical structures and pharmacological data of the most potent imidazothiazinone derivatives at human GPR18 and human GPR55.

7.3. Development of potent and selective GPR18 agonists

In order to develop potent and selective agonists for GPR18, we screened a xanthine sublibrary of the Pharma-Zentrum Bonn compound library. We discovered compound **182** (Figure 121), originally synthesized in the group of Prof. Dr. Katarzyna Kieć-Kononowicz, Jagiellonian University, Cracow, Poland, as a potent GPR18 agonist with an EC$_{50}$ value of **0.556** µM. Compound **182** displays peptide-like features and consists of an 8-indolylethylaminoxanthine core structure. The compound showed high selectivity for GPR18 versus GPR55, CB$_1$ and CB$_2$ receptors.

The identified scaffold was further optimized in cooperation with the research group of Prof. Kieć-Kononowicz. Firstly, the third heterocycle was varied and later on completely omitted. Further variations were made at the *N1* and *N7* of the xanthine core structure. However, no substitutions except for methyl were tolerated at the *N1*-position. At the *N7*-position different substituents with varying chain-length were introduced. The most potent compound was a *p*-chloro-substituted derivative, compound **162** (Figure 120). The indole residue turned out to be crucial for GPR18

activation. A whole library of compounds with different residues instead of the indole were tested and none of them was active at GPR18. Structure-activity relationships are summarized in Figure 122.

GPR18 agonists

182

GPR18 EC_{50} = **0.556** ± 0.126 μM
efficacy: 106%

GPR55 EC_{50}/IC_{50} > 10 μM
CB_1 K_i > 10 μM
CB_2 K_i > 10 μM

potency↑

potency↑
selectivity↑

162

GPR18 EC_{50} = **0.0191** ± 0.0034 μM
efficacy: 141%

GPR55 EC_{50}/IC_{50} > 10 μM
CB_1 K_i = **1.18** ± 0.44 μM
CB_2 K_i = **0.481** ± 0.104 μM

161

GPR18 EC_{50} = **0.0454** ± 0.0081 μM
efficacy: 84%

GPR55 EC_{50}/IC_{50} > 10 μM
CB_1 K_i > 10 μM
CB_2 K_i > 10 μM
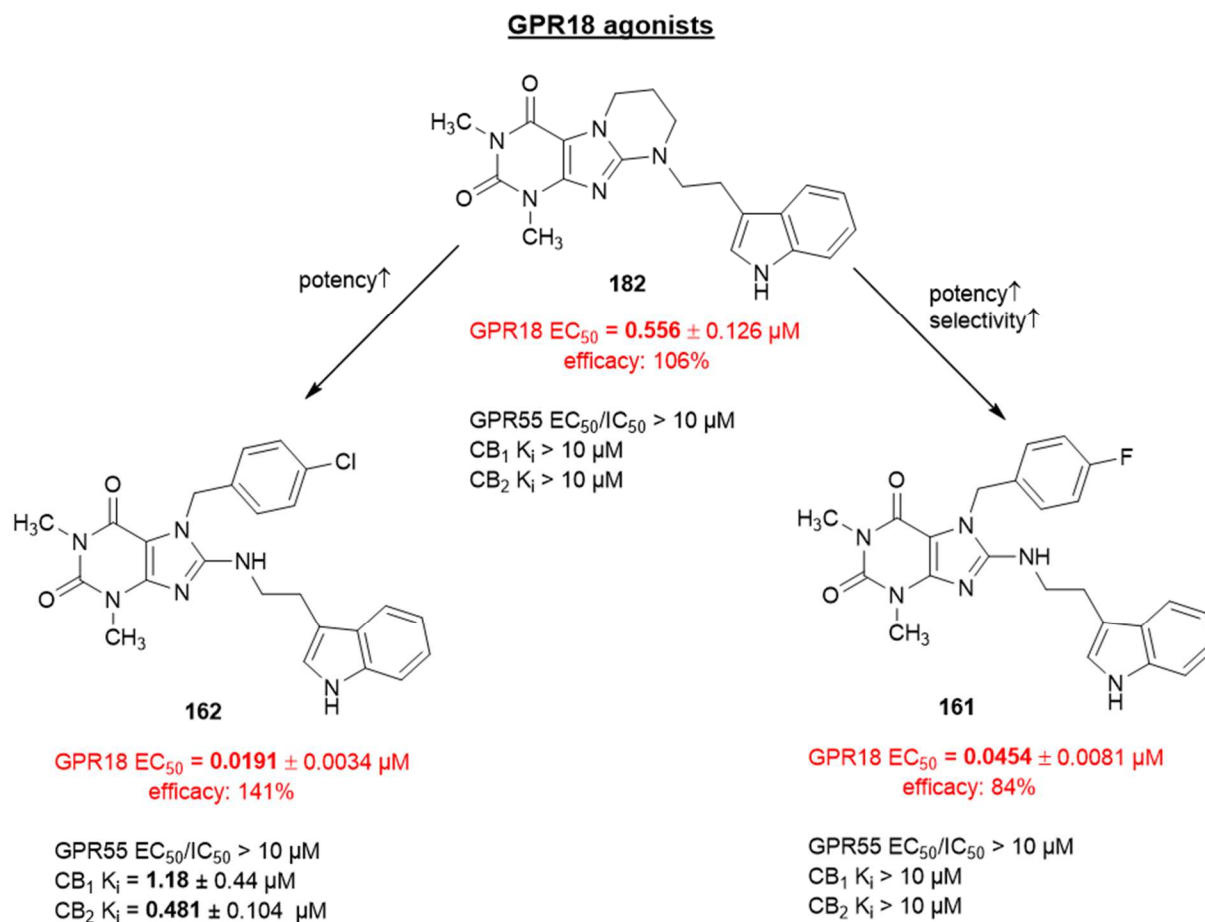
Figure 121: Most potent GPR18 agonist of indolylethylaminoxanthine series; efficacy was compared to the maximum response of Δ^9-THC.

R^2: *p*-Cl-Benzyl > *p*-Br-benzyl > *p*-F-benzyl >> benzyl
p-Cl-benzyl > *m*-Cl benzyl >> *o*-Cl benzyl

R^2: 2-Isobutyl > isopropyl > pentyl > hexyl > butyl > propyl > ethyl > methyl

Diazepane > diazinane >> imidazolidine

R^1: -CH$_3$ >> H, ethyl, propyl → methyl substitution essential

Indolylethylamine >> 5-hydroxy-indolylethylamine

Indole is required, alkyl and aryl residues are inactive
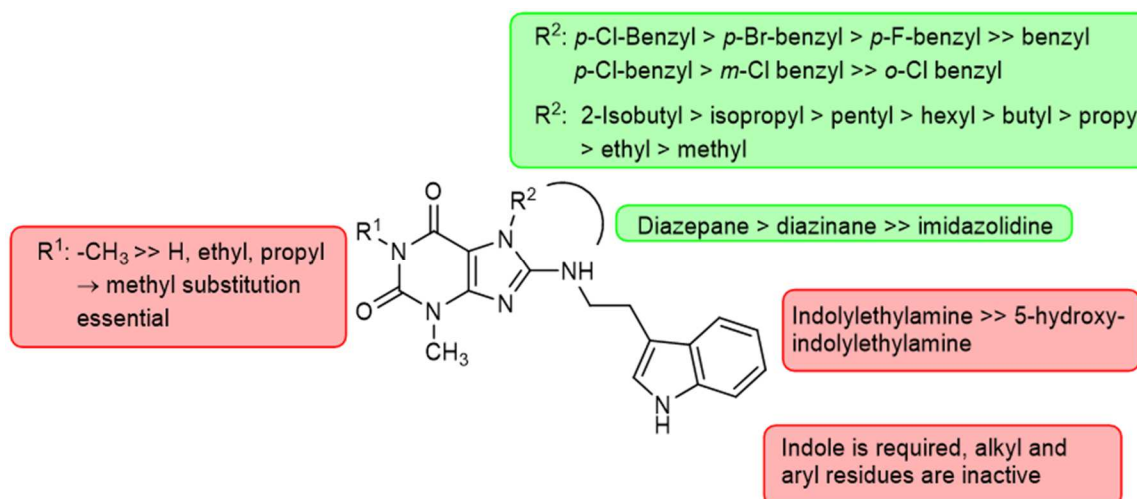
Figure 122: Structure-activity relationships of the indolylethylaminoxanthines at GPR18.

The compounds were tested for their selectivity versus the closely related GPR55 in the same assay system and showed no activating or inhibiting activity. They were further investigated at CB$_1$ and CB$_2$

receptors in radioligand binding studies. Some compounds showed affinity for the CB_2 receptor. The most selective compound was **161**, which showed no affinity to the CB receptors up to 10 µM, but a high potency at GPR18 with an EC_{50} value of **0.0454** µM. The most potent CB_2 receptor ligand within this class of compounds was **168** with a K_i value of **0.344** µM. Compound **162** also showed nanomolar affinity for the CB_2 receptor (K_i = **0.481** µM).

We further investigated the potencies of the newly discovered agonists at the mouse GPR18. This murine orthologue shares a high degree of sequence similarity with the human GPR18. We expressed it in the same assay system and tested the agonists at the mouse receptor. Similar potencies were observed: the EC_{50} values of the agonists were slightly, but insignificantly higher at the mouse as compared to the human GPR18, while the structure-activity relationship were identical. The lipid-like compound *N*-arachidonoylglycine neither interacted with the mouse nor with the human GPR18 in our experiments.

Concentration-dependent inhibition of Δ^9-THC versus compound **182**-induced β-arrestin recruitment by the antagonist **PSB-CB-5** (**17**) indicated different binding sites for both receptors. The antagonist was 40-fold weaker versus compound **182** than versus Δ^9-THC. Thus, **PSB-CB-5** (**17**) appears to occupy the same binding site as Δ^9-THC, which is plausible since both are lipid-like compounds, while Δ^9-THC and the new indole antagonists probably have different binding sites on GPR18.

In order to get more insight into the binding sites of GPR18, we performed a molecular modeling study. To this end, we used the Rosetta protein design modeling suite in the laboratory of Prof. Dr. Jens Meiler at Vanderbilt University, Nashville, TN, USA. Twenty GPCR crystal structures were provided as templates together with the human GPR18 sequence resulting in an ensemble of models, which were selected by energy scores, clustering and reasonable visual appearance. By subsequent optimization the extracellular loops of the receptor models were individually adapted to the proposed secondary structure prediction (Figure 123). GPR18 shows the unusual DVILY instead of the conserved NPxxY motif found in most other GPCR. The effects of this sequence variation are unknown. The β-strand prediction for the extracellular loop 2 could not be captured in the loop refinement study, although it seemed likely by secondary structure prediction.
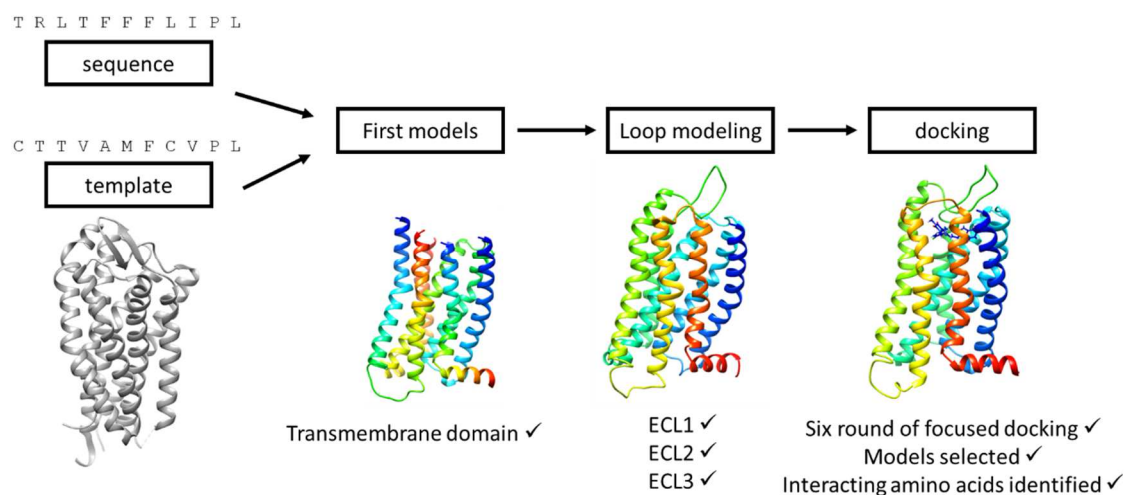
Figure 123: Homology modeling and docking of GPR18.

An ensemble of well-scoring models from different clusters with reasonable appearance were selected for ligand docking. The potent agonist **162** was selected as a ligand. The docking was conducted over six rounds, where ligand mobility was decreased in each step. A final ensemble of models was selected based on energy scoring and clustering. Out of each cluster the best models were evaluated concerning the ligand pose and the interaction profile with the amino acids of the receptor. Four different poses deemed reasonable and eleven suggestions for mutagenesis studies were made based on the models (Figure 124).
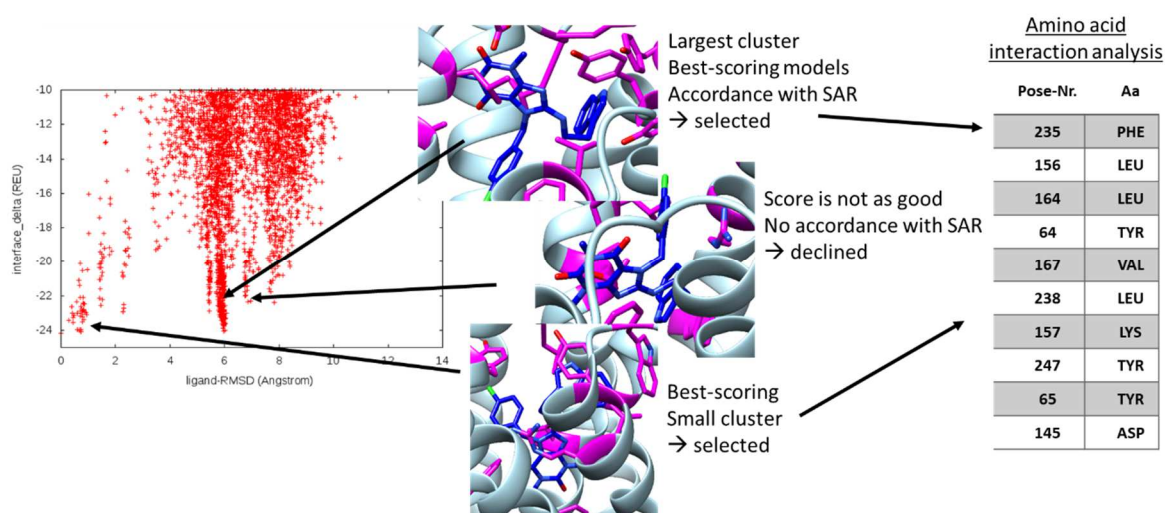
Figure 124: Procedure and results from the docking of compound **162** into the GPR18 homology models.

Experiments are in the progress to confirm or discard the proposed agonist-receptor interactions.

7.4. Chromen-4-ones as GPR55 agonists

In another subproject, we investigated and optimized a series of chromen-4-one derivative as GPR55 ligands (Figure 126). Based on chromen-4ones that had been identified as weak GPR55 antagonists we performed a number of structural modifications to increase their potency and to modulate their functionality. By aliphatic *meta*-substitution of the 8-benzamido residue, compounds with partial agonistic activity were obtained as compared to the full agonist lysophosphatidylinositol (LPI). Interestingly, the agonistic properties were lost when the compounds were substituted with an aromatic residue (for example, compound **283**, Figure 126). By subsequent optimization, we developed compound **299**, which showed an EC_{50} value of **0.196** µM and a high efficacy of 86%. The optimized compounds proved to be selective versus the phylogenetically most closely related GPR35 and GPR18. Compound **299** was 75-fold selective for GPR55 versus the cannabinoid receptors and 8-fold selective versus GPR17. Structure-activity relationships are summarized in Figure 125.
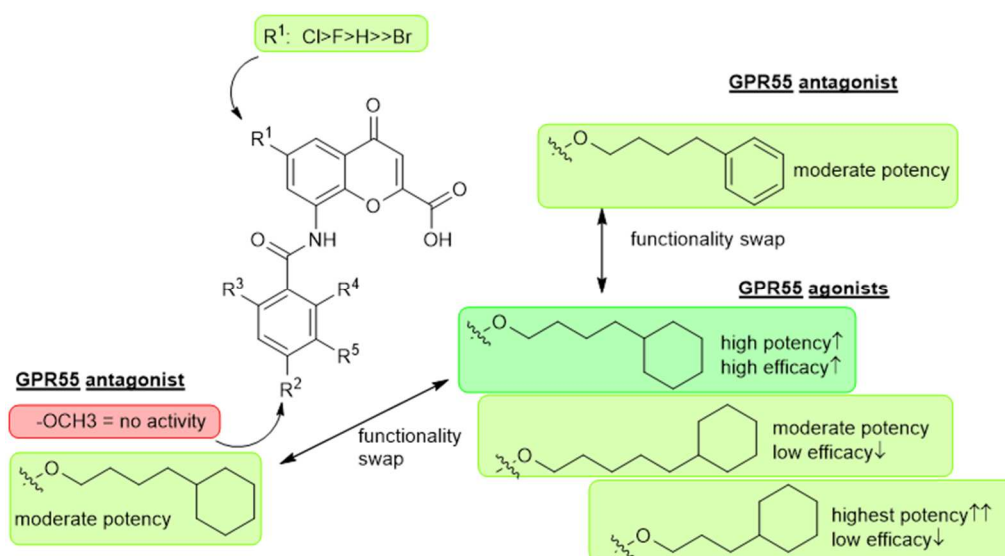
Figure 125: Structure-activity relationships for chromen-4-ones as GPR55 agonists.
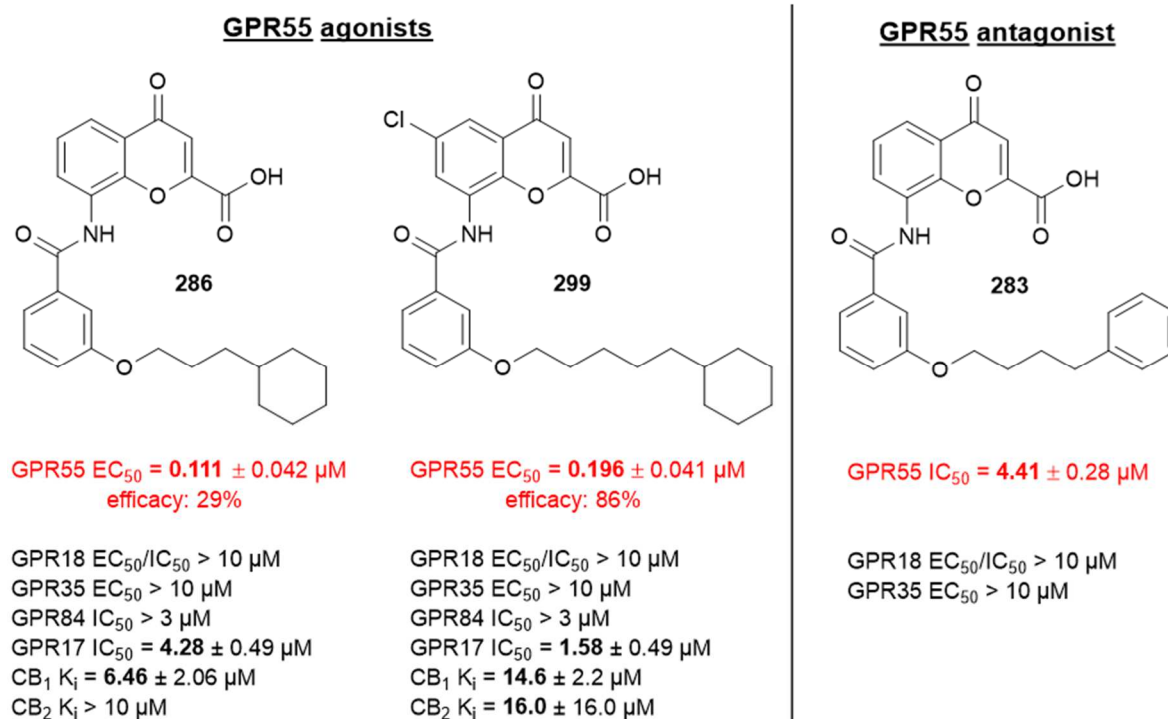
Figure 126: The most potent compounds of the chromen-4-one series.

7.5. Pharmacological evaluation of synthetic cannabinoids derived from "spice"

In a further subproject we pharmacologically investigated constituents of "Spice". The abuse of synthetic cannabinoids in incenses called 'spice' has increased in the last years. Highly potent synthetic CB_1 agonists that had been published in the scientific literature, were sprayed onto herbal materials which are sold as legal highs. These synthetic compounds are psychoactive and cause severe side effects up to lethal intoxications. As soon as the structure of a compound, its potential abuse and its effects on CB_1 receptors are known, these compounds will be restricted by law. The illicit sellers often circumvent restrictions by preparing compounds with slightly changed structure.

In cooperation with the Institute of Forensic Medicine, University of Bonn, we investigated a large set of compounds that had been reported to be distributed in herbal blends ("spice"). We determined their ability to bind to the CB receptors and also investigated the interaction of selected compounds with GPR18 and GPR55.

Our results confirmed that the majority of the investigated compounds behaved as highly potent CB receptor agonists with affinities in the low nanomolar to subnanomolar concentration range combined with high efficacy (see Figure 127). The main structural variations of the compounds represent typical bioisosteric exchanges altering the structure of the compounds in order to circumvent restriction by law, but retaining the intended psychoactive effects. Knowledge of medicinal chemistry provides powerful strategies to bypass controlled substances. In our study, we have

provided a comprehensive analysis of the structure-activity relationships of spice constituents including 41 compounds of previously unknown potency and efficacy. The obtained data were compared to those of established CB receptor ligands. In the future, this may help to predict pharmacological behavior of novel compounds that appear on the illicit drug market.

The compounds were further investigated at the CB receptor-related orphan GPCRs GPR18 and GPR55. While no interaction with GPR18 was detected, some derivatives behaved as weak antagonists of GPR55. Since knowledge about these newly discovered orphan receptors is still very limited our results contribute to a better understanding of their ligands' structural requirements. Moreover we have identified novel GPR55 antagonists that could be used as starting points for future optimization.

MDMB-FUBINACA (348)
hCB$_1$: K$_i$ = **0.0985** ± 0.0291 nM
hCB$_2$: K$_i$ = **0.130** ± 0.010 nM

EAM-2201 (383)
hCB$_1$: K$_i$ = **0.380** ± 0.111 nM
hCB$_2$: K$_i$ = **0.371** ± 0.052 nM
hGPR55: IC$_{50}$ = **1860** ± 160 nM

Figure 127: Chemical structure of the most potent CB receptor ligand **MDMB-FUBINACA (348)** and **EAM-2201 (383)**, the most potent GPR55 antagonist.

7.6. Conclusion

The discovered structure-activity relationships of several classes of compounds at cannabinoid and cannabinoid-like orphan GPCRs, namely GPR18 and GPR55, the new optimized and characterized tool compounds, and performed molecular modeling studies will be highly useful since they will allow studies towards validation of GPR18 and GPR55 as drug targets. Extensive studies on spice constituents will help to limit their illegal use.

8. EXPERIMENTAL METHODS

8.1. Cell culture

8.1.1. Cell culture

Cells were cultured in their respective medium in incubators, maintaining 37° and 5% or 10% CO_2. They were passaged under a laminar air flow when reaching a confluence of 80-90% up to 35 passages. To remove cells from cell culture flask, initial medium was removed and cells were rinsed with 10 ml PBS buffer. After removing this buffer, cells were treated with 3 ml trypsin/EDTA solution (for 175 cm^2 tissue culture flasks, 1.5 ml for 75 cm^2 and 1 ml for 25 cm^2) for up to five minutes at 37° degrees. When cells were detached, the reaction was stopped by adding their respective medium up to 10 ml. Cells were resuspended by pipetting and then split into prepared cell culture flask.

8.1.2. Thawing and freezing of cells

Cells were thawed from kryo-stocks (-80°/-150°/nitrogen stored) by warming them, until the medium could be removed from the kryo-stocks directly into cell culture medium.

To produce kryo stocks, cells were removed as described in 8.1.1. Detached cells were transferred into prepared falcon tubes. They were centrifuged for 5 minutes at 1200 rpm to spin down cell material. Subsequently, the supernatant was removed and cells were resuspended in FCS containing 10% DMSO (microbiological grade) and transferred into prepared kryo stocks. Initially, they were stored in freezing devices in a -80° freezer to ensure moderate freezing rates. On the next day, they were transferred to long time storage (-80° freezer, -150° freezer or nitrogen tank).

8.1.3. Membrane preparations

For membrane preparations, cell suspensions were split into petri dishes (75 cm^2) in a total volume of 20 ml cell culture medium and grown, until the density reached >80%. The medium was removed and the petri dish rinsed with 10 ml PBS buffer. The PBS buffer was discarded and petri dishes were frozen at -20° degrees. Upon thawing, 1 ml dissociation buffer (5 mM Tris, 2 mM NaEDTA, pH 7.4) was transferred on every dish. Cells were removed and collected, and always kept on ice. The total amount of cell suspension was homogenized with an Ultra-Turrax at maximum speed. After this, the suspension was further treated with a potter at maximum speed. This suspension was transferred into centrifuge tubes and centrifuged for 10 min and 1000g at 4° in a Beckman centrifuge (Beckman-Coulter, Brea, CA, USA). The supernatant was collected, the pellet discarded. The supernatant was further centrifuged with 48,300g for 1h at 4°. The supernatant was discarded and the pellet was

resuspended in radioligand binding assay wash buffer (50 mM Tris, pH 7.4) in an amount that corresponded to 0.1 ml per initial dish. All pellets were collected and homogenized, transferred into Eppendorf tubes and stored in a -80° freezer.

8.1.4. Protein determination in membrane preparations using the Lowry assay

For determining the protein amount, a stock solution of BSA (1 mg/ml in 50 mM Tris, pH 7.4) was used for calibration. The solution was diluted in 50 mM Tris, pH 7.4 to the following concentrations: 50, 100, 200, 300, 400 and 500 µg/ml. The test solution was diluted 1:10, 1:20 and 1:50. As a control 50 mM Tris buffer, pH 7.4 was used. 200 µl of the test solutions or the calibration dilutions were initially disposed in reaction tubes in duplicates. A fresh solution of copper sulfate was prepared by mixing 50 parts of a 2% Na_2CO_3 solution in 0.1 N NaOH and 1 part of a $CuSO_4*5\ H_2O$ 0.5%, sodium tartrate 1% in aqua bidest. 1000 µl of this solution was transferred to each reaction tube, mixed by vortexing and incubated for 20 min at room temperature. 100 µl of the Folin's Ciocalteau Phenol Reagent Working Solution (1:5 solution of Folin's Reagent in aqua bidest.) were transferred to each reaction tube, mixed by vortexing and incubated for 30 min at room temperature. The content of each reagent tube was transferred to cuvettes, suitable for determination of absorption at 550 nm. The absorption of the control was put to zero in a photometer from Beckman, Brea, CA, USA (pre-warmed for 30 min). Subsequently, all following dilutions were measured and the absorptions determined. From the calibration with BSA, a linear equation was obtained for calculating the amount of protein in the membrane preparartions.[312]

8.2. Pharmacological assays

8.2.1. Preparation of cAMP binding protein

cAMP binding protein (proteinkinase A) was extracted from bovine adrenals, as described by Nordstedt *et al*.[313] The adrenals were transferred to 4° cold buffer (100 mM Tris*HCl, 250 mM NaCl, 10 mM NaEDTA, 0.25 M sucrose and 0.1% mercaptoethanol, pH 7.4) or stored frozen in -80° until the cAMP binding protein was prepared. Adrenals were cleared of visual fat and other tissue with a knife or a scalpel and kept on ice or in ice-cold buffer. Then, the adrenal cortex was divided from the adrenal mark as complete as possible. Hence, the slices were cut into small pieces, covered with buffer and crushed with an Ultra-Turrax in varying speeds. The mixture was transferred to a potter and processed at varying speeds. The suspension was filtered over mull with a water-jet vacuum pump to separate tissue pieces and fat from the flow-through. The whole amount of liquid was divided in centrifuge

tubes and spinned for 1 h at 30.000g and 4°. The pellet was discarded and the supernatant was aliquoted in 2 ml tubes and stored at -20° (ready-to be used stocks), or at -80° (long-time storage).

8.2.2. cAMP assay

Inhibition of adenylate cyclase activity was determined in Chinese Hamster Ovary (CHO) cells stably expressing the CB_1 or the CB_2 receptor subtype, respectively, using a competition binding assay for cAMP, adapted from the procedure described by Nordstedt *et al.*[313] Cells were seeded into a 24-well plate at a density of 200 000 cells/well 24 h before performing the assay. After the incubation, the cells were washed with Hank's buffered saline solution (HBSS) consisting of NaCl (13 mM), HEPES (20 mM), glucose (5.5 mM), KCl (5.4 mM), $NaHCO_3$ (4.2 mM), $CaCl_2 \times 2\ H_2O$ (1.25 mM), $MgSO_4$ (0.8 mM), $MgCl_2$ (1 mM), KH_2PO_4 (0.44 mM), and Na_2HPO_4 (0.34 mM) dissolved in deionized, autoclaved water. After addition of 190 µL of HBSS per well, cells were incubated for 2 h at 37°C. After this period of time, 20 µl of the phosphodiesterase inhibitor Ro-20-1724 (4-(3-butoxy-4-methoxybenzyl)-2-imodazolidinone), final concentration 40 µM, dissolved in HBSS, was added and the suspension incubated for 10 min. 15 µl of test compound was diluted in HBSS containing 10% dimethylsulfoxide (DMSO) to the desired concentration and added to the suspension. After 5 min of incubation 15 µl forskolin (final concentration: 10 µM), prepared in HBSS containing 10% DMSO, were added to each well. Antagonists were added at the desired concentration 20 min before adding the agonist. The final DMSO concentration was 1.9%. The suspension was incubated for 10 min after the addition of Ro-20-1724, again for 5 min after the addition of test compound, and for another 15 min after adding forskolin. cAMP accumulation was stopped by removing the supernatant from the cell suspension and subsequently lysing the cells with 500 µL of hot lysis buffer (100 °C; 4 mM EDTA, 0.01% Triton X-100). Aliquots of 50 µL of cell suspension were transferred to 2.5 mL tubes, 30 µL of [^{3}H]cAMP (3 nM) and 40 µL of cAMP-binding protein (50 µg per well) were added, followed by 1 h of incubation on ice. The cAMP binding protein was obtained from bovine adrenal cortex as described above. Bound and free radioligand were separated by rapid filtration through GF/B glass fiber filters using a Brandel 48-channel cell harvester (Brandel, Gaithersburg, MD). Radioactivity on the filters was determined in a liquid scintillation counter (TRICARB 2900TR, Packard/Perkin-Elmer) after 6 h of preincubation with 3 mL of scintillation cocktail (LumaSafeplus, Perkin-Elmer). Data were obtained from three independent experiments, performed in duplicates.

8.2.3. Radioligand binding studies at cannabinoid receptors

Competition binding assays were performed using the CB agonist radioligand [^{3}H](−)-cis-3-[2-hydroxy-4-(1,1-dimethylheptyl)phenyl]-trans-4-(3-hydroxypropyl)¬cyclohexanol ([^{3}H]CP55,940, final

234

concentration 0.1 nM). As a source for human CB_1 and CB_2 receptors membrane preparations of Chinese hamster ovary (CHO) cells stably expressing the respective receptor subtype were used (30 μg of protein/well for CB_1 and 8 μg of protein/well for CB_2-receptor preparations) as described above. Stock solutions of the test compound were prepared in DMSO. The final DMSO concentration in the assay was 2.5%. After addition of 15 μL of the test compound in DMSO, 60 μL of [^{3}H]CP55,940 solution in assay buffer, and 60 μL of membrane preparation to 465 μL of assay buffer (50 mM TRIS, 3 mM $MgCl_2$, 0.1% BSA, pH 7.4), the suspension was incubated for 2h at room temperature. Total binding was determined by adding DMSO without test compound. Nonspecific binding was determined in the presence of 10 μM of unlabeled CP55,940. Incubation was terminated by rapid filtration through GF/C glass fiber filters presoaked for 0.5 h with 0.3% aq. polyethyleneimine solution, using a Brandel 96-channel cell harvester (Brandel, Gaithersburg, MD). Filters were washed three times with ice-cold washing buffer (50 mM TRIS, 0.1% BSA, pH 7.4) and then dried for 1.5 h at 50 °C. Radioactivity on the filters was determined in a liquid scintillation counter (Topcount NXT, Packard/Perkin-Elmer) after 10 h of preincubation with 50 μl of scintillation cocktail (Multiscint 25, Perkin-Elmer). Data were obtained in three independent experiments, performed in duplicates. Data were analyzed using GraphPad Prism Version 4.02 (San Diego, CA, USA). For the calculation of K_i values the Cheng-Prusoff equation[314] and a K_D value of 2.4 nM ([^{3}H]CP55,940 at CB_1) and 0.7 nM ([^{3}H]CP55,940 at CB_2) were used.[315]

8.2.4. β-Arrestin recruitment assay (PathHunter®)

In white 96-well-plates, 20.000 cells per well, stably expressing GPR18 or GPR55 and prolink1, were seeded in 90 μl medium (Opti-Mem, 2% FCS, 100 U/ml Penicillin, 100 μg/ml Streptomycin, 800 μg/ml Geneticin and 300 μg Hygromycin) and incubated for 24h at 37°C and 5-10% CO_2. Antagonist and agonists (stocks in 10 mM DMSO were diluted in PBS containing 0.1% BSA, until the final concentration of DSMO is 1% and the final concentration of screens was 10 μM). Antagonists were added to the wells in an amount of 5 μl, incubated 60 min at 37°, than agonist was added in an amount of 5 μl and incubated for 90 min. The final assay volume was 100 μl. 50 μl detection reagent per well (for GPR18 by mixing 220 μl of Galacton-StaR® (2 mM), with 1000 μl the luminescence enhancer Emerald-II™ and a lysis buffer consisting of 5 mM K_2HPO_4, 5 mM KH_2PO_4, 150 mM NaCl, 10 mM $MgAc_2$ and 2% Chaps, pH7,4; and for GPR55 by mixing the chemiluminescent substrate Galacton-StarR® (2 mM), with the luminescence enhancer Emerald-II™ and a lysis buffer (10 mM TRIS, 1 mM EDTA, 100 mM NaCl, 5 mM MgCl2, 1 % Triton-X; pH 8) in a ratio of 1:5:19) were added and incubated for 60 min at room temperature. After that luminescence signals were counted in a TopCount NXT, Packard, Perkin-Elmer, in one second per well. For the human GPR18, $Δ^9$-THC as agonist was used in concentration of 10 μM, and later on the agonist **162** in a concentration of 0.1 μM. As maximum response of the respective agonist $Δ^9$-THC was used at 30 μM and compound **162** at 1 μM. For the human GPR55, LPI was used as

agonist in a concentration of 1 µM, as maximal response at 10 µM. For the mouse GPR18, compound **162** was used at 0.3 µM and 3 µM to obtain the maximal response.

8.2.5. Radioligand binding studies at GABA$_A$ receptor channels

Test compounds were diluted in DMSO to obtain a final test concentration of 10 µM in the assay. For unspecific binding diazepam was used in a concentration 10 µM, for determining total binding DMSO was added. As the assay did not tolerate a DMSO concentration higher than 1%, 10 µl of the DMSO dilutions were transferred onto 790 µl of assay buffer (50 mM Tris, pH 7.4). As radioligand [^{3}H]diazepam in a concentration of 2 nM and rat cortex preparations with a protein amount of 100 µg per well were added to the assay buffer each in 100 µl of assay buffer. After 1h of incubation (shaking on ice), the assay was filtered through a 48-well harvester (Brandel, Gaithersburg, MD, USA) using GF/B-filters and washed three times with 4°C cold Tris 50 mM buffer, pH 7.4. Filters were then transferred to scintillation vials, soaked in 2 ml scintillation cocktail (LumaSafePlus, Perkin-Elmer, Waltham, MA, USA) and counted after 6h in a luminescence counter (TRICARB 2900 TR, Canberra Packard, Perkin-Elmer) for 1 min.[316]

For the calculation of K$_i$ values the Cheng –Prusoff equation[314] and a K$_d$ of 4 nM for diazepam were used.

8.2.6. Data Analysis

All data were processed with Microsoft Excel (2007, 2010 and 2013) and further analyzed using Prism 4.02 or Prism 5.01 for Windows, GraphPad Software, San Diego California USA, www.graphpad.com.

8.3. Molecular biology

8.3.1. Production of competent bacteria

Untransformed Top10 E. coli bacteria were cultivated in 4 ml of LB-medium (without antibiotics) at 37° and 220 rpm overnight. They were transferred into 40 ml LB-medium on the next day and incubated for 40 min. Optical density was controlled, until it reached 0.5. The bacterial suspension was then centrifuged for 20 min at 1700g and 4°C. The supernatant was removed and the cells resuspended in 20 ml of an ice-cold 0.1 mM CaCl$_2$ solution. They were incubated for 30 min on ice. After that, they were centrifuged again for 20 min at 1700g and 4°. The supernatant was removed again and the cells

resuspended in 2 ml of ice-cold 0.1 mM CaCl$_2$ solution. 0.5 ml glycerol was added and the suspension was aliquoted (100 µl each) and stored at -80°C.

8.3.2. Transformation of competent bacteria

The competent bacteria were removed from the -80°C freezer and stored on ice for 30 min. 10 ng of the plasmid of interest were gently mixed into the suspension with a tip and everything was incubated for further 30 min on ice. After that, the bacterial suspension underwent a heat shock (either in a thermomixer plate or in a water bath at 37°C for 2 min). Subsequently, they were stored on ice for further 2 min. Then, 200 µl of LB-medium was added and the culture was incubated at 37°C and 220 rpm for one hour. After that, the suspension was added to an agar-plate containing the corresponding antibiotic for selection and was spread with a Drigalski-spatula. After air drying, the agar plate was stored in an incubator at 37°C upside down overnight.

8.3.3. Single colony picking and growth

From the agar plate, one colony was picked with a pipette tip and transferred to 4 ml of the corresponding liquid bacterial culture medium (LB-medium with selection antibiotics). The tubes were incubated over night (or 18 h) in a 37° incubator in shaking mode (220 rpm). For DNA mini-preparations 3 ml of the medium were used, for larger scales, the bacterial colony were transferred into a 150 ml LB-medium containing heat-sterilized Erlenmeyer flask and shaken overnight.

8.3.4. Glycerin cultures for long time storage

For long time storage, the bacterial culture of interest in their overnight culture medium was gently mixed with glycerin (5:1) and immediately deep-frozen at -20°C and for long-time storage at -80°C.

8.3.5. Purification of plasmid-DNA (Mini-prep, Midi-prep)

The ZR plasmid Miniprep™ - Classic kit (Zymo Research Corporation, Irvine, CA, USA) was used for plasmid purification according to the instructions of the supplier. In the last step, the DNA was eluted with 30 µl purified water.

The PureLink® HiPure Plasmid Filter Midiprep Kit (Invivogen, ThermoScientific, Waltham, MA, USA) was used to obtain larger amounts of DNA according to the instructions of the supplier. Only the last centrifugation step was prolonged to 30 min.

8.3.6. Gel electrophoresis of DNA

To verify DNA length and purity, the plasmid DNA was assessed via gel electrophoresis on an agarose gel (1%; 0,25 mg agarose were dissolved in 25 ml TAE buffer (Tris-acetat-EDTA-buffer) by carefully heating in a microwave, then 1.75 µl Gel-Red™ were added). For cooling, the gel was transferred on a gel trail, where a comb was put in the liquid gel. The samples were prepared by mixing 2 µl 6x loading dye, the volume of DNA necessary for detection, normally, 1-3 µl. Then purified water was added to a total volume of 12 µl. The gel was posed in the electrophoresis chamber, covered with TAE-buffer and loaded with 10 µl of the samples, along with a DNA marker (λ-marker). After applying a voltage of 105 V, the gel was run for 30 -60 minutes.

8.3.7. DNA purification out of a gel

With the Zymoclean™ Gel DNA Recovery Kit (Zymo Research Corporation, Irvine, CA, USA), the DNA was purified according to the instructions of the supplier.

8.3.8. Sequencing

The sequencing of plasmid DNA and PCR products was carried out by the biotech company GATC. Therefore, up to 1000 ng of the DNA in Aqua bidest. and if necessary primer suitable for sequencing were sent to GATC. The data analysis was done with Chromas Lite 2.01.

8.3.9. Restriction digest of plasmid DNA

Restriction was performed with 0.5 µl of each of the corresponding restriction enzymes (for the prolink1 and pBlueskripthGPR18 digest HindIII and NheI) with 1 µl reaction buffer (CutSmart®), the purified plasmid DNA (not less than 50 ng) and filled with sterile H_2O up to a total volume of 10 µl. The mixture was incubated for one hour at 37° in a heat block. In controls, samples are prepared lacking one of the restriction enzyme and also one lacking the plasmid DNA.

8.3.10. Ligation

For the ligation, at least 50 ng (but possibly more) cut plasmid DNA from step 8.3.9 and at least 150 ng of the insert DNA piece (this ratio can be adapted depending on performance and molecular weight) were put together with 1 µl of ligation buffer, 0.5 µl of T4-ligase and filled up with sterile H_2O up to 10

µl. As control, the ligation was performed lacking the insert and further lacking the enzyme and the insert.

8.3.11. Transfection of mammalian cells with Lipofectamine®

The parent cell line was grown in a minimum of three 25 cm^2 tissue culture flasks, till the cells reached a density of 80%. On the day of transfection, 4 hours prior to the transfection procedure, the medium was removed and the cells were incubated in their normal medium and 10% FCS, without any antibiotics. The transfection was carried out with Lipofectamine® according to the instructions of the supplier. 10 µl Lipofectamine® were gently mixed in 620 µl F12 Nutri-Mix (without anything) for 5 min. The volume containing 10 µg of the plasmid DNA was filled-up to 625 µl total volume with F-12 Nutri-Mix (without anything). Both solutions were gently mixed and incubated for 20 min. After this time, the solution was transferred to the respective tissue culture flask. As controls, in a second tissue culture flask the procedure above was performed without adding DNA. As further control, one flask was not treated at all. On the next day, the medium was removed and exchanged for the medium of the untransfected cells. One day later, the medium was exchanged once more to the selection medium. The third control was not exchanged, as it was necessary for controlling transfected versus untransfected cells in the pharmacological assay. Whenever the cells reached confluence, they were transferred to a 75 cm^2 flask. After some days of incubation with selection medium the untransfected cells (second control) were dead. When the transfected cells were confluent, kryo-stocks were made and pharmacological assays could be performed with untransfected cells as control.

This procedure was used to produce the CHO prolink1 mGPR18 cell line. Here, the parent cell line was already stably expressing a β-arrestin construct (selection on 0.3 mg/ml hygromycin B) and was further transfected with a pCMV-prolink1 mGPR18 vector (selection on 0.8 mg/ml G418).

8.3.12. Monoclone selection

For monoclone selection, the polyclonal mixture was removed from the tissue culture flask and cells were counted and further passaged, so that in 100 µl one cell could be expected. The suspension was transferred to a flat bottom adherent cell suitable 96-well plate (100 µl each) and incubated for some days. Cell growth was controlled regularly. When growth was detected, every well was controlled and only those were passaged to a 25 cm^2 flask, where exclusively one colony could be detected. Clones were cultured until they filled a 75 cm^2 tissue culture flask and then seeded according to the protocol of the assay. Maximum response to a standard agonist was measured and compared. The clones with

the highest differences in baseline to maximum response and a suitable background were chosen and retested. After the retest, one clone was chosen to be used for further assays.

8.3.13. Determining DNA concentration

The DNA concentration was either estimated by comparing the results from the gel electrophoresis samples to the λ-ladder, which shows characteristic bands of defined DNA amounts, or it was determined using 1 µl of the DNA solution with a nano-drop instrument (Colibri, Titertek-Berthold, Pfortzheim, Germany).

8.3.14. Used DNA sequence

For the cloning of the mouse GPR18, a pBluescript-mGPR18 sequence was ordered, containing restriction sites for NheI and HindIII and no stop-codon, with the following sequence:

```
>mGPR18

ggtaccgctagcaccATGGCCACCCTGAGCAATCACAACCAGCTTGATCTTTCTAATGGCTCACACCC
AGAGGAATACAAAATCGCAGCCCTAGTCTTCTACAGCTGCATCTTCCTGATTGGGCTGTTTGTTAATG
TCACTGCGTTGTGGGTTTTCAGCTGTACGACCAAGAAAAGAACCACAGTGACCATCTACATGATGAAC
GTTGCACTACTGGACCTCGTATTTATACTCAGTCTGCCCTTTCGGATGTTTTACTATGCAAAAGGCGA
GTGGCCATTTGGAGAGTACTTCTGCCACATTCTTGGGGCCCTGGTGGTGTGTTTTACCCAAGCCTCGCTC
TGTGGCTTCTTGCTTTCATTAGTGCTGACAGATACATGGCCATCGTACAGCCAAAATATGCCAAGGAG
CTGAAGAACACCGGCAAGGCCGTGCTTGCGTGTGGGGGGGTCTGGGTAATGACCCTGACCACCACTGT
CCCCCTGCTACTGCTCTACGAAGACCCAGACAAGGCCTCCTCCCCGGCCACCTGCCTGAAGATCTCCG
ACATCACCCACTTAAAAGCTGTCAACGTGCTCAACTTCACGCGACTCATATTTTTCTTCCTGATCCCT
TTGTTCATCATGATCGGGTGCTACGTGGTCATCATTCACAGTCTCCTCCGAGGGCAGACGTCTAAGCT
GAAGCCCAAGGTCAAGGAGAAGTCCATACGGATCATCATGACCCTCCTGCTGCAGGTGCTCGTCTGCT
TCGTGCCCTTCCACATCTGCTTTGCCGTCCTGATGCTACAAGGACAGGAGAACAGCTATAGCCCCTGG
GGAGCCTTCACCACCTTCCTCATGAACCTCAGCACCTGTCTCGATGTAGTCCTCTACTACATCGTTTC
CAAACAGTTCCAGGCTCGAGTCATCAGCGTCATGCTGTACCGCAATTACCTTCGCAGTGTTCGCAGAA
AAAGTGTCCGATCGGGCAGTTTACGGTCACTTAGCAACATGAACAGTGAGATGCTTtcaagcttaTGA
gaattc
```

8.4. LC/MS analyses

The purities of specific products were determined by ESI-mass spectra obtained on an LC/MS instrument (Applied Biosystems API 2000 LCMS/MS, HPLC Agilent 1100) using the following procedure: the compounds were diluted to 10 mM or 1 mM in DMSO. Then, 5-10 µL of the sample were injected into a HPLC column (Macherey-Nagel Nucleodur 3 µ C18, 50 mm × 2.00 mm). Elution was performed with a gradient of water/acetonitrile (containing 2 mM ammonium acetate) from 90:10 to 0:100 for

20 min at a flow rate of 300 µL/min, starting the gradient after 10 min. UV absorption was detected from 200 to 950 nm using a diode array detector.[257]

8.5. Chemicals, materials, devices and software

Table 47: Materials.

Materials	
Safe Seal® microtubes 1.5 and 5 ml	Eppendorf AG, Hamburg, Germany
Tips, nonsterile	Sarstedt, Nümbrecht, Germany
Ri-tips®	Ritter GmbH Medical, Schwabmünchen, Germany
Disposable pipettes 1, 5, 10 and 25 ml	Sarstedt, Nümbrecht, Germany
Megablocks	VWR International, Darmstadt, Germany
Falcons 15 ml and 50 ml	Corning Science Tanaulipas, Mexiko
GF/B filters Whatman	GE Healthcare, Little Chalfont, UK
GF/C filters	Perkin-Elmer, Waltham, MA, USA
Tissue culture flasks (25 cm^2, 75 cm^2 and 175 cm^2)	Sarstedt, Nümbrecht, Germany
NUNClon™ Delta Surface	Thermo Fisher Scientific, Rosenkilde, Denmark
TipOne filter tips sterile 10, 100 and 1000 µl	STARLAB, Hamburg, Germany
Reservoirs, nonsterile 50 ml	VWR International, Darmstadt, Germany
Rotilabo® microtest plates, V profile, 96 Well	Carl Roth GmbH & Co. KG, Karlsruhe, Germany
Reservoirs, sterile 50 ml	VWR International, Darmstadt, Germany
Sterile, disposable pipettes 1, 5, 10 and 25 ml	Sarstedt, Nümbrecht, Germany
Scinti-Vials, 3.5 ml, 10 ml	VWR International, Darmstadt, Germany; Perkin-Elmer, Waltham, MA, USA
Biozym® steril aerosol pipette tips	Labcon, Petatunia, CA, USA
Cuvettes for UV-Vis photometry	Ratiolab, Dreieich, Germany
Kryo vials	Sarstedt, Nümbrecht, Germany
Disposable petri-dishes (25 cm^2) and sterile disposable petri-dishes	Sarstedt, Nümbrecht, Germany
Bacterial tubes, 4 ml	Sarstedt, Nümbrecht, Germany

Table 48: Chemicals.

Chemicals	
Agarose TE	Biozym Scientific GmbH, Hessisch-Oldendorf, Germany
Tris	Carl Roth GmbH & Co. KG, Karlsruhe, Gemany
Glucose	Sigma Aldrich Corp., St. Louis, MO, USA
Sodium EDTA (ethylenediaminetetraacetic acid)	Sigma Aldrich Corp., St. Louis, MO, USA
NaCl	Carl Roth GmbH & Co. KG, Karlsruhe, Gemany
MgCl$_2$	Alfa Aesar, Ward Hill, MA, USA
Triton X-100	Sigma Aldrich Corp., St. Louis, MO, USA
Cut-Smart	New England Biolabs, Ipswich, MA, USA
λ-DNA/EcoRI/Hind III	New England Biolabs, Ipswich, MA, USA
K$_2$HPO$_4$	Carl Roth GmbH & Co. KG, Karlsruhe, Gemany
KH$_2$PO$_4$	Carl Roth GmbH & Co. KG, Karlsruhe, Gemany
Magnesiumacetata (MgAc$_2$)	Carl Roth GmbH & Co. KG, Karlsruhe, Gemany
Chaps	
Tropix® Emerald II	Applied Biosystems, Thermo Fisher Scientific

Galacton StaR®	Applied Biosystems, Thermo Fisher Scientific
Lipofectamie™	Thermo Fisher Scientific, Waltham, MA, USA
NaOH	Fluka, Sigma Aldrich Corp., St. Louis, MO, USA
Na-Tartrat	Riedel-de-Haen, Seelze, Germany
LB-medium	Carl Roth GmbH & Co. KG, Karlsruhe, Gemany
LB-agar	Carl Roth GmbH & Co. KG, Karlsruhe, Gemany
HEPES	Sigma Aldrich Corp., St. Louis, MO, USA
Na-Ampicillin	Carl Roth GmbH & Co. KG, Karlsruhe, Gemany
Glycerol	Sigma Aldrich Corp., St. Louis, MO, USA,
methyleneparabene	Acros Organics, Thermo Fisher Scientific, Waltham, MA, USA
Kanamycinsulfat	Carl Roth GmbH & Co. KG, Karlsruhe, Gemany
DMSO, micobiological grade	Carl Roth GmbH & Co. KG, Karlsruhe, Gemany
Polyethyleneimine 50%	Fluka, Sigma Aldrich Corp., St. Louis, MO, USA
BSA (bovine serum albumin)	Carl Roth GmbH & Co. KG, Karlsruhe, Gemany
FCS (fetal calf serum)	Sigma Aldrich Corp., St. Louis, MO, USA
Trypsin	PANBiotech GmbH, Aidenbach, Germany
NheI-HF, restriction enzyme	New England Biolabs, Ipswich, MA, USA
HindIII-HF, restriction enzyme	New England Biolabs, Ipswich, MA, USA
Hygromycin	InvivoGen, San Diego, CA, USA
PenStrep (Penicillin-streptomycin 10 000 I.E./ml, 10 mg/ml)	Gibco®, Life Technologies, Thermo Fisher Scientific, Waltham, MA, USA
Ultraglutamin / L-Glutamin	Gibco®, Life Technologies, Thermo Fisher Scientific, Waltham, MA, USA
G418 (Geneticin) 100 mg/ml and Paneticin G418 100 mg/ml	Invitrogen, Life Technologies, Thermo Fisher Scientific, Waltham, MA, USA and PANBiotech GmbH, Aidenbach, Germany
F-12 (Nutri-Mix)	Gibco®, Life Technologies, Thermo Fisher Scientific, Waltham, MA, USA
DMEM/F-12	Gibco®, Life Technologies, Thermo Fisher Scientific, Waltham, MA, USA
DMEM (Dulbecco's Modified Eagle Medium)	Gibco®, Life Technologies, Thermo Fisher Scientific, Waltham, MA, USA
Opti-MEM	Gibco®, Life Technologies, Thermo Fisher Scientific, Waltham, MA, USA
$CaCl_2$	Sigma Aldrich Corp., St. Louis, MO, USA
DMSO	AppliChem GmbH, Darmstadt, Germany
Hydrochloric Acid 37%	Carl Roth GmbH & Co. KG, Karlsruhe, Gemany
LumaSafe™	Perkin-Elmer, Waltham, MA, USA
MicroScint 25™	Perkin-Elmer, Waltham, MA, USA
mercaptoethanol	AppliChem, Damstadt, Germany
Ethanol, pure	Sigma Aldrich Corp., St. Louis, MO, USA

Table 49: Devices and instruments.

Devices	
Eppendorf pipette Research plus	Eppendorf AG, Hamburg, Germany
Biometra® Thermocycler	Biometra GmbH, Göttingen, Germany
Hettich centrifuge for tubes	Hettich, Tuttlingen, Germany
UV/Vis spectrometer	Beckman, Brea, CA, USA
Hettich centrifuge for falcons	Hettich, Tuttlingen, Germany
Beckman centrifuge Avanti J-20 I	Beckman, Brea, CA, USA
Tricarb 2900TR, luminescence Counter	Perkin-Elmer, Waltham, MA, USA
Topcount NXT	Perkin-Elmer, Waltham, MA, USA

Brandel Harvester 96	Brandel, Gaithersberg, MD, USA
Brandel Harvester 48	Brandel, Gaithersberg, MD, USA
UltraTurrax	IKA®-Werke GmbH & Co. KG, Staufen, Germany
Potter	Büchi, Flawil, Switzerland
Shaker Thermostat	Elmi, Riga, Latvia.
Vortexer	IKA®-Werke GmbH & Co. KG, Staufen, Germany
Accu-Jet® pipetting controller	Brand, Wertheim, Germany
Analytical balance 440-47N (max. 2000 g)	Kern & Sohn GmbH, Balingen-Frommern, Germany
Analytical balance CP225D	Sartorius, Göttingen, Germany
Axiovert 25 microscope	Carl Zeiss AG, Oberkochen, Germany
Neubauer Counting chamber 10 mm^2/ 0.0025 mm^2	Paul Marienfeld GmbH & Co. KG, Lauda Königshofen, Germany
Eppendorf Multipette® plus	Eppendorf AG, Hamburg, Germany
NUNC® BIOFLOW workbench	Nunc GmbH & Co. KG, Langenselbold, Germany
NUNC® Safe flow 1.2 workbench	Nunc GmbH & Co. KG, Langenselbold, Germany
Ultrasonic bath Bandelin Sonorex	Bandelin, Berlin, Germany
Systec 3850 ELV autoclave	Systec, Wettenberg, Germany
pH-Meter	Mettler-Toledo, Columbus, OH, USA
Rotofix 32 centrifuge	Hettich, Tuttlingen, Germany

Compounds were stored at 4° in 10 mM solution in DMSO. In exception, they were stored at -20° due to a lack of stability, or solutions were made in 1 mM due to a lack of solubility in DMSO. Compounds were diluted in DMSO. For cell assays, the last solution step was performed in the according assay buffer.

Table 50: Compounds

Compounds	
LPI	Sigma Aldrich Corp., St. Louis, MO, USA
Δ^9-THC (as Dronabinol)	Bionorica, Neumarkt in der Oberpflaz, Germany
Ro-20-1724	Sigma Aldrich Corp., St. Louis, MO, USA
Forskolin	Enzo Biochem Inc., Farmingsdale, NY, USA
CP55,940	Sigma Aldrich Corp., St. Louis, MO, USA
[^{3}H]CP55,940	ARC American radiolabeled chemicals. St. Louis, MO, USA
[^{3}H]cAMP	Perkin-Elemer, Waltham, MA, USA
[^{3}H]Diazepame	Perkin-Elemer, Waltham, MA, USA
CB-compounds	Synthesized by the group of Professor Katarzyna Kiec-Kononowicz
MZ and KD compounds	Synthesized by the group of Professor Katarzyna Kiec-Kononowicz
O-1918	Tocris Bioscience, Bristol, UK
abn-CBD	Tocris Bioscience, Bristol, UK
O-1602	Tocris Bioscience, Bristol, UK
Cannabidiol (CBD)	Tocris Bioscience, Bristol, UK
Xanthine sublibrary	PharmaZentrum Bonn, Prof. Christa E. Müller, Bonn, Germany
THV-compounds	Synthezised by The Hung Vu, lab of Prof. Christa E. Müller, Bonn, Germany
AF compounds	Synthezised by Alexander Fuchs, lab of Prof. Christa E. Müller, Bonn, Germany

Stemphol, epipyrone, 4-butyl-3,5-dihydroxy-benzoic acid, coriolide	Supplied by the group of Prof. Gabriele König, Bonn, Germany
RmF compounds	Supplied by Dr. Mahmoud Elsebai, Oulu, Finland
SZ compounds	Synthesized by the group of Prof. Stefan Bräse, Karlsruhe, Germany

8.6. Computational methods

Two main procedures were employed in this computational approach. With comparative modeling using the Rosetta protein design software suite, mainly its applications RosettaCM, homology models were built. In the second step small molecule docking was performed using RosettaLigand. The evaluation of all computational work was done by using the BioChemicalLibrary (BCL). Note that every command documented here was constructed for the environment it was used in and refers to the used data paths. In other systems with differently organized file paths the command has to be changed accordingly. Further, in the depicted options files some options have been commented out by a "#" - but as this options have been used in some other steps, they are also written down here.

8.6.1. Alignment

The alignment to suitable protein sequences was done based on the PDB search of BLAST from NCBI. Main criteria were sequence homology, e-value, resolution of crystal structures and conformation of the crystal structure. 20 structures were used as templates for the comparative modeling approach. A preliminary alignment was done with ClustalOmega, EMBL-EBI.[317; 318] The alignment was transferred to Excel, where it was manually adapted for each hybridization step and according to the sequence part that was build.

8.6.2. Threading

In this step, the aligned sequences wee used to give every amino acid the coordinates of the aligned template amino acid. To use the basic alignment for this procedure, it had to be transferred into a so-called grishin-alignment. An example can be found below:

```
## hGPR18 3VW7.pdb
#
scores from program: 0
0 -----------PDEYKIAALVFYSCIFIIGLFVNITALWVFSCTT---KKRTTVTIYMMNVALVDLIF-
IMTLPFRMFYYAK-D--EWPFGEYFCQILGALTVFYPSIALWLLAFISADRYMAIVQPKY---
AKELKNTCKAVLACVGVWIMTLTTTTPLLLLYK------------------------------
IYLKAVNVLNLTRLTFFFLIPLFIMIGCYLVIIHNLLHGR---
TSKLKPKVKEKSIRIIITLLVQVLVCFMPFHICFAFLML---GTGENS-----------
YNPWGAFTTFLMNLSTCLDVILYYIVSKQFQARVISVMLY----
0 -------------------------------------------------------------------
---------------------------------------------------------------------
---------------------------------------------------------------------
-----------------------------------------------PTNVLLIAHYS---FLSHTS------
TTEAAYFAYLLCV-CV------------------------------
```

All template pdb-files were downloaded from the RCSB PDB protein data bank (www.rcsb.org).[319] Further, the pdb-templates had to be transformed into so-called cleaned-up pdb-files by removing all unnecessary information, e.g. ligands, crystallization relicts in the structure, water etc. This can be accomplished by using the following command:

```
~/rosetta/rosetta_2015.12.57698/tools/protein_tools/scripts/clean_pdb.py
*.pdb
```

The grishin-alignments and the cleaned templates were transformed into threaded templates by the following command:

```
~/rosetta/rosetta_2015.12.57698/main/source/bin/partial_thread.default.linu
xgccrelease -in:file:fasta hGPR18_3.fasta -in:file:alignment
"$a"_L1.grishin -in:file:template_pdb "$a".pdb -database
~/rosetta/rosetta_2015.12.57698/main/database/
```

8.6.3. Fragment generation

For fragment insertion, 3mers and 9mers had to be created (these are fragments with 3 or 9 amino acids). For fragment generation the Rosetta fragmentpicker was used.[320] In an initial step of the fragmentpicker secondary-structure predictions were made, based on which the fragments were extracted from the RCSB PDB. For secondary structure prediction the fragmentpicker uses jufo_2 and psipred: The jufo_2 application as a built-in in rosetta and the BCL with a smooth prediction profile[217] and the open-source secondary structure prediction tool psipred distributed from University College London (UCL)[218].

The secondary structure predictions were created in the first step with the following command:

```
~/scripts/rosetta_tools/fragmentpicker_runss hGPR18.fasta
```

Fragments are further created with the command below:

```
~/rosetta/rosetta_2015.12.57698/main/source/bin/fragment_picker.linuxgccrel
ease –database ~/rosetta/rosetta_2015.12.57698/main/database
@fragment_picker_quota.options
```

For processing the request, the fragmentpicker further needs some information concerning scoring options, library paths, etc. They were written down in the fragment_picker_quota.options.

```
#input databases
-in:file:vall
~/rosetta/rosetta_2015.31.58019/tools/fragment_tools/vall.jul19.2011.gz

#query-related input files ##generated in the previous step
-in:file:checkpoint hGPR18_3.checkpoint
-in:file:fasta hGPR18_3.fasta
-frags:ss_pred hGPR18_3.psipred_ss2 psipred hGPR18_3.jufo9d_ss jufo

#the name root for the output fragment files
-out:file:frag_prefix hGPR18_frags

#show score components for each selected fragment
-frags:describe_fragments hGPR18_frags.fsc

#weights
-frags:scoring:config ./fragment_picker_quota.wghts

#we need 9-mers and 3-mers ##could be 5-mers or whatever you need
-frags:frag_sizes 9 5 3

#select 500 fragments from 2500 candidates. we need more candidates than
fragments to fill quota pools
-frags:n_candidates 2500
-frags:n_frags 500

#quota.def file defines the shares between different quota pools. the total
should be 1.0
-frags:picking:quota_config_file ./fragment_picker_quota.cfg
```

fragment_picker_quota.cfg:

```
#pool_id pool_namefraction
1 psipred 0.6
2 jufo 0.4
```

fragment_picker_quota.wghts:

```
#score name priority weight min_allowed extras
SecondarySimilarity 350 0.5 - psipred
SecondarySimilarity 250 0.5 - jufo
RamaScore 150 1.0 - psipred
RamaScore 150 1.0 - jufo
ProfileScoreL1 200 1.0 -
```

8.6.4. Creating models

In the so-called hybridize step, the models were built from sequence, fragment insertion and threaded templates. The required format of this application in Rosetta was a so-called .xml file, where rosetta task operations were defined. Further, the already created files are needed, and additionally,

a span file, that defines the transmembrane domains. These domains are predicted using the online

tool octopus (http://octopus.cbr.su.se).[213]

```
<dock_design>
    <TASKOPERATIONS>
    </TASKOPERATIONS>
    <SCOREFXNS>
        <stage1 weights="stage1_membrane.wts" symmetric=0>
            <Reweight scoretype=atom_pair_constraint weight=1/>
        </stage1>
        <stage2 weights="stage2_membrane.wts" symmetric=0>
            <Reweight scoretype=atom_pair_constraint weight=0.5/>
        </stage2>
        <fullatom weights="stage3_rlx_membrane.wts" symmetric=0>
            <Reweight scoretype=atom_pair_constraint weight=0.5/>
        </fullatom>
    </SCOREFXNS>
    <FILTERS>
    </FILTERS>
    <MOVERS>
        <Hybridize name=hybridize stage1_scorefxn=stage1
stage2_scorefxn=stage2 fa_scorefxn=fullatom batch=1
stage1_increase_cycles=1.0 stage2_increase_cycles=1.0
linmin_only=1 add_hetatm=0 disulf_file="hGPR18.disulfide" realign_domains=0>
            <Fragments 3mers="hGPR18_frags.500.3mers"
9mers="hGPR18_frags.500.9mers"/>
            Template pdb="3ODU_thread.pdb.pdb" cst_file="AUTO"
weight=   0.000 />
    <Template pdb="01_10_relax_16_ECL3_S_0028_0001_0018.pdb" cst_file="AUTO"
weight=   1.000 />
  </Hybridize>
    </MOVERS>
    <APPLY_TO_POSE>
    </APPLY_TO_POSE>
    <PROTOCOLS>
        <Add mover=hybridize/>
    </PROTOCOLS>
</dock_design>
```

Options-file:

```
# i/o
-in:file:fasta hGPR18_full.fasta
-in:file:psipred_ss2 hGPR18_full.psipred_ss2
-constraints:cst_fa_file angle.cst
#-constraints:cst_fa_weight 10
-in:file:extra_res_fa LG.params #Ligand file
-in:file:extra_res_cen LG.cen.params #Ligand centroid file
-score:extra_improper_file LG.tors #Ligand torsion angles file
-parser:protocol hybridize1.xml
#-nstruct 10 # for testruns
#-nstruct 2000 # for production run

# membrane options
-in:file:spanfile hGPR18.span
-membrane:no_interpolate_Mpair
-membrane:Menv_penalties
-rg_reweight .1

# relax options
-relax:minimize_bond_angles
```

```
-relax:minimize_bond_lengths
-relax:jump_move true
-default_max_cycles 200
-relax:min_type lbfgs_armijo_nonmonotone
-relax:jump_move true
-score:weights stage3_rlx.wts
-score:weights stage3_rlx_membrane.wts
-use_bicubic_interpolation
-hybridize:stage1_probability 1.0
-sog_upper_bound 15
-in:fix_disulf hGPR18.disulfide
# loop options

# reduce memory footprint
-chemical:exclude_patches LowerDNA  UpperDNA Cterm_amidation SpecialRotamer
VirtualBB ShoveBB VirtualDNAPhosphate VirtualNTerm CTermConnect sc_orbitals
pro_hydroxylated_case1 pro_hydroxylated_case2 ser_phosphorylated
thr_phosphorylated  tyr_phosphorylated tyr_sulfated lys_dimethylated
lys_monomethylated  lys_trimethylated lys_acetylated glu_carboxylated
cys_acetylated tyr_diiodinated N_acetylated C_methylamidated
MethylatedProteinCterm

# run multiple processors to produce output for one file
-multiple_processes_writing_to_one_directory
```

Further, Rosetta needs some options (called "weights"), due to the fact that the here performed modelling concerns a membrane embedded protein rather than a soluble protein.

stage1_membrane.wts:

```
# stage1 weights for hybridization: membrane score weights added
Menv 2.019
Mpair 1.0
Mcbeta 2.5
cenpack 1.0
hs_pair 1.0
ss_pair 1.0
rsigma  1.0
sheet   1.0
vdw     3.0
rg      .1
rama    0.15
linear_chainbreak    2.0
atom_pair_constraint 1.0
Menv_non_helix 2.019
Menv_termini 2.019
Menv_tm_proj 2.019
Mlipo 1.0
```

stage2_membrane.wts:

```
STRAND_STRAND_WEIGHTS 0 6
# stage2 weights for hybridization: membrane scoring weights added
hbond_sr_bb 1.17
hbond_lr_bb 1.17
rama        0.15
omega       0.2
rg          0.1
vdw         3.0
Menv 2.019
```

```
Mpair 1.0
Mcbeta 2.5
cenpack_smooth  1.0
cart_bonded     0.05
atom_pair_constraint 0.5
Mlipo 1.0
rsigma 1.0
sheet 1.0
ss_pair 1.0
hs_pair 1.0
Menv_non_helix 2.019
Menv_termini 2.019
Menv_tm_proj 2.019
```

stage3_rlx_membrane.wts:

```
# stage3 fullatom weights for hybridization: adopted with membrane scores.
METHOD_WEIGHTS ref  0.16 1.7 -0.67 -0.81 0.63 -0.17 0.56 0.24 -0.65 -0.1 -
0.34 -0.89 0.02 -0.97 -0.98 -0.37 -0.27 0.29 0.91 0.51
fa_atr  0.8
fa_rep  0.44
fa_sol  0.00
fa_intra_rep 0.004
fa_pair 0.49
fa_plane 0
fa_dun  0.56
ref     1
hbond_lr_bb 1.17
hbond_sr_bb 1.17
hbond_bb_sc 2.34
hbond_sc 2.2
p_aa_pp     0.32
dslf_ss_dst 0.5
dslf_cs_ang 2
dslf_ss_dih 5
dslf_ca_dih 5
pro_close   1.0
rama    0.2
omega   0.5
atom_pair_constraint    0.5
coordinate_constraint   0.0
cart_bonded     0.5
fa_mbenv 0.3
fa_mbsolv 0.35
Menv_smooth 0.5
```

The command to run hybridize is the following:

```
~/rosetta/rosetta_2015.12.57698/main/source/bin/rosetta_scripts.default.lin
uxgccrelease @hybridize.options -out:prefix loop_01_ -out:file:scorefile
cmloops_1_3.sc -nstruct 1 -database
~/rosetta/rosetta_2015.12.57698/main/database/
```

In total between 4000 and 8800 models were created in each hybridize step.

Another option can be introduced, when a restraint in the model was known before. This was called constrain in Rosetta. An example, where this option was taken, was the loop modeling in chapter 3.5.4.2. There, the orientation of a certain amino acid side chain was defined by angles and ranges in the following way:

```
### trp-proline orientation
#
Dihedral CG 70 CB 70 CA 70 O 70 SCALARWEIGHTEDFUNC 10 CIRCULARHARMONIC 1.13 0.35
Dihedral NE1 70 CD1 70 CG 70 CB 70 SCALARWEIGHTEDFUNC 10 CIRCULARHARMONIC 3.14 0.35
Dihedral O 70 C 70 N 71 CD 71 SCALARWEIGHTEDFUNC 10 CIRCULARHARMONIC 3.14 0.35
AtomPair NE1 70 O 73 SCALARWEIGHTEDFUNC 10 BOUNDED 2.5 4.0 0.5 NOE
AtomPair O 70 N 73 SCALARWEIGHTEDFUNC 10 BOUNDED 2.5 4.0 0.5 NOE
AtomPair CH2 70 CD2 72 SCALARWEIGHTEDFUNC 10 FLAT_HARMONIC 8 2 4
AtomPair CZ2 70 CD2 80 SCALARWEIGHTEDFUNC 10 FLAT_HARMONIC 8 2 4
```

This constraint was also used in relax, which still defines the noted orientation.

8.6.5. Energy optimization

The primarily built structures were further optimized in their overall conformational structure by running through a so-called relax, a refinement of the full-atom model. This was achieved by the relax application, which runs with the command:

```
~/rosetta/rosetta_2015.31.58019/main/source/bin/relax.default.linuxgccrelea
se  @relax.options  -l  $PDB  -nstruct  1  -out:prefix  relax_  -database
~/rosetta/rosetta_2015.31.58019/main/database/
```

In the options for the relax protocol, the extent to which side chains and backbone are moved can be defined – and have to be defined - according to the problem to solve. For example, different options were needed, when a small molecule was present in the models.

```
#-in:fix_disulf hGPR18.disulfide #read disulfide connectivity information
-in:file:spanfile hGPR18.span #read predicted transmembrane regions
-in:file:extra_res_fa LG.params
-in:file:extra_res_cen LG.cen.params
-score:extra_improper_file LG.tors

-membrane:no_interpolate_Mpair # membrane scoring specification
-membrane:Menv_penalties # turn on membrane penalty scores

-score:weights membrane_highres_Menv_smooth.wts

-relax:dualspace #use dualspace relax protocol
-relax:minimize_bond_angles #dualspace relax protocol setting
-set_weights cart_bonded .5 pro_close 0 #score proline ring closure using
energy term for all bond lengths (pro_close uses virtual atom NV for
proline ring scores)
-default_max_cycles 200
#-flip_HNQ
#-no_optH false
#-relax:constrain_relax_to_start_coords
#relax:coord_constrain_sidechains
#-relax:ramp_constraints false
-constraints:cst_fa_file angle.cst
-constraints:cst_fa_weight 10


 -out:file:fullatom
-out:pdb
```

8.6.6. Model selection I - Scoring and Clustering

To evaluate the models and select models that were suitable to be further processed two procedures were chosen: scoring by the energy scores rosetta creates with every model, and clustering, which means to sample those models that resemble the biggest groups that were created. The visualization of this similarity was achieved by comparing the models by their RMSD (root mean square deviation of the alpha carbon atom). The BCL was used to generate the necessary calculations.

By the following command RMSD calculations against the best scoring model were done:

```
bcl.exe  protein:Compare  -quality  RMSD  -specify_residues  residues.ls  -
reference_pdb relax_80_ECL3_S_0021_0001.pdb -pdb_list ../evaluate_models.txt
-prefix ECL1_RMSD_ -atoms All -aaclass AAComplete -convert_to_natural_aa_type
-scheduler PThread 12
```

A plot of the RMSD versus the score was done with Gnuplot, 5.0.

For the Clustering, one model was compared to each other model based on their RMSD. A linker defined groups of models that were more similar to another. Results can afterwards be processed so that all best scoring models of the biggest clusters can be collected.

```
bcl.exe PDBCompare -quality RMSD -atoms CA -specify_residues residues.ls -
pdb_list models.pdb.ls -prefix ECL2_cluster_ -aaclass AACaCb -
convert_to_natural_aa_type -scheduler PThread 12
bcl.exe Cluster -distance_input_file "ECL2_cluster_RMSD.txt" -input_format
TableLowerTriangle -output_format Rows Centers -output_file cluster_ECL2_ -
linkage Average -remove_internally_similar_nodes 0.05 -scheduler PThread 12
grep "Leaf : 1 : " *.Centers. | sort -nk10 | tail
```

8.6.7. Docking of small molecules

The first step of ligand docking is to create an ensemble of possible rotamers of the small molecule of interest. This was achived by using the bcl application bcl::conf – the ConformerGenerator.[219] Therefore, the ligand had to be processed to a sdf file and the following command was executed:

```
bcl.exe  molecule:ConformerGenerator  -ensemble_filenames  THC.sdf  -add_h  -
sample_all_rotamers -generate_3D -conformers_single_file Conformer.sdf
```

The ligand has to be positioned in the receptor models of the chosen models for the docking step. In PyMOL the receptor model was loaded, the ligand positioned and everything was saved together as pdb file. Rosetta itself cannot deal with typical small molecule information files as "sdf" because it is only comparable to pdb file format. Therefore, a so-called params file had to be made, that gives Rosetta coordinates and ligand information in a pdb file friendly format.

```
~/rosetta/mini/mini_trunk/src/python/apps/public/molfile_to_params.py
conformers0.sdf
```

The docking protocol needs an options file that defined some basic parameters:

```
-database ~/rosetta/rosetta_2015.31.58019/main/database/
-in
  -file
      -extra_res_fa MZ1415.params
-packing
 -ex1
 -ex1aro
 -ex2
-parser
 -protocol dock_MZ1415.xml

-out
 -file
  -fullatom
 -pdb

-score
```

All other information for the program were again defined in an xml file:

```
<ROSETTASCRIPTS>
    <SCOREFXNS>
        <ligand_soft_rep weights=ligand_soft_rep>
            <Reweight scoretype=fa_elec weight=0.42/>
            <Reweight scoretype=hbond_bb_sc weight=1.3/>
            <Reweight scoretype=hbond_sc weight=1.3/>
            <Reweight scoretype=rama weight=0.2/>
        </ligand_soft_rep>
        <hard_rep weights=ligand>
            <Reweight scoretype=fa_intra_rep weight=0.004/>
            <Reweight scoretype=fa_elec weight=0.42/>
            <Reweight scoretype=hbond_bb_sc weight=1.3/>
            <Reweight scoretype=hbond_sc weight=1.3/>
            <Reweight scoretype=rama weight=0.2/>
        </hard_rep>
    </SCOREFXNS>
    <LIGAND_AREAS>
            <docking_sidechain_X chain=X cutoff=6.0 add_nbr_radius=true
all_atom_mode=true minimize_ligand=10/>
                <final_sidechain_X chain=X cutoff=6.0 add_nbr_radius=true
all_atom_mode=true/>
                 <final_backbone_X chain=X cutoff=7.0 add_nbr_radius=false
all_atom_mode=true Calpha_restraints=0.3/>
    </LIGAND_AREAS>

    <INTERFACE_BUILDERS>
        <side_chain_for_docking ligand_areas=docking_sidechain_X/>
        <side_chain_for_final ligand_areas=final_sidechain_X/>
        <backbone ligand_areas=final_backbone_X extension_window=3/>
    </INTERFACE_BUILDERS>
    <MOVEMAP_BUILDERS>
        <docking sc_interface=side_chain_for_docking minimize_water=true/>
        <final sc_interface=side_chain_for_final bb_interface=backbone
minimize_water=true/>
    </MOVEMAP_BUILDERS>
    <MOVERS>
        StartFrom name=start_from_X chain=X >
            Coordinates x=-38.5825 y=69.8486 z=39.1026/>
        /StartFrom>
```

```
            <CompoundTranslate name=compound_translate randomize_order=false
allow_overlap=false>
                <Translate chain=X distribution=uniform angstroms=4.0 cycles=50/>
            </CompoundTranslate>
            <Rotate name=rotate_X chain=X distribution=uniform degrees=360
cycles=500/>
            <SlideTogether name=slide_together chains=X/>
            <HighResDocker name=high_res_docker cycles=6 repack_every_Nth=3
scorefxn=ligand_soft_rep movemap_builder=docking/>
            <FinalMinimizer name=final scorefxn=hard_rep movemap_builder=final/>
            <InterfaceScoreCalculator name=add_scores chains=X
scorefxn=hard_rep/>
            <ParsedProtocol name=low_res_dock>
                Add mover_name=start_from_X/>
                <Add mover_name=compound_translate/>
                <Add mover_name=rotate_X/>
                <Add mover_name=slide_together/>
            </ParsedProtocol>
            <ParsedProtocol name=high_res_dock>
                <Add mover_name=high_res_docker/>
                <Add mover_name=final/>
            </ParsedProtocol>
        </MOVERS>
        <PROTOCOLS>
            <Add mover_name=low_res_dock/>
            <Add mover_name=high_res_dock/>
            <Add mover_name=add_scores/>
        </PROTOCOLS>
</ROSETTASCRIPTS>
```

Usually, up to 10.000 models were constructed. Everything can be executed by typing the following command (example):

```
~/rosetta/rosetta_2015.31.58019/main/source/bin/rosetta_scripts.default.lin
uxgccrelease @dock_Mz1415_in_hGPR18.options -out:prefix test_02_ -nstruct 3
-database ~/rosetta/rosetta_2015.31.58019/main/database/ -s
templates/10_ECL2_1_S_0005_0001.pdb
```

8.6.8. Model selection II – scoring and clustering

The docking results had to be evaluated and suitable results had to be taken forward. The suitability of the models was judged based on their scoring (in this case either ddg or interface_energy can be taken as parameters). These parameters describe the energy that was gained by binding the ligand in the corresponding way, so lower, negative values were better than higher values. To compare this energy term, normally depicted in RosettaEnergyUnits (REU), all models had to be aligned and the position of the ligand in comparison had to be determined.

The alignment of all models was done with the program ProFit (Martin, A.C.R. and Porter, C.T., http://www.bioinf.org.uk/software/profit/), which uses the McLachlan algorithm (McLachlan, 1982)[321] as depited below, whereby all aligned structures were written down in `align.script`.

```
profit -h -f align.script
```

Further, the position of the ligand had to be described. This was achieved by calculating the ligand-RMSD. Therefore, the ligand had to be separated out of the models, and all had to be compared to one ligand position. This was accomplished by the BCL with the following command (example):

```
bcl.exe molecule:Compare all_ligand.sdf model.pdb_ligand.sdf -method
RealSpaceRMSD -output ligand_reference_rmsd
```

Again, the ligand position was also clustered to know which positions had been proposed more often than others and how they look like. Therefore, the ligand_RMSD had to be calculated with respect to each other model. An example command can be found below:

```
bcl.exe molecule:Compare cluster_ligands.sdf -method RealSpaceRMSD -output
ligand_rmsd -bcl_table_format
bcl.exe Cluster -distance_input_file ECL1_ligand_rmsd -input_format
TableLowerTriangle -output_format Rows Centers -output_file Cluster_ECL1 -
linkage Average -remove_internally_similar_nodes 4
grep "Leaf : 1 : " *.Centers. | sort -nk10 | tail
```

Out of 10000 models between 100 and 500 models were collected to further be processed in another round of docking. For each following round of docking, the dimension of the ligand movement was narrowed down in the xml protocol by adapting the torsion angle and the rotation of the ligand in the enzyme pocket. After each docking round, the models were processed as described above, sorted and chosen for further docking rounds. When the interface_score cannot be further decreased, the docking cannot improve further. Out of the last round of focused docking a final selection of models had to be chosen by scoring and clustering.

8.6.9. Amino acid interaction

As a last step of the docking procedure, crucial amino acid interactions had to be determined to predict possible mutagenesis candidates. An application of rosetta that is called energy-breakdown was used for this purpose. It calculates which residue participates in the allover Rosetta energy score with which impact on the atom level. An example command is depicted below:

```
~/rosetta/rosetta_2016.08.58479/main/source/bin/residue_energy_breakdown.de
fault.linuxgccrelease -in:file:s model.pdb -in:file:extra_res_fa
MZ1415.params -database ~/rosetta/rosetta_2016.08.58479/main/database/
```

Out of the resulting table, only the interactions with the ligand were extracted and transferred to Excel, where they were calculated in percentages and for up to ten bestscoring models out of one cluster. This was done for every cluster of interest.

8.6.10. Visualization tools

Models (as pdb format text-files) and chemical structures (sdf) were visualized in PyMol (The PyMOL Molecular Graphics System, Version 1.8 Schrödinger, LLC) or with the UCSF Chimera package. Chimera was developed by the Resource for Biocomputing, Visualization, and Informatics at the University of California, San Francisco (supported by NIGMS P41-GM103311).[322]

8.7. *In-silico* prediction of drug properties

Properties of compounds were predicted with the program Stardrop 5.5 (Optibrium) using the ADME QSAR (Quantitative Structure-Activity Relationship) tool predicting the Lipinski rule of five, oral CNS scoring profile and intravenous CNS scoring profile with standard conditions.

9. LIST OF ABBREVIATIONS

2-AG	2-arachidonoylglycerol
2-AG-PI	2-arachidonoylphoyphatidylinositol
5-HT	5-Hydroxy-tryptamine, serotonine
AA-5-HT	Arachidonoylserotonine
Abn-CBD	abnormal cannabidiol
AEA	anandamide, arachidonoylethanolamine
BCL	BioChemical Library
BSA	bovine serum albumin
cAMP	cyclic adenosine monophosphate
CASP	Critical Assessment of Techniques for Protein Structure Prediction
CBD	cannabidiol
CB receptor	cannabinoid receptor
CHO cells	chinease hamster ovary cells
CNS	central nervous system
Compd.	compound
CTX	cholera toxin
CysLT1 receptor	cysteinyl leukotriene receptor
DAG	diacylglycerol
DAGL	diacylglycerol lipase
DMEM	Dulbecco's Modified Eagle's Medium
DMSO	dimethylsulfoxide
EC_{50}	halfmaximal activatory concentration
ECL	extracellular loop
EDTA	ethylenediaminetetraacetic acid
ELISA	enzyme linked immunosorbent assay
ENT	equilibrative nucleoside transporter
EMCDDA	European Monitoring Centre for Drugs and Drug Addiction
ERK	extracellular singal-regulated kinase
ESI	electronspray ionization
FAAH	fatty acid amide hydrolase
FCS	fetal calf serum

FRET	Förster-resonance energy transfer
GABA	γ-aminobutyric acid
GlYT1 receptor	glycine transporter 1
GlYT2a receptor	glycine transporter 2a
GPCR	G protein-coupled receptor
GDP	guanosine diphosphate
GIRK	G protein-coupled inwardly-rectifying potassium channels
GRK	G protein-coupled receptor kinase
GSK	GlaxoSmithKline
GTP	guanosine triphosphate
GTPγS	guanosine 5'-*O*-[γ-thio]triphosphate
HBSS	Hank's Balanced Salt Solution
HEK293	human embryonic kidney cell line
HEPES	(4-(2-Hydroxyethyl)-1-piperazineethanesulfonic acid
HPLC	high performance liquid chromatography
HUVEC	human umbilical vein endothelial cells
IC_{50}	half-maximal inhibitory concentration
ICL	intracellular loop
IP_3	inositoltriphosphate
IUPHAR	International Union of Basic and Clinical Pharmacology
LB medium	Lysogeny broth medium
LogP	partition coefficient
LPI	lysophosphatidylinositol
LPS	lipopolysaccharide
MAGL	monoacylglycerol lipase
MAPkinase	mitogen activated protein kinase
NAGly	*N*-arachidonoylglycine
NAPE	*N*-acyl phosphatidylethanolamine
NAPE-PDL	*N*-acyl phosphatidylethanolamine-specific phospholipase D
NCBI	National Center for Biotechnology Information
NFAT	nuclear factor of activated T-cells
NFκB	nuclear factor kappa-light-chain-enhancer of activated B-cells
NIH	National Insitute of Health

NMDA-receptor	*N*-methyl-D-aspartate receptor, a glutamate receptor
NMR	nuclear magnetic resonance spectroscopy
NOS	nitric oxide synthase
PAR1	protease-activated receptor 1
PCR	polymerase chain reaction
PDB	protein data bank
PPARγ receptor	peroxisome proliferator-activated receptor gamma
PTX	pertussis toxin
PZB	Pharma-Zentrum Bonn
QSAR	Quantitative structure-activity relationships
REU	Rosetta Energy Units
RLU	relative luminescence units
RMSD	root mean square deviation
SAR	structure-activity relationships
SRE	serum response element
TAE buffer	Tris-acetate-EDTA buffer
Δ^9-THC	Δ^9-tetrahydrocannabinol
TM	transmembrane
tPSA	total polar surface area
Tris	tris(hydroxymethyl)-aminomethan
TRPA	transient receptor potential cation channels
TRPV	transient receptor potential cation channels subfamily V ("Vanilloid")

NMDA-receptor   *N*-methyl-D-aspartate receptor, a glutamate receptor

10. REFERENCES

(1) Fredriksson, R.; Lagerstrom, M. C.; Lundin, L.-G.; Schioth, H. B. The G-protein-coupled receptors in the human genome form five main families. Phylogenetic analysis, paralogon groups, and fingerprints. *Mol. Pharmacol.* **2003**, *63*, 1256–1272.

(2) Rasmussen, Soren G F; Choi, H.-J.; Rosenbaum, D. M.; Kobilka, T. S.; Thian, F. S.; Edwards, P. C.; Burghammer, M.; Ratnala, Venkata R P; Sanishvili, R.; Fischetti, R. F.; Schertler, Gebhard F X; Weis, W. I.; Kobilka, B. K. Crystal structure of the human β_2 adrenergic G-protein-coupled receptor. *Nature* **2007**, *450*, 383–387.

(3) Santos, R.; Ursu, O.; Gaulton, A.; Bento, A. P.; Donadi, R. S.; Bologa, C. G.; Karlsson, A.; Al-Lazikani, B.; Hersey, A.; Oprea, T. I.; Overington, J. P. A comprehensive map of molecular drug targets. *Nat. Rev. Drug Discov.* **2017**, *16*, 19–34.

(4) Williams, C. cAMP detection methods in HTS: selecting the best from the rest. *Nat. Rev. Drug Discov.* **2004**, *3*, 125–135.

(5) Rajagopal, S.; Rajagopal, K.; Lefkowitz, R. J. Teaching old receptors new tricks: biasing seven-transmembrane receptors. *Nat. Rev. Drug Discov.* **2010**, *9*, 373–386.

(6) Bylund, D. B.; Toews, M. L. Radioligand binding methods: practical guide and tips. *Am. J. Physiol.* **1993**, *265*, L421-9.

(7) Rankovic, Z.; Brust, T. F.; Bohn, L. M. Biased agonism: An emerging paradigm in GPCR drug discovery. *Bioorg. Med. Chem. Lett.* **2016**, *26*, 241–250.

(8) Zhang, J.; Feng, H.; Xu, S.; Feng, P. Hijacking GPCRs by viral pathogens and tumor. *Biochem. Pharmacol.* **2016**, *114*, 69–81.

(9) Jacobson, K. A. New paradigms in GPCR drug discovery. *Biochem. Pharmacol.* **2015**, *98*, 541–555.

(10) Devane, W. A.; Dysarz, F A 3rd; Johnson, M. R.; Melvin, L. S.; Howlett, A. C. Determination and characterization of a cannabinoid receptor in rat brain. *Mol Pharmacol* **1988**, *34*, 605–613.

(11) Matsuda, L. A.; Lolait, S. J.; Brownstein, M. J.; Young, A. C.; Bonner, T. I. Structure of a cannabinoid receptor and functional expression of the cloned cDNA. *Nature* **1990**, *346*, 561–564.

(12) Devane, W. A.; Hanus, L.; Breuer, A.; Pertwee, R. G.; Stevenson, L. A.; Griffin, G.; Gibson, D.; Mandelbaum, A.; Etinger, A.; Mechoulam, R. Isolation and structure of a brain constituent that binds to the cannabinoid receptor. *Science* **1992**, *258*, 1946–1949.

(13) Vogel, Z.; Barg, J.; Levy, R.; Saya, D.; Heldman, E.; Mechoulam, R. Anandamide, a brain endogenous compound, interacts specifically with cannabinoid receptors and inhibits adenylate cyclase. *J Neurochem.* **1993**, *61*, 352–355.

(14) Felder, C. C.; Briley, E. M.; Axelrod, J.; Simpson, J. T.; Mackie, K.; Devane, W. A. Anandamide, an endogenous cannabimimetic eicosanoid, binds to the cloned human cannabinoid receptor and stimulates receptor-mediated signal transduction. *PNAS* **1993**, *90*, 7656–7660.

(15) Munro, S.; Thomas, K. L.; Abu-Shaar, M. Molecular characterization of a peripheral receptor for cannabinoids. *Nature* **1993**, *365*, 61–65.

(16) Mechoulam, R.; Ben-Shabat, S.; Hanus, L.; Ligumsky, M.; Kaminski, N. E.; Schatz, A. R.; Gopher, A.; Almog, S.; Martin, B. R.; Compton, D. R. Identification of an endogenous 2-monoglyceride, present in canine gut, that binds to cannabinoid receptors. *Biochem. Pharmacol.* **1995**, *50*, 83–90.

(17) Shao, Z.; Yin, J.; Chapman, K.; Grzemska, M.; Clark, L.; Wang, J.; Rosenbaum, D. M. High-resolution crystal structure of the human CB_1 cannabinoid receptor. *Nature* **2016**,

(18) Hua, T.; Vemuri, K.; Pu, M.; Qu, L.; Han, G. W.; Wu, Y.; Zhao, S.; Shui, W.; Li, S.; Korde, A.; Laprairie, R. B.; Stahl, E. L.; Ho, J.-H.; Zvonok, N.; Zhou, H.; Kufareva, I.; Wu, B.; Zhao, Q.; Hanson, M. A.; Bohn, L. M.; Makriyannis, A.; Stevens, R. C.; Liu, Z.-J. Crystal Structure of the Human Cannabinoid Receptor CB_1. *Cell* **2016**, *167*, 750-762.

(19) Mackie, K. Distribution of cannabinoid receptors in the central and peripheral nervous system. *Handb. Exp. Pharmacol.* **2005**, 299–325.

(20) Ohno-Shosaku, T.; Tsubokawa, H.; Mizushima, I.; Yoneda, N.; Zimmer, A.; Kano, M. Presynaptic cannabinoid sensitivity is a major determinant of depolarization-induced retrograde suppression at hippocampal synapses. *J. Neurosci.* **2002**, *22*, 3864–3872.

(21) Kreitzer, A. C.; Regehr, W. G. Retrograde inhibition of presynaptic calcium influx by endogenous cannabinoids at excitatory synapses onto Purkinje cells. *Neuron* **2001**, *29*, 717–727.

(22) Wilson, R. I.; Nicoll, R. A. Endogenous cannabinoids mediate retrograde signalling at hippocampal synapses. *Nature* **2001**, *410*, 588–592.

(23) Silvestri, C.; Di Marzo, V. The endocannabinoid system in energy homeostasis and the etiopathology of metabolic disorders. *Cell Metab.* **2013**, *17*, 475–490.

(24) Heinemann, J. C.; Duerr, G. D.; Keppel, K.; Breitbach, M.; Fleischmann, B. K.; Zimmer, A.; Wehner, S.; Welz, A.; Dewald, O. CB2 receptor-mediated effects of pro-inflammatory macrophages influence survival of cardiomyocytes. *Life Sci.* **2015**, *138*, 18–28.

(25) Montecucco, F.; Di Marzo, V. At the heart of the matter: the endocannabinoid system in cardiovascular function and dysfunction. *Trends Pharmacol. Sci.* **2012**, *33*, 331–340.

(26) Basu, S.; Dittel, B. N. Unraveling the complexities of cannabinoid receptor 2 (CB_2) immune regulation in health and disease. *Immunol. Res.* **2011**, *51*, 26–38.

(27) Rieder, S. A.; Chauhan, A.; Singh, U.; Nagarkatti, M.; Nagarkatti, P. Cannabinoid-induced apoptosis in immune cells as a pathway to immunosuppression. *Immunobiology* **2010**, *215*, 598–605.

(28) Ofek, O.; Karsak, M.; Leclerc, N.; Fogel, M.; Frenkel, B.; Wright, K.; Tam, J.; Attar-Namdar, M.; Kram, V.; Shohami, E.; Mechoulam, R.; Zimmer, A.; Bab, I. Peripheral cannabinoid receptor, CB2, regulates bone mass. *PNAS* **2006**, *103*, 696–701.

(29) Pertwee, R. G. Targeting the endocannabinoid system with cannabinoid receptor agonists: pharmacological strategies and therapeutic possibilities. *Philos. Trans. Soc. Lond. Biol. Sci.* **2012**, *367*, 3353–3363.

(30) Pertwee, R. G.; Howlett, A. C.; Abood, M. E.; Alexander, S P H; Di Marzo, V.; Elphick, M. R.; Greasley, P. J.; Hansen, H. S.; Kunos, G.; Mackie, K.; Mechoulam, R.; Ross, R. A. International Union of Basic and Clinical Pharmacology. LXXIX. Cannabinoid receptors and their ligands: beyond CB_1 and CB_2. *Pharmacol. Rev.* **2010**, *62*, 588–631.

(31) Lakhan, S. E.; Rowland, M. Whole plant cannabis extracts in the treatment of spasticity in multiple sclerosis: a systematic review. *BMC Neurology* **2009**, *9*, 59.

(32) Russo, M.; Naro, A.; Leo, A.; Sessa, E.; D'Aleo, G.; Bramanti, P.; Calabro, R. S. Evaluating Sativex® in neuropathic pain management: A clinical and neurophysiological assessment in multiple sclerosis. *Pain Med.* **2016**, *17*, 1145–1154.

(33) Ward, A.; Holmes, B. Nabilone. A preliminary review of its pharmacological properties and therapeutic use. *Drugs* **1985**, *30*, 127–144.

(34) Fowler, C. J. The Potential of inhibitors of indocannabinoid metabolism for drug development: A critical review. *Handb. Exp. Pharmacol.* **2015**, *231*, 95–128.

(35) Mallet, C.; Dubray, C.; Duale, C. FAAH inhibitors in the limelight, but regrettably. *Int. J. Clin. Pharmacol. Ther.* **2016**, *54*, 498–501.

(36) O'Keefe, L.; Simcocks, A. C.; Hryciw, D. H.; Mathai, M. L.; McAinch, A. J. The cannabinoid receptor 1 and its role in influencing peripheral metabolism. *Diabetes Obes. Metab.* **2014**, *16*, 294–304.

(37) Curioni, C.; Andre, C. Rimonabant for overweight or obesity. *Cochrane Database Syst. Rev.* **2006**, CD006162.

(38) Chorvat, R. J. Peripherally restricted CB1 receptor blockers. *Bioorg. Med. Chem. Lett.* **2013**, *23*, 4751–4760.

(39) Racz, I.; Nadal, X.; Alferink, J.; Banos, J. E.; Rehnelt, J.; Martin, M.; Pintado, B.; Gutierrez-Adan, A.; Sanguino, E.; Manzanares, J.; Zimmer, A.; Maldonado, R. Crucial role of CB2 cannabinoid receptor in the regulation of central immune responses during neuropathic pain. *J. Neurosci.* **2008**, *28*, 12125–12135.

(40) Di Marzo, V.; Stella, N.; Zimmer, A. Endocannabinoid signalling and the deteriorating brain. *Nat. Rev. Neurosci.* **2015**, *16*, 30–42.

(41) Ashton, J. C.; Glass, M. The cannabinoid CB2 receptor as a target for inflammation-dependent neurodegeneration. *Curr. Neuropharmacol.* **2007**, *5*, 73–80.

(42) Navarro, G.; Morales, P.; Rodriguez-Cueto, C.; Fernandez-Ruiz, J.; Jagerovic, N.; Franco, R. Targeting cannabinoid CB2 receptors in the central nervous system. Medicinal chemistry approaches with focus on neurodegenerative disorders. *Front. Neurosci.* **2016**, *10*, 406.

(43) Ferreira, S. G.; Lomaglio, T.; Avelino, A.; Cruz, F.; Oliveira, C. R.; Cunha, R. A.; Kofalvi, A. *N*-acyldopamines control striatal input terminals via novel ligand-gated cation channels. *Neuropharmacol.* **2009**, *56*, 676–683.

(44) Bradshaw, H. B.; Raboune, S.; Hollis, J. L. Opportunistic activation of TRP receptors by endogenous lipids: exploiting lipidomics to understand TRP receptor cellular communication. *Life Sci.* **2013**, *92*, 404–409.

(45) Lake, K. D.; Compton, D. R.; Varga, K.; Martin, B. R.; Kunos, G. Cannabinoid-induced hypotension and bradycardia in rats mediated by CB1-like cannabinoid receptors. *J. Pharmacol. Exp. Ther.* **1997**, *281*, 1030–1037.

(46) Jarai, Z.; Wagner, J. A.; Varga, K.; Lake, K. D.; Compton, D. R.; Martin, B. R.; Zimmer, A. M.; Bonner, T. I.; Buckley, N. E.; Mezey, E.; Razdan, R. K.; Zimmer, A.; Kunos, G. Cannabinoid-induced mesenteric vasodilation through an endothelial site distinct from CB1 or CB2 receptors. *PNAS* **1999**, *96*, 14136–14141.

(47) Offertaler, L.; Mo, F.-M.; Batkai, S.; Liu, J.; Begg, M.; Razdan, R. K.; Martin, B. R.; Bukoski, R. D.; Kunos, G. Selective ligands and cellular effectors of a G protein-coupled endothelial cannabinoid receptor. *Mol. Pharmacol.* **2003**, *63*, 699–705.

(48) Vassilatis, D. K.; Hohmann, J. G.; Zeng, H.; Li, F.; Ranchalis, J. E.; Mortrud, M. T.; Brown, A.; Rodriguez, S. S.; Weller, J. R.; Wright, A. C.; Bergmann, J. E.; Gaitanaris, G. A. The G protein-coupled receptor repertoires of human and mouse. *PNAS* **2003**, *100*, 4903–4908.

(49) Civelli, O.; Reinscheid, R. K.; Zhang, Y.; Wang, Z.; Fredriksson, R.; Schiöth, H. B. G protein-coupled receptor deorphanizations. *Annu. Rev. Pharmacol. Toxicol.* **2013**, *53*, 127–146.

(50) Chung, S.; Funakoshi, T.; Civelli, O. Orphan GPCR research. *Br. J. Pharmacol.* **2008**, *153 Suppl 1*, S339-46.

(51) Gantz, I.; Muraoka, A.; Yang, Y. K.; Samuelson, L. C.; Zimmerman, E. M.; Cook, H.; Yamada, T. Cloning and chromosomal localization of a gene (GPR18) encoding a novel seven transmembrane receptor highly expressed in spleen and testis. *Genomics* **1997**, *42*, 462–466.

(52) Kitamura, H.; Makide, K.; Shuto, A.; Ikubo, M.; Inoue, A.; Suzuki, K.; Sato, Y.; Nakamura, S.; Otani, Y.; Ohwada, T.; Aoki, J. GPR34 is a receptor for lysophosphatidylserine with a fatty acid at the sn-2 position. *J. Biochem.* **2012**, *151*, 511–518.

(53) Hannedouche, S.; Zhang, J.; Yi, T.; Shen, W.; Nguyen, D.; Pereira, J. P.; Guerini, D.; Baumgarten, B. U.; Roggo, S.; Wen, B.; Knochenmuss, R.; Noel, S.; Gessier, F.; Kelly, L. M.; Vanek, M.; Laurent, S.; Preuss, I.; Miault, C.; Christen, I.; Karuna, R.; Li, W.; Koo, D.-I.; Suply, T.; Schmedt, C.; Peters, E. C.; Falchetto, R.; Katopodis, A.; Spanka, C.; Roy, M.-O.; Detheux, M.; Chen, Y. A.; Schultz, P. G.; Cho, C. Y.; Seuwen, K.; Cyster, J. G.; Sailer, A. W. Oxysterols direct immune cell migration via EBI2. *Nature* **2011**, *475*, 524–527.

(54) Dereeper, A.; Audic, S.; Claverie, J.-M.; Blanc, G. BLAST-EXPLORER helps you building datasets for phylogenetic analysis. *BMC Evol. Biol*. **2010**, *10*, 8.

(55) Dereeper, A.; Guignon, V.; Blanc, G.; Audic, S.; Buffet, S.; Chevenet, F.; Dufayard, J.-F.; Guindon, S.; Lefort, V.; Lescot, M.; Claverie, J.-M.; Gascuel, O. Phylogeny.fr: robust phylogenetic analysis for the non-specialist. *Nucleic Acids Res.* **2008**, *36*, W465-9.

(56) Edgar, R. C. MUSCLE: multiple sequence alignment with high accuracy and high throughput. *Nucleic Acids Res.* **2004**, *32*, 1792–1797.

(57) Guindon, S.; Gascuel, O. A simple, fast, and accurate algorithm to estimate large phylogenies by maximum likelihood. *Syst. Biol.* **2003**, *52*, 696–704.

(58) Wilhelmsen, K.; Khakpour, S.; Tran, A.; Sheehan, K.; Schumacher, M.; Xu, F.; Hellman, J. The endocannabinoid/endovanilloid *N*-arachidonoyl dopamine (NADA) and synthetic cannabinoid WIN55,212-2 abate the inflammatory activation of human endothelial cells. *J. Biol. Chem.* **2014**, *289*, 13079–13100.

(59) Hasko, J.; Fazakas, C.; Molnar, J.; Nyul-Toth, A.; Herman, H.; Hermenean, A.; Wilhelm, I.; Persidsky, Y.; Krizbai, I. A. CB2 receptor activation inhibits melanoma cell transmigration through the blood-brain barrier. *Int. J. Mol. Sci.* **2014**, *15*, 8063–8074.

(60) Kohno, M.; Hasegawa, H.; Inoue, A.; Muraoka, M.; Miyazaki, T.; Oka, K.; Yasukawa, M. Identification of *N*-arachidonylglycine as the endogenous ligand for orphan G-protein-coupled receptor GPR18. *Biochem. Biophys. Res. Commun.* **2006**, *347*, 827–832.

(61) Huang, S. M.; Bisogno, T.; Petros, T. J.; Chang, S. Y.; Zavitsanos, P. A.; Zipkin, R. E.; Sivakumar, R.; Coop, A.; Maeda, D. Y.; Petrocellis, L. de; Burstein, S.; Di Marzo, V.; Walker, J. M. Identification of a new class of molecules, the arachidonyl amino acids, and characterization of one member that inhibits pain. *J. Biol. Chem.* **2001**, *276*, 42639–42644.

(62) Sheskin, T.; Hanus, L.; Slager, J.; Vogel, Z.; Mechoulam, R. Structural requirements for binding of anandamide-type compounds to the brain cannabinoid receptor. *J. Med. Chem.* **1997**, *40*, 659–667.

(63) Wiles, A. L.; Pearlman, R.-J.; Rosvall, M.; Aubrey, K. R.; Vandenberg, R. J. N-Arachidonyl-glycine inhibits the glycine transporter, GLYT2a. *J. Neurochem*. **2006**, *99*, 781–786.

(64) Ikeda, Y.; Iguchi, H.; Nakata, M.; Ioka, R. X.; Tanaka, T.; Iwasaki, S.; Magoori, K.; Takayasu, S.; Yamamoto, T. T.; Kodama, T.; Yada, T.; Sakurai, T.; Yanagisawa, M.; Sakai, J. Identification of *N*-arachidonylglycine, U18666A, and 4-androstene-3,17-dione as novel insulin Secretagogues. *Biochem. Biophys. Res. Commun.* **2005**, *333*, 778–786.

(65) Burstein, S. H.; Adams, J. K.; Bradshaw, H. B.; Fraioli, C.; Rossetti, R. G.; Salmonsen, R. A.; Shaw, J. W.; Walker, J. M.; Zipkin, R. E.; Zurier, R. B. Potential anti-inflammatory actions of the elmiric (lipoamino) acids. *Bioorg. Med. Chem.* **2007**, *15*, 3345–3355.

(66) Rempel, V.; Atzler, K.; Behrenswerth, A.; Karcz, T.; Schoeder, C.; Hinz, S.; Kaleta, M.; Thimm, D.; Kiec-Kononowicz, K.; Müller, C. E. Bicyclic imidazole-4-one derivatives: a new class of antagonists for the orphan G protein-coupled receptors GPR18 and GPR55. *Med. Chem. Commun.* **2014**, *5*, 632.

(67) Rimmerman, N.; Bradshaw, H. B.; Hughes, H. V.; Chen, J. S.-C.; Hu, S. S.-J.; McHugh, D.; Vefring, E.; Jahnsen, J. A.; Thompson, E. L.; Masuda, K.; Cravatt, B. F.; Burstein, S.; Vasko, M. R.; Prieto, A. L.; O'Dell, D. K.; Walker, J. M. N-palmitoyl glycine, a novel endogenous lipid that acts as a modulator of calcium influx and nitric oxide production in sensory neurons. *Mol. Pharmacol.* **2008**, *74*, 213–224.

(68) McHugh, D.; Tanner, C.; Mechoulam, R.; Pertwee, R. G.; Ross, R. A. Inhibition of human neutrophil chemotaxis by endogenous cannabinoids and phytocannabinoids: evidence for a site distinct from CB1 and CB2. *Mol. Pharmacol.* **2008**, *73*, 441–450.

(69) McHugh, D.; Hu, Sherry S J; Rimmerman, N.; Juknat, A.; Vogel, Z.; Walker, J. M.; Bradshaw, H. B. N-arachidonoyl glycine, an abundant endogenous lipid, potently drives directed cellular migration through GPR18, the putative abnormal cannabidiol receptor. *BMC Neurosci.* **2010**, *11*, 44.

(70) McHugh, D.; Wager-Miller, J.; Page, J.; Bradshaw, H. B. siRNA knockdown of GPR18 receptors in BV-2 microglia attenuates N-arachidonoyl glycine-induced cell migration. *J. Mol. Signal.* **2012**, *7*, 10.

(71) Malek, N.; Popiolek-Barczyk, K.; Mika, J.; Przewlocka, B.; Starowicz, K. Anandamide, Acting via CB2 Receptors, Alleviates LPS-Induced Neuroinflammation in Rat Primary Microglial Cultures. *Neural. Plast.* **2015**, *2015*, 130639.

(72) McHugh, D.; Page, J.; Dunn, E.; Bradshaw, H. B. Delta(9) -Tetrahydrocannabinol and N-arachidonyl glycine are full agonists at GPR18 receptors and induce migration in human endometrial HEC-1B cells. *Br. J. Pharmacol.* **2012**, *165*, 2414–2424.

(73) Caldwell, M. D.; Hu, S. S.-J.; Viswanathan, S.; Bradshaw, H.; Kelly, Melanie E M; Straiker, A. A GPR18-based signalling system regulates IOP in murine eye. *Br. J. Pharmacol.* **2013**, *169*, 834–843.

(74) MacIntyre, J.; Dong, A.; Straiker, A.; Zhu, J.; Howlett, S. E.; Bagher, A.; Denovan-Wright, E.; Yu, D.-Y.; Kelly, Melanie E M. Cannabinoid and lipid-mediated vasorelaxation in retinal microvasculature. *Eur J. Pharmacol.* **2014**, *735*, 105–114.

(75) Burstein, S. H.; McQuain, C. A.; Ross, A. H.; Salmonsen, R. A.; Zurier, R. E. Resolution of inflammation by *N*-arachidonoylglycine. *J. Cell Biochem.* **2011**, *112*, 3227–3233.

(76) Takenouchi, R.; Inoue, K.; Kambe, Y.; Miyata, A. *N*-arachidonoyl glycine induces macrophage apoptosis via GPR18. *Biochem. Biophys. Res. Commun.* **2012**, *418*, 366–371.

(77) Jablonski, K. A.; Amici, S. A.; Webb, L. M.; Ruiz-Rosado, Juan de Dios; Popovich, P. G.; Partida-Sanchez, S.; Guerau-de-Arellano, M. Novel markers to delineate murine M1 and M2 macrophages. *PLoS One* **2015**, *10*, e0145342.

(78) Wynn, T. A.; Chawla, A.; Pollard, J. W. Macrophage biology in development, homeostasis and disease. *Nature* **2013**, *496*, 445–455.

(79) Penumarti, A.; Abdel-Rahman, A. A. The novel endocannabinoid receptor GPR18 is expressed in the rostral ventrolateral medulla and exerts tonic restraining influence on blood pressure. *J. Pharmacol. Exp. Ther.* **2014**, *349*, 29–38.

(80) Penumarti, A.; Abdel-Rahman, A. A. Neuronal nitric oxide synthase-dependent elevation in adiponectin in the rostral ventrolateral medulla underlies g protein-coupled receptor 18-mediated hypotension in conscious rats. *J. Pharmacol. Exp. Ther.* **2014**, *351*, 44–53.

(81) Qin, Y.; Verdegaal, E M E; Siderius, M.; Bebelman, J. P.; Smit, M. J.; Leurs, R.; Willemze, R.; Tensen, C. P.; Osanto, S. Quantitative expression profiling of G-protein-coupled receptors (GPCRs) in metastatic melanoma: the constitutively active orphan GPCR GPR18 as novel drug target. *Pigment Cell Melanoma Res.* **2011**, *24*, 207–218.

(82) Yin, H.; Chu, A.; Li, W.; Wang, B.; Shelton, F.; Otero, F.; Nguyen, D. G.; Caldwell, J. S.; Chen, Y. A. Lipid G protein-coupled receptor ligand identification using beta-arrestin PathHunter assay. *J. Biol. Chem.* **2009**, *284*, 12328–12338.

(83) van Lu, B.; Puhl, Henry L 3rd; Ikeda, S. R. *N*-Arachidonyl glycine does not activate G protein-coupled receptor 18 signaling via canonical pathways. *Mol. Pharmacol.* **2013**, *83*, 267–282.

(84) Wang, X.; Sumida, H.; Cyster, J. G. GPR18 is required for a normal CD8αα intestinal intraepithelial lymphocyte compartment. *J. Exp. Med.* **2014**, *211*, 2351–2359.

(85) Taylor, L.; Christou, I.; Kapellos, T. S.; Buchan, A.; Brodermann, M. H.; Gianella-Borradori, M.; Russell, A.; Iqbal, A. J.; Greaves, D. R. Primary macrophage chemotaxis induced by cannabinoid receptor 2 agonists occurs independently of the CB2 Receptor. *Sci. Rep.* **2015**, *5*, 10682.

(86) Becker, A. M.; Callahan, D. J.; Richner, J. M.; Choi, J.; DiPersio, J. F.; Diamond, M. S.; Bhattacharya, D. GPR18 controls reconstitution of mouse small intestine intraepithelial lymphocytes following bone marrow transplantation. *PLoS One* **2015**, *10*, e0133854.

(87) Console-Bram, L.; Brailoiu, E.; Brailoiu, G. C.; Sharir, H.; Abood, M. E. Activation of GPR18 by cannabinoid compounds: a tale of biased agonism. *Br. J. Pharmacol.* **2014**, *171*, 3908–3917.

(88) Chiang, N.; Dalli, J.; Colas, R. A.; Serhan, C. N. Identification of resolvin D2 receptor mediating resolution of infections and organ protection. *J. Exp. Med.* **2015**, *212*, 1203–1217.

(89) Finlay, D. B.; Joseph, W. R.; Grimsey, N. L.; Glass, M. GPR18 undergoes a high degree of constitutive trafficking but is unresponsive to *N*-Arachidonoylglycine. *PeerJ.* **2016**, *4*, e1835.

(90) Flegel, C.; Vogel, F.; Hofreuter, A.; Wojcik, S.; Schoeder, C.; Kiec-Kononowicz, K.; Brockmeyer, N. H.; Muller, C. E.; Becker, C.; Altmuller, J.; Hatt, H.; Gisselmann, G. Characterization of non-olfactory GPCRs in human sperm with a focus on GPR18. *Sci. Rep.* **2016**, *6*, 32255.

(91) Li, J.; Leong, M. M.; Stewart, A.; Rizzacasa, M. A. Total synthesis of the endogenous inflammation resolving lipid resolvin D2 using a common lynchpin. *Beilstein J. Org. Chem.* **2013**, *9*, 2762–2766.

(92) Spite, M.; Norling, L. V.; Summers, L.; Yang, R.; Cooper, D.; Petasis, N. A.; Flower, R. J.; Perretti, M.; Serhan, C. N. Resolvin D2 is a potent regulator of leukocytes and controls microbial sepsis. *Nature* **2009**, *461*, 1287–1291.

(93) Tian, Y.; Zhang, Y.; Zhang, R.; Qiao, S.; Fan, J. Resolvin D2 recovers neural injury by suppressing inflammatory mediators expression in lipopolysaccharide-induced Parkinson's disease rat model. *Biochem. Biophys. Res. Commun.* **2015**, *460*, 799–805.

(94) Zhang, M. J.; Sansbury, B. E.; Hellmann, J.; Baker, J. F.; Guo, L.; Parmer, C. M.; Prenner, J. C.; Conklin, D. J.; Bhatnagar, A.; Creager, M. A.; Spite, M. Resolvin D2 Enhances Postischemic Revascularization While Resolving Inflammation. *Circulation* **2016**, *134*, 666–680.

(95) Park, C.-K.; Xu, Z.-Z.; Liu, T.; Lu, N.; Serhan, C. N.; Ji, R.-R. Resolvin D2 is a potent endogenous inhibitor for transient receptor potential subtype V1/A1, inflammatory pain, and spinal cord synaptic plasticity in mice: distinct roles of resolvin D1, D2, and E1. *J. Neurosci.* **2011**, *31*, 18433–18438.

(96) Harms, H.; Rempel, V.; Kehraus, S.; Kaiser, M.; Hufendiek, P.; Müller, C. E.; König, G. M. Indoloditerpenes from a marine-derived fungal strain of *Dichotomomyces cejpii* with antagonistic activity at GPR18 and cannabinoid receptors. *J. Nat. Prod.* **2014**, *77*, 673–677.

(97) Nazir, M.; Harms, H.; Loef, I.; Kehraus, S.; El Maddah, F.; Arslan, I.; Rempel, V.; Müller, C. E.; König, G. M. GPR18 inhibiting amauromine and the novel triterpene glycoside auxarthonoside from the sponge-derived fungus *Auxarthron reticulatum. Planta Med.* **2015**, *81*, 1141–1145.

(98) Sawzdargo, M.; Nguyen, T.; Lee, D. K.; Lynch, K. R.; Cheng, R.; Heng, H. H.; George, S. R.; O'Dowd, B. F. Identification and cloning of three novel human G protein-coupled receptor genes GPR52, PsiGPR53 and GPR55: GPR55 is extensively expressed in human brain. *Brain. Res. Mol. Brain. Res.* **1999**, *64*, 193–198.

(99) Baker, D.; Pryce, G.; Davies, W. L.; Hiley, C. R. In silico patent searching reveals a new cannabinoid receptor. *Trends Pharmacol Sci* **2006**, *27*, 1–4.

(100) Petitet, F.; Donlan, M.; Michel, A. GPR55 as a new cannabinoid receptor: still a long way to prove it. *Chem. Biol. Drug. Des*. **2006**, *67*, 252–253.

(101) Mackenzie, A. E.; Milligan, G. The emerging pharmacology and function of GPR35 in the nervous system. *Neuropharmacol.* **2017**, *113*, 661–671.

(102) Oka, S.; Nakajima, K.; Yamashita, A.; Kishimoto, S.; Sugiura, T. Identification of GPR55 as a lysophosphatidylinositol receptor. *Biochem. Biophys. Res. Commun.* **2007**, *362*, 928–934.

(103) Oka, S.; Toshida, T.; Maruyama, K.; Nakajima, K.; Yamashita, A.; Sugiura, T. 2-Arachidonoyl-sn-glycero-3-phosphoinositol: a possible natural ligand for GPR55. *J. Biochem.* **2009**, *145*, 13–20.

(104) Okuno, T.; Yokomizo, T. What is the natural ligand of GPR55? *J. Biochem.* **2011**, *149*, 495–497.

(105) Guy, A. T.; Nagatsuka, Y.; Ooashi, N.; Inoue, M.; Nakata, A.; Greimel, P.; Inoue, A.; Nabetani, T.; Murayama, A.; Ohta, K.; Ito, Y.; Aoki, J.; Hirabayashi, Y.; Kamiguchi, H. Neuronal development. Glycerophospholipid regulation of modality-specific sensory axon guidance in the spinal cord. *Science* **2015**, *349*, 974–977.

(106) Ryberg, E.; Larsson, N.; Sjogren, S.; Hjorth, S.; Hermansson, N.-O.; Leonova, J.; Elebring, T.; Nilsson, K.; Drmota, T.; Greasley, P. J. The orphan receptor GPR55 is a novel cannabinoid receptor. *Br. J. Pharmacol.* **2007**, *152*, 1092–1101.

(107) Henstridge, C. M.; Balenga, Nariman A B; Ford, L. A.; Ross, R. A.; Waldhoer, M.; Irving, A. J. The GPR55 ligand L-alpha-lysophosphatidylinositol promotes RhoA-dependent Ca2+ signaling and NFAT activation. *FASEB J* **2009**, *23*, 183–193.

(108) Oka, S.; Kimura, S.; Toshida, T.; Ota, R.; Yamashita, A.; Sugiura, T. Lysophosphatidylinositol induces rapid phosphorylation of p38 mitogen-activated protein kinase and activating transcription factor 2 in HEK293 cells expressing GPR55 and IM-9 lymphoblastoid cells. *J. Biochem.* **2010**, *147*, 671–678.

(109) Hiley, C. R.; Kaup, S. S. GPR55 and the vascular receptors for cannabinoids. *Br. J. Pharmacol.* **2007**, *152*, 559–561.

(110) Johns, D. G.; Behm, D. J.; Walker, D. J.; Ao, Z.; Shapland, E. M.; Daniels, D. A.; Riddick, M.; Dowell, S.; Staton, P. C.; Green, P.; Shabon, U.; Bao, W.; Aiyar, N.; Yue, T.-L.; Brown, A. J.; Morrison, A. D.; Douglas, S. A. The novel endocannabinoid receptor GPR55 is activated by atypical cannabinoids but does not mediate their vasodilator effects. *Br. J. Pharmacol.* **2007**, *152*, 825–831.

(111) Kargl, J.; Balenga, N.; Parzmair, G. P.; Brown, A. J.; Heinemann, A.; Waldhoer, M. The cannabinoid receptor CB1 modulates the signaling properties of the lysophosphatidylinositol receptor GPR55. *J. Biol. Chem.* **2012**, *287*, 44234–44248.

(112) Martinez-Pinilla, E.; Reyes-Resina, I.; Onatibia-Astibia, A.; Zamarbide, M.; Ricobaraza, A.; Navarro, G.; Moreno, E.; Dopeso-Reyes, I. G.; Sierra, S.; Rico, A. J.; Roda, E.; Lanciego, J. L.; Franco, R. CB1 and GPR55 receptors are co-expressed and form heteromers in rat and monkey striatum. *Exp. Neurol.* **2014**, *261*, 44–52.

(113) Moreno, E.; Andradas, C.; Medrano, M.; Caffarel, M. M.; Perez-Gomez, E.; Blasco-Benito, S.; Gomez-Canas, M.; Pazos, M. R.; Irving, A. J.; Lluis, C.; Canela, E. I.; Fernandez-Ruiz, J.; Guzman, M.; McCormick, P. J.; Sanchez, C. Targeting CB2-GPR55 receptor heteromers modulates cancer cell signaling. *J. Biol. Chem.* **2014**, *289*, 21960–21972.

(114) Balenga, N. A.; Martinez-Pinilla, E.; Kargl, J.; Schroder, R.; Peinhaupt, M.; Platzer, W.; Balint, Z.; Zamarbide, M.; Dopeso-Reyes, I. G.; Ricobaraza, A.; Perez-Ortiz, J. M.; Kostenis, E.; Waldhoer, M.; Heinemann, A.; Franco, R. Heteromerization of GPR55 and cannabinoid CB2 receptors modulates signalling. *Br. J. Pharmacol.* **2014**, *171*, 5387–5406.

(115) Anavi-Goffer, S.; Baillie, G.; Irving, A. J.; Gertsch, J.; Greig, I. R.; Pertwee, R. G.; Ross, R. A. Modulation of L-alpha-lysophosphatidylinositol/GPR55 mitogen-activated protein kinase (MAPK) signaling by cannabinoids. *J. Biol. Chem.* **2012**, *287*, 91–104.

(116) Henstridge, C. M.; Balenga, N. A.; Schroder, R.; Kargl, J. K.; Platzer, W.; Martini, L.; Arthur, S.; Penman, J.; Whistler, J. L.; Kostenis, E.; Waldhoer, M.; Irving, A. J. GPR55 ligands promote receptor coupling to multiple signalling pathways. *Br. J. Pharmacol.* **2010**, *160*, 604–614.

(117) Lauckner, J. E.; Jensen, J. B.; Chen, H.-Y.; Lu, H.-C.; Hille, B.; Mackie, K. GPR55 is a cannabinoid receptor that increases intracellular calcium and inhibits M current. *PNAS* **2008**, *105*, 2699–2704.

(118) Kapur, A.; Zhao, P.; Sharir, H.; Bai, Y.; Caron, M. G.; Barak, L. S.; Abood, M. E. Atypical responsiveness of the orphan receptor GPR55 to cannabinoid ligands. *J. Biol. Chem.* **2009**, *284*, 29817–29827.

(119) Sharir, H.; Console-Bram, L.; Mundy, C.; Popoff, S. N.; Kapur, A.; Abood, M. E. The endocannabinoids anandamide and virodhamine modulate the activity of the candidate cannabinoid receptor GPR55. *J. Neuroimmune Pharmacol.* **2012**, *7*, 856–865.

(120) Brown, A. J.; Daniels, D. A.; Kassim, M.; Brown, S.; Haslam, C. P.; Terrell, V. R.; Brown, J.; Nichols, P. L.; Staton, P. C.; Wise, A.; Dowell, S. J. Pharmacology of GPR55 in yeast and identification of GSK494581A as a mixed-activity glycine transporter subtype 1 inhibitor and GPR55 agonist. *J Pharmacol. Exp. The.r* **2011**, *337*, 236–246.

(121) Heynen-Genel, S.; Dahl, R.; Shi, S.; Milan, L.; Hariharan, S.; Bravo, Y.; Sergienko, E.; Hedrick, M.; Dad, S.; Stonich, D.; Su, Y.; Vicchiarelli, M.; Mangravita-Novo, A.; Smith, L. H.; Chung, T. D. Y.; Sharir, H.; Barak, L. S.; Abood, M. E. Screening for Selective Ligands for GPR55 - Agonists. *Probe Reports from NIH Mol. Libr. Progr*. **2010.**

(122) Kotsikorou, E.; Madrigal, K. E.; Hurst, D. P.; Sharir, H.; Lynch, D. L.; Heynen-Genel, S.; Milan, L. B.; Chung, Thomas D Y; Seltzman, H. H.; Bai, Y.; Caron, M. G.; Barak, L.; Abood, M. E.; Reggio, P. H. Identification of the GPR55 agonist binding site using a novel set of high-potency GPR55 selective ligands. *Biochemistry* **2011**, *50*, 5633–5647.

(123) Lingerfelt, M. A.; Zhao, P.; Sharir, H. P.; Hurst, D. P.; Reggio, P. H.; Abood, M. E. Identification of crucial amino acid residues involved in agonist signaling at the GPR55 receptor. *Biochemistry* **2017**, *56*, 473–486.

(124) Elbegdorj, O.; Westkaemper, R. B.; Zhang, Y. A homology modeling study toward the understanding of three-dimensional structure and putative pharmacological profile of the G-protein coupled receptor GPR55. *J. Mol. Graph. Model.* **2013**, *39*, 50–60.

(125) Morales, P.; Whyte, L. S.; Chicharro, R.; Gomez-Canas, M.; Pazos, M. R.; Goya, P.; Irving, A. J.; Fernandez-Ruiz, J.; Ross, R. A.; Jagerovic, N. Identification of novel GPR55 modulators using cell-impedance-based label-free technology. *J. Med. Chem.* **2016**, *59*, 1840–1853.

(126) Yrjola, S.; Parkkari, T.; Navia-Paldanius, D.; Laitinen, T.; Kaczor, A. A.; Kokkola, T.; Adusei-Mensah, F.; Savinainen, J. R.; Laitinen, J. T.; Poso, A.; Alexander, A.; Penman, J.; Stott, L.; Anskat, M.; Irving, A. J.; Nevalainen, T. J. Potent and selective *N*-(4-sulfamoylphenyl)thiourea-based GPR55 agonists. *Eur J Med. Chem.* **2016**, *107*, 119–132.

(127) Heynen-Genel, S.; Dahl, R.; Shi, S.; Milan, L.; Hariharan, S.; Sergienko, E.; Hedrick, M.; Dad, S.; Stonich, D.; Su, Y.; Vicchiarelli, M.; Mangravita-Novo, A.; Smith, L. H.; Chung, T. D. Y.; Sharir, H.; Caron, M. G.; Barak, L. S.; Abood, M. E. Screening for Selective Ligands for GPR55 - Antagonists. *Probe Reports from NIH Mol. Libr. Progr*. **2011**.

(128) Meza-Avina, M. E.; Lingerfelt, M. A.; Console-Bram, L. M.; Gamage, T. F.; Sharir, H.; Gettys, K. E.; Hurst, D. P.; Kotsikorou, E.; Shore, D. M.; Caron, M. G.; Rao, N.; Barak, L. S.; Abood, M. E.; Reggio, P. H.; Croatt, M. P. Design, synthesis, and analysis of antagonists of GPR55: Piperidine-substituted 1,3,4-oxadiazol-2-ones. *Bioorg. Med. Chem. Lett.* **2016**, *26*, 1827–1830.

(129) Rempel, V.; Volz, N.; Hinz, S.; Karcz, T.; Meliciani, I.; Nieger, M.; Wenzel, W.; Bräse, S.; Müller, C. E. 7-Alkyl-3-benzylcoumarins: a versatile scaffold for the development of potent and selective cannabinoid receptor agonists and antagonists. *J. Med. Chem.* **2012**, *55*, 7967–7977.

(130) Kargl, J.; Brown, A. J.; Andersen, L.; Dorn, G.; Schicho, R.; Waldhoer, M.; Heinemann, A. A selective antagonist reveals a potential role of G protein-coupled receptor 55 in platelet and endothelial cell function. *J. Pharmacol. Exp. Ther.* **2013**, *346*, 54–66.

(131) Kotsikorou, E.; Sharir, H.; Shore, D. M.; Hurst, D. P.; Lynch, D. L.; Madrigal, K. E.; Heynen-Genel, S.; Milan, L. B.; Chung, Thomas D Y; Seltzman, H. H.; Bai, Y.; Caron, M. G.; Barak, L. S.; Croatt, M. P.; Abood, M. E.; Reggio, P. H. Identification of the GPR55 antagonist binding site using a novel set of high-potency GPR55 selective ligands. *Biochemistry* **2013**, *52*, 9456–9469.

(132) Rempel, V.; Volz, N.; Gläser, F.; Nieger, M.; Bräse, S.; Müller, C. E. Antagonists for the orphan G-protein-coupled receptor GPR55 based on a coumarin scaffold. *J. Med. Chem.* **2013**, *56*, 4798–4810.

(133) Fuchs, A.; Rempel, V.; Muller, C. E. The natural product magnolol as a lead structure for the development of potent cannabinoid receptor agonists. *PLoS One* **2013**, *8*, e77739.

(134) Wu, C.-S.; Chen, H.; Sun, H.; Zhu, J.; Jew, C. P.; Wager-Miller, J.; Straiker, A.; Spencer, C.; Bradshaw, H.; Mackie, K.; Lu, H.-C. GPR55, a G-protein coupled receptor for lysophosphatidylinositol, plays a role in motor coordination. *PLoS One* **2013**, *8*, e60314.

(135) Cherif, H.; Argaw, A.; Cecyre, B.; Bouchard, A.; Gagnon, J.; Javadi, P.; Desgent, S.; Mackie, K.; Bouchard, J.-F. Role of GPR55 during axon growth and target innervation. *eNeuro* **2015**, *2*.

(136) Bondarenko, A.; Waldeck-Weiermair, M.; Naghdi, S.; Poteser, M.; Malli, R.; Graier, W. F. GPR55-dependent and -independent ion signalling in response to lysophosphatidylinositol in endothelial cells. *Br. J. Pharmacol.* **2010**, *161*, 308–320.

(137) Gangadharan, V.; Selvaraj, D.; Kurejova, M.; Njoo, C.; Gritsch, S.; Skoricova, D.; Horstmann, H.; Offermanns, S.; Brown, A. J.; Kuner, T.; Tappe-Theodor, A.; Kuner, R. A novel biological role for the phospholipid lysophosphatidylinositol in nociceptive sensitization via activation of diverse G-protein signalling pathways in sensory nerves in vivo. *Pain* **2013**, *154*, 2801–2812.

(138) Pietr, M.; Kozela, E.; Levy, R.; Rimmerman, N.; Lin, Y. H.; Stella, N.; Vogel, Z.; Juknat, A. Differential changes in GPR55 during microglial cell activation. *FEBS Lett* **2009**, *583*, 2071–2076.

(139) Kallendrusch, S.; Kremzow, S.; Nowicki, M.; Grabiec, U.; Winkelmann, R.; Benz, A.; Kraft, R.; Bechmann, I.; Dehghani, F.; Koch, M. The G protein-coupled receptor 55 ligand l-alpha-lysophosphatidylinositol exerts microglia-dependent neuroprotection after excitotoxic lesion. *Glia* **2013**, *61*, 1822–1831.

(140) Obara, Y.; Ueno, S.; Yanagihata, Y.; Nakahata, N. Lysophosphatidylinositol causes neurite retraction via GPR55, G13 and RhoA in PC12 cells. *PLoS One* **2011**, *6*, e24284.

(141) Staton, P. C.; Hatcher, J. P.; Walker, D. J.; Morrison, A. D.; Shapland, E. M.; Hughes, J. P.; Chong, E.; Mander, P. K.; Green, P. J.; Billinton, A.; Fulleylove, M.; Lancaster, H. C.; Smith, J. C.; Bailey, L. T.; Wise, A.; Brown, A. J.; Richardson, J. C.; Chessell, I. P. The putative cannabinoid receptor GPR55 plays

a role in mechanical hyperalgesia associated with inflammatory and neuropathic pain. *Pain* **2008**, *139*, 225–236.

(142) Andradas, C.; Caffarel, M. M.; Perez-Gomez, E.; Salazar, M.; Lorente, M.; Velasco, G.; Guzman, M.; Sanchez, C. The orphan G protein-coupled receptor GPR55 promotes cancer cell proliferation via ERK. *Oncogene* **2011**, *30*, 245–252.

(143) Pineiro, R.; Falasca, M. Lysophosphatidylinositol signalling: new wine from an old bottle. *Biochim. Biophys. Acta.* **2012**, *1821*, 694–705.

(144) Ross, R. A. L-alpha-lysophosphatidylinositol meets GPR55: a deadly relationship. *Trends Pharmacol. Sci* .**2011**, *32*, 265–269.

(145) Andradas, C.; Blasco-Benito, S.; Castillo-Lluva, S.; Dillenburg-Pilla, P.; Diez-Alarcia, R.; Juanes-Garcia, A.; Garcia-Taboada, E.; Hernando-Llorente, R.; Soriano, J.; Hamann, S.; Wenners, A.; Alkatout, I.; Klapper, W.; Rocken, C.; Bauer, M.; Arnold, N.; Quintanilla, M.; Megias, D.; Vicente-Manzanares, M.; Uriguen, L.; Gutkind, J. S.; Guzman, M.; Perez-Gomez, E.; Sanchez, C. Activation of the orphan receptor GPR55 by lysophosphatidylinositol promotes metastasis in triple-negative breast cancer. *Oncotarget* **2016**, *7*, 47565–47575.

(146) Ford, L. A.; Roelofs, A. J.; Anavi-Goffer, S.; Mowat, L.; Simpson, D. G.; Irving, A. J.; Rogers, M. J.; Rajnicek, A. M.; Ross, R. A. A role for L-alpha-lysophosphatidylinositol and GPR55 in the modulation of migration, orientation and polarization of human breast cancer cells. *Br. J. Pharmacol.* **2010**, *160*, 762–771.

(147) Kargl, J.; Balenga, N. A.; Platzer, W.; Martini, L.; Whistler, J. L.; Waldhoer, M. The GPCR-associated sorting protein 1 regulates ligand-induced down-regulation of GPR55. *Br. J. Pharmacol.* **2012**, *165*, 2611–2619.

(148) Kargl, J.; Andersen, L.; Hasenohrl, C.; Feuersinger, D.; Stancic, A.; Fauland, A.; Magnes, C.; El-Heliebi, A.; Lax, S.; Uranitsch, S.; Haybaeck, J.; Heinemann, A.; Schicho, R. GPR55 promotes migration and adhesion of colon cancer cells indicating a role in metastasis. *Br. J. Pharmacol.* **2016**, *173*, 142–154.

(149) Balenga, Nariman A B; Aflaki, E.; Kargl, J.; Platzer, W.; Schroder, R.; Blattermann, S.; Kostenis, E.; Brown, A. J.; Heinemann, A.; Waldhoer, M. GPR55 regulates cannabinoid 2 receptor-mediated responses in human neutrophils. *Cell Res*. **2011**, *21*, 1452–1469.

(150) Stancic, A.; Jandl, K.; Hasenohrl, C.; Reichmann, F.; Marsche, G.; Schuligoi, R.; Heinemann, A.; Storr, M.; Schicho, R. The GPR55 antagonist CID16020046 protects against intestinal inflammation. *Neurogastroenterol. Motil.* **2015**, *27*, 1432–1445.

(151) Wlodarczyk, M.; Sobolewska-Wlodarczyk, A.; Cygankiewicz, A. I.; Jacenik, D.; Krajewska, W. M.; Stec-Michalska, K.; Piechota-Polanczyk, A.; Wisniewska-Jarosinska, M.; Fichna, J. G protein-coupled receptor 55 (GPR55) expresses differently in patients with Crohn's disease and ulcerative colitis. *Scand J. Gastroenterol.* **2017**, 1–5.

(152) Moreno-Navarrete, J. M.; Catalan, V.; Whyte, L.; Diaz-Arteaga, A.; Vazquez-Martinez, R.; Rotellar, F.; Guzman, R.; Gomez-Ambrosi, J.; Pulido, M. R.; Russell, W. R.; Imbernon, M.; Ross, R. A.; Malagon, M. M.; Dieguez, C.; Fernandez-Real, J. M.; Fruhbeck, G.; Nogueiras, R. The L-alpha-lysophosphatidylinositol/GPR55 system and its potential role in human obesity. *Diabetes* **2012**, *61*, 281–291.

(153) McKillop, A. M.; Moran, B. M.; Abdel-Wahab, Y H A; Flatt, P. R. Evaluation of the insulin releasing and antihyperglycaemic activities of GPR55 lipid agonists using clonal beta-cells, isolated pancreatic islets and mice. *Br. J. Pharmacol.* **2013**, *170*, 978–990.

(154) Yu, J.; Deliu, E.; Zhang, X.-Q.; Hoffman, N. E.; Carter, R. L.; Grisanti, L. A.; Brailoiu, G. C.; Madesh, M.; Cheung, J. Y.; Force, T.; Abood, M. E.; Koch, W. J.; Tilley, D. G.; Brailoiu, E. Differential activation of cultured neonatal cardiomyocytes by plasmalemmal versus intracellular G protein-coupled receptor 55. *J. Biol. Chem.* **2013**, *288*, 22481–22492.

(155) Walsh, S. K.; Hector, E. E.; Andreasson, A.-C.; Jonsson-Rylander, A.-C.; Wainwright, C. L. GPR55 deletion in mice leads to age-related ventricular dysfunction and impaired adrenoceptor-mediated inotropic responses. *PLoS One* **2014**, *9*, e108999.

(156) Meadows, A.; Lee, J. H.; Wu, C.-S.; Wei, Q.; Pradhan, G.; Yafi, M.; Lu, H.-C.; Sun, Y. Deletion of G-protein-coupled receptor 55 promotes obesity by reducing physical activity. *Int. J. Obes.* **2016**, *40*, 417–424.

(157) Bjursell, M.; Ryberg, E.; Wu, T.; Greasley, P. J.; Bohlooly-Y, M.; Hjorth, S. Deletion of GPR55 results in subtle effects on energy metabolism, motor activity and thermal pain sensation. *PLoS One* **2016**, *11*, e0167965.

(158) Whyte, L. S.; Ryberg, E.; Sims, N. A.; Ridge, S. A.; Mackie, K.; Greasley, P. J.; Ross, R. A.; Rogers, M. J. The putative cannabinoid receptor GPR55 affects osteoclast function in vitro and bone mass in vivo. *PNAS* **2009**, *106*, 16511–16516.

(159) Zhang, X.; Maor, Y.; Wang, J. F.; Kunos, G.; Groopman, J. E. Endocannabinoid-like N-arachidonoyl serine is a novel pro-angiogenic mediator. *Br. J. Pharmacol.* **2010**, *160*, 1583–1594.

(160) Agrawal, A.; Lynskey, M. T. Candidate genes for cannabis use disorders: findings, challenges and directions. *Addiction* **2009**, *104*, 518–532.

(161) Leweke, F. M.; Piomelli, D.; Pahlisch, F.; Muhl, D.; Gerth, C. W.; Hoyer, C.; Klosterkotter, J.; Hellmich, M.; Koethe, D. Cannabidiol enhances anandamide signaling and alleviates psychotic symptoms of schizophrenia. *Transl. Psychiatry.* **2012**, *2*, e94.

(162) Pertwee, R. G. The diverse CB1 and CB2 receptor pharmacology of three plant cannabinoids: delta9-tetrahydrocannabinol, cannabidiol and Δ^9-tetrahydrocannabivarin. *Br. J. Pharmacol.* **2008**, *153*, 199–215.

(163) Castillo, A.; Tolon, M. R.; Fernandez-Ruiz, J.; Romero, J.; Martinez-Orgado, J. The neuroprotective effect of cannabidiol in an in vitro model of newborn hypoxic-ischemic brain damage in mice is mediated by CB2 and adenosine receptors. *Neurobiol. Dis.* **2010**, *37*, 434–440.

(164) Lin, X.-H.; Yuece, B.; Li, Y.-Y.; Feng, Y.-J.; Feng, J.-Y.; Yu, L.-Y.; Li, K.; Li, Y.-N.; Storr, M. A novel CB receptor GPR55 and its ligands are involved in regulation of gut movement in rodents. *Neurogastroenterol. Motil.* **2011**, *23*, 862-e342.

(165) Schicho, R.; Bashashati, M.; Bawa, M.; McHugh, D.; Saur, D.; Hu, H.-M.; Zimmer, A.; Lutz, B.; Mackie, K.; Bradshaw, H. B.; McCafferty, D.-M.; Sharkey, K. A.; Storr, M. The atypical cannabinoid O-1602 protects against experimental colitis and inhibits neutrophil recruitment. *Inflamm. Bowel. Dis.* **2011**, *17*, 1651–1664.

(166) Romero-Zerbo, S. Y.; Rafacho, A.; Diaz-Arteaga, A.; Suarez, J.; Quesada, I.; Imbernon, M.; Ross, R. A.; Dieguez, C.; Rodriguez de Fonseca, Fernando; Nogueiras, R.; Nadal, A.; Bermudez-Silva, F. J. A role for the putative cannabinoid receptor GPR55 in the islets of Langerhans. *J. Endocrinol.* **2011**, *211*, 177–185.

(167) Diaz-Arteaga, A.; Vazquez, M. J.; Vazquez-Martinez, R.; Pulido, M. R.; Suarez, J.; Velasquez, D. A.; Lopez, M.; Ross, R. A.; de Fonseca, F Rodriguez; Bermudez-Silva, F. J.; Malagon, M. M.; Dieguez, C.; Nogueiras, R. The atypical cannabinoid O-1602 stimulates food intake and adiposity in rats. *Diabetes Obes. Metab.* **2012**, *14*, 234–243.

(168) McHugh, D. GPR18 in microglia: implications for the CNS and endocannabinoid system signalling. *Br. J. Pharmacol.* **2012**, *167*, 1575–1582.

(169) Kieć-Kononowicz, K.; Karolak-Wojciechowska, J.; Michalak, B.; Pekala, E.; Schumacher, B.; Müller, C. E. Imidazo[2,1-*b*]thiazepines: synthesis, structure and evaluation of benzodiazepine receptor binding. *Eur. J. Med. Chem.* **2004**, *39*, 205–218.

(170) Alexander, S P H. So what do we call GPR18 now? *Br. J. Pharmacol.* **2012**, *165*, 2411–2413.

(171) Drabczyńska, A.; Müller, C. E.; Schumacher, B.; Hinz, S.; Karolak-Wojciechowska, J.; Michalak, B.; Pekala, E.; Kieć-Kononowicz, K. Tricyclic oxazolo[2,3-*f*]purinediones: potency as adenosine receptor ligands and anticonvulsants. *Bioorg. Med. Chem.* **2004**, *12*, 4895–4908.

(172) Drabczyńska, A.; Müller, C. E.; Lacher, S. K.; Schumacher, B.; Karolak-Wojciechowska, J.; Nasal, A.; Kawczak, P.; Yuzlenko, O.; Pekala, E.; Kieć-Kononowicz, K. Synthesis and biological activity of tricyclic aryloimidazo-, pyrimido-, and diazepinopurinediones. *Bioorg. Med. Chem.* **2006**, *14*, 7258–7281.

(173) Drabczyńska, A.; Müller, C. E.; Karolak-Wojciechowska, J.; Schumacher, B.; Schiedel, A.; Yuzlenko, O.; Kieć-Kononowicz, K. N9-benzyl-substituted 1,3-dimethyl- and 1,3-dipropyl-pyrimido[2,1-*f*]purinediones: synthesis and structure-activity relationships at adenosine A_1 and A_{2A} receptors. *Bioorg. Med. Chem.* **2007**, *15*, 5003–5017.

(174) Drabczyńska, A.; Müller, C. E.; Schiedel, A.; Schumacher, B.; Karolak-Wojciechowska, J.; Fruziński, A.; Zobnina, W.; Yuzlenko, O.; Kieć-Kononowicz, K. Phenylethyl-substituted pyrimido[2,1-*f*]purinediones and related compounds: Structure–activity relationships as adenosine A_1 and A_{2A} receptor ligands. *Bioorg. Med. Chem.* **2007**, *15*, 6956–6974.

(175) Drabczyńska, A.; Yuzlenko, O.; Köse, M.; Paskaleva, M.; Schiedel, A. C.; Karolak-Wojciechowska, J.; Handzlik, J.; Karcz, T.; Kuder, K.; Müller, C. E.; Kieć-Kononowicz, K. Synthesis and biological activity of tricyclic cycloalkylimidazo-, pyrimido- and diazepinopurinediones. *Eur. J. Med. Chem.* **2011**, *46*, 3590–3607.

(176) Wang, J.; Simonavicius, N.; Wu, X.; Swaminath, G.; Reagan, J.; Tian, H.; Ling, L. Kynurenic acid as a ligand for orphan G protein-coupled receptor GPR35. *J. Biol. Chem.* **2006**, *281*, 22021–22028.

(177) Milligan, G. Orthologue selectivity and ligand bias: translating the pharmacology of GPR35. *Trends Pharmacol. Sci.* **2011**, *32*, 317–325.

(178) Jenkins, L.; Alvarez-Curto, E.; Campbell, K.; Munnik, S. de; Canals, M.; Schlyer, S.; Milligan, G. Agonist activation of the G protein-coupled receptor GPR35 involves transmembrane domain III and is transduced via Gα_{13} and β-arrestin-2. *Br. J. Pharmacol.* **2011**, *162*, 733–748.

(179) Funke, M.; Thimm, D.; Schiedel, A. C.; Müller, C. E. 8-Benzamidochromen-4-one-2-carboxylic acids: Potent and selective agonists for the orphan G protein-coupled receptor GPR35. *J. Med. Chem.* **2013**, *56*, 5182–5197.

(180) Thimm, D.; Funke, M.; Meyer, A.; Müller, C. E. 6-Bromo-8-(4-[^{3}H]methoxybenzamido)-4-oxo-4*H*-chromene-2-carboxylic acid: a powerful tool for studying orphan G protein-coupled receptor GPR35. *J. Med. Chem.* **2013**, *56*, 7084–7099.

(181) McHugh, D.; Roskowski, D.; Xie, S.; Bradshaw, H. B. Delta(9)-THC and N-arachidonoyl glycine regulate BV-2 microglial morphology and cytokine release plasticity: implications for signaling at GPR18. *Front. Pharmacol.* **2014**, *4*, 162.

(182) Stansley, B.; Post, J.; Hensley, K. A comparative review of cell culture systems for the study of microglial biology in Alzheimer's disease. *J. Neuroinflamm.* **2012**, *9*, 115.

(183) Kenakin, T. P. *A pharmacology primer*; Academic Press/Elsevier: Amsterdam, Boston, 2009.

(184) Zhang, D.; Gao, Z.-G.; Zhang, K.; Kiselev, E.; Crane, S.; Wang, J.; Paoletta, S.; Yi, C.; Ma, L.; Zhang, W.; Han, G. W.; Liu, H.; Cherezov, V.; Katritch, V.; Jiang, H.; Stevens, R. C.; Jacobson, K. A.; Zhao, Q.; Wu, B. Two disparate ligand-binding sites in the human P2Y$_1$ receptor. *Nature* **2015**, *520*, 317–321.

(185) Kruse, A. C.; Ring, A. M.; Manglik, A.; Hu, J.; Hu, K.; Eitel, K.; Hubner, H.; Pardon, E.; Valant, C.; Sexton, P. M.; Christopoulos, A.; Felder, C. C.; Gmeiner, P.; Steyaert, J.; Weis, W. I.; Garcia, K. Christopher; Wess, J.; Kobilka, B. K. Activation and allosteric modulation of a muscarinic acetylcholine receptor. *Nature* **2013**, *504*, 101–106.

(186) Jazayeri, A.; Doré, A. S.; Lamb, D.; Krishnamurthy, H.; Southall, S. M.; Baig, A. H.; Bortolato, A.; Koglin, M.; Robertson, N. J.; Errey, J. C.; Andrews, S. P.; Teobald, I.; Brown, Alastair J. H.; Cooke, R. M.; Weir, M.; Marshall, F. H. Extra-helical binding site of a glucagon receptor antagonist. *Nature* **2016**, *533*, 274–277.

(187) Sliwoski, G.; Kothiwale, S.; Meiler, J.; Lowe, Edward W Jr. Computational methods in drug discovery. *Pharmacol. Rev.* **2014**, *66*, 334–395.

(188) Richter, F.; Leaver-Fay, A.; Khare, S. D.; Bjelic, S.; Baker, D. De novo enzyme design using Rosetta3. *PLoS One* **2011**, *6*, e19230.

(189) Ovchinnikov, S.; Kim, D. E.; Wang, R. Y.-R.; Liu, Y.; DiMaio, F.; Baker, D. Improved de novo structure prediction in CASP11 by incorporating coevolution information into Rosetta. *Proteins* **2016**, *84 Suppl 1*, 67–75.

(190) Nguyen, E. D.; Norn, C.; Frimurer, T. M.; Meiler, J. Assessment and challenges of ligand docking into comparative models of G-protein coupled receptors. *PLoS One* **2013**, *8*, e67302.

(191) Zhang, C.; Srinivasan, Y.; Arlow, D. H.; Fung, J. J.; Palmer, D.; Zheng, Y.; Green, H. F.; Pandey, A.; Dror, R. O.; Shaw, D. E.; Weis, W. I.; Coughlin, S. R.; Kobilka, B. K. High-resolution crystal structure of human protease-activated receptor 1. *Nature* **2012**, *492*, 387–392.

(192) Rasmussen, Soren G F; DeVree, B. T.; Zou, Y.; Kruse, A. C.; Chung, K. Y.; Kobilka, T. S.; Thian, F. S.; Chae, P. S.; Pardon, E.; Calinski, D.; Mathiesen, J. M.; Shah, Syed T A; Lyons, J. A.; Caffrey, M.; Gellman, S. H.; Steyaert, J.; Skiniotis, G.; Weis, W. I.; Sunahara, R. K.; Kobilka, B. K. Crystal structure of the β2 adrenergic receptor-Gs protein complex. *Nature* **2011**, *477*, 549–555.

(193) Meiler, J.; Baker, D. ROSETTALIGAND: protein-small molecule docking with full side-chain flexibility. *Proteins* **2006**, *65*, 538–548.

(194) Lemmon, G.; Meiler, J. Rosetta Ligand docking with flexible XML protocols. *Methods. Mol. Biol.* **2012**, *819*, 143–155.

(195) Butkiewicz, M.; Lowe, Edward W Jr; Mueller, R.; Mendenhall, J. L.; Teixeira, P. L.; Weaver, C. D.; Meiler, J. Benchmarking ligand-based virtual High-Throughput Screening with the PubChem database. *Molecules* **2013**, *18*, 735–756.

(196) Madden T. The BLAST Sequence Analysis Tool. *The NCBI Handbook.* **2002**.

(197) Zhang, K.; Zhang, J.; Gao, Z.-G.; Zhang, D.; Zhu, L.; Han, G. W.; Moss, S. M.; Paoletta, S.; Kiselev, E.; Lu, W.; Fenalti, G.; Zhang, W.; Müller, C. E.; Yang, H.; Jiang, H.; Cherezov, V.; Katritch, V.; Jacobson, K. A.; Stevens, R. C.; Wu, B.; Zhao, Q. Structure of the human $P2Y_{12}$ receptor in complex with an antithrombotic drug. *Nature* **2014**, *509*, 115–118.

(198) Miller, R. L.; Thompson, A. A.; Trapella, C.; Guerrini, R.; Malfacini, D.; Patel, N.; Han, G. W.; Cherezov, V.; Caló, G.; Katritch, V.; Stevens, R. C. The Importance of Ligand-Receptor Conformational Pairs in Stabilization: Spotlight on the N/OFQ G Protein-Coupled Receptor. *Structure* **2015**, *23*, 2291–2299.

(199) Wu, H.; Wacker, D.; Mileni, M.; Katritch, V.; Han, G. W.; Vardy, E.; Liu, W.; Thompson, A. A.; Huang, X.-P.; Carroll, F. Ivy; Mascarella, S. Wayne; Westkaemper, R. B.; Mosier, P. D.; Roth, B. L.; Cherezov, V.; Stevens, R. C. Structure of the human κ-opioid receptor in complex with JDTic. *Nature* **2012**, *485*, 327–332.

(200) Huang, W.; Manglik, A.; Venkatakrishnan, A. J.; Laeremans, T.; Feinberg, E. N.; Sanborn, A. L.; Kato, H. E.; Livingston, K. E.; Thorsen, T. S.; Kling, R. C.; Granier, S.; Gmeiner, P.; Husbands, S. M.; Traynor, J. R.; Weis, W. I.; Steyaert, J.; Dror, R. O.; Kobilka, B. K. Structural insights into μ-opioid receptor activation. *Nature* **2015**, *524*, 315–321.

(201) Fenalti, G.; Giguere, P. M.; Katritch, V.; Huang, X.-P.; Thompson, A. A.; Cherezov, V.; Roth, B. L.; Stevens, R. C. Molecular control of δ-opioid receptor signalling. *Nature* **2014**, *506*, 191–196.

(202) Zhang, H.; Unal, H.; Desnoyer, R.; Han, G. W.; Patel, N.; Katritch, V.; Karnik, S. S.; Cherezov, V.; Stevens, R. C. Structural basis for ligand recognition and functional selectivity at angiotensin receptor. *J. Biol. Chem.* **2015**, *290*, 29127–29139.

(203) Tan, Q.; Zhu, Y.; Li, J.; Chen, Z.; Han, G. W.; Kufareva, I.; Li, T.; Ma, L.; Fenalti, G.; Li, J.; Zhang, W.; Xie, X.; Yang, H.; Jiang, H.; Cherezov, V.; Liu, H.; Stevens, R. C.; Zhao, Q.; Wu, B. Structure of the CCR5 chemokine receptor-HIV entry inhibitor maraviroc complex. *Science* **2013**, *341*, 1387–1390.

(204) Park, S. H.; Das, B. B.; Casagrande, F.; Tian, Y.; Nothnagel, H. J.; Chu, M.; Kiefer, H.; Maier, K.; De Angelis, Anna A.; Marassi, F. M.; Opella, S. J. Structure of the chemokine receptor CXCR1 in phospholipid bilayers. *Nature* **2012**, *491*, 779–783.

(205) Wu, B.; Chien, Ellen Y T; Mol, C. D.; Fenalti, G.; Liu, W.; Katritch, V.; Abagyan, R.; Brooun, A.; Wells, P.; Bi, F. C.; Hamel, D. J.; Kuhn, P.; Handel, T. M.; Cherezov, V.; Stevens, R. C. Structures of the

CXCR4 chemokine GPCR with small-molecule and cyclic peptide antagonists. *Science* **2010**, *330*, 1066–1071.

(206) Krumm, B. E.; White, J. F.; Shah, P.; Grisshammer, R. Structural prerequisites for G-protein activation by the neurotensin receptor. *Nat. Commun.* **2015**, *6*, 7895.

(207) Lebon, G.; Warne, T.; Edwards, P. C.; Bennett, K.; Langmead, C. J.; Leslie, Andrew G. W.; Tate, C. G. Agonist-bound adenosine A$_{2A}$ receptor structures reveal common features of GPCR activation. *Nature* **2011**, *474*, 521–525.

(208) Chien, Ellen Y T; Liu, W.; Zhao, Q.; Katritch, V.; Han, G. W.; Hanson, M. A.; Shi, L.; Newman, A. H.; Javitch, J. A.; Cherezov, V.; Stevens, R. C. Structure of the human dopamine D3 receptor in complex with a D2/D3 selective antagonist. *Science* **2010**, *330*, 1091–1095.

(209) Weichert, D.; Kruse, A. C.; Manglik, A.; Hiller, C.; Zhang, C.; Hubner, H.; Kobilka, B. K.; Gmeiner, P. Covalent agonists for studying G protein-coupled receptor activation. *PNAS* **2014**, *111*, 10744–10748.

(210) Wang, C.; Jiang, Y.; Ma, J.; Wu, H.; Wacker, D.; Katritch, V.; Han, G. W.; Liu, W.; Huang, X.-P.; Vardy, E.; McCorvy, J. D.; Gao, X.; Zhou, X. E.; Melcher, K.; Zhang, C.; Bai, F.; Yang, H.; Yang, L.; Jiang, H.; Roth, B. L.; Cherezov, V.; Stevens, R. C.; Xu, H. E. Structural basis for molecular recognition at serotonin receptors. *Science* **2013**, *340*, 610–614.

(211) Shimamura, T.; Shiroishi, M.; Weyand, S.; Tsujimoto, H.; Winter, G.; Katritch, V.; Abagyan, R.; Cherezov, V.; Liu, W.; Han, G. W.; Kobayashi, T.; Stevens, R. C.; Iwata, S. Structure of the human histamine H1 receptor complex with doxepin. *Nature* **2011**, *475*, 65–70.

(212) Haga, K.; Kruse, A. C.; Asada, H.; Yurugi-Kobayashi, T.; Shiroishi, M.; Zhang, C.; Weis, W. I.; Okada, T.; Kobilka, B. K.; Haga, T.; Kobayashi, T. Structure of the human M2 muscarinic acetylcholine receptor bound to an antagonist. *Nature* **2012**, *482*, 547–551.

(213) Viklund, H.; Elofsson, A. OCTOPUS: improving topology prediction by two-track ANN-based preference scores and an extended topological grammar. *Bioinformatics* **2008**, *24*, 1662–1668.

(214) Ballesteros, J. A.; Weinstein, H. Integrated methods for the construction of three-dimensional models and computational probing of structure-function relations in G protein-coupled receptors. *Methods in Neurosci.* pp. 366–428.

(215) Isberg, V.; Graaf, C. de; Bortolato, A.; Cherezov, V.; Katritch, V.; Marshall, F. H.; Mordalski, S.; Pin, J.-P.; Stevens, R. C.; Vriend, G.; Gloriam, D. E. Generic GPCR residue numbers - aligning topology maps while minding the gaps. *Trends Pharmacol. Sci.* **2015**, *36*, 22–31.

(216) Bender, B. J.; Cisneros, A. 3.; Duran, A. M.; Finn, J. A.; Fu, D.; Lokits, A. D.; Mueller, B. K.; Sangha, A. K.; Sauer, M. F.; Sevy, A. M.; Sliwoski, G.; Sheehan, J. H.; DiMaio, F.; Meiler, J.; Moretti, R. Protocols for molecular modeling with Rosetta3 and RosettaScripts. *Biochemistry* **2016**, *55*, 4748–4763.

(217) Meiler, J.; Müller, M.; Zeidler, A.; Schmäschke, F. Generation and evaluation of dimension-reduced amino acid parameter representations by artificial neural networks. *Molecular modeling annual* **2001**, *7*, 360–369.

(218) Buchan, Daniel W A; Minneci, F.; Nugent, Tim C O; Bryson, K.; Jones, D. T. Scalable web services for the PSIPRED Protein Analysis Workbench. *Nucleic Acids Res.* **2013**, *41*, W349-57.

(219) Kothiwale, S.; Mendenhall, J. L.; Meiler, J. BCL::Conf: small molecule conformational sampling using a knowledge based rotamer library. *J. Cheminform.* **2015**, *7*, 47.

(220)   Bauer, A.; Bronstrup, M. Industrial natural product chemistry for drug discovery and development. *Nat. Prod. Rep.* **2014**, *31*, 35–60.

(221) Klebe, G. *Wirkstoffdesign*; Spektrum Akademischer Verlag: Heidelberg, 2009.

(222) Steinegger, E. *Pharmakognosie - Phytopharmazie*; Springer: Heidelberg, 2007.

(223) Nobelförsammlingen - The Nobel Assembly at Karolinska Institute - Nobelprize.org. *The 2015 Nobel Prize in Physiology or Medicine - Advanced Information*.

(224) Lachance, H.; Wetzel, S.; Kumar, K.; Waldmann, H. Charting, navigating, and populating natural product chemical space for drug discovery. *J. Med. Chem.* **2012**, *55*, 5989–6001.

(225) Elsebai, M. F.; Rempel, V.; Schnakenburg, G.; Kehraus, S.; Müller, C. E.; König, G. M. Identification of a potent and selective cannabinoid CB1 receptor antagonist from *Auxarthron reticulatum. ACS Med. Chem. Lett.* **2011**, *2*, 866–869.

(226) Kim, S. Y.; Kim, J.; Jeong, S.-I.; Jahng, K. Y.; Yu, K.-Y. Antimicrobial effects and resistant regulation of magnolol and honokiol on methicillin-resistant *Staphylococcus aureus. Biomed. Res. Int.* **2015**, *2015*, 283630.

(227) Bai, X.; Cerimele, F.; Ushio-Fukai, M.; Waqas, M.; Campbell, P. M.; Govindarajan, B.; Der, C. J.; Battle, T.; Frank, D. A.; Ye, K.; Murad, E.; Dubiel, W.; Soff, G.; Arbiser, J. L. Honokiol, a small molecular weight natural product, inhibits angiogenesis in vitro and tumor growth in vivo. *J. Biol. Chem.* **2003**, *278*, 35501–35507.

(228) Watanabe, K.; Watanabe, H.; Goto, Y.; Yamaguchi, M.; Yamamoto, N.; Hagino, K. Pharmacological properties of magnolol and hōnokiol extracted from *Magnolia officinalis*: central depressant effects. *Planta Med.* **1983**, *49*, 103-108.

(229) Kuribara, H.; Kishi, E.; Kimura, M.; Weintraub, S. T.; Maruyama, Y. Comparative assessment of the anxiolytic-like activities of honokiol and derivatives. *Pharmacol. Biochem. Behav.* **2000**, *67*, 597–601.

(230) Woodbury, A.; Yu, S. P.; Wei, L.; García, P. Neuro-modulating effects of honokiol: a review. *Front. Neurol.* **2013**, *4*, 130.

(231) Li, L.-F.; Yang, J.; Ma, S.-P.; Qu, R. Magnolol treatment reversed the glial pathology in an unpredictable chronic mild stress-induced rat model of depression. *Eur. J. Pharmacol.* **2013**, *711*, 42–49.

(232) Lee, Y.-J.; Choi, D.-Y.; Yun, Y.-P.; Han, S. B.; Kim, H. M.; Lee, K.; Choi, S. H.; Yang, M.-P.; Jeon, H. S.; Jeong, J.-H.; Oh, K.-W.; Hong, J. T. Ethanol extract of *Magnolia officinalis* prevents lipopolysaccharide-induced memory deficiency via its antineuroinflammatory and antiamyloidogenic effects. *Phytother. Res.* **2013**, *27*, 438–447.

(233) Shen, J.-L.; Man, K.-M.; Huang, P.-H.; Chen, W.-C.; Chen, D.-C.; Cheng, Y.-W.; Liu, P.-L.; Chou, M.-C.; Chen, Y.-H. Honokiol and magnolol as multifunctional antioxidative molecules for dermatologic disorders. *Molecules* **2010**, *15*, 6452–6465.

(234) Chuang, D. Y.; Chan, M.-H.; Zong, Y.; Sheng, W.; He, Y.; Jiang, J. H.; Simonyi, A.; Gu, Z.; Fritsche, K. L.; Cui, J.; Lee, J. C.; Folk, W. R.; Lubahn, D. B.; Sun, A. Y.; Sun, G. Y. Magnolia polyphenols attenuate oxidative and inflammatory responses in neurons and microglial cells. *J. Neuroinflamm.* **2013**, *10*, 15.

(235) Wang, L.; Waltenberger, B.; Pferschy-Wenzig, E.-M.; Blunder, M.; Liu, X.; Malainer, C.; Blazevic, T.; Schwaiger, S.; Rollinger, J. M.; Heiss, E. H.; Schuster, D.; Kopp, B.; Bauer, R.; Stuppner, H.; Dirsch, V. M.; Atanasov, A. G. Natural product agonists of peroxisome proliferator-activated receptor gamma (PPARγ): a review. *Biochem. Pharmacol.* **2014**, *92*, 73–89.

(236) Squires, R. F.; Ai, J.; Witt, M. R.; Kahnberg, P.; Saederup, E.; Sterner, O.; Nielsen, M. Honokiol and magnolol increase the number of 3H muscimol binding sites three-fold in rat forebrain membranes in vitro using a filtration assay, by allosterically increasing the affinities of low-affinity sites. *Neurochem. Res.* **1999**, *24*, 1593–1602.

(237) Chen, C. R.; Tan, R.; Qu, W. M.; Wu, Z.; Wang, Y.; Urade, Y.; Huang, Z. L. Magnolol, a major bioactive constituent of the bark of Magnolia officinalis, exerts antiepileptic effects via the GABA/benzodiazepine receptor complex in mice. *Br. J. Pharmacol.* **2011**, *164*, 1534–1546.

(238) Ma, H.; Kim, C.-S.; Ma, Y.; Nam, S.-Y.; Kim, D.-S.; Woo, S.-S.; Hong, J.-T.; Oh, K.-W. Magnolol enhances pentobarbital-induced sleeping behaviors: possible involvement of GABAergic systems. *Phytother. Res.* **2009**, *23*, 1340–1344.

(239) Ai, J.; Wang, X.; Nielsen, M. Honokiol and magnolol selectively interact with GABA_A receptor subtypes in vitro. *Pharmacology* **2001**, *63*, 34–41.

(240) Alexeev, M.; Grosenbaugh, D. K.; Mott, D. D.; Fisher, J. L. The natural products magnolol and honokiol are positive allosteric modulators of both synaptic and extra-synaptic GABA_A receptors. *Neuropharmacology* **2012**, *62*, 2507–2514.

(241) Baur, R.; Schuehly, W.; Sigel, E. Moderate concentrations of 4-*O*-methylhonokiol potentiate GABA$_A$ receptor currents stronger than honokiol. *Biochim. Biophys. Acta* **2014**, *1840*, 3017–3021.

(242) Clark, A. M.; El-Feraly, F. S.; Li, W. S. Antimicrobial activity of phenolic constituents of *Magnolia grandiflora L. J Pharm Sci* **1981**, *70*, 951–952.

(243) Schuehly, W.; Paredes, Juan Manuel Viveros; Kleyer, J.; Huefner, A.; Anavi-Goffer, S.; Raduner, S.; Altmann, K.-H.; Gertsch, J. Mechanisms of osteoclastogenesis inhibition by a novel class of biphenyl-type cannabinoid CB$_2$ receptor inverse agonists. *Chem. Biol.* **2011**, *18*, 1053–1064.

(244) Gertsch, J.; Anavi-Goffer, S. Methylhonokiol attenuates neuroinflammation: a role for cannabinoid receptors? *J. Neuroinflamm.* **2012**, *9*, 135.

(245) Rempel, V.; Fuchs, A.; Hinz, S.; Karcz, T.; Lehr, M.; Koetter, U.; Müller, C. E. Magnolia Extract, magnolol, and metabolites: Activation of cannabinoid CB2 Receptors and blockade of the related GPR55. *ACS Med. Chem. Lett.* **2013**, *4*, 41–45.

(246) Fuchs, A.; Baur, R.; Schoeder, C.; Sigel, E.; Müller, C. E. Structural analogues of the natural products magnolol and honokiol as potent allosteric potentiators of GABA$_A$ receptors. *Bioorg. Med. Chem.* **2014**, *22*, 6908–6917.

(247) Sigel, E.; Baur, R.; Racz, I.; Marazzi, J.; Smart, T. G.; Zimmer, A.; Gertsch, J. The major central endocannabinoid directly acts at GABA$_A$ receptors. *PNAS* **2011**, *108*, 18150–18155.

(248) Solfrizzo, M.; Strange, R. N.; Sabia, C.; Visconti, A. Production of a toxin stemphol by *Stemphylium* species. *Nat. Toxins* **1994**, *2*, 14–18.

(249) Schulz, S.; Yildizhan, S.; Stritzke, K.; Estrada, C.; Gilbert, L. E. Macrolides from the scent glands of the tropical butterflies Heliconius cydno and Heliconius pachinus. *Org. Biomol. Chem.* **2007**, *5*, 3434–3441.

(250) Andersen, B.; Frisvad, J. C. Natural occurrence of fungi and fungal metabolites in moldy tomatoes. *J. Agric. Food Chem.* **2004**, *52*, 7507–7513.

(251) Casapullo, A.; Minale, L.; Zollo, F. Paniceins and related sesquiterpenoids from the Mediterranean sponge Reniera fulva. *J. Nat. Prod.* **1993**, *56*, 527–533.

(252) Takase, S.; Iwame, M.; Ando, T.; Okamoto, M.; Yoshida, K., Horiai, H; Kohsaka, M.; Aoki, H, Imanaka, H. Amouromine, a new vasodilator: taxonomy, isolation and characterization. *J. Antibiotics* **1984**, *28*, 1320–1323.

(253) Gross, U.; Nieger, M.; Bräse, S. A unified strategy targeting the thiodiketopiperazine mycotoxins exserohilone, gliotoxin, the epicoccins, the epicorazines, rostratin A and aranotin. *Chemistry* **2010**, *16*, 11624–11631.

(254) Aharony, D. Pharmacology of leukotriene receptor antagonists. *Am. J. Respir. Crit. Care Med.* **1998**, *157*, S214-8; discussion S218-9, S247-8.

(255) Hennen, S.; Wang, H.; Peters, L.; Merten, N.; Simon, K.; Spinrath, A.; Blattermann, S.; Akkari, R.; Schrage, R.; Schroder, R.; Schulz, D.; Vermeiren, C.; Zimmermann, K.; Kehraus, S.; Drewke, C.; Pfeifer, A.; Konig, G. M.; Mohr, K.; Gillard, M.; Muller, C. E.; Lu, Q. R.; Gomeza, J.; Kostenis, E. Decoding signaling and function of the orphan G protein-coupled receptor GPR17 with a small-molecule agonist. *Sci. Signal.* **2013**, *6*, ra93.

(256) Anne Meyer. Chromen-4-ones as novel potent and selective ligands for Chromen-4-ones as novel potent and selective ligands for purinoceptor-related class A delta-branch orphan G protein-coupled receptors. *Dissertation*, Bonn, 2017.

(257) Funke, M.; Thimm, D.; Schiedel, A. C.; Müller, C. E. 8-Benzamidochromen-4-one-2-carboxylic acids: potent and selective agonists for the orphan G protein-coupled receptor GPR35. *J. Med. Chem.* **2013**, *56*, 5182–5197.

(258) Lynch, K. R.; O'Neill, G. P.; Liu, Q.; Im, D. S.; Sawyer, N.; Metters, K. M.; Coulombe, N.; Abramovitz, M.; Figueroa, D. J.; Zeng, Z.; Connolly, B. M.; Bai, C.; Austin, C. P.; Chateauneuf, A.; Stocco, R.; Greig, G. M.; Kargman, S.; Hooks, S. B.; Hosfield, E.; Williams, D L Jr; Ford-Hutchinson, A. W.; Caskey, C. T.; Evans, J. F. Characterization of the human cysteinyl leukotriene CysLT1 receptor. *Nature* **1999**, *399*, 789–793.

(259) Zhao, P.; Lane, T. R.; Gao, Helen G L; Hurst, D. P.; Kotsikorou, E.; Le, L.; Brailoiu, E.; Reggio, P. H.; Abood, M. E. Crucial positively charged residues for ligand activation of the GPR35 receptor. *J. Biol. Chem.* **2014**, *289*, 3625–3638.

(260) Mario Funke. Medizinische Chemie G-Protein-gekoppelter P2Y- und verwandter Waisen-Rezeptoren: Synthese, Optimierung und Charakterisierung selektiver Liganden als pharmakologische Tools. *Dissertation*, Bonn, 2014.

(261) Dominik Thimm. Medizinische Chemie und molekulare Pharmakologie G-Protein-gekoppelter Purin- und verwandter Waisen-Rezeptoren. *Dissertation*, Bonn, 2013.

(262) Kotsikorou, E.; Lynch, D. L.; Abood, M. E.; Reggio, P. H. Lipid bilayer molecular dynamics study of lipid-derived agonists of the putative cannabinoid receptor, GPR55. *Chem. Phys. Lipids* **2011**, *164*, 131–143.

(263) Lipinski, C. A.; Lombardo, F.; Dominy, B. W.; Feeney, P. J. Experimental and computational approaches to estimate solubility and permeability in drug discovery and development settings. *Adv. Drug Deliv. Rev.* **2001**, *46*, 3–26.

(264) Oka, S.; Toshida, T.; Maruyama, K.; Nakajima, K.; Yamashita, A.; Sugiura, T. 2-Arachidonoyl-sn-glycero-3-phosphoinositol: a possible natural ligand for GPR55. *J. Biochem.* **2009**, *145*, 13–20.

(265) Rempel, V.; Volz, N.; Gläser, F.; Nieger, M.; Bräse, S.; Müller, C. E. Antagonists for the orphan G-protein-coupled receptor GPR55 based on a coumarin scaffold. *J. Med. Chem.* **2013**, *56*, 4798–4810.

(266) Mechoulam, R.; GAONI, Y. A total synthesis of DL-Δ-1-tetrahydrocannabinol, the active constituent of hashish. *J. Am. Chem. Soc.* **1965**, *87*, 3273–3275.

(267) Mechoulam, R.; GAONI, Y. The absolute configuration of Δ-1-tetrahydrocannabinol, the major active constituent of hashish. *Tetrahedron Lett.* **1967**, *12*, 1109–1111.

(268) Mechoulam, R.; Lander, N.; Srebnik, M.; Breuer, A.; Segal, M.; Feigenbaum, J. J.; Jarbe, T. U.; Consroe, P. Stereochemical requirements for cannabimimetic activity. *NIDA Res. Monogr.* **1987**, *79*, 15–30.

(269) Mechoulam, R.; Lander, N.; Varkony, T. H.; Kimmel, I.; Becker, O.; Ben-Zvi, Z.; Edery, H.; Porath, G. Stereochemical requirements for cannabinoid activity. *J. Med. Chem.* **1980**, *23*, 1068–1072.

(270) Mechoulam, R.; Devane, W. A.; Breuer, A.; Zahalka, J. A random walk through a cannabis field. *Pharmacol. Biochem. Behav.* **1991**, *40*, 461–464.

(271) Adams, I. B.; Martin, B. R. Cannabis: pharmacology and toxicology in animals and humans. *Addiction* **1996**, *91*, 1585–1614.

(272) Gabriel G. Nahas. Toxicology and pharmacology of cannabis sativa with special reference to Δ^9-THC; United Nations Office on Drugs and Crime (UNODC), 01.01.1972.

(273) Ameri, A. The effects of cannabinoids on the brain. *Prog. Neurobiol.* **1999**, *58*, 315–348.

(274) Scallet, A. C. Neurotoxicology of cannabis and THC: a review of chronic exposure studies in animals. *Pharmacol. Biochem. Behav.* **1991**, *40*, 671–676.

(275) Europäische Beobachtungsstelle für Drogen und Drogensucht. Europäischer Drogenbericht 2015 **2015**.

(276) Auwarter, V.; Dresen, S.; Weinmann, W.; Muller, M.; Putz, M.; Ferreiros, N. 'Spice' and other herbal blends: harmless incense or cannabinoid designer drugs? *J Mass Spectrom* **2009**, *44*, 832–837.

(277) Uchiyama, N.; Kikura-Hanajiri, R.; Kawahara, N.; Haishima, Y.; Goda, Y. Identification of a cannabinoid analog as a new type of designer drug in a herbal product. *Chem. Pharm. Bull.* **2009**, *57*, 439–441.

(278) Huffman, J. W.; Dai, D.; Martin, B. R.; Compton, D. R. Design, synthesis and pharmacology of cannabimimetic indoles. *Bioorg. Med. Chem. Lett.* **1994**, *4*, 563–566.

(279) Little, P. J.; Compton, D. R.; Johnson, M. R.; Melvin, L. S.; Martin, B. R. Pharmacology and stereoselectivity of structurally novel cannabinoids in mice. *J. Pharmacol. Exp. Ther.* **1988**, *247*, 1046–1051.

(280) Darmani, N. A.; Sim-Selley, L. J.; Martin, B. R.; Janoyan, J. J.; Crim, J. L.; Parekh, B.; Breivogel, C. S. Antiemetic and motor-depressive actions of CP55,940: cannabinoid CB1 receptor characterization, distribution, and G-protein activation. *Eur. J. Pharmacol.* **2003**, *459*, 83–95.

(281) Sacerdote, P.; Massi, P.; Panerai, A. E.; Parolaro, D. In vivo and in vitro treatment with the synthetic cannabinoid CP55,940 decreases the in vitro migration of macrophages in the rat: involvement of both CB1 and CB2 receptors. *J. Neuroimmunol.* **2000**, *109*, 155–163.

(282) Sañudo-Peña, M. C.; Patrick, S. L.; Khen, S.; Patrick, R. L.; Tsou, K.; Walker, J. M. Cannabinoid effects in basal ganglia in a rat model of Parkinson's disease. *Neurosci. Lett.* **1998**, *248*, 171–174.

(283) Every-Palmer, S. Synthetic cannabinoid JWH-018 and psychosis: an explorative study. *Drug Alcohol. Depend.* **2011**, *117*, 152–157.

(284) Hermanns-Clausen, M.; Kneisel, S.; Szabo, B.; Auwarter, V. Acute toxicity due to the confirmed consumption of synthetic cannabinoids: clinical and laboratory findings. *Addiction* **2013**, *108*, 534–544.

(285) Lapoint, J.; James, L. P.; Moran, C. L.; Nelson, L. S.; Hoffman, R. S.; Moran, J. H. Severe toxicity following synthetic cannabinoid ingestion. *Clin. Toxicol.* **2011**, *49*, 760–764.

(286) Behonick, G.; Shanks, K. G.; Firchau, D. J.; Mathur, G.; Lynch, C. F.; Nashelsky, M.; Jaskierny, D. J.; Meroueh, C. Four postmortem case reports with quantitative detection of the synthetic cannabinoid, 5F-PB-22. *J. Anal. Toxicol.* **2014**, *38*, 559–562.

(287) Adams, A. J.; Banister, S. D.; Irizarry, L.; Trecki, J.; Schwartz, M.; Gerona, R. "Zombie" Outbreak Caused by the Synthetic Cannabinoid AMB-FUBINACA in New York. *N. Engl. J. Med.* **2017**, *376*, 235–242.

(288) Springer, Y. P.; Gerona, R.; Scheunemann, E.; Shafer, S. L.; Lin, T.; Banister, S. D.; Cooper, M. P.; Castrodale, L. J.; Levy, M.; Butler, J. C.; McLaughlin, J. B. Increase in adverse reactions associated with use of synthetic cannabinoids - Anchorage, Alaska, 2015-2016. *MMWR Morb. Mortal Wkly. Rep.* **2016**, *65*, 1108–1111.

(289) Lindigkeit, R.; Boehme, A.; Eiserloh, I.; Luebbecke, M.; Wiggermann, M.; Ernst, L.; Beuerle, T. Spice: a never ending story? *Forensic. Sci. Int.* **2009**, *191*, 58–63.

(290) Perspective on Drugs: Synthetic cannabinoids in Europe; EMCDDA (European Monitoring Centre on Drug and Drug Addiction), 31.05.2016.

(291) Huffman, J. W.; Zengin, G.; Wu, M.-J.; Lu, J.; Hynd, G.; Bushell, K.; Thompson, Alicia L S; Bushell, S.; Tartal, C.; Hurst, D. P.; Reggio, P. H.; Selley, D. E.; Cassidy, M. P.; Wiley, J. L.; Martin, B. R. Structure-activity relationships for 1-alkyl-3-(1-naphthoyl)indoles at the cannabinoid CB_1 and CB_2 receptors: steric and electronic effects of naphthoyl substituents. New highly selective CB_2 receptor agonists. *Bioorg. Med. Chem.* **2005**, *13*, 89–112.

(292) Frost, J. M.; Dart, M. J.; Tietje, K. R.; Garrison, T. R.; Grayson, G. K.; Daza, A. V.; El-Kouhen, O. F.; Miller, L. N.; Li, L.; Yao, B. B.; Hsieh, G. C.; Pai, M.; Zhu, C. Z.; Chandran, P.; Meyer, M. D. Indol-3-yl-tetramethylcyclopropyl ketones: effects of indole ring substitution on CB2 cannabinoid receptor activity. *J. Med. Chem.* **2008**, *51*, 1904–1912.

(293) Blaazer, A. R.; Lange, Jos H M; van der Neut, Martina A W; Mulder, A.; den Boon, Femke S; Werkman, T. R.; Kruse, C. G.; Wadman, W. J. Novel indole and azaindole (pyrrolopyridine) cannabinoid (CB) receptor agonists: design, synthesis, structure-activity relationships, physicochemical properties and biological activity. *Eur. J. Med. Chem.* **2011**, *46*, 5086–5098.

(294) Banister, S. D.; Stuart, J.; Kevin, R. C.; Edington, A.; Longworth, M.; Wilkinson, S. M.; Beinat, C.; Buchanan, A. S.; Hibbs, D. E.; Glass, M.; Connor, M.; McGregor, I. S.; Kassiou, M. Effects of bioisosteric fluorine in synthetic cannabinoid designer drugs JWH-018, AM-2201, UR-144, XLR-11, PB-22, 5F-PB-22, APICA, and STS-135. *ACS Chem. Neurosci.* **2015**, *6*, 1445–1458.

(295) Banister, S. D.; Longworth, M.; Kevin, R.; Sachdev, S.; Santiago, M.; Stuart, J.; Mack, James B C; Glass, M.; McGregor, I. S.; Connor, M.; Kassiou, M. Pharmacology of Valinate and tert-Leucinate Synthetic Cannabinoids 5F-AMBICA, 5F-AMB, 5F-ADB, AMB-FUBINACA, MDMB-FUBINACA, MDMB-CHMICA, and Their Analogues. *ACS Chem. Neurosci.* **2016**, *7*, 1241–1254.

(296) Banister, S. D.; Moir, M.; Stuart, J.; Kevin, R. C.; Wood, K. E.; Longworth, M.; Wilkinson, S. M.; Beinat, C.; Buchanan, A. S.; Glass, M.; Connor, M.; McGregor, I. S.; Kassiou, M. Pharmacology of Indole and Indazole Synthetic Cannabinoid Designer Drugs AB-FUBINACA, ADB-FUBINACA, AB-PINACA, ADB-PINACA, 5F-AB-PINACA, 5F-ADB-PINACA, ADBICA, and 5F-ADBICA. *ACS Chem. Neurosci.* **2015**, *6*, 1546–1559.

(297) Buchler, I.; Hayes, M. J.; Hedge, S. G.; Hockerman, S.; Jones, D.; Kortum, S.; Rico, J.; Tenbrick, R.; Wu, K. Indazole derivatives, *patent*. **2009**, WO2019/106982A1

(298) Wiley, J. L.; Marusich, J. A.; Lefever, T. W.; Antonazzo, K. R.; Wallgren, M. T.; Cortes, R. A.; Patel, P. R.; Grabenauer, M.; Moore, K. N.; Thomas, B. F. AB-CHMINACA, AB-PINACA, and FUBIMINA: Affinity and potency of novel synthetic cannabinoids in producing Δ^9-tetrahydrocannabinol-like effects in mice. *J. Pharmacol. Exp. Ther.* **2015**, *354*, 328–339.

(299) Bowden, M.; Williamson, J. Cannabinoid compounds, *patent*, **2014**, WO2014/167530A1.

(300) Banister, S. D.; Stuart, J.; Conroy, T.; Longworth, M.; Manohar, M.; Beinat, C.; Wilkinson, S. M.; Kevin, R. C.; Hibbs, D. E.; Glass, M.; Connor, M.; McGregor, I. S.; Kassiou, M. Structure–activity relationships of synthetic cannabinoid designer drug RCS-4 and its regioisomers and C4 homologues. *Forensic Toxicol.* **2015**, *33*, 355–366.

(301) Banister, S. D.; Wilkinson, S. M.; Longworth, M.; Stuart, J.; Apetz, N.; English, K.; Brooker, L.; Goebel, C.; Hibbs, D. E.; Glass, M.; Connor, M.; McGregor, I. S.; Kassiou, M. The synthesis and pharmacological evaluation of adamantane-derived indoles: cannabimimetic drugs of abuse. *ACS Chem. Neurosci.* **2013**, *4*, 1081–1092.

(302) Frost, J. M.; Dart, M. J.; Tietje, K. R.; Garrison, T. R.; Grayson, G. K.; Daza, A. V.; El-Kouhen, O. F.; Yao, B. B.; Hsieh, G. C.; Pai, M.; Zhu, C. Z.; Chandran, P.; Meyer, M. D. Indol-3-ylcycloalkyl ketones: effects of N1 substituted indole side chain variations on CB_2 cannabinoid receptor activity. *J. Med. Chem.* **2010**, *53*, 295–315.

(303) Wrobleski, S. T.; Chen, P.; Hynes, J., JR; Lin, S.; Norris, D. J.; Pandit, C. R.; Spergel, S.; Wu, H.; Tokarski, J. S.; Chen, X.; Gillooly, K. M.; Kiener, P. A.; McIntyre, K. W.; Patil-Koota, V.; Shuster, D. J.; Turk, L. A.; Yang, G.; Leftheris, K. Rational design and synthesis of an orally active indolopyridone as a novel conformationally constrained cannabinoid ligand possessing antiinflammatory properties. *J. Med. Chem.* **2003**, *46*, 2110–2116.

(304) Huffman, J. W.; Mabon, R.; Wu, M. J.; Lu, J.; Hart, R.; Hurst, D. P.; Reggio, P. H.; Wiley, J. L.; Martin, B. R. 3-Indolyl-1-naphthylmethanes: new cannabimimetic indoles provide evidence for aromatic stacking interactions with the CB_1 cannabinoid receptor. *Bioorg. Med. Chem.* **2003**, *11*, 539–549.

(305) Uchiyama, N.; Matsuda, S.; Kawamura, M.; Kikura-Hanajiri, R.; Goda, Y. Two new-type cannabimimetic quinolinyl carboxylates, QUPIC and QUCHIC, two new cannabimimetic carboxamide derivatives, ADB-FUBINACA and ADBICA, and five synthetic cannabinoids detected with a thiophene derivative α-PVT and an opioid receptor agonist AH-7921 identified in illegal products. *Forensic Toxicol.* **2013**, *31*, 223–240.

(306) Irie, T.; Kikura-Hanajiri, R.; Usami, M.; Uchiyama, N.; Goda, Y.; Sekino, Y. MAM-2201, a synthetic cannabinoid drug of abuse, suppresses the synaptic input to cerebellar Purkinje cells via activation of presynaptic CB1 receptors. *Neuropharmacology* **2015**, *95*, 479–491.

(307) Wiley, J. L.; Marusich, J. A.; Martin, B. R.; Huffman, J. W. 1-Pentyl-3-phenylacetylindoles and JWH-018 share in vivo cannabinoid profiles in mice. *Drug Alcohol. Depend.* **2012**, *123*, 148–153.

(308) The Senate of the United States. An act to amend the Controlled Substances Act to place synthetic drugs in Schedule I, 08.12.2011.

(309) Louis, A.; Peterson, B. L.; Couper, F. J. XLR-11 and UR-144 in Washington state and state of Alaska driving cases. *J Anal. Toxicol.* **2014**, *38*, 563–568.

(310) Karinen, R.; Tuv, S. S.; Oiestad, E. L.; Vindenes, V. Concentrations of APINACA, 5F-APINACA, UR-144 and its degradant product in blood samples from six impaired drivers compared to previous reported concentrations of other synthetic cannabinoids. *Forensic Sci. Int.* **2015**, *246*, 98–103.

(311) Schep, L. J.; Slaughter, R. J.; Hudson, S.; Place, R.; Watts, M. Delayed seizure-like activity following analytically confirmed use of previously unreported synthetic cannabinoid analogues. *Hum. Exp. Toxicol.* **2015**, *34*, 557–560.

(312) Lowry, O. H.; Rosebrough, N. J.; Farr, A. L.; Randall, R. J. Protein measurement with the Folin phenol reagent. *J. Biol. Chem.* **1951**, *193*, 265–275.

(313) Nordstedt, C.; Fredholm, B. B. A modification of a protein-binding method for rapid quantification of cAMP in cell-culture supernatants and body fluid. *Anal. Biochem.* **1990**, *189*, 231–234.

(314) Cheng, Y.; Prusoff, W. H. Relationship between the inhibition constant (K_i) and the concentration of inhibitor which causes 50 per cent inhibition (IC_{50}) of an enzymatic reaction. *Biochem. Pharmacol.* **1973**, *22*, 3099–3108.

(315) Behrenswerth, A.; Volz, N.; Torang, J.; Hinz, S.; Brase, S.; Muller, C. E. Synthesis and pharmacological evaluation of coumarin derivatives as cannabinoid receptor antagonists and inverse agonists. *Bioorg. Med. Chem.* **2009**, *17*, 2842–2851.

(316) Geis, U.; Kiec-Kononowicz, K.; Müller, C. E. Benzylidene-substituted imidazo-thiazole, - thiazine and -thiazepine derivatives: a new class of ligands for the benzodiazepine binding site of $GABA_A$ receptors. *Sci. Pharma.* **1996**, 383–390.

(317) McWilliam, H.; Li, W.; Uludag, M.; Squizzato, S.; Park, Y. M.; Buso, N.; Cowley, A. P.; Lopez, R. Analysis Tool Web Services from the EMBL-EBI. *Nucleic Acids Res.* **2013**, *41*, W597-600.

(318) Sievers, F.; Wilm, A.; Dineen, D.; Gibson, T. J.; Karplus, K.; Li, W.; Lopez, R.; McWilliam, H.; Remmert, M.; Soding, J.; Thompson, J. D.; Higgins, D. G. Fast, scalable generation of high-quality protein multiple sequence alignments using Clustal Omega. *Mol. Syst. Biol.* **2011**, *7*, 539.

(319) Berman, H. M.; Westbrook, J.; Feng, Z.; Gilliland, G.; Bhat, T. N.; Weissig, H.; Shindyalov, I. N.; Bourne, P. E. The Protein Data Bank. *Nucleic Acids Res.* **2000**, *28*, 235–242.

(320) Vernon, R.; Shen, Y.; Baker, D.; Lange, O. F. Improved chemical shift based fragment selection for CS-Rosetta using Rosetta3 fragment picker. *J. Biomol. NMR* **2013**, *57*, 117–127.

(321) McLachlan, A. D. Rapid comparison of protein structures. *Acta Crystallograph. A* **1982**, *38*, 871–873.

(322) Pettersen, E. F.; Goddard, T. D.; Huang, C. C.; Couch, G. S.; Greenblatt, D. M.; Meng, E. C.; Ferrin, T. E. UCSF Chimera--a visualization system for exploratory research and analysis. *J. Comput. Chem.* **2004**, *25*, 1605–1612.

11.DANKSAGUNG

12. PUBLICATION LIST

Publications

Angerer, V.; Mogler, L.; Steitz, J.; Bisel, P.; Hess, C.; <u>Schoeder, C.</u>; Müller, C.E.; Huppertz, L.; Westphal, F.; Schäper, J.; Auwärter, V. Structural characterization and pharmacological evaluation of the new synthetic cannabinoid 'Cumyl-PEGACLONE' *Drug Test. Anal.* **2017**, doi: 10.1002/dta.2237.

Flegel, C.; Vogel, F.; Hofreuter, A.; Wojcik, S.; <u>Schoeder, C.</u>; Kiec-Kononowicz, K.; Brockmeyer N, Müller CE, Becker C, Altmüller J, Hatt H, Gisselmann G. Characterization of non-olfactory GPCRs in human sperm with a focus on GPR18. *Sci. Rep.* **2016**, *6*, 32255.

Hess, C.; <u>Schoeder, C.</u>; Pillaiyar, T.; Madea, B.; Müller, C. E. Pharmacological evaluation of synthetic cannabinoids identified as constituents of spice. *Forensic Toxicol.* **2016**, *34,* 329-343.

Rempel, V.; Atzler, K.; Behrenswert, A.; Karcz, T.; <u>Schoeder, C.</u>; Hinz, S.; Kelta, M. ; Thimm, D.; Kieć-Kononowicz, K.; Müller, C. E. Bicyclic imidazole-4-one derivatives: a new class of antagonists for the orphan G protein-coupled receptors GPR18 and GPR55. *Med. Chem. Commun.* **2014**, *5*, 632-349.

Fuchs, A.; Baur, R.; <u>Schoeder, C</u>.; Sigel, E.; Müller, C. E. Structural Analogues of the Natural Products Magnolol and Honokiol as Potent Allosteric Potentiators of GABA$_A$ Receptors. *Bioorg. Med. Chem*. **2014**, *22*, 6908-6917.

Conference participation – Oral presentations

DPhG Doktorandentagung 2017
March -30-31, 2017, Frankfurt, Germany
"Pharmacological evaluation of synthetic cannabinoids identified as constituents of spice"
<u>Schoeder, C.;</u> Hess, C.; Pillaiyar, T.; Madea, B.; Müller, C. E.

International Symposium of the RTG1873
September 21-22, 2016, Bonn, Germany
"Pharmacological evaluation of synthetic cannabinoids identified as constituents of spice"
<u>Schoeder, C.;</u> Hess, C.; Pillaiyar, T.; Madea, B.; Müller, C. E.

Summer Academy Pharmacology
September 27-29, 2015, Bonn, Germany
"Development and characterization of agonists and antagonists for GPR18"
<u>Schoeder, C</u>.; Rempel, V.; Kieć-Kononowcz, K.; Müller, C. E.

Conference participation – Poster presentations

Keystone GPCR
February 23-17, 2016, Keystone, CO, USA.
"New antagonists and agonists for orphan G protein-coupled receptors GPR18"
(<u>Schoeder, C.;</u> Rempel, V.; Karcz, T.; Kieć-Kononowicz, K.; Müller, C. E.)

ESN Tartu
June 14-17, 2015, Tartu, Estonia
"New antagonists for the orphan G-protein coupled receptor GPR18, a new player in microglial migration"
(<u>Schoeder, C</u>.; Rempel, V.; Karcz, T.; Kieć-Kononowcz, K.; Müller, C. E.)

DPhG Jahrestagung
September 23-26, 2015, Düsseldorf, Germany
"Pharmacological evaluation of synthetic cannabinoids identified as constituents of spice"
<u>Schoeder, C.;</u> Hess, C.; Madea, B.; Müller, C. E.

Purines 2014
July 23-27, 2014, Bonn, Germany.
"P2Y-like orphan receptors: new antagonist for GPR18 and GPR55"
(<u>Schoeder, C</u>.; Rempel, V.; Karcz, T.; Kieć-Kononowcz, K.; Müller, C. E.)

EFMC International Symposium on Medicinal Chemistry
September 7-11, 2014, Lisbon, Portugal.
"New antagonists for orphan G protein-coupled receptors GPR18 and GPR55: Structure activity relationships of bicyclic imidazole-4-one derivatives"
(<u>Schoeder, C.;</u> Rempel, V.; Karcz, T.; Kieć-Kononowcz, K.; Müller, C. E.)

ESN Tartu
June 14-17, 2015, Tartu, Estonia